Understanding CO_2 diffusion in C_4 plants:

An investigation of CO_2 permeable aquaporins and carbonic anhydrase in the C_4 grass *Setaria viridis*

Hannah Louise Osborn

October 2017

A thesis submitted for the degree of Doctor of Philosophy of

The Australian National University

Australian National University

DECLARATION

This thesis contains research undertaken at the Australian National University, Canberra, ACT. Except where otherwise indicated, this thesis is my own original work performed under the supervision of Professor Susanne von Caemmerer, Professor Robert T Furbank, Dr Hugo Alonso Cantabrana and Dr Robert E Sharwood.

Hannah Louise Osborn

October 2017

ACKNOWLEDGEMENTS

This research was carried out at the Australian National University, Canberra and financially supported by the Australian Government Research Training Program in collaboration with CSIRO Agriculture OCE Postgraduate Studentship.

I would like to thank my supervisory panel, Susanne von Caemmerer, Robert Furbank, Robert Sharwood and Hugo Alonso-Cantabrana for their support and guidance throughout this PhD. They have all been extremely positive, encouraging, challenging and inspiring as mentors. It has been a privilege to learn from them and to share in their genuine enthusiasm for research.

I would like to acknowledge the technical support I have received from Soumi Bala for running the tunable diode laser and advice on many other lab assays, Dimitri Tolleter for running the membrane inlet mass spectrometer, Daryl Webb for his help using the confocal microscope and Wendy Sullivan for her assistance at the University of Adelaide running the stopped flow spectrophotometer. I would also like to thank the von Caemmerer lab group and the many friendly faces within the ARC Centre of Excellence for Translational Photosynthesis for all their advice, lovely chats and morning tea breaks.

I would especially like to thank the productive discussions I have had with Michael Groszmann and for his continued encouragement, support and advice. I would also like to thank Steve Tyerman and John Evans for their advice and comments regarding aquaporins.

I am extremely grateful for the genuine friendships I have made whilst at ANU with Elena Martin Avila, Hannah Birke and Anne-Sophie Dielen who have all helped me throughout this PhD providing many morale boosting conversations and valued coffee breaks, thank you girls!

Finally, I would like to thank my great family and partner Eric who have loved and supported me through this entire journey, even when it didn't make sense to them. Thank you Eric, you have been my rock and travelled this challenging and emotional PhD rollercoaster by my side.

ABSTRACT

The productive yield of key C_4 crops must increase in the future to meet the demands of an increasing global population. We are therefore endeavouring to improve the availability of CO_2 for photosynthesis, one of the fundamental limitations to photosynthetic carbon fixation. The initial steps of CO_2 assimilation in leaf mesophyll cells involve the diffusion of CO_2 from the intercellular airspace to the mesophyll cytosol (mesophyll conductance). This involves CO_2 passing through the liquid phase and the plasma membrane, a process believed to be both passive and possibly facilitated by protein pores, known as aquaporins. Within the cytosol of mesophyll cells, carbonic anhydrase (CA) catalyses the hydration of CO_2 to HCO_3^- which PEP Carboxylase uses in the first CO_2 fixation step of C_4 photosynthesis. Here, I have examined the role of CO_2 permeable aquaporins and CA from a C_4 photosynthesis perspective using the model monocot species *Setaria viridis* (Foxtail millet).

CO_2 permeable aquaporins have been demonstrated to increase CO_2 diffusion in C_3 plants. However, to date very little is known about the role of CO_2 permeable aquaporins in the highly efficient and specialised C_4 photosynthetic pathway. After bioinformatic identification of all twelve Setaria PIPs (plasma membrane intrinsic proteins) I first used yeast as a heterologous expression system to confirm plasma membrane localisation and determine CO_2 permeability of the plasma membrane using CO_2 triggered intracellular acidification on a stopped flow spectrophotometry. This *in vitro* approach identified SiPIP2;7 as a putative CO_2 permeable aquaporin, adding a third CO_2 pore to the list of C_4 plant aquaporins characterised to date. I also examined the effect of PIP1 and PIP2 co-expression and found improved localisation to the plasma membrane but no improvement to CO_2 permeability compared to the single PIP1s.

The effects of modifying CA activity in C_4 photosynthesis was examined *in planta*. I silenced the major leaf CA in *Setaria viridis* in three independent, stably transformed lines. At low CO_2 a strong correlation between photosynthetic assimilation rate and CA hydration rates was observed in the transformed lines, which have as little as 13% of wild type CA activity. Significantly, no visual phenotype or photosynthetic effect was observed in the transformed

lines at ambient CO_2. $C^{18}O^{16}O$ isotope discrimination was used to estimate the mesophyll conductance to CO_2 diffusion from the intercellular air space to the mesophyll cytosol in control plants, which allowed us to calculate CA activities in the mesophyll cytosol. These results indicated that CA is not rate limiting for C_4 photosynthesis in *S. viridis* under current atmospheric conditions.

We conclude that CO_2 permeable aquaporins and CA activity are factors with variable importance to CO_2 diffusion in C_4 photosynthesis, with both factors becoming rate limiting under extreme environmental conditions that result in low intercellular CO_2 such as drought stress.

TABLE OF CONTENTS

LIST OF FIGURES

LIST OF TABLES

ABBREVIATIONS AND SYMBOLS

A (μmol m^{-2} s^{-1})	Rate of CO_2 assimilation
a_{18bs}	Weighted discrimination of $C^{16}O^{18}O$ diffusion across the boundary layer and stomata in series
C_a (μbar)	Ambient air CO_2 partial pressure
C_i (μbar)	Intracellular airspace CO_2 partial pressure
C_c (μbar)	Chloroplastic CO_2 partial pressure
C_m (μbar)	Mesophyll cytosol CO_2 partial pressure
C_i/C_a	Ratio of C_i to C_a
$C_i - C_m$ (μbar)	Drawdown of CO_2 from the intercellular airspace to the site of fixation
C_{in} and C_{out} (μbar)	Molar fraction of $^{12}CO_2$ in dry air entering (C_{in}) and leaving (C_{out}) the leaf chamber
C_s	CO_2 partial pressure at the leaf surface
E	Transpiration rate
g_{ac}	Total conductance to CO_2
g_m (μmol m^{-2} s^{-1} bar^{-1})	Mesophyll conductance for CO_2
g_s (mol m^{-2} s^{-1})	Stomatal conductance for CO_2
k_{CA} (mol m^{-2} s^{-1} bar^{-1})	Rate constant of CA hydration
K_{CO2}	Rate constant of the exponential kinetics of decrease in fluorescence
P_{CO2} (m s^{-1})	CO_2 permeability
pH_f	Final intracellular pH
pK_a	Acid dissociation constant for HCO_3^-
S_m (m^2 m^{-2})	Mesophyll surface area exposed to intercellular airspace to leaf area ratio
$\Delta^{18}O$ (‰)	Oxygen isotope discrimination
ϑ	Isotopic equilibrium (theta)

δ_{in} and δ_{out}	Isotopic composition of the CO_2 entering δ_{in} and leaving δ_{out} the leaf chamber
δ_A	Isotopic composition of ambient air (in our case $\delta_a = \delta_{out}$)
δ_i	Oxygen isotope composition of CO_2 in the intercellular airspaces
δ_{io}	Isotopic composition of intercellular CO_2
V/A (m)	Volume to surface area ratio
w_{in} and w_{out}	Water vapour concentration entering (w_{in}) and exiting (w_{out})

CHAPTER 1: GENERAL INTRODUCTION

Publications arising from this chapter:

Groszmann M., Osborn H.L., Evans J.R. 2016. Carbon dioxide and water transport through plant aquaporins. *Plant Cell and Environment*, 40, 938-961.

1.1 Food security

Substantial increases in food production are needed to meet the world's rapidly increasing population, predicted to hit 9 billion by 2050. Previous major advances in agriculture production occurred during the green revolution in the 1950's by increasing crop yield potential, primarily due to better biomass partitioning to the grain. Yield potential was also improved by the expansion of irrigation infrastructure, modernisation of farming techniques, and wide distribution of hybridised seeds, synthetic nitrogen fertilisers and pesticides. However, over the past decade, the annual gains in yield have reached a plateau and these benefits are not enough to match demand from expected population growth. Today, the amount of arable land is limited and under competition from increased urbanisation, land degradation, biofuel crops and the threat of climate change (Parry and Hawkesford, 2010). To continue to provide sufficient food there is clearly a need for advances in crop yields, a second "green revolution" above the incremental advances currently observed by traditional breeding technologies is required (Furbank *et al.*, 2015). Indeed, if we continue following current crop yield trends (Figure 1.1 solid lines) we will not achieve the required doubling of yield predicted to be necessary for different key agriculture crops such as maize, rice, wheat and soybean by 2050 (Figure 1.1 dashed lines; Ray *et al.*, 2013).

There are a number of factors which limit crop productivity. Environmental issues such as weather, soil nutrients and biotic factors can all influence a plant's growth rate. Ultimately, however, a plant's growth is determined by its photosynthetic efficiency, a process in which plants convert light energy into chemical energy and assimilate atmospheric CO_2 to form sugars for growth. Improvements to key aspects of photosynthesis such as water use efficiency, light capture and the catalytic rate of the key enzyme Rubisco (Ribulose-1, 5-bisphosphate carboxylase/oxygenase), all have the potential to increase crop yield (Ort *et al.*, 2015; Richards, 2000; Sharwood, 2017). Indeed, manipulation of photosynthesis is cited as the only remaining major trait available to improve yield potential (Long *et al.*, 2006; Raines, 2011). Efforts to achieve improvements in photosynthesis are already yielding rewards, as demonstrated recently by Kromdijk *et al.* (2016) achieving a 15% increase in crop biomass by modifying the plants response to light fluctuations.

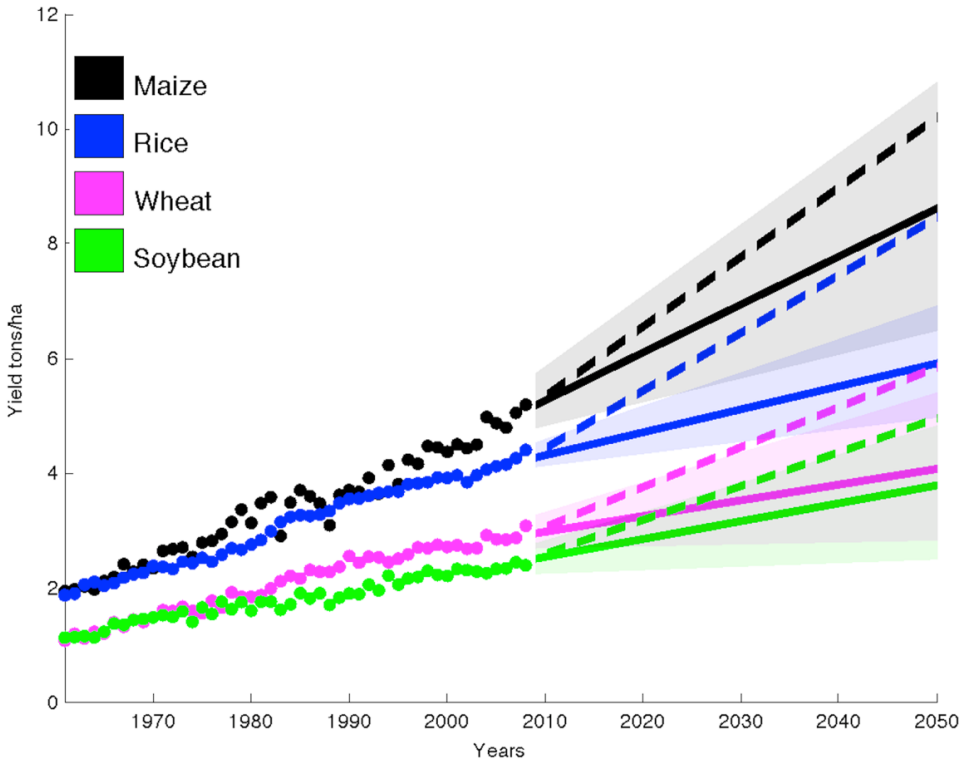

Figure 1.1: Global prediction of yield from 1961 – 2008 and projections (solid line) to 2050 for maize, rice, wheat and soybean. Dashed lines show the improvement to crop yield needed to achieve the required doubling of yield production in these crops by 2050 (Image from Ray *et al.*, 2013).

1.2 Photosynthesis

There are three different photosynthetic mechanisms in plants: C_3, C_4 and CAM (Crassulacean Acid Metabolism) photosynthesis. The C_3 photosynthetic mechanism evolved first, early in the history of life in a high CO_2 environment (Ehleringer *et al.*, 1991). Around 24-35 million years ago a number of contributing factors including low atmospheric CO_2, global acidification and regions of heat, drought and salinity lead to the evolution of C_4 photosynthesis (Sage, 2004). CAM photosynthesis evolved earlier, around 40-100 million years ago, under similar conditions but is not a focus of this study (Silvera *et al.*, 2010). The C_4 photosynthetic pathway has evolved multiple times in both dicot and monocot genera, with more than 60 independent origins of C_4 photosynthesis estimated (Christin and Osborne, 2013; Sage, 2004; Sage *et al.*, 2011; Sage *et al.*, 2012).

In C_3 plants, atmospheric CO_2 is fixed in the mesophyll cells (Figure 1.2A). In contrast, the defining advantageous feature of C_4 photosynthesis is the concentration of CO_2 in the bundle

sheath cells where Rubisco is located (Figure 1.2C) and with the mesophyll cells serving as a biochemical CO_2 pump. The C_4 photosynthesis pathway (Hatch and Slack, 1966) is characterised by both biochemical and anatomical specialisation. Important biofuel and agriculturally productive crops including *Zea mays* (maize), *Sorghum bicolor* (sorghum), *Saccharum officinarum* (sugarcane) and *Panicum virgatum* (switchgrass) all carry out this C_4 pathway. Notably, despite C_3 photosynthesis being the most common photosynthetic pathway, C_4 plants contribute approximately 25% of the primary production on the planet and yet, represent only 3% of the total terrestrial plants (Lloyd and Farquhar, 1994; Sage *et al.*, 1999).

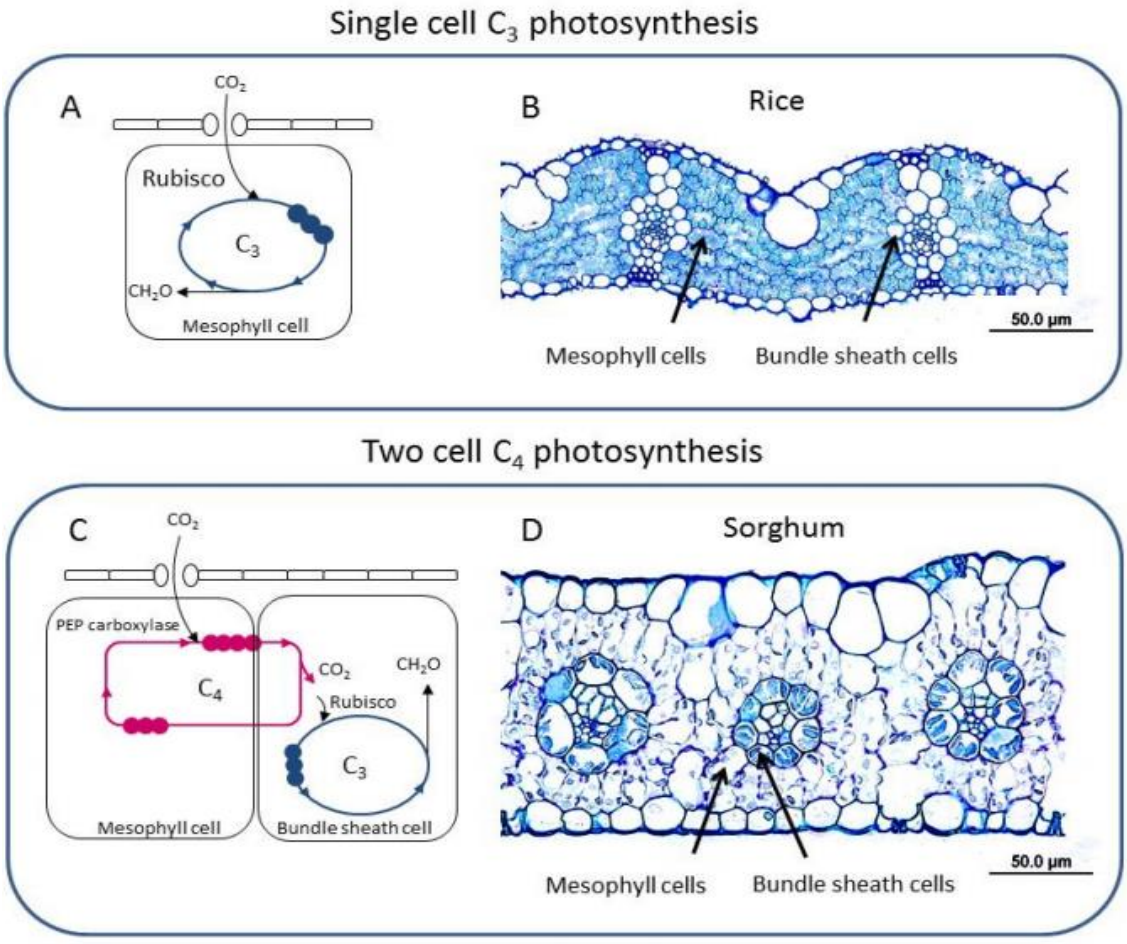

Figure 1.2: Comparison of biochemistry and anatomy of plants operating C_3 and C_4 photosynthetic pathways. A) C_3 photosynthesis fixes atmospheric CO_2 with Rubisco in single cells. B) A transverse light microscopy image of a C_3 rice leaf. C) C_4 photosynthesis is separated over two cells, with atmospheric CO_2 fixed in the mesophyll cell and Rubisco localised to the bundle sheath cells. D) A transverse light microscopy image of a C_4 sorghum leaf (Image from von Caemmerer *et al.*, 2012).

1.2.1 C_4 photosynthetic cycle

In the specialised C_4 photosynthetic cycle, CO_2 enters the mesophyll cell where it is converted to HCO_3^- by carbonic anhydrase (CA) and then fixed by phosphoenolpyruvate carboxylase (PEPC). This produces oxaloacetate (OAA) which is converted into four carbon acids, either malate or aspartate, which diffuse into the bundle sheath cell. Once in the bundle sheath, the C_4 acids are decarboxylated releasing CO_2 and consequently increasing CO_2 concentrations in this compartment up to 10-fold above ambient air levels (Furbank and Hatch, 1987). CO_2 is then refixed by Rubisco and the photosynthetic carbon reduction cycle producing a 3 carbon sugar phosphate, triose-P.

Plants carrying out C_4 photosynthesis can be further divided into three sub groups based on the enzyme involved in the decarboxylation step within the bundle sheath cells (Figure 1.3). These are NADP-malic enzyme (NADP-ME), NAD-malic enzyme (NAD-ME) and PEP carboxykinase (PEP-CK); however there is a degree of flexibility within these groups (Furbank, 2011). Common to all decarboxylation types is PEPC which produces OAA. In the case of NADP-ME types, OAA enters the mesophyll chloroplast where it is reduced to malate, diffuses to the bundle sheath and is decarboxylated by NADP-ME and then converted into pyruvate in the chloroplast. In the case of NAD-ME and PEP-CK types, OAA is converted in the cytosol to aspartate by asparate aminotransferase. Once in the bundle sheath, NAD-ME types decarboxylate in the mitochondria and PEP-CK types decarboxylate predominately in the cytosol.

Anatomically, C_4 plants are also highly specialised. The C_4 pathway is separated over two cells in the leaf, the mesophyll and bundle sheath cells which are arranged in a wreath like formation known as Kranz anatomy (Figure 1.2D). The primary function of this specific anatomy is to provide an advantageous environment for Rubisco to operate, thereby avoiding photorespiration. The two rings of cells surround the vascular bundle, the inner ring are bundle sheath cells where CO_2 accumulates and which contains Rubisco, and the outer ring are mesophyll cells where CO_2 is initially fixed by PEPC.

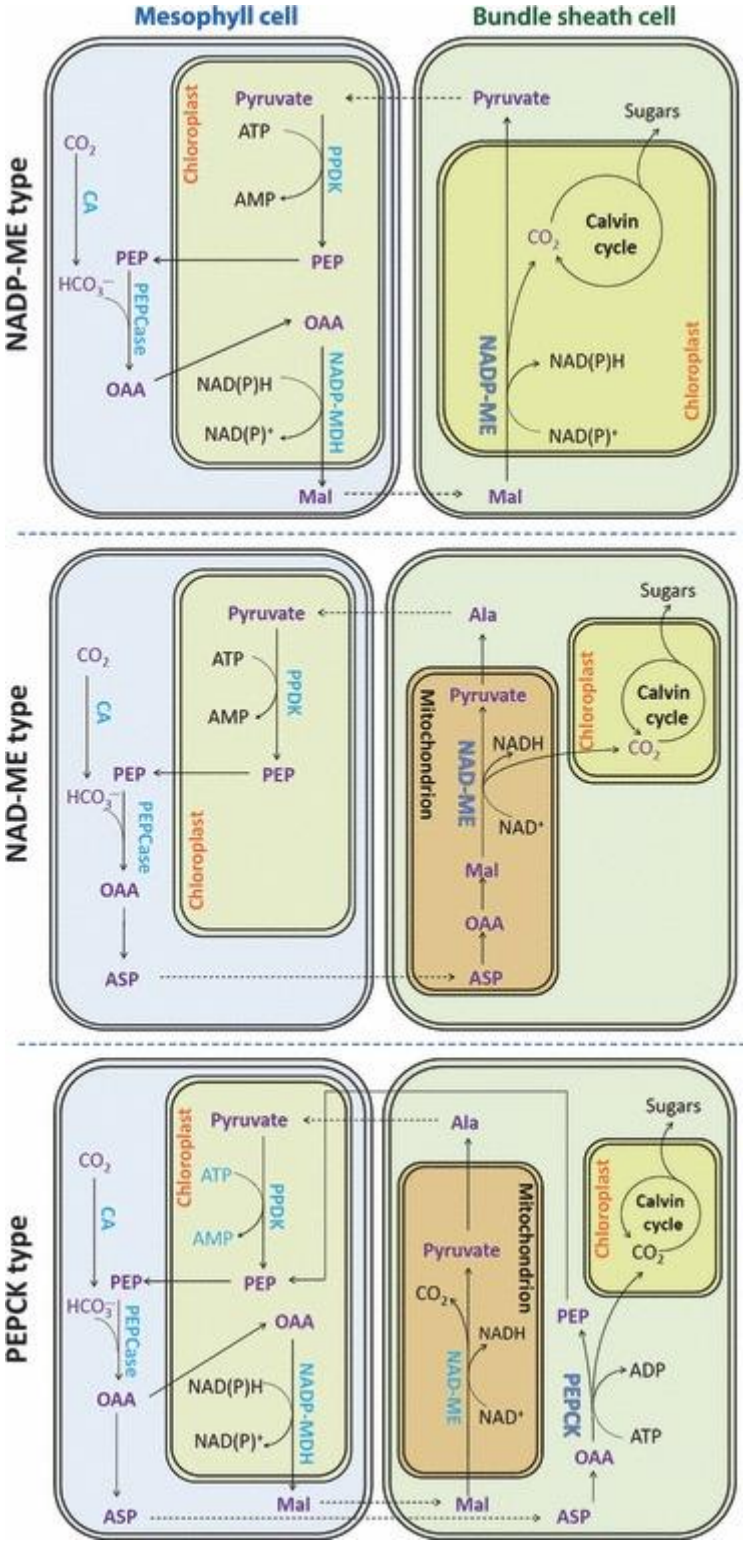

Figure 1.3: Subtypes of C_4 photosynthesis. There are three major types of C_4 photosynthesis divided based on the primary decarboxylation enzyme utilised: NADP-ME, NAD-ME and PEPCK (Image from Wang *et al.*, 2011). Note: Ala, alanine; ASP, aspartate; CA, carbonic anhydrase; Mal, malate; MDH, malate dehydrogenase; NAD-ME, NAD-dependent malic enzyme; NADP-ME, NADP-dependent malic enzyme; OAA, oxaloacetate; PEP, phosphoenolpyruvate; PEPCase, phosphoenolpyruvate carboxylase; PEPCK, phosphoenolpyruvate carboxykinase; PPDK, pyruvate orthophosphate dikinase.

1.1.2 Recent model C_4 species

Setaria viridis (green foxtail) is a C_4 grass closely related to important NADP-ME cereal crops including maize, sorghum and sugarcane and is found worldwide in both temperate and subtropical regions (Defelice, 2002). It is a member of the Paniceae tribe and Poaceae family and *S. viridis* is genetically very similar to *S. italica* (foxtail millet), a cereal crop widely grown in Northern China and India. *S. viridis* has become a recent model C_4 species due to its many desirable features including its rapid generation time, small stature, high seed production, small sequenced genome (~515 MB) and the ability to be genetically transformed (Brutnell *et al.*, 2010; Doust *et al.*, 2009; Li and Brutnell, 2011).

1.3 CO_2 diffusion

High photosynthetic rates require high rates of CO_2 diffusion from the intercellular airspace to the site of CO_2 fixation (von Caemmerer *et al.*, 2012). Both C_3 and C_4 photosynthetic plants can be physiologically limited by the availability of CO_2. Within C_3 plants, the importance of CO_2 has been demonstrated on a large scale using free-air CO_2 enrichment (FACE) experiments which show the effect of elevated CO_2 on plants, including increased photosynthetic rate and increased yield (Ainsworth and Long, 2005). The diffusion pathway of CO_2 from ambient air to its site of carboxylation differs slightly depending on the photosynthetic pathway. For C_3 plants, CO_2 must diffuse across the cell wall, the plasma membrane and into the chloroplast through the envelope and stroma to reach Rubisco. For C_4 plants, CO_2 must cross the cell wall and plasma membrane of the mesophyll cell, be converted to HCO_3^- by CA and then be fixed by PEPC. The movement of CO_2 from sub-stomatal cavities to the site of fixation can be quantified by mesophyll conductance, g_m, which can be defined by Fick's law:

$$g_m = A/(C_i - C_c) \qquad \text{Equation 1}$$

where A is the CO_2 assimilation rate, C_i is the CO_2 concentration in the intercellular air space and C_c is the CO_2 concentration in the chloroplast stroma. For C_4 photosynthesis C_c is actually C_m the CO_2 concentration in the mesophyll cytosol.

The bulk of information on CO_2 diffusion through leaves has been discovered through studying C_3 plants. To further understand CO_2 diffusion in C_4 photosynthetic plants we can build on this existing knowledge within C_3 plants. On a cellular level, the resistance to diffusion of CO_2 from ambient air to the site of carboxylation within the leaf can occur at multiple levels. These barriers to diffusion are difficult to measure and can depend on leaf thickness, cell shape, mesophyll surface area exposed to the intercellular air space and, within C_3 plants, chloroplast position relative to stomata location (Evans *et al.*, 2009; Evans and von Caemmerer, 1996). Resistances in the leaf can occur in the gaseous or liquid phase, with the latter generally assumed to be higher (Evans *et al.*, 2009; Niinemets and Reichstein, 2003). Currently, none of these resistances can be directly measured independently in an intact leaf. However, it is possible to estimate the importance of each component of resistance by mathematical modelling based on diffusion path length, the porosity of the element and the diffusivity of CO_2 in the solvent (water or lipid). Cell walls are believed to impose a significant proportion of the total resistance; 25 – 50% depending on assumed porosity (Evans *et al.*, 2009). There is also significant resistance to CO_2 diffusion across membranes such as plasma membrane and the chloroplast membrane (Flexas *et al.*, 2012).

1.3.1 Limitations to mesophyll conductance

Mesophyll conductance, g_m, describes the flux of CO_2 diffusion from the intercellular airspace to the site of fixation (Equation 1). This equation applies to C_3 photosynthetic species; however, in C_4 photosynthesis measuring g_m is more complex. There are a number of techniques available to measure g_m in C_3 plants including combining gas exchange measurements with carbon isotope discrimination (Evans *et al.*, 1986) or with chlorophyll fluorescence (Harley *et al.*, 1992). However, as alluded to, these techniques are not possible for C_4 plants and consequently, there is very little published data on g_m in C_4 plants. Pfeffer and Peisker (1998) calculated g_m in maize as approximately 1.07 mol m^{-2} s^{-1} based on gas exchange data and PEPC activity. Pengelly *et al.* (2010) suggested a reduction in g_m in *Flaveria bidentis* based on changes in leaf anatomy due to low irradiance and calculated g_m in low light as 0.55 mol m^{-2} s^{-1} bar^{-1} compared to g_m in medium light of 0.92 mol m^{-2} s^{-1} bar^{-1}. More recent methods have used oxygen isotope discrimination (Gillon and Yakir, 2000) to demonstrate variations in g_m in C_4 plants. Barbour *et al.* (2016) demonstrated g_m decreased with leaf age in some C_4 species with g_m decreasing 61% in old leaves compared to young leaves with g_m of 0.72 mol m^{-2} s^{-1} bar^{-1} in *F. bidentis*. Alonso-Cantabrana and von Caemmerer

(2016) also measured g_m in *F. bidentis* estimating g_m decreased with increasing intercellular CO_2 concentrations from 0.79 to 0.38 mol m^{-2} s^{-1} bar^{-1}. Ubierna *et al.* (2017) demonstrated the effects of temperature on g_m in various C_4 species using oxygen isotope discrimination and the effect of modifying CA activity using *in vitro* V_{pmax} modelling.

In addition to these factors of leaf age, light availability and CO_2 concentrations, there are other environmental factors hypothesised to influence g_m in C_4 plants which have been demonstrated experimentally in C_3 species such as temperature, salinity and drought (see review by Flexas *et al.*, 2008). There are also membrane proteins such as aquaporins which have been implicated in g_m in both chloroplast and plasma membranes in C_3 plants (Flexas *et al.*, 2006; Kaldenhoff, 2012) which most likely also influence g_m in C_4 photosynthetic plants, therefore I have discussed aquaporins in the following sections.

1.4 General features of aquaporins

1.4.1 Classification, subcellular localisation and structural characteristics

Aquaporins are pore forming integral membrane proteins that allow facilitated diffusion of water and other small uncharged molecules across membranes (Groszmann *et al.*, 2016; Kaldenhoff *et al.*, 1998). They are present in most living organisms and belong to the ancient superfamily of major intrinsic proteins (MIPs). Plant aquaporins have been classified into five main subfamilies, based on sequence homology and sub cellular localisation: plasma membrane intrinsic proteins (PIPs), tonoplast intrinsic proteins (TIPs), nodulin 26-like intrinsic proteins (NIPs) which are found in the plasma membrane and endoplasmic reticulum (ER), small basic intrinsic proteins (SIPs) which are found in the ER and X intrinsic proteins (XIPs) which are localised in the plasma membrane (Johanson *et al.*, 2001; Maurel *et al.*, 2008). Members of the GlpF-like intrinsic proteins (GIPs) and hybrid intrinsic proteins (HIPs) subfamilies are present exclusively in moss and not found in vascular plants (Figure 1.4; Anderberg *et al.*, 2011; Li *et al.*, 2014).

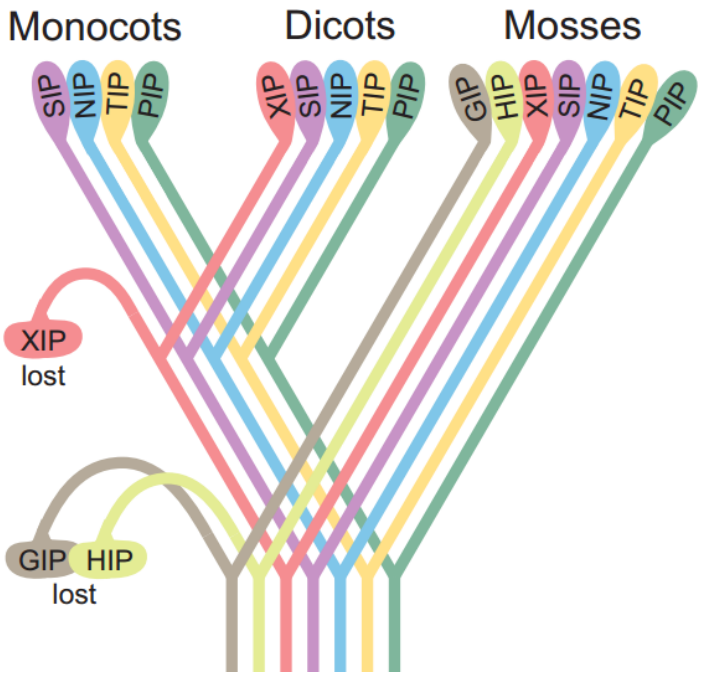

Figure 1.4: Evolution of the MIP superfamily in plants. GIPs and HIPs were lost during the evolution of higher plants and subsequently the XIP subfamily were lost in monocots (Image from Danielson and Johanson, 2008). Note: PIPs (plasma membrane intrinsic proteins), TIPs (tonoplast intrinsic proteins), NIPs (nodulin 26-like intrinsic proteins), SIPs (small basic intrinsic proteins), XIPs (X intrinsic proteins), GIPs (GlpF-like intrinsic proteins) and HIPs (hybrid intrinsic proteins).

Multiple aquaporins are present within each species, for instance there are 35 aquaporins in *Arabidopsis thaliana* (Johanson *et al.*, 2001) and 33 in *Oryza sativa* (Sakurai *et al.*, 2005). The total number of aquaporins found in plants is considerably higher than that found in other kingdoms: for instance there are only two native aquaporins in *Saccharomyces cerevisiae* (Carbrey *et al.*, 2001) and 13 in humans (Moshelion *et al.*, 2015). The large number of plant aquaporins is suggested to be due to their importance in water regulation and maintenance of cellular water homeostasis at different developmental stages and environmental conditions (Hachez *et al.*, 2006; Tyerman *et al.*, 2002).

Structurally, aquaporins are small proteins (21 – 34 kDa), comprising six membrane spanning helices with N and C-termini facing the cytosol (Figure 1.5A; Heymann *et al.*, 1998). The loops form a pore with high specificity based on two filter regions. Firstly, the NPA motif (asparagine-proline-alanine) constitutes a first size exclusion zone in the centre of the channel, and secondly the Ar/R (aromatic/arginine) selectivity filter, comprising four amino

acids, contributes to a size exclusion and hydrogen bond environment for the substrate transport (Chaumont and Tyerman, 2014; Murata *et al.*, 2000).

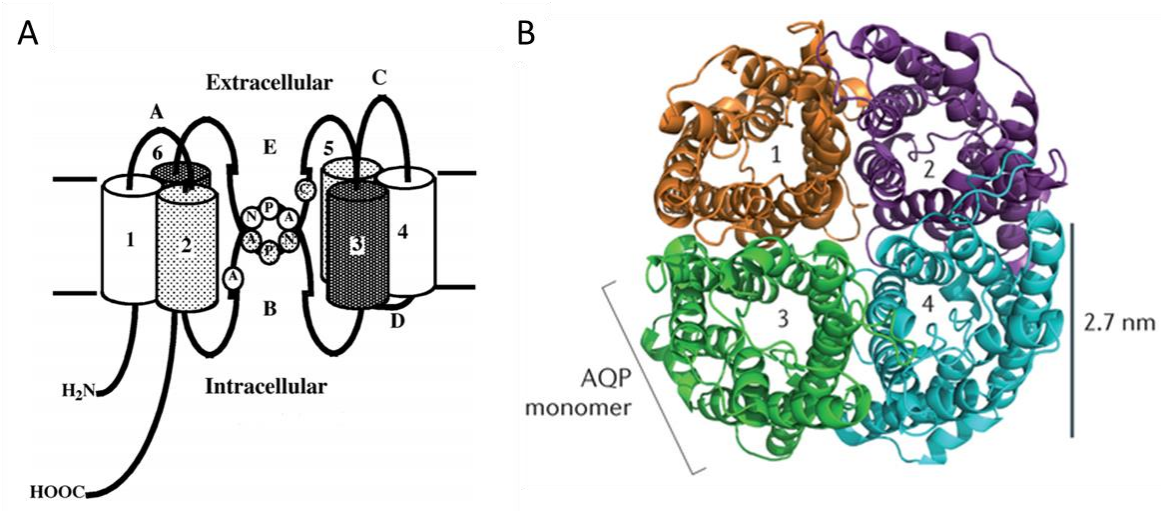

Figure 1.5: Comparison of aquaporin structures. A) The aquaporin structure comprises six membrane spanning domains with N and C termini facing the intracellular cytosol (Image from Heymann *et al.*, 1998). B) Four aquaporin monomers assemble as a tetramer in the membrane, from a top view perspective (Image from Verkman *et al.*, 2014).

Aquaporins assemble as homo and/or heterotetramers in the membrane (Figure 1.5B) with each monomer acting as an independent channel and a fifth channel created in the centre by this formation (Murata *et al.*, 2000). There are two major PIP subgroups in plants, PIP1 and PIP2. These are separated based on sequence homology and typically vary in water permeability; in general PIP2s have a higher capacity to transport water (Chaumont *et al.*, 2000; Johanson *et al.*, 2001). The interactions of different PIPs to form these tetramers are important in determining permeability efficiency, as well as correct localisation to the membrane. Artificial heterotetramers with defined proportions of PIP1 to PIP2 have demonstrated altered substrate permeability to water in yeast membranes (Otto *et al.*, 2010). Additionally, fluorescence experiments in maize have demonstrated ZmPIP1s localise to the ER and ZmPIP2s localise to the plasma membrane when expressed alone. However when co-expressed, ZmPIP1 localises to the plasma membrane due to physical interaction with a ZmPIP2 (Fetter *et al.*, 2004; Zelazny *et al.*, 2007). Different motifs have since been identified in PIP2s which are required for trafficking to the plasma membrane (Chevalier *et al.*, 2014; Zelazny *et al.*, 2009). The activity of aquaporins can also be regulated by post-

translational mechanisms such as gating, driven by divalent cations and pH in the cytosol, trafficking or redistribution of aquaporins (Groszmann *et al.*, 2016).

1.4.2 CO_2 permeable aquaporins

In addition to their role in water permeability, aquaporins are also important for the membrane-selective pathway of other small uncharged molecules such as ammonia, glycerol, urea, hydrogen peroxide, oxygen, boric acid, arsenite and CO_2 (Biela *et al.*, 1999; Meinild *et al.*, 1998; Terashima and Ono, 2002; Tyerman *et al.*, 2002; Zwiazek *et al.*, 2017). The permeability of aquaporins to diverse substrates is not only important in maintaining water homeostasis but also plays significant roles in plant metabolism, nutrition, signalling processes and photosynthesis (Chaumont and Tyerman, 2014). It is hypothesised that CO_2 permeable aquaporins are important in plants for photosynthesis and that, in theory, the expression of these CO_2 permeable aquaporins may be manipulated to maximise CO_2 diffusion rates to increase photosynthesis while not affecting transpiration or water loss (Moshelion *et al.*, 2015).

CO_2 is a hydrophobic gas and according to the Meyer-Overton rule can rapidly cross all cell membranes (Missner and Pohl, 2009). However, recent research demonstrating the presence of CO_2 permeable aquaporins in animal and plant cells has resulted in significant debate within the literature (Boron, 2010; Uehlein *et al.*, 2012). The Meyer-Overton rule implies there is no need for aquaporins and that the rate limiting step to CO_2 diffusion is the unstirred layer adjacent to the membrane rather than the membrane itself (Missner *et al.*, 2008; Missner and Pohl, 2009). The energy barrier for CO_2 through an aquaporin is also argued to be greater than the energy barrier through the lipid bilayer and therefore aquaporins would actually reduce transport rates (Hub and De Groot, 2008). In biological systems, however, the CO_2 transport rates are much lower than predicted, reportedly 10-1000 times lower than expected from a pure lipid bilayer (Endeward *et al.*, 2006; Evans *et al.*, 2009; Otto *et al.*, 2010; Uehlein *et al.*, 2012). This is supported by gas exchange measurements indicating g_m is not as large or as constant as previously thought (Flexas *et al.*, 2006). Under these conditions, membrane characteristics and the role of CO_2 permeable aquaporins need to be considered.

Evidence for CO_2 permeable aquaporins has been generated through two heterologous expression systems; either *Xenopus laevis* oocytes or yeast (Heckwolf *et al.*, 2011; Mori *et al.*, 2014; Nakhoul *et al.*, 1998; Otto *et al.*, 2010). CO_2 permeability of the oocyte or yeast plasma

membrane can then be measured via three main approaches. In all cases, CA is added to increase the catalysed rate of $CO_2 + H_2O \leftrightarrow HCO_3^- + H^+$. One approach to measure CO_2 permeability is using a stopped flow spectrophotometer which monitors changes in fluorescence intensity due to CO_2 triggered intracellular acidification (Ding *et al.*, 2013; Heckwolf *et al.*, 2011; Otto *et al.*, 2010; Uehlein *et al.*, 2008). Here, cells are incubated in a pH sensitive dye and uptake of CO_2 results in CA converting CO_2 to HCO_3^- ions and protons which decreases the intracellular pH and consequently, decreases the fluorescence of the dye. This decrease in fluorescence is then measured spectrophotometrically and used to determine CO_2 permeability.

A second approach to measure CO_2 permeability is from mass spectrometry measurements of ^{18}O exchange (Badger and Price, 1989; Endeward *et al.*, 2006; Itel *et al.*, 2012; Price and Badger, 1989; Tu *et al.*, 1986; Wunder *et al.*, 1997). This measures the exchange of ^{18}O from CO_2, HCO_3^- and H_2O. CA catalyses the reversible reaction of CO_2 to HCO_3^-; as this hydration-dehydration reaction continues, the ^{18}O label can be lost to the larger water pool within the cell. This causes a slow decay in the $C^{18}O^{16}O$ pool which is then measured via a membrane inlet mass spectrometer (MIMS). CO_2 permeability is then calculated by comparing the rate of ^{18}O loss due to the uncatalysed kinetics of CO_2 to HCO_3^- to the catalysed rate of ^{18}O loss due to cells with CA activity (Badger and Price, 1989; von Caemmerer *et al.*, 2004).

The third approach is to measure the intracellular pH change directly by a pH microelectrode (Mori *et al.*, 2014; Nakhoul *et al.*, 1998; Uehlein *et al.*, 2003). This technique is specific for oocytes, the oocytes are placed in a CO_2 enriched buffer and then impaled with a microelectrode and the internal cytosolic pH determined. Acidification within the cytosol indicates CO_2 permeability.

In addition to these *in vitro* expression systems, Uehlein *et al.,* (2012) have demonstrated CO_2 permeability of aquaporins using a synthetic triblock copolymer to mimic a biological membrane. Two chambers were separated by the artificial membrane with a solution maintaining high CO_2 concentrations on one side and the other with depleted CO_2 concentrations. This approach measured pH change resulting from CO_2 diffusion through different plant aquaporins inserted into the artificial membrane.

1.4.3 In planta effects of CO_2 permeable aquaporins

Evidence for the role of CO_2 permeable aquaporins *in vivo* has been explored through manipulation of PIP expression in plants. Specifically, overexpression studies have demonstrated increased g_m, stomatal conductance (g_s) and net photosynthetic rates in tobacco overexpressing *Nicotiana tabacum NtAQP1* (Flexas *et al.*, 2006) and *Mesembryanthemum crystallinum McMIPB* (Kawase *et al.*, 2013); in rice overexpressing *Hordeum vulgare HvPIP2;1* (Hanba *et al.*, 2004), and in tomato overexpressing *NtAQP1* (Sade *et al.*, 2010). Similarly, knockout approaches have shown decreased g_m to CO_2. For instance, insertion of a T-DNA in *AtPIP1;2* in *Arabidopsis thaliana* decreased g_m approximately 40% (Heckwolf *et al.*, 2011), RNAi mediated suppression of *NtAQP1* expression (Uehlein *et al.*, 2008) and *NtAQP1* antisense (Flexas *et al.*, 2006) studies in tobacco also resulted in decreased g_m and g_s.

Some aquaporins, NtAQP1 for instance, have a dual function being permeable to both water and CO_2. Consequently, altering the expression of this aquaporin can result in changes which are potentially attributable more to the water than the CO_2 permeability of the aquaporin. This may be the case for g_s when *NtAQP1* expression is altered in tobacco (Flexas *et al.*, 2006). However, when expression of *AtPIP1;2*, which is CO_2 permeable only, was altered in Arabidopsis no change in g_s was observed (Heckwolf *et al.*, 2011). Overexpression of *NtAQP1* in tomato was shown to significantly improve plant growth and height compared to wild type plant (Kelly *et al.*, 2014). Net photosynthetic rate and g_m were not altered suggesting the increase in plant growth in this study was due to NtAQP1 acting as a water aquaporin not as a CO_2 pore. Studies on the localisation of NtAQP1 revealed the aquaporin changes function, switching from water to CO_2 permeable, depending on cellular location or the permeability of different membranes e.g. plasma membrane or chloroplast membrane (Sade *et al.*, 2014; Sade *et al.*, 2010; Uehlein *et al.*, 2008).

Interestingly, distinct aquaporin transcript profiles to changes in CO_2 concentrations have been observed in tobacco leaves (Secchi *et al.*, 2016). Growth in low atmospheric CO_2 concentrations increased the expression of the CO_2 permeable *NtAQP1*, whereas the water permeable *NtPIP2;1* did not change under these conditions. Another study examined the transcript profile of Arabidopsis *AtPIP1;2* knockout lines and compared it to wild type plants grown under drought or low CO_2 conditions. The transcript profile of the *AtPIP1;2* knockout plants was most similar to that of plants grown under low CO_2 conditions (Boudichevskaia *et*

al., 2015), consistent with its function as a CO_2 pore determined in heterologous expression systems (Heckwolf *et al.*, 2011).

1.4.4 CO_2 permeable aquaporins in C_4 plants

To date, there are very few studies investigating the presence of CO_2 permeable aquaporins in C_4 species. Despite the importance of CO_2 transport for maintaining high photosynthetic rates in C_4 plants, there are still many gaps in our knowledge surrounding its diffusion, the properties of mesophyll plasma membranes and what role aquaporins, which are implicated in C_3 photosynthesis as described above, may play in CO_2 diffusion in C_4 species.

The presence of CO_2 permeable aquaporins in C_4 plants is indicated in the comparative transcriptomic study of two closely related C_3 (*Cleome spinosa*) and C_4 (*Cleome gynandra*) species (Bräutigam *et al.*, 2011). A transcript putatively involved in CO_2 diffusion was observed to be 20-fold higher in the C_4 leaf compared to the C_3 leaf, suggestive of a role for CO_2 permeable aquaporins in C_4 plants (Kaldenhoff, 2012; Weber and von Caemmerer, 2010). Indeed, experimental evidence using a heterologous expression system have identified two maize aquaporins, ZmPIP1;5 and ZmPIP1;6 as CO_2 permeable (Heinen *et al.*, 2014). Additionally, a transcriptomic study comparing aquaporin expression in two C_4 species, maize and sorghum under drought stress suggested that PIP1;6 may play a putative role in CO_2 transport (Hasan *et al.*, 2017). The number of aquaporins in the genome of C_4 species is also comparable to their C_3 counterparts: there are 41 aquaporins identified in sorghum (Reddy *et al.*, 2015), 33 in sugarcane (de Andrade *et al.*, 2016) and 33 in maize (Heinen *et al.*, 2014).

Another argument for the importance of CO_2 permeable aquaporins in C_4 plants comes from an anatomical perspective. The specialised Kranz anatomy of C_4 species means there is limited surface area for CO_2 diffusion from the intercellular air space into the mesophyll cell due to contact with the bundle sheath. The surface area is less than that in C_3 plants (Dengler *et al.*, 1994) and consequently the surface area available for CO_2 diffusion to enter the photosynthetic cells in C_4 plants is reduced. In C_4 photosynthesis, CO_2 permeable aquaporins are predicted to be localised to the mesophyll plasma membrane. This is firstly due to the high photosynthetic rates typical of C_4 plants which require high g_m and secondly if they were located on the bundle sheath plasma membrane this would reduce the efficiency of the CO_2 concentrating mechanism, which provides the unique advantage to C_4 photosynthesis. In C_3 plants, CO_2 permeable aquaporins also localise on the chloroplast envelope membranes

(Uehlein *et al.*, 2008), in a C_4 species the absence of Rubisco from the mesophyll chloroplast may mean that CO_2 permeable aquaporins are not needed in the chloroplast envelope membranes.

1.5 Carbonic anhydrase

Another key component influencing CO_2 diffusion into a C_4 leaf is carbonic anhydrase. CA is a zinc metalloenzyme that catalyses the reversible conversion of CO_2 and HCO_3^-. CA is important in many physiological functions that involve carboxylation or decarboxylation reactions, including photosynthesis and respiration. There are multiple forms of CA which have evolved independently across all kingdoms of life. These include five distinct families of CA (α, β, γ, δ, ζ) which have little sequence similarity, though all catalyse the hydration of CO_2 (Moroney *et al.*, 2001). The α-CAs are widely distributed and have been found in animals, plants, eubacteria and viruses. The β-CAs have been found in plants, algae, eubacteria and yeast. β-CAs are most abundant in land plants, though they have differing significance in C_3 compared to C_4 photosynthetic plants (Ludwig, 2012). The γ-CAs have been found in eubacteria and plants. There are many CA genes present in plants, for instance, rice has 16 CA genes and sorghum has 17 (DiMario *et al.*, 2017). In plants, CAs have been localised to different subcellular compartments, including the chloroplast, cytosol and mitochondria. The activity of these CA enzymes varies significantly across evolutionary lineages (Gillon and Yakir, 2000).

CA is an abundant enzyme in C_3 plants, representing up to 2% of the soluble leaf protein (Okabe *et al.*, 1984). In C_3 plants, CA activity is involved in a number of roles (Figure 1.6; DiMario *et al.*, 2017). It is localised to the stroma of the chloroplasts where it facilitates the diffusion of CO_2 across the chloroplast stroma. It also influences guard cell movement and amino acid biosynthesis (DiMario *et al.*, 2016; Engineer *et al.*, 2016; Hu *et al.*, 2010). Conversely, in C_4 plants CA is localised primarily to the cytosol of mesophyll cells and is crucial in C_4 photosynthesis (Hatch and Burnell, 1990). CA is the first enzyme in a pathway catalysing the fixation of CO_2 in the mesophyll cells, providing HCO_3^- as a substrate for PEPC to produce the C_4 acid, OAA.

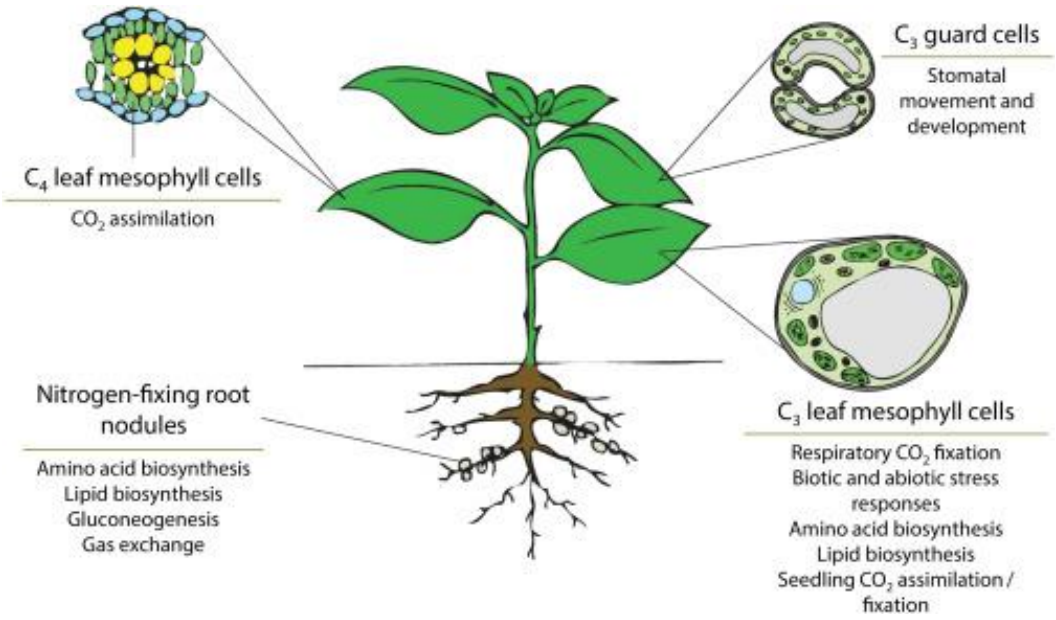

Figure 1.6: Diagram of the physiological functions of CA in plant cells and organs. CA is involved in a number of roles including stomatal movement and development, amino acid biosynthesis and, in C_4 plants, CO_2 assimilation (Image from DiMario *et al.*, 2017).

The level of *in vivo* CA activity within C_4 leaves is reportedly only just sufficient to ensure the conversion of CO_2 to HCO_3^- to support measured rates of photosynthesis. Without CA activity, uncatalysed CO_2 hydration would be approximately 10^4 fold lower and would not sustain C_4 photosynthesis (Hatch and Burnell, 1990). C_4 photosynthetic species have high CA activity, although this activity varies widely between species. For example, the leaves of C_4 dicot *Flaveria bidentis* have CA activity 10-fold higher than maize leaves, a C_4 monocot (Cousins *et al.*, 2008; Hatch and Burnell, 1990). This range of activities suggests that the importance of CA may also vary across C_4 species (Studer *et al.*, 2014).

Manipulating the expression of CA has been attempted in C_4 species by overexpressing a tobacco *CA* in *F. bidentis* under a constitutive 35S promoter (Ludwig *et al.*, 1998; von Caemmerer *et al.*, 1997). Expression of *CA* increased in the cytosol of both the mesophyll and bundle sheath cells and resulted in increased leakiness to the bundle sheath and disruption of the CO_2 concentrating mechanism. There was less CO_2 available for Rubisco and consequently a decrease in photosynthesis. This study confirms earlier work suggesting that the absence of CA in bundle sheath cells is a requirement for C_4 photosynthesis (Burnell and Hatch, 1988; Furbank and Hatch, 1987).

Antisense studies in *F. bidentis* have shown that CA is essential for C_4 photosynthesis (von Caemmerer *et al.*, 2004). Transgenic plants with less than 20% of wild type CA activity in leaves showed reduced CO_2 assimilation and plants with less than 10% of wild type CA activity required high CO_2 for growth. Conversely, using a knockout approach in maize, it was shown that CA is not rate limiting, even in mutants with only 3% of wild type CA activity (Studer *et al.*, 2014).

1.6 Project overview

It is evident that the productive yield of key C_4 crops must increase in the future to meet the demands of an increasing global population. A fundamental limitation to photosynthetic carbon fixation is the availability of CO_2. To further understand and potentially improve the initial steps of CO_2 assimilation within the leaf, I have examined aquaporins and carbonic anhydrase in the model C_4 monocot species *Setaria viridis* (green foxtail).

The overall objectives of this thesis were to firstly identify aquaporins in Setaria based on publicly available transcriptomic data (Chapter 2) and to characterise their CO_2 permeability and membrane localisation using yeast as a heterologous expression system (Chapter 3). The *in planta* effects of factors affecting CO_2 diffusion, namely CO_2 permeable aquaporins (Chapter 4) and CA (Chapter 5) were then investigated in *S. viridis*. Finally, I have modelled the importance of improving CO_2 diffusion in C_4 photosynthesis by increasing mesophyll conductance on both a leaf level and a canopy level (Chapter 6).

CHAPTER 2: PHYLOGENY AND COMPARATIVE TRANSCRIPTOMICS OF SETARIA AQUAPORINS

Publications arising from this chapter:

McGaughey S.A., Osborn H.L., Chen L., Pegler J.L., Tyerman S.D., Furbank R.T., Byrt C.S., Grof C.P.L. 2016. Roles of Aquaporins in *Setaria viridis* Stem Development and Sugar Storage. *Frontiers in Plant Science* 7, 1-13.

2.1 Introduction

Setaria is a C_4 grass of the Paniceae tribe and Poaceae family. Both *Setaria italica* (foxtail millet) and *Setaria viridis* (green foxtail) are closely related to important agronomical crops such as *Zea mays* (maize), *Sorghum bicolor* (sorghum) and *Saccharum officinarum* (sugarcane). *S. viridis* is an important model species for photosynthesis research as it has many desirable features including a small sequenced genome (~515 MB) and the ability to be transformed (Brutnell *et al.*, 2010; Doust *et al.*, 2009; Li and Brutnell, 2011).

There are multiple aquaporins present in all species; within C_4 plants, for instance, there are 33 aquaporins predicted in maize (Chaumont *et al.*, 2001), 33 aquaporins in sugarcane (de Andrade *et al.*, 2016) and 41 aquaporins in sorghum (Reddy *et al.*, 2015). The total number of aquaporins found in plants is considerably higher than that found in other kingdoms as compared to two aquaporins in yeast (Carbrey *et al.*, 2001) and 13 aquaporins in humans (Moshelion *et al.*, 2015). The large number of plant aquaporins is suggested to be due to their importance in water regulation and maintaining cellular water homeostasis at different developmental stages and environmental conditions, but also indicative of the many roles aquaporins may play in plant metabolism, nutrition, signalling processes and photosynthesis (Chaumont and Tyerman, 2014; Hachez *et al.*, 2006; Tyerman *et al.*, 2002).

Aquaporins are permeable to a wide range of small uncharged molecules (Biela *et al.*, 1999; Meinild *et al.*, 1998; Terashima and Ono, 2002; Tyerman *et al.*, 2002). Plant aquaporins have been classified into five main subfamilies, based on sequence homology and cellular location: plasma membrane intrinsic proteins (PIPs), tonoplast intrinsic proteins (TIPs), nodulin 26-like intrinsic proteins (NIPs), small basic intrinsic proteins (SIPs) and X intrinsic proteins (XIPs) (Johanson *et al.*, 2001; Maurel *et al.*, 2008). Each subfamily of aquaporins characterised have different substrate permeability's identified to date: PIPs are permeable to water, carbon dioxide, hydrogen peroxide, glycerol, boron and urea; TIPs are permeable to water, glycerol, urea and ammonia; NIPs usually have low permeability to water but are permeable to a number of metalloids such as silicon, boron, antimony and arsenite as well as glycerol, urea and lactic acid; to date SIPs have only been identified as water permeable and XIPs are permeable to water, glycerol, urea and boron (see reviews: Gomes *et al.*, 2009; Maurel *et al.*, 2015). Though, the XIP subfamily has since been lost in monocots (Maurel *et al.*, 2015).

The specificity of aquaporins to different substrates is not well understood. There are highly conserved regions such as the NPA motif (asparagine-proline-alanine), which is thought to constitute a first size exclusion zone in the centre of the channel (Guan *et al.*, 2010). The Ar/R

(aromatic/arginine) selectivity filter is the mechanism predicted to allow an aquaporin to selectively bind water molecules (hence allowing them through) and prevent other molecules from entering. This constriction site varies in size depending on the permeability of the aquaporin, in water specific aquaporins it is 2.8 Å in diameter, identical to that of a water molecule, and about 3.4 Å in aquaglyceroporins, matching the diameter of glycerol (Wu and Beitz, 2007). CO_2 is a neutral, linear molecular with a similar diameter to water; however, not all water permeable aquaporins are also permeable to CO_2. For example AtPIP2;3 (Heckwolf *et al.*, 2011) and NtPIP2;1 (Otto *et al.*, 2010) both have high water permeability but low CO_2 permeability.

S. viridis aquaporin genes were identified in this chapter from transcriptomic data, and their expression profile investigated based on homology to *S. italica* published transcriptomic data (John *et al.*, 2014). Specific motifs for substrate specificity were then identified and compared to those of known CO_2 permeable aquaporins in other plants.

2.2 Methods

2.2.1 Phylogenetic tree

S. viridis aquaporins were identified as described in McGaughey *et al.* (2016), which included using *S. italica* (Azad *et al.*, 2016), *Arabidopsis thaliana* (Johanson *et al.*, 2001), *Oryza sativa* (Sakurai *et al.*, 2005), *Hordeum vulgare* (Hove *et al.*, 2015) and maize (Chaumont *et al.*, 2001) aquaporins, and predicted *S. viridis* aquaporins from transcriptomic data (Martin *et al.*, 2016) as search items using the sequence analysis online HMMER tool (Finn *et al.*, 2015).

Protein sequences used to generate the phylogenetic tree were obtained for *S. italica, S. viridis* and maize from Phytozome 11.0.5 (*S. italica* v2.2, *S. viridis* v1.1, last accessed July 19, 2016) (See Supplementary Table S2 in McGaughey *et al*., 2016). The phylogenetic tree was generated using the neighbor-joining method in the Geneious Tree Builder program (Geneious 9.0.2).

2.2.2 Sequence analysis

Prediction of transmembrane helices in Setaria PIPs were made using TMpred (Hofmann and Stoffel, 1993). The *S. italica* and *S. viridis* PIP amino acid sequences obtained above were aligned using ClustalW in Geneious 9.0.2. Residues occurring at the 'NPA', Ar/R selectivity filter and "Froger's position" were determined from published literature (Froger *et al.*, 1998; Hove and Bhave, 2011). Known CO_2 permeable aquaporins (Groszmann *et al.*, 2016) were aligned and predicted CO_2 selectivity motifs searched in the Setaria PIPs (Mori *et al.*, 2014).

2.2.3 In situ transcriptomic analysis

Using available datasets present in the literature, Setaria PIPs were identified and transcriptomic data used to investigate their expression profiles. This included analysis of Setaria PIP expression profiles available in Phytozome (Phytomine; data supplied by Thomas Brutnell, Danforth Centre) and analysis of mesophyll and bundle sheath cell specific *S. italica* PIP expression (John *et al.*, 2014). This data was analysed using ClustVis: a web tool for visualizing clustering of multivariate data (BETA) to create a heat map (Metsalu and Vilo, 2015).

2.2.4 Gene co-expression network analysis

Raw FPKM values (Fragments Per Kilobase of transcript per Million mapped reads) of *S. viridis* PIPs were extracted from the expression data available in Phytomine. This included transcriptome data for different experimental conditions and leaf and root tissues for *S. viridis*. These values were normalized by Log2 transformation and Pearson's correlation coefficients calculated by Metscape (Karnovsky *et al.*, 2012). A gene network was then generated for Pearson's correlation coefficients between 0.7 and 1.0 and visualized with the Metscape app in Cytoscape v3.1.1.

2.3 Results

2.3.1 Identification of Setaria aquaporins

As described in McGaughey *et al.* (2016), we identified *S. viridis* aquaporin genes using previously published *S. viridis* elongating internode transcriptome data (Martin *et al.*, 2016), and protein sequences of aquaporins identified in Arabidopsis, *S. italica*, barley, maize and rice.

We assigned the nomenclature to the putative *S. viridis* aquaporins following their relative homology to previously named maize aquaporins (Chaumont *et al.*, 2001) as determined by phylogenetic analysis of protein sequences (Figure 2.1). *S. viridis* proteins separated as expected into the major aquaporin subfamilies referred to as PIPs, TIPs, NIPs and SIPs. Within *S. viridis,* 41 full length aquaporins were identified: 12 PIPs, 14 TIPs, 12 NIPs and three SIPs.

Within *S. italica* there are 42 aquaporins (Azad *et al.*, 2016), which can be divided into 12 PIPs, 15 TIPs, 12 NIPs and three SIPs. The additional aquaporin in *S. italica* is a TIP, *Seita.7G175600*, which has no identifiable homolog in *S. viridis.*

The overall focus of my study is on CO_2 diffusion so I will concentrate on the expression and function of PIPs which, to date, are the only aquaporin subfamily which have been identified containing aquaporins permeable to CO_2. There is very high similarity between *S. italica* and *S. viridis* PIPs (Figure 2.2). 10 out of the 12 PIPs share 100% amino acid sequence identity, PIP1;2 has 90% and PIP2;4 has 99% identity between *S. italica* and *S. viridis*.

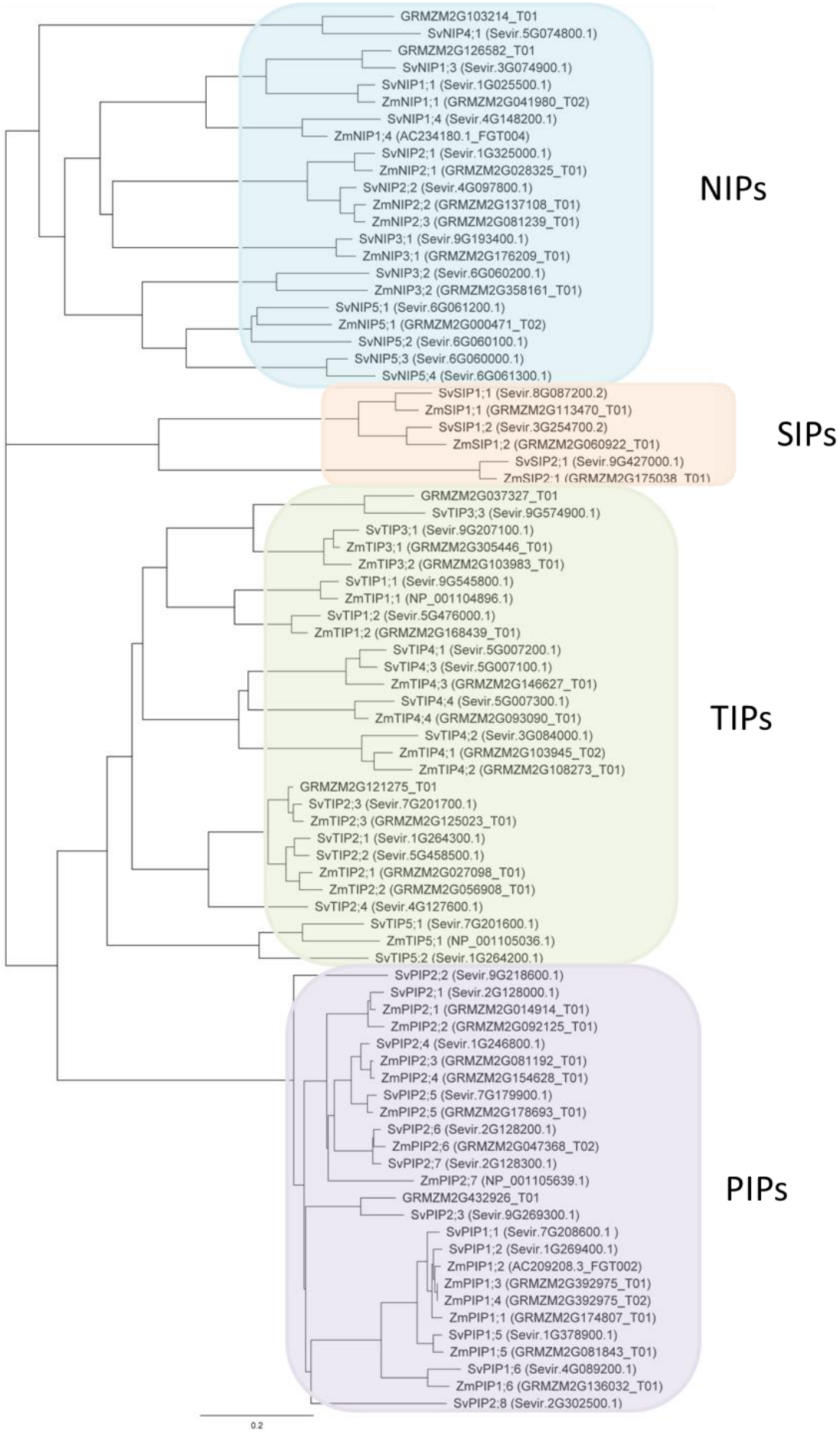
GRMZM2G103214_T01
SvNIP4;1 (Sevir.5G074800.1)
GRMZM2G126582_T01
SvNIP1;3 (Sevir.3G074900.1)
SvNIP1;1 (Sevir.1G025500.1)
ZmNIP1;1 (GRMZM2G041980_T02)
SvNIP1;4 (Sevir.4G148200.1)
ZmNIP1;4 (AC234180.1_FGT004)
SvNIP2;1 (Sevir.1G325000.1)
ZmNIP2;1 (GRMZM2G028325_T01)
SvNIP2;2 (Sevir.4G097800.1)
ZmNIP2;2 (GRMZM2G137108_T01)
ZmNIP2;3 (GRMZM2G081239_T01)
SvNIP3;1 (Sevir.9G193400.1)
ZmNIP3;1 (GRMZM2G176209_T01)
SvNIP3;2 (Sevir.6G060200.1)
ZmNIP3;2 (GRMZM2G358161_T01)
SvNIP5;1 (Sevir.6G061200.1)
ZmNIP5;1 (GRMZM2G000471_T02)
SvNIP5;2 (Sevir.6G060100.1)
SvNIP5;3 (Sevir.6G060000.1)
SvNIP5;4 (Sevir.6G061300.1)
NIPs
SvSIP1;1 (Sevir.8G087200.2)
ZmSIP1;1 (GRMZM2G113470_T01)
SvSIP1;2 (Sevir.3G254700.2)
ZmSIP1;2 (GRMZM2G060922_T01)
SvSIP2;1 (Sevir.9G427000.1)
SIPs
GRMZM2G037327_T01
SvTIP3;3 (Sevir.9G574900.1)
SvTIP3;1 (Sevir.9G207100.1)
ZmTIP3;1 (GRMZM2G305446_T01)
ZmTIP3;2 (GRMZM2G103983_T01)
SvTIP1;1 (Sevir.9G545800.1)
ZmTIP1;1 (NP_001104896.1)
SvTIP1;2 (Sevir.5G476000.1)
ZmTIP1;2 (GRMZM2G168439_T01)
SvTIP4;1 (Sevir.5G007200.1)
SvTIP4;3 (Sevir.5G007100.1)
ZmTIP4;3 (GRMZM2G146627_T01)
SvTIP4;4 (Sevir.5G007300.1)
ZmTIP4;4 (GRMZM2G093090_T01)
SvTIP4;2 (Sevir.3G084000.1)
ZmTIP4;1 (GRMZM2G103945_T02)
ZmTIP4;2 (GRMZM2G108273_T01)
GRMZM2G121275_T01
SvTIP2;3 (Sevir.7G201700.1)
ZmTIP2;3 (GRMZM2G125023_T01)
SvTIP2;1 (Sevir.1G264300.1)
SvTIP2;2 (Sevir.5G458500.1)
ZmTIP2;1 (GRMZM2G027098_T01)
ZmTIP2;2 (GRMZM2G056908_T01)
SvTIP2;4 (Sevir.4G127600.1)
SvTIP5;1 (Sevir.7G201600.1)
ZmTIP5;1 (NP_001105036.1)
SvTIP5;2 (Sevir.1G264200.1)
TIPs
SvPIP2;2 (Sevir.9G218600.1)
SvPIP2;1 (Sevir.2G128000.1)
ZmPIP2;1 (GRMZM2G014914_T01)
ZmPIP2;2 (GRMZM2G092125_T01)
SvPIP2;4 (Sevir.1G246800.1)
ZmPIP2;3 (GRMZM2G081192_T01)
ZmPIP2;4 (GRMZM2G154628_T01)
SvPIP2;5 (Sevir.7G179900.1)
ZmPIP2;5 (GRMZM2G178693_T01)
SvPIP2;6 (Sevir.2G128200.1)
ZmPIP2;6 (GRMZM2G047368_T02)
SvPIP2;7 (Sevir.2G128300.1)
ZmPIP2;7 (NP_001105639.1)
GRMZM2G432926_T01
SvPIP2;3 (Sevir.9G269300.1)
SvPIP1;1 (Sevir.7G208600.1)
SvPIP1;2 (Sevir.1G269400.1)
ZmPIP1;2 (AC209208.3_FGT002)
ZmPIP1;3 (GRMZM2G392975_T01)
ZmPIP1;4 (GRMZM2G392975_T02)
ZmPIP1;1 (GRMZM2G174807_T01)
SvPIP1;5 (Sevir.1G378900.1)
ZmPIP1;5 (GRMZM2G081843_T01)
SvPIP1;6 (Sevir.4G089200.1)
ZmPIP1;6 (GRMZM2G136032_T01)
SvPIP2;8 (Sevir.2G302500.1)
PIPs
0.2

Figure 2.1: Phylogenetic comparison of aquaporins. Through the alignment of aquaporin protein sequences from *S. viridis* (Sv) and *Zea mays* (Zm) the phylogenetic tree was generated by the neighbor-joining method using the Geneious Tree Builder program, Geneious 9.0.2. The scale bar indicates the evolutionary distance, expressed as changes per amino acid residue. These aquaporins can be grouped into four subfamilies: PIPs (plasma membrane intrinsic proteins), TIPs (tonoplast intrinsic proteins), NIPs (nodulin-like intrinsic proteins) and SIPs (small basic intrinsic proteins).

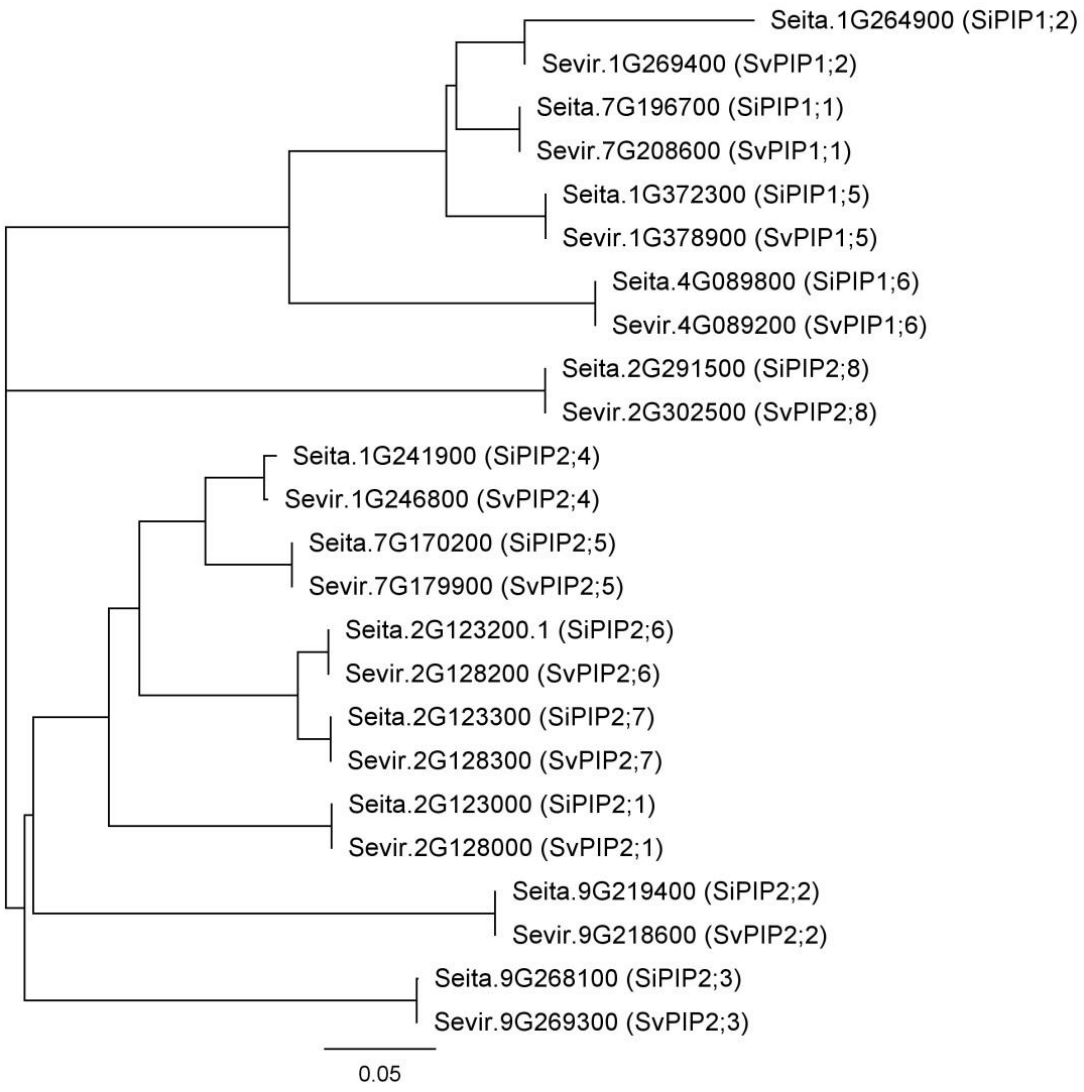

Figure 2.2: Phylogenetic tree of *S. italica* and *S. viridis* PIPs. Aquaporins are labelled with accession number (Seita or Sevir) and common name (Si or Sv) based on McGaughey *et al.* (2016) for *S. italica* and *S. viridis*. The tree was generated by neighbor-joining method using the Geneious Tree Builder program, Geneious 9.0.2. The scale bar indicates the evolutionary distance, expressed as changes per amino acid residue.

2.3.2 Identification of selectivity-related motifs

Using transmembrane prediction software, six transmembrane domains were identified in all 12 of the Setaria PIPs. Key conserved residues for substrate selectivity were identified in Setaria and are numbered according to alignment with hAQP1 (Figure 2.3). These are also summarised for both *S. viridis* and *S. italica* in Table 2.1. The Ar/R selectivity filter includes positions labelled as H2 which is located in transmembrane helix 2 (TM2), H5 which is in TM5, and LE1 and LE2 which are located in the inter-helical loop E. Froger *et al.* (1998) identified a

number of key residues which are predicted to determine substrate specificity, these are labelled as “Froger’s position” and are designated P1 – P5 numbered from N to C terminus. The Ar/R selectivity motifs are the same for all PIPs in both *S. italica* and *S. viridis* apart from at H5 (position 163) which is a histidine (H) for all PIPs expect for PIP2;8 which has a phenylalanine (F). This changes the hydrophobicity of this amino acid from non-polar to basic polar. The residues at the Froger’s positions P1- P5 are the same for PIPs in both *S. italica* and *S. viridis* with the exception of SiPIP1;2 which has aspartic acid (D) at P4 (position 212) not a phenylalanine (F), and a leucine (L) at P5 (position 213) rather than a tryptophan (W) residue. The residues in P1 (position 116) are variable for both *S. italica* and *S. viridis* PIPs with the majority a glutamine (Q). PIP1;6 has a valine (V), PIP2;2 and PIP2;3 have a histidine (H) whilst PIP2;8 has a threonine (T) in positon P1. All Setaria PIPs have two conserved NPA motifs: the first in loop B and the second in loop E.

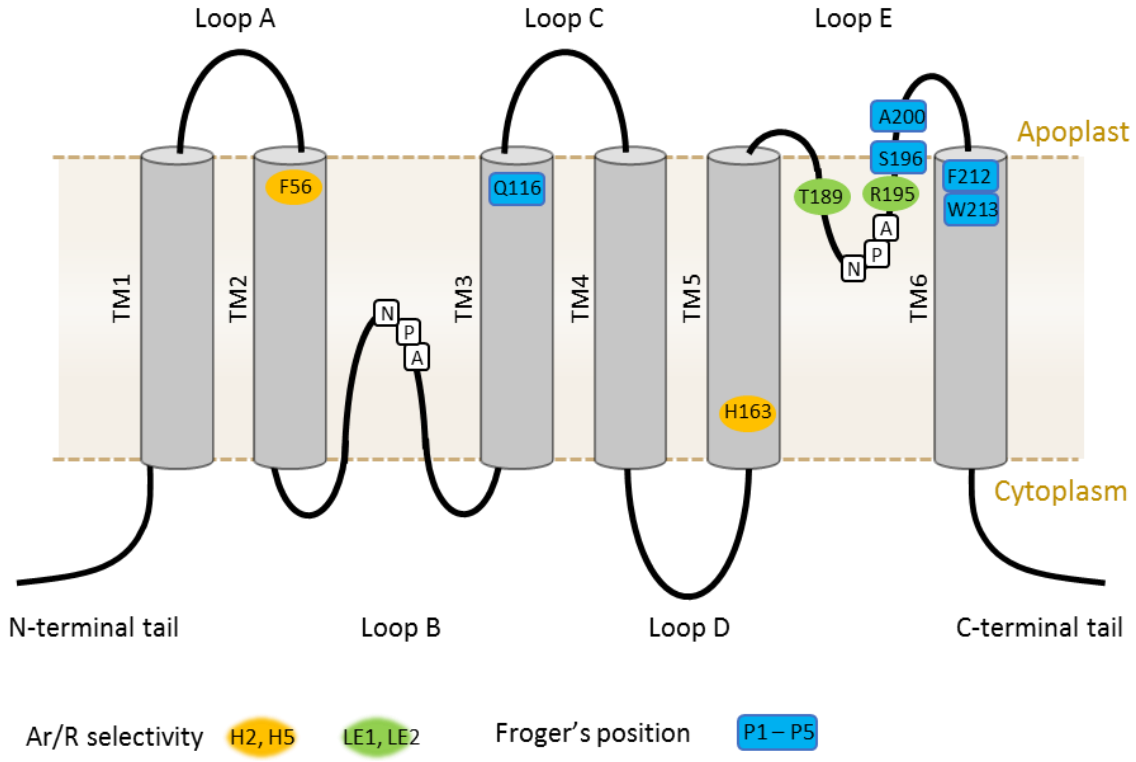

Figure 2.3: Diagram of a PIP aquaporin showing key conserved amino acid residues common to Setaria PIPs. Amino acids are numbered based on alignment to hAQP1. The transmembrane helices (TM) are numbered 1 to 6. The Ar/R selectivity filter includes H2 (phenylalanine, F, at position 56), H5 (histidine, H, at position 163), LE1 (threonine, T, at position 189) and LE2 (arginine, R, at position 195). “Froger’s position” P1- P5 are P1 (glutamine, Q, 116), P2 (serine, S, 196), P3 (alanine, A, 200), P4 (phenylalanine, F, 212) and P5 (tryptophan, W, 213). This figure is modified from Groszmann *et al.* (2016).

Table 2.1: Summary of conserved amino acid residues and prediction of transmembrane domains of Setaria PIPs.

Name	Ar/R selectivity filter				Froger's Position					TMH
	H2	H5	LE1	LE2	P1	P2	P3	P4*	P5*	
PIP1;1	F	H	T	R	Q	S	A	F	W	6
PIP1;2	F	H	T	R	Q	S	A	D/F	L/W	5/6
PIP1;5	F	H	T	R	Q	S	A	F	W	6
PIP1;6	F	H	T	R	V	S	A	F	W	6
PIP2;1	F	H	T	R	Q	S	A	F	W	6
PIP2;2	F	H	T	R	H	S	A	F	W	6
PIP2;3	F	H	T	R	H	S	A	F	W	6
PIP2;4	F	H	T	R	Q	S	A	F	W	6
PIP2;5	F	H	T	R	Q	S	A	F	W	6
PIP2;6	F	H	T	R	Q	S	A	F	W	6
PIP2;7	F	H	T	R	Q	S	A	F	W	6
PIP2;8	F	F	T	R	T	S	A	F	W	6

*Difference between *S. italica*/ *S. viridis* PIP1;2 at P4 and P5 residues. Note TMH (transmembrane helices) and amino acids: F (phenylalanine), H (histidine), T (threonine), R (arginine), Q (glutamine), S (serine), A (alanine), W (tryptophan), L (leucine) and D (aspartic acid).

2.3.3 Setaria PIP expression analysis

Transcriptomic data publically available on Phytomine was mined to investigate the expression profiles of Setaria PIPs. Transcriptomic data for *S. italica* and *S. viridis* leaves and roots in different experimental treatments were analysed. Figure 2.4 shows the Phytomine expression data for *S. viridis* PIPs under different treatments including leaves 2 – 6 from two week old Setaria plants under high light conditions and Setaria roots exposed to ammonia, drought, nitrate or urea conditions. Whole leaves were examined with leaf 2 the oldest leaf at the base of the plant and leaf 6 the youngest leaf at the top of the plant. The transcript abundance is colour coded in the heat map with higher transcript expression in red and low expression in blue. Overall, there is higher transcript abundance of PIPs in the roots compared to the leaf samples for the majority of the PIPs. Under drought conditions there is a strong increase in transcript abundance for all the PIPs, except for *PIP2;8*. In the leaf material, *PIP1;1, PIP2;1* and *PIP2;8* show an increase in transcript abundance from leaves 2 – 6 indicating expression is higher in the younger leaves (leaf 5 and 6) compared to the older leaf 2.

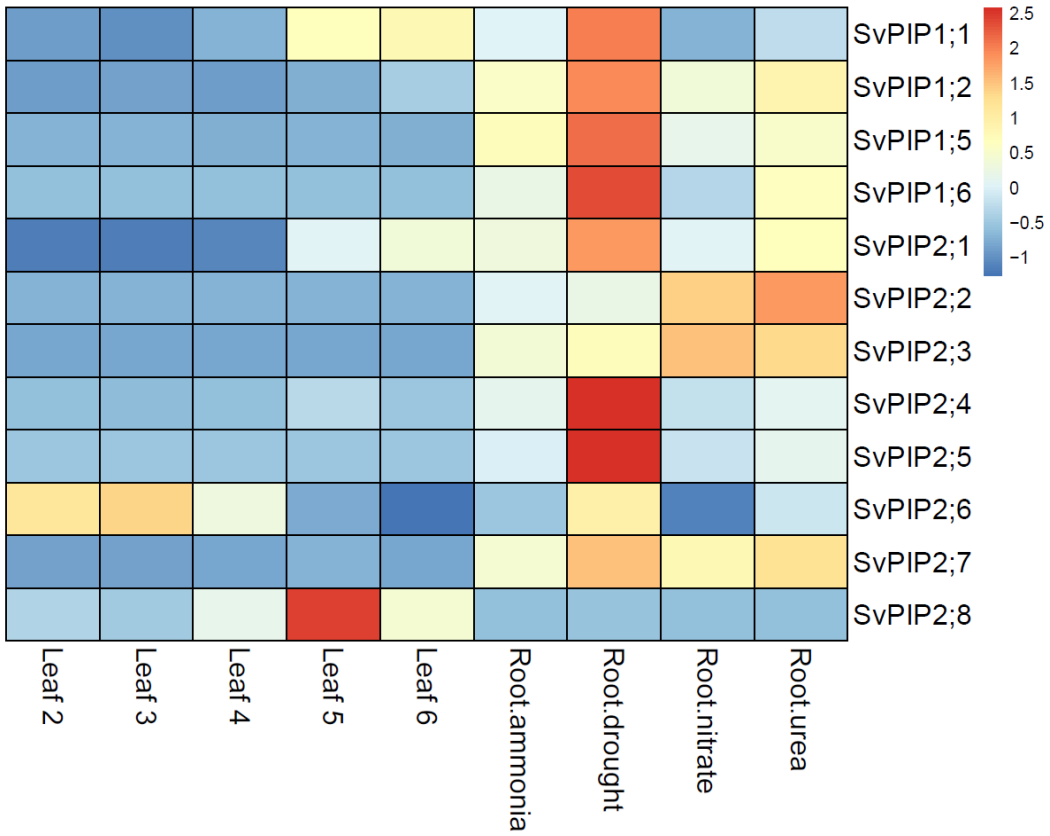

Figure 2.4: Expression data of *S. viridis* PIPs analysed using ClustVis to create a heat map. Colours indicate transcript abundance, red is high, blue is low. Expression data is reported for different treatments: leaves 2 – 6 from two week old Setaria plants under highlight and roots exposed to ammonia, drought, nitrate and urea conditions (Phytomine, Thomas Brutnell).

S. italica and *S. viridis* share very high sequence similarity (Figure 2.2) and so very similar expression patterns for each individual PIP from both species were found (Figure 2.5). Interestingly, despite the high similarity between the aquaporins PIP2;6 and PIP2;7 (97% amino acid sequence identity) they exhibit different expression profiles in the leaf and root tissues (Figure 2.4, Figure 2.5). *PIP2;6* has higher expression in leaves 2 – 4 whereas *PIP2;7* has low expression in the leaves and high expression in the roots under different conditions (Figure 2.5).

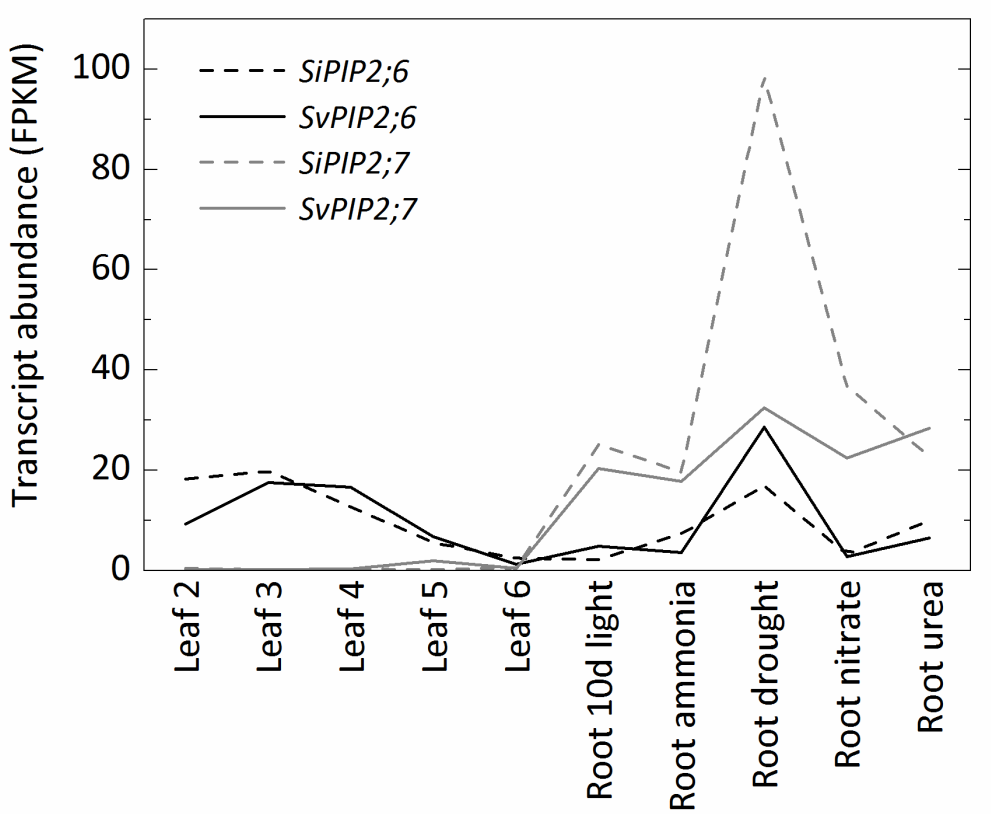

Figure 2.5: Comparison of expression data of *S. italica* and *S. viridis PIP2;6* and *PIP2;7* in leaves and roots under different conditions. Conditions include: leaves 2 – 6 from two week old Setaria plants under highlight and roots exposed to high light, ammonia, drought, nitrate and urea conditions (Phytomine, Thomas Brutnell).

Transcriptomic data was also mined from John *et al.* (2014) to examine PIP expression in the leaf which was specific to either the mesophyll or bundle sheath cells. John *et al.* (2014) separated the different cell types from 17 day old *S. viridis* plants and using *S. italica* homologs identified RNA transcript expression specific to the mesophyll or bundle sheath cell. Setaria PIPs were identified (Supplementary file 2 within John *et al.*, 2014), however *PIP1;6, PIP2;2, PIP2;3* and *PIP2;7* were not present. Figure 2.6 presents the transcript abundance of Setaria PIPs in the mesophyll and bundle sheath cells. Only two PIPs, *PIP2;4* and *PIP2;8* have higher transcript abundance in the mesophyll cell relative to the bundle sheath. *PIP2;8* is substantially more abundant in the leaf compared to the remaining PIPs.

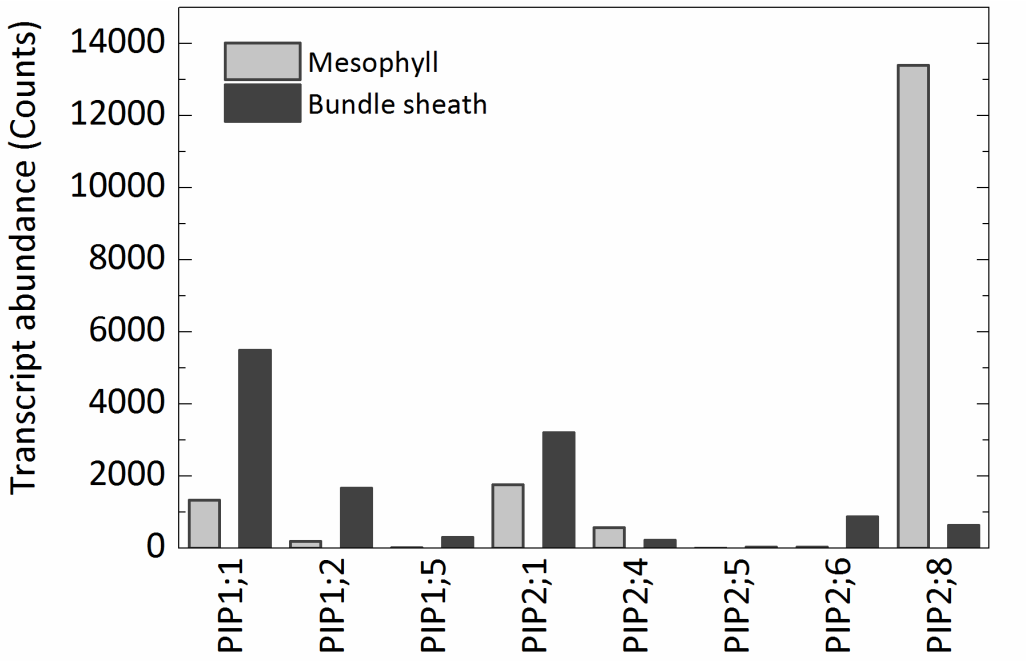

Figure 2.6: Cell specific transcript abundance for Setaria PIPs in either the mesophyll or bundle sheath cells. Data mined from Supplementary file 2 in John *et al.* (2014).

2.3.4 Prediction of CO_2 permeability

CO_2 permeable aquaporins are thought to be important for CO_2 diffusion across plasma membranes in C_4 photosynthesis as discussed in Section 1.4.4 so to help predict which Setaria PIPs may be permeable to CO_2 I compared amino acid sequences to known CO_2 permeable aquaporins and presented the data as a heat map (Figure 2.7). The exact sequence identity percentages are overlaid. There was no clear, stand out Setaria aquaporin candidate which aligned best to the published CO_2 permeable aquaporins. Rather, the *S. viridis* PIPs cluster based on their subgroup, PIP1s or PIP2s. Also, the plant aquaporins showed higher similarity to each other compared to the evolutionary distant CO_2 permeable aquaporins human (hAQP1) and desert truffle *Terfezia claveryi* (TcAQP1). Alignment of the whole amino acid sequence may, however, hide any small correlations specific to CO_2 permeability.

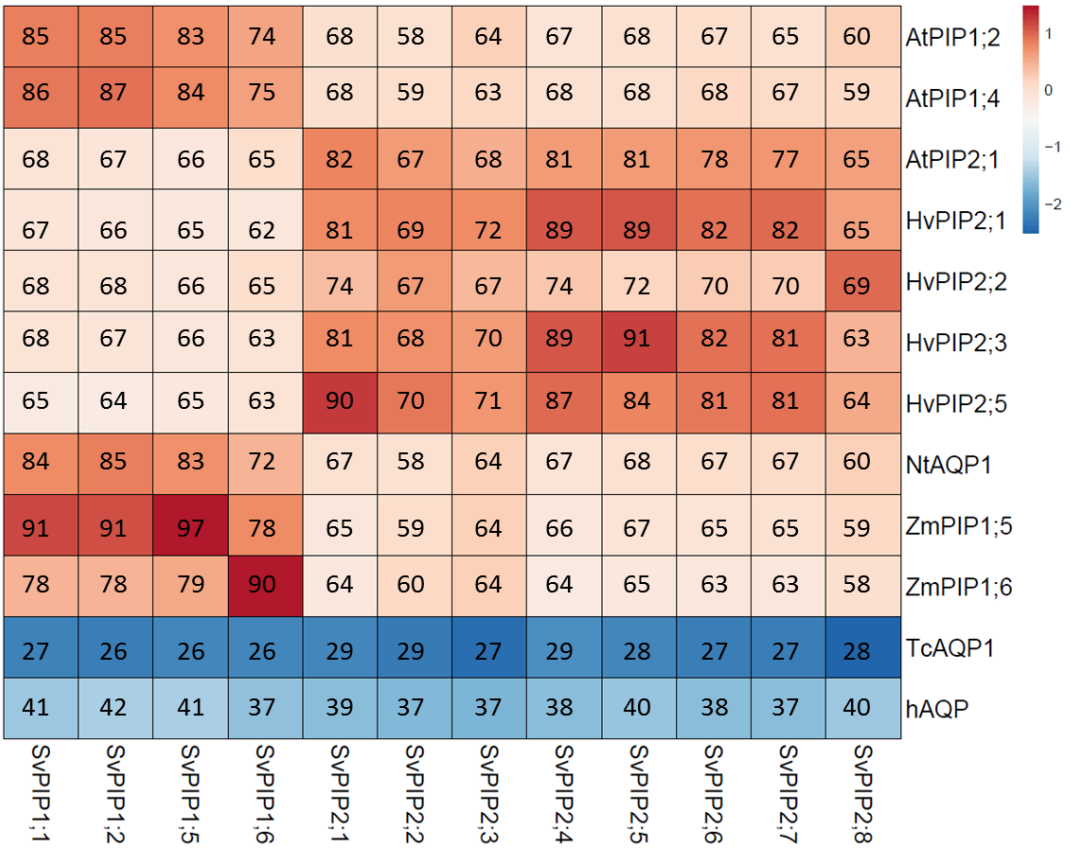

Figure 2.7: Alignment of known CO_2 permeable aquaporins analysed using ClustVis to create a heat map. Colours indicate amino acid sequence identity, red is high, blue is low. References for CO_2 permeable aquaporins include AtPIP1;2 (Heckwolf *et al.*, 2011), AtPIP1;4 (Li *et al.*, 2015), AtPIP2;1 (Wang *et al.*, 2016), HvPIP2;1, HvPIP2;2, HvPIP2;3, HvPIP2;5 (Mori *et al.*, 2014), NtAQP1 (Uehlein *et al.*, 2003), ZmPIP1;5, ZmPIP1;6 (Heinen *et al.*, 2014), TcAQP1 (Navarro-Rodenas *et al.*, 2012) and hAQP1 (Itel *et al.*, 2012).

A specific, semi conserved region of amino acids common to all CO_2 permeable aquaporins has been identified at the end of the E-loop, WIFWVGP (Mori *et al.*, 2014). It was demonstrated in Mori *et al.* (2014) that changing an amino acid in this sequence (see arrow Figure 2.8) from isoleucine, I, to methionine, M, reduced CO_2 permeability in the barley PIP HvPIP2;3. This region is highlighted in the alignment of 12 Setaria PIPs and HvPIP2;3 (CO_2 permeable) and HvPIP2;4 (not CO_2 permeable and possess a methionine) in Figure 2.8. All of the Setaria PIPs have the same semi conserved sequence except for SvPIP2;3 which has a methionine (M) at position 278. This may suggest that SvPIP2;3 is not CO_2 permeable.

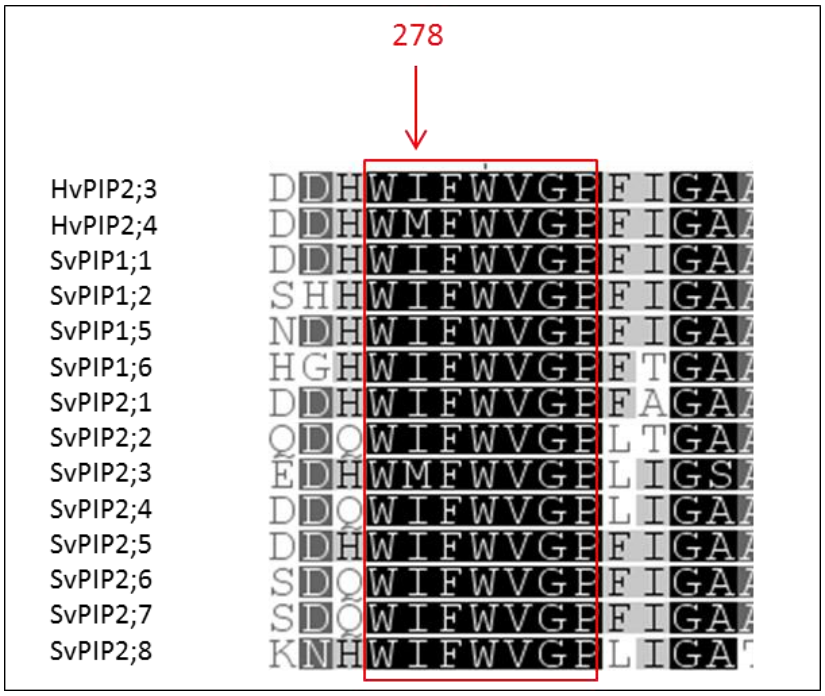

Figure 2.8: Alignment of *S. viridis* SvPIPs with *Hordeum vulgare* HvPIP2;3 (CO_2 permeable) and HvPIP2;4 (not CO_2 permeable) to identify a predicted conserved region (red box).Changing an amino acid residue in this conserved region has experimentally been shown to alter CO_2 permeability in *H. vulgare* (Mori *et al.*, 2014). SvPIP2;3 has a methionine (red arrow) similar to HvPIP2;4 indicating it may not be CO_2 permeable. Alignment performed with ClustalW in Geneious (9.0.2), shading indicates amino acid similarity.

The movement of CO_2 through an aquaporin is suggested to permeate through the central pore. Hub *et al.* (2009) computed possible pathways for CO_2 movement through an aquaporin tetramer and found the potentials of mean force were lowest for the central cavity, indicating it was more likely to contribute to CO_2 flux rather than the four other pores. The key residues lining this pore were identified by Yu *et al.* (2006) in a bovine aquaporin and I then investigated these key residues for the twelve *S. viridis* PIPs in Figure 2.9. The residues were identified in Setaria as V104 and L107 which localise within the TMH (transmembrane helices) 2 and L233 and F237 which localise within TMH 5. Valine (V) at position 104 is present in all PIPs except for SvPIP2;3 which has an alanine (A); leucine (L) is at position 107 in all PIP2s but is a glutamine (Q) in the PIP1s; leucine (L) is present at positon 233 in all PIPs; and phenylalanine (F) is present at position 237 in all PIPs except for SvPIP1;6 which has a leucine (L). The hydrophobic lining of the central pore is hypothesised to prevent water permeating (Yu *et al.*, 2006), all four key residues and changes are hydrophobic, except for the change at

position 107 to glutamine (Q) in the SvPIP1s. This may indicate that in Setaria, these PIP1s may permeate water through the central pore.

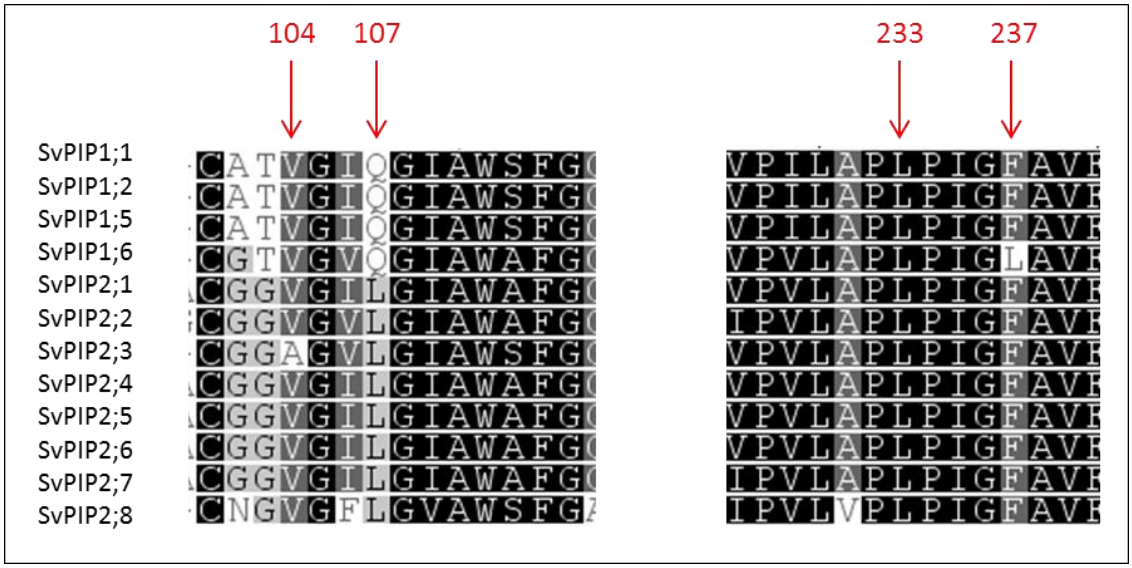

Figure 2.9: Alignment of *S. viridis* SvPIPs to identify key residues predicted to line the central pore of the aquaporin tetramer. Alignment performed with ClustalW in Geneious (9.0.2), shading indicates amino acid similarity.

2.3.5 Co-expression analysis to indicate possible aquaporin interactions

Aquaporin permeability can be affected by its physical interactions (Otto *et al.*, 2010). To examine these possible interactions, specifically between different PIPs, the co-expression of transcriptomic data was investigated. Expression data of *S. viridis* PIPs generated by other groups were collated for different tissues (including whole plant, leaf and roots) and under different experimental conditions. The co-expression analysis indicates which PIPs interact (Figure 2.10), however FRET (Fluorescence Resonance Energy Transfer) analysis or co-precipitation experiments would be required to identify this *in vivo*. This preliminary analysis shows there is strong co-expression of some of the aquaporins within the PIP2 clade (Pearson's correlation coefficient between 0.95 – 1.0). There is also a strong co-expression of *SvPIP1;2* to *SvPIP2;2* and *SvPIP2;3*. *SvPIP2;8* has a strong interaction with *SvPIP2;1* and weaker interactions with *SvPIP1;2*, *SvPIP1;6, SvPIP2;6* and *SvPIP2;2*.

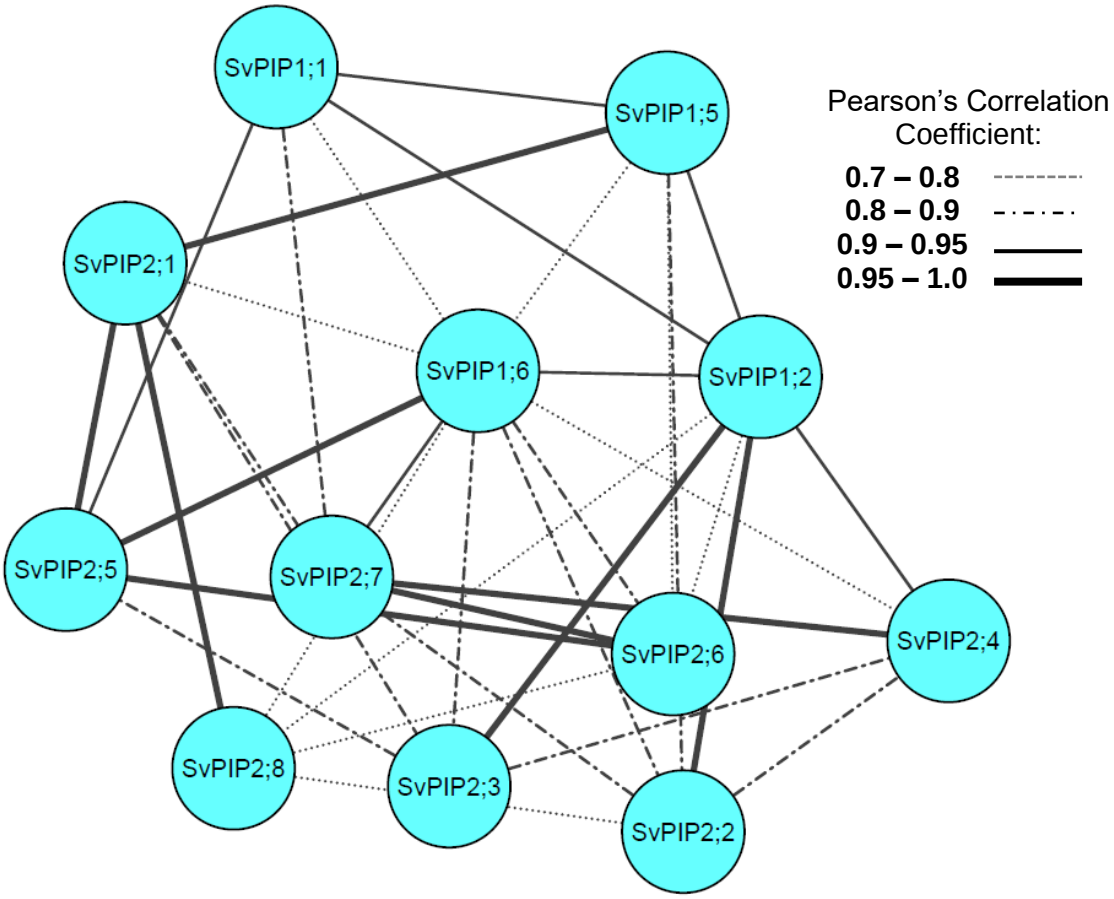

Figure 2.10: Co-expression analysis of *S. viridis* PIPs. Line thickness indicates higher co-expression of PIP transcripts. Raw FPKM values from Phytomine were analysed and Pearson's correlation coefficient calculated. Metscape app in Cytoscape v3.1.1 was used to visualise the gene expression network for those correlations greater than 0.7.

2.4 Discussion

2.4.1 Expression profile of Setaria aquaporins

In *S. viridis*, 41 aquaporin encoding genes were identified that group into four subfamilies including PIPs, TIPs, NIPs and SIPs (Figure 2.1). Azad *et al.* (2016) named the *S. italica* aquaporins in an order consecutive with where they are found in the genome. In our paper, McGaughey *et al.* (2016), we named the *S. viridis* aquaporins based on their homology to previously named maize aquaporins (Chaumont *et al.*, 2001), for ease of comparing related aquaporins in C_4 grasses of interest. Of course, high homology and the same name does not necessarily infer the same function.

The aim of this study was to determine which Setaria aquaporin(s) are likely to be permeable to CO_2. Despite increasing research on CO_2 permeable aquaporins in C_3 photosynthetic plants, their role in CO_2 diffusion in C_4 plants is largely unknown (von Caemmerer and Furbank, 2016). CO_2 permeable aquaporins are expected to be localised to the mesophyll plasma membrane in C_4 leaves. This is due to a number of reasons, firstly the high photosynthetic rates typical of C_4 plants requires high mesophyll conductance to CO_2 (CO_2 diffusion from the intercellular airspace to the mesophyll cytosol), and secondly, high CO_2 permeability of the bundle sheath plasma membrane would be undesirable as it could increase the escape of CO_2 from the bundle sheath and reduce the efficiency of the C_4 pump.

Of the eight Setaria aquaporins identified in John *et al.* (2014), only two PIPs (*PIP2;4* and *PIP2;8*) showed preferential expression in the mesophyll cells compared to the bundle sheath cells (Figure 2.6). In terms of tissue specificity, *PIP2;8* also showed very high expression in the leaf relative to root tissue (Figure 2.4). Each PIP showed a different expression profile under the different treatments, however, most of the aquaporins had the highest transcript expression under drought stress in the roots, consistent with the most common role of aquaporins in water movement (Figure 2.4). Surprisingly, PIP2;6 and PIP2;7, which share 97% amino acid sequence identity, showed very different expression profiles in different tissue types with *PIP2;6* higher in the leaf relative to *PIP2;7*, and *PIP2;7* much higher in Setaria roots under different conditions (Figure 2.5).

Interestingly, along a maize developmental leaf gradient, the function of maize aquaporins, CO_2 or H_2O permeable, loosely correlates with photosynthetic gene expression. In the base region of the maize leaf, genes are largely related to basic cellular functions such as DNA

synthesis (Li *et al.*, 2010). Water permeability of isolated maize protoplasts is also highest at the base of the leaf compared to the leaf tip (Hachez *et al.*, 2008). Additionally, maize aquaporins permeable to water, *ZmPIP2;1*, *ZmPIP2;4* and *ZmPIP2;5* (Fetter *et al.*, 2004), all have high transcript expression at the base of the leaf (Hachez *et al.*, 2008), indicating these aquaporins may be involved in cell growth and regulating turgor. Whereas, in the photosynthetically active region of the leaf, the mature zone, genes encoding the calvin cycle enzymes, photosystems I and II, and carbon shuttle enzymes are highly abundant (Li *et al.*, 2010). Interestingly, the two maize aquaporins identified as CO_2 permeable, *ZmPIP1;5* and *ZmPIP1;6* (Heinen *et al.*, 2014) also increase in transcript expression in this mature zone (Hachez *et al.*, 2008). The expression of photosynthesis related genes along the developmental gradient of *S. viridis* leaf is similar to that of maize (Ding *et al.*, 2015). In addition, SvPIP2;1 has been identified as water permeable in oocytes (McGaughey *et al.*, 2016), similar to ZmPIP2;1. It would be interesting to investigate the transcript profile of PIPs along a Setaria leaf gradient to see if aquaporin expression similarly correlates with leaf function, as have been observed in maize.

2.4.2 Predicting CO_2 permeable aquaporin candidates

Conserved motifs or residues which are predicted to confer specificity to a certain substrate were also investigated in this chapter. The Ar/R selectivity filter did not reveal any interesting candidates as all the predicted regions were identical for all 12 Setaria PIPs (Hove and Bhave, 2011). The motif Mori *et al.* (2014) experimentally demonstrated to confer CO_2 permeability in barley was also present and identical for all PIPs except for SvPIP2;3, possibly indicating this PIP is not CO_2 permeable. However, the presence of this motif in 11 out of 12 Setaria aquaporins indicates that this motif alone is unlikely the only key criteria conferring CO_2 permeability in Setaria.

Ultimately, it is very difficult to predict CO_2 permeability, or indeed any substrate permeability, based on either amino acid sequence similarity or directly from its expression profile. Alignment to the known CO_2 permeable aquaporins only highlights the homologs within other species, with the different clades, PIP1 and PIP2, strongly driving the alignment (Figure 2.7). Large scale statistical coupling analysis have been performed previously to identify possible functional residues which separate aquaporins and aquaglyceroporins as water or glycerol permeable (Lin *et al.*, 2012). However, reversal of substrate specificity by

point mutagenesis has only resulted in partial success from this approach (Savage *et al.*, 2010). It is likely, however, that other factors, such as the interactions of different PIPs (Figure 2.10) when they form a tetramer, are more important in determining substrate permeability. Artificial heterotetramers with defined proportions of PIP1 to PIP2 (NtAQP1 to NtPIP2;1) have been demonstrated to alter water or CO_2 permeability activities (Otto *et al.*, 2010). In addition, the interaction of different PIPs is also important for correct localisation to the membrane for the aquaporin to function, and allow substrates through, as expected (Fetter *et al.*, 2004; Zelazny *et al.*, 2007).

2.4.3 Conclusions

Using published transcriptomic data I have examined the expression profile of *S. viridis* PIPs and used specific motifs for substrate specificity to identify potential aquaporins which are CO_2 permeable. This *in silico* approach was difficult and did not readily predict a CO_2 permeable aquaporin candidate in Setaria. Therefore, in the next chapter I have expressed the *S. italica* aquaporins in yeast and examined their sub-cellular localisation with GFP tags. I have also examined the effect of PIP1 and PIP2 co-expression on localisation and function, and measured CO_2 permeability of the Setaria aquaporins in yeast using CO_2 triggered intracellular acidification detected with a stopped flow spectrophotometer.

CHAPTER 3: CHARACTERISATION OF SETARIA AQUAPORINS

3.1 Introduction

The transport of gaseous substances across biological membranes is essential in all forms of life. Traditionally, it was thought that CO_2 can easily cross a cell membrane since it is lipophilic and any barriers to CO_2 diffusion was likely due to the unstirred layers adjacent to the membrane (Missner *et al.*, 2008; Missner and Pohl, 2009). This view has been challenged however, since in biological systems the rate of CO_2 transport is much lower than predicted; reportedly 10-1000 times lower than expected from a pure lipid bilayer (Endeward *et al.*, 2006; Evans *et al.*, 2009; Otto *et al.*, 2010; Uehlein *et al.*, 2012). In addition, plant plasma membranes have been estimated to contain an equal amount of phospholipids and sterols while proteins account for about 40% of the mass (Yoshida and Uemura, 1986). This high content of proteins within the lipid bilayer blocks the membrane and under these biological conditions it is suggested that plant plasma membranes may not be very permeable to CO_2 and the inclusion of aquaporins permeable to CO_2 could impact on overall membrane permeability (Endeward *et al.*, 2013).

Plant aquaporins were discovered in 1993 (Maurel *et al.*, 1993) and evidence has since been accumulating to challenge the concept that CO_2 diffuses solely through the lipid bilayer. The evidence for CO_2 permeable aquaporins has largely been generated through studies of membrane permeability in two heterologous expression systems; either *Xenopus laevis* oocytes or yeast (Heckwolf *et al.*, 2011; Mori *et al.*, 2014; Nakhoul *et al.*, 1998; Otto *et al.*, 2010). More CO_2 permeable aquaporins are being reported every year. To date, the plant aquaporins identified as CO_2 permeable include *Arabidopsis thaliana AtPIP1;2* (Heckwolf *et al.*, 2011), *AtPIP1;4* (Li *et al.*, 2015) and *AtPIP2;1* (Wang *et al.*, 2016); *Hordeum vulgare HvPIP2;1*, *HvPIP2;2*, *HvPIP2;3* and *HvPIP2;5* (Mori *et al.*, 2014); *Nicotiana tabacum NtAQP1* (Uehlein *et al.*, 2003) and *Zea mays ZmPIP1;5* and *ZmPIP1;6* (Heinen *et al.*, 2014).

There are two main approaches to determining CO_2 permeability of an aquaporin in a heterologous expression system, either detecting a change in pH (e.g. using a pH microelectrode probe or a pH sensitive fluorescent dye detected using a stopped flow spectrophotometer) or by following ^{18}O isotope exchange on a membrane inlet mass spectrometer (MIMS). CO_2 is a difficult substrate to assay and for both approaches there needs to be sufficient carbonic anhydrase (CA) activity to catalyse CO_2 exchange with HCO_3^-. Initially, we tried both the stopped flow spectrophotometer and the MIMS approach, however settled on just the stopped flow spectrophotometer. This technique monitors

changes in fluorescence intensity due to CO_2 triggered intracellular acidification (Ding *et al.*, 2013; Heckwolf *et al.*, 2011; Otto *et al.*, 2010; Uehlein *et al.*, 2008).

The importance of CO_2 permeable aquaporins in C_4 photosynthesis is not well understood. To date only ZmPIP1;5 and ZmPIP1;6 have been shown to be CO_2 permeable in yeast and both have been suggested to play a physiological role in guard cell CO_2 permeability based on their diurnal expression pattern in stomatal complexes (Heinen *et al.*, 2014). In this chapter, the main aim was to characterise the aquaporins in the C_4 grass, Setaria for CO_2 permeability, however, as a part of the translational aim of the ARC Centre of Excellence for Translational Photosynthesis I also looked at a subset of aquaporins from the important agricultural crop *Sorghum bicolor*.

The Setaria PIP subfamily of aquaporins can be divided into two clades: PIP1 and PIP2, based on amino acid sequences. All 12 Setaria PIPs were examined, including 4 PIP1s and 8 PIP2s. The *Setaria italica* PIP sequences were used here, instead of *Setaria viridis*, as *S. italica* was available and fully sequenced and annotated (Bennetzen *et al.*, 2012; Zhang *et al.*, 2012). Typically PIP2s have higher water permeability than the PIP1 clade (Chaumont *et al.*, 2001). However, PIP1s have been found to require interaction with PIP2s to correctly localise to the plasma membrane (Fetter *et al.*, 2004; Zelazny *et al.*, 2007). Using yeast as a heterologous expression system, I have examined CO_2 permeability and additionally, localisation of Setaria PIPs tagged with GFP. I generated separate yeast constructs to confirm the localisation in yeast and to avoid GFP interfering with the spectrophotometry assay used for detecting permeability. I also observed improved GFP expression for PIP1s when co-expressed with a PIP2 and, further to this result, I measured the effect of PIP1 and PIP2 co-expression on CO_2 permeability. Finally, I hypothesised candidate amino acid residues involved in CO_2 permeability.

3.2 Methods

3.2.1 Summary of genes and yeast vectors

The coding sequence of aquaporin genes of interest (Table 3.1) were codon optimised for expression in yeast (IDT DNA codon optimisation tool) and synthesised by GeneScript (US) into pUC57 (ampicillin resistant). Each sequence was designed with restriction enzyme sites for future cloning and Kozak sequence at the 5' end to increase translation (Nakagawa *et al.*, 2008). A glycine rich region was added as a spacer before the addition of the sequence encoding a Myc tag at the 3' end of each aquaporin sequence. For the hCAII (*Homo sapiens* α carbonic anhydrase II) sequence, a sequence encoding a single Flag tag was added at the 3' end (Figure 3.1D).

Table 3.1: Summary of aquaporin and CA gene IDs used for expression in yeast.. Si = *Setaria italica*, h = *Homo sapiens*, At = *Arabidopsis thaliana*, Nt = *Nicotiana tabacum.*

Name	**Gene ID**
SiPIP1;1	*Seita.7G196700*
SiPIP1;2	*Seita.1G264900*
SiPIP1;5	*Seita.1G372300*
SiPIP1;6	*Seita.4G089800*
SiPIP2;1	*Seita.2G123000*
SiPIP2;2	*Seita.9G219400*
SiPIP2;3	*Seita.9G268100*
SiPIP2;4	*Seita.1G241900*
SiPIP2;5	*Seita.7G170200*
SiPIP2;6	*Seita.2G123200*
SiPIP2;7	*Seita.2G123300*
SiPIP2;8	*Seita.2G291500*
AtPIP1;2	*AT2G45960.3*
AtPIP2;1	*AT3G53420.1*
AtPIP2;3	*AT2G37180*
NtAQP1	*AJ001416.1*
NtPIP2;1	*AAL33586*
hCAII	*AK312978*
NtCA	*M94135*

Yeast vectors pSF-TPI1-URA3 and pSF-TEF1-LEU2 were ordered from Oxford Genetics (UK) and pRS423-GPD-HIS was obtained from AddGene (Alberti *et al.*, 2007). A C-terminal tagged version of pSF-TPI1-URA3 with eGFP was generated using synthesised eGFP from GeneScript by restriction/ligation cloning as described in Section 3.2.2. Transgene expression in each yeast vector is driven by a strong, constitutively expressed promoter and all are high copy number plasmids. There are different amino acid markers on each yeast vector to allow for selection based on amino acid complementation, either uracil (URA), histidine (HIS) or leucine (LEU) (Figure 3.1).

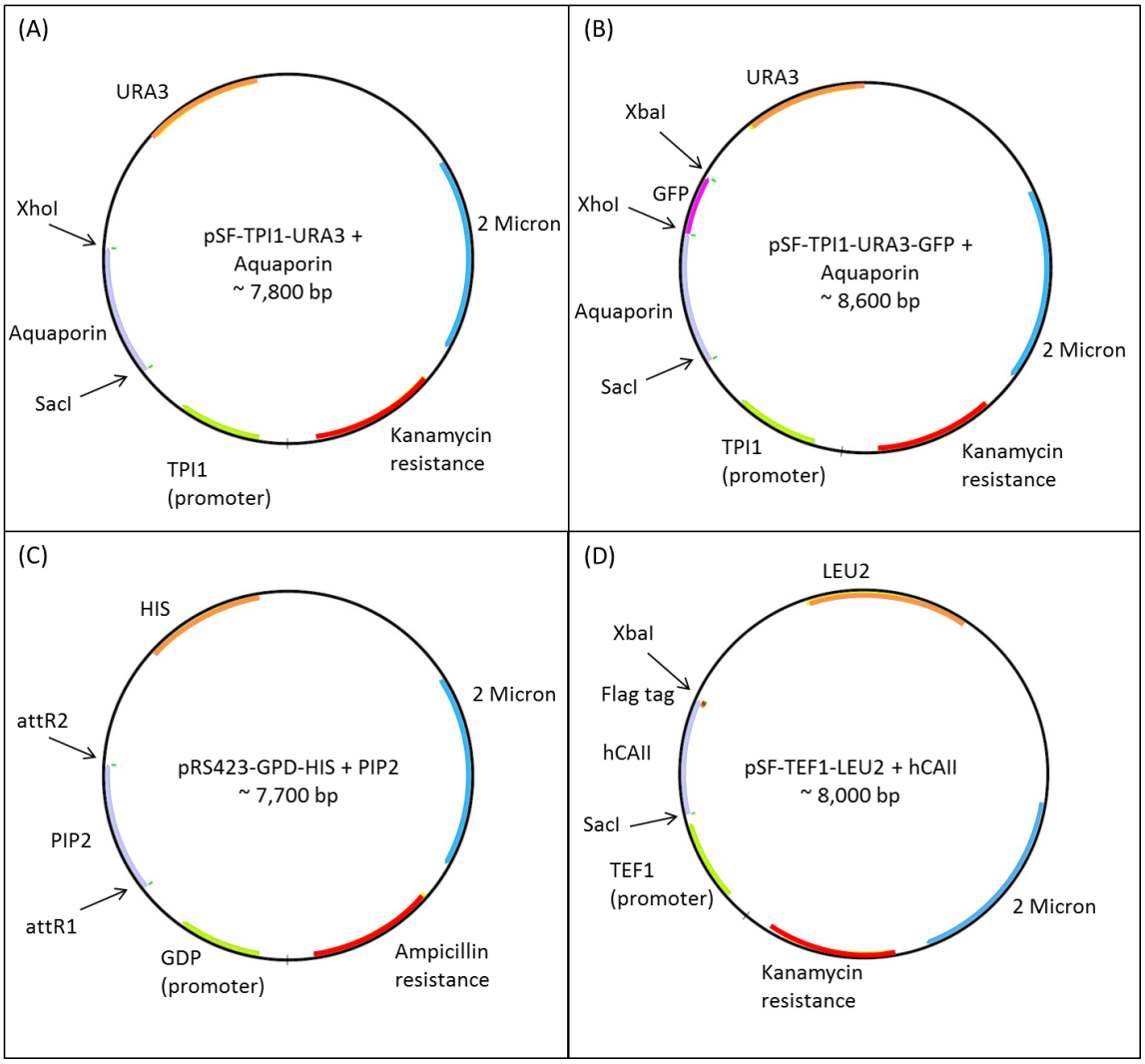

Figure 3.1: Transformed yeast vectors. (A) pSF-TPI1-URA3 with aquaporin, (B) pSF-TPI1-URA3-GFP with aquaporin, (C) pRS423-GPD-HIS with PIP2 and (D) pSF-TEF1-LEU2 with hCAII. Restriction enzyme sites used for ligation cloning are labelled in (A), (B) and (D); gateway cloning sites are labelled in (C). Constitutive promoters are present in all yeast vectors, which include the triose phosphate isomerase (TPI1), triose phosphate dehydrogenase (GPD) and elongation factor alpha-1 (TEF1); and all vectors are a high copy number as indicated by the 2 Micron.

3.2.2 Molecular cloning into yeast vectors

For cloning and plasmid propagation, chemically competent *Escherichia coli* Top10 cells (Thermo Fisher Scientific) were used for bacterial transformation. 100 ng of plasmid DNA was transformed into 50 µL of chemically competent cells. Cells were incubated on ice for 30 min and then heat shocked at 42 °C for 30 s and placed on ice for another 2 min. 450 µL of Luria Broth (LB) media was then added to the cells and these were grown at 37 °C shaking at 200 rpm for 1 h. 20 – 100 µL of transformation mix was then spread on LB agar plates with the appropriate antibiotic selection and grown at 37 °C overnight (Table 3.2). A colony was then selected and grown overnight in 4 mL of liquid LB with the appropriate antibiotic at 37 °C shaking at 200 rpm. Plasmid DNA was purified using Promega Plus Sv Minipreps DNA Purification System as per the manufacturer's instructions and for restriction/ligation cloning DNA was digested with the relevant restriction enzymes (Promega) at 37 °C for 90 min. All aquaporins, pSF-TPI1-URA3 and pSF-TPI1-URA3-GFP were cut with SacI and XhoI, whereas hCA, SiPIP2;4, SiPIP2;5 and pSF-TEF1-LEU2 were cut with SacI and XbaI. The digestion was then run on an agarose gel (1%) containing Gel Safe for 30 min at 100 V. The digested product was then cut out from the gel and purified using Promega Wizard SV Gel and PCR Clean-Up System. Using restriction/ligation cloning both the digested vector and gene of interest were ligated using T4 DNA ligase (Promega) and incubated at 15 °C overnight.

Table 3.2: General solutions and growth media.

Media	**Components**
Luria broth (LB)	0.5% (w/v) yeast extract (Sigma Aldrich), 0.5% (w/v) NaCl, 1% (w/v) tryptone pH 7.5, for plates: + 1.5% (w/v) agar
LB/ Kan	LB + 50 µg mL^{-1} of kanamycin
LB/ Amp	LB + 100 µg mL^{-1} of ampicillin
10 x TAE	0.4 M Tris, 0.01 M EDTA disodium salt, 0.2 M acetic acid
Agarose gel	1% (w/v) agarose dissolved in 1 x TAE buffer
SC Minimal drop out media	6.7% (w/v) yeast nitrogen base without amino acids, 20% (w/v) glucose and: Leucine drop out: 1.16% (w/v) Leucine drop out medium supplement; Leucine + Uracil drop out: 1.15% (w/v) Leucine, Histidine, Uracil, Tryptophan drop out media supplement, 0.05% (w/v) Histidine media supplement, 0.1% (w/v) Tryptophan media supplement;

	Leucine + Uracil + Histidine drop out: 1.15% (w/v) Leucine, Histidine, Uracil, Tryptophan drop out media supplement, 0.1% (w/v) Tryptophan media supplement; For plates: 2% (w/v) agar.

The ligation products (5 µL) were then transformed into chemically competent *E. coli* cells as described above using the heat shock method. Colonies were selected and then grown overnight in liquid LB. Plasmid DNA was purified as described above. The products were digested to confirm the correct sized product and were verified by sequencing using primers in Table 3.3. Alignment of the sequences was performed with ClustalW in Geneious (v9.0.2).

Table 3.3: Primers used in this study.

Description	**Sequence (5' – 3')**
Sequencing For_URA3	TCGATCCTACCATCCACTCGA
Sequencing Rev_URA3	CCTGCGGATCCAGAAATCGA
Sequencing Rev_URA3 + GFP	GGAAAAACACTGCACACCGT
Sequencing For_LEU2	AGAAAGCATAGCAATCTAATCTAAGT
Sequencing Rev_LEU2	CCTGCGGATCCAGAAATCGA
Sequencing For_HIS	GAACTTAGTTTCGACGGATTCTAGA
Sequencing Rev_HIS	TTTCGGTTAGAGCGGATGTG
AttL1	GGGGACAAGTTTGTACAAAAAAGCAGGCTTAGAGCTCCACAAAATGTC
AttL2	GGGGACCACTTTGTACAAGAAAGCTGGGTATCACTCGAGTAGGTCTTCTTC

Gateway cloning was followed for SiPIP2;4 and SiPIP2;5 into the yeast vector pRS423-GPD-HIS. AttL1 and AttL2 sites were added to these aquaporins by PCR (Table 3.3). The PCR cycling conditions followed the Phusion High-Fidelity DNA Polymerase (Thermo-Fisher) instructions: 98 °C 30 s; 98 °C 10 s, 56 °C 20 s, 72 °C 30 s for 35 cycles; 72 °C 5 min. The PCR products were then purified using Promega Wizard SV PCR Clean-Up System and ligated into the entry vector, pDONR (Invitrogen) and then into the final vector pRS423-GPD-HIS following standard Gateway cloning using BP and LR clonase (Invitrogen). The ligation mixture was transformed into OmniMAX competent cells (Thermo Fisher Scientific) as described above using the heat

shock method. Plasmid DNA was purified as described previously using Promega Minipreps and products were verified by sequencing (Table 3.3).

3.2.3 Expression in yeast

Saccharomyces cerevisiae wild type strain INV*Sc*1 (*MATa his3D1 leu2 trp1-289 ura3-52 MA*T *his3D1 leu2 trp1-289 ura3-52*) (Thermo Fisher Scientific) was used for the yeast transformations. Competent yeast cells were made using the Frozen-EZ yeast transformation II kit (Zymo Research) and transformed with different yeast vectors as outlined in Table 3.4. Briefly, 5 µL DNA were added to competent yeast cells, incubated for 3 h at 30 °C and then spread on SC Minimal media plates (Table 3.2). Plates were incubated at 29 °C for 4 days to allow for growth of transformants. Selection of transformants was based on amino acid complementation (Table 3.4). Yeast transformants were cultured in SC Minimal drop out media (same as plate media without agar) shaking at 200 rpm overnight at 29 °C. Glycerol stocks were made and stored at -80 °C.

Table 3.4: Summary of yeast transformations.

Yeast construct	**Yeast strain**	**Selection**	**Purpose**
pSF-TEF1-LEU2 + CA	INV*Sc*1	Leucine	CO_2 permeability assay control
pSF-TEF1-LEU2 + CA and pSF-TPI1-URA3 + aquaporin	INV*Sc*1	Leucine and Uracil	CO_2 permeability assay
pSF-TEF1-LEU2 + CA and pSF-TPI1-URA3-GFP + aquaporin	INV*Sc*1	Leucine and Uracil	GFP localisation
pSF-TEF1-LEU2 + SiPIP2;4/SiPIP2;5 and pSF-TPI1-URA3-GFP + SiPIP1s	INV*Sc*1	Leucine and Uracil	Test co-expression of PIP1 and PIP2 for GFP localisation
pSF-TEF1-LEU2 + CA, pSF-TPI1-URA3 + SiPIP1s, and pRS423-GPD-HIS + SiPIP2;4/SiPIP2;5	INV*Sc*1	Leucine, Uracil and Histidine	Co-expression of PIP1 and PIP2 for CO_2 permeability assay

3.2.4 CO_2 permeability of selected sorghum aquaporins

Five sorghum aquaporin genes were selected as co-locating with quantitative trait loci (QTLs) for putative photosynthetic traits (Mace et al., unpublished 2017, University of Queensland). These included *SbPIP1;6, SbPIP2;6, SbPIP2;7, SbTIP1;1, and SbTIP5;2*. *SbPIP2;7* was codon optimised for expression in yeast and cloned as described previously (Section 3.2.2). The remaining sorghum aquaporins were cloned by Michael Groszmann into the yeast strain, aqy1/2 a mutant strain deficient in aquaporins (Suga and Maeshima, 2004) and I then determined the CO_2 permeability of these sorghum aquaporins (Table 3.5).

Table 3.5: Summary of sorghum aquaporins used for expression in yeast.

Name	**Gene ID**	**Yeast vector***	**Yeast strain**
SbPIP1;6	*Sobic.010G087900*	pRS423-GPD-HIS	Aqy1/2
SbPIP2;6	*Sobic.002G125700*	pRS423-GPD-HIS	Aqy1/2
SbPIP2;7	*Sobic.002G125300*	pSF-TPI1-URA3-GFP pRS423-GPD-HIS	INV*Sc*1 Aqy1/2
SbTIP1;1	*Sobic.001G505100*	pRS423-GPD-HIS	Aqy1/2
SbTIP5;2	*Sobic.007G124600*	pRS423-GPD-HIS	Aqy1/2

*Note yeast vectors are described in Section 3.2.1.

3.2.5 GFP localisation

Localisation and expression of aquaporins was inferred from GFP expression using confocal microscopy. Overnight cultures of individual aquaporins tagged with GFP (pSF-TEF1-LEU2 + CA and pSF-TPI1-URA3-GFP + aquaporin), and PIP1s tagged with GFP and co-expressed with a PIP2 (pSF-TEF1-LEU2 + SiPIP2;4/SiPIP2;5 and pSF-TPI1-URA3-GFP + SiPIP1s) were viewed under x40 magnification using oil on a Zeiss 780 confocal at the Centre for Advanced Microscopy at the Australian National University. Settings for fluorescence detection were channel 1 (ChS1) excitation 488 nm and emission 530 nm with a digital gain 750. Transmitted light images were also collected. A plasmid with cytosolic GFP expression (pAG426GPD-eGFP-ccDB; Alberti *et al.*, 2007) was also used as a positive control, kindly provided by Michael Groszmann.

3.2.6 CA activity

Relative CA activity of yeast transformed for CO_2 permeability assays (Table 3.4) was determined using a membrane inlet mass spectrometer (MIMS; Isoprime100, Elementar, UK). Highly ^{18}O enriched $NaH^{13}CO_3$ equilibrated against 99% $H_2{}^{18}O$ in a sealed vial at room temperature for 24 h was used for these assays. 2.5 mmol L^{-1} of this highly enriched bicarbonate was added to the reaction buffer (100 mM EPPS pH 7.8) in the MIMS cuvette to a final volume of 600 μL (S4 PTFE membrane, Hansatech). Dextran-bound acetazolamide (Ramidus AB, Sweden) was added (1.2 μg mL^{-1}) to eliminate external CA activity. An overnight culture of yeast were concentrated 10x and once chemical equilibration on the MIMS was reached (~300 s) 10 μL yeast were added. The concentration of CO_2 species: $^{13}C^{16}O^{16}O$ (mass 45), $^{13}C^{18}O^{16}O$ (mass 47) and $^{13}C^{18}O^{18}O$ (mass 49) were monitored over time. Figure 3.2A illustrates the exchange of ^{18}O. When the highly enriched sodium bicarbonate buffer is added (*) there is an initial increase in mass 49 CO_2 as the uncatalysed reaction of $HCO_3{}^- + H^+ \leftrightarrow CO_2 + H_2O$ occurs. There is also movement of the ^{18}O between the CO_2 and H_2O pool and an increase in mass 47 and mass 45 is observed. When the yeast cells are added (arrow) there is an increase in CA activity and this rapidly increases the exchange of the ^{18}O, with more ^{18}O entering the H_2O pool and the unlabelled CO_2 (mass 45) becoming the most abundant CO_2 species detected by the MIMS.

In-house Python scripts were used to record and process data from the Mass Spectrometer. These measurements were made on intact yeast cells and further assumptions would be required to calculate CA hydration rates inside the cell. Consequently, we have calculated a relative CA activity of the intact yeast cells using the enrichment rate of mass 49 (Figure 3.2B), described by:

$$Enrichment\ rate = \frac{\log \frac{Mass\ 49}{Mass\ 49 + Mass\ 47 + Mass\ 45}}{Time} \qquad \text{Equation 2}$$

An average of 10 sec (** Figure 3.2B) is taken at the peak rate of mass 49 once the yeast cells are added. The final OD_{600} in the MIMS cuvette was measured and used to normalise the CA activity between the different cultures.

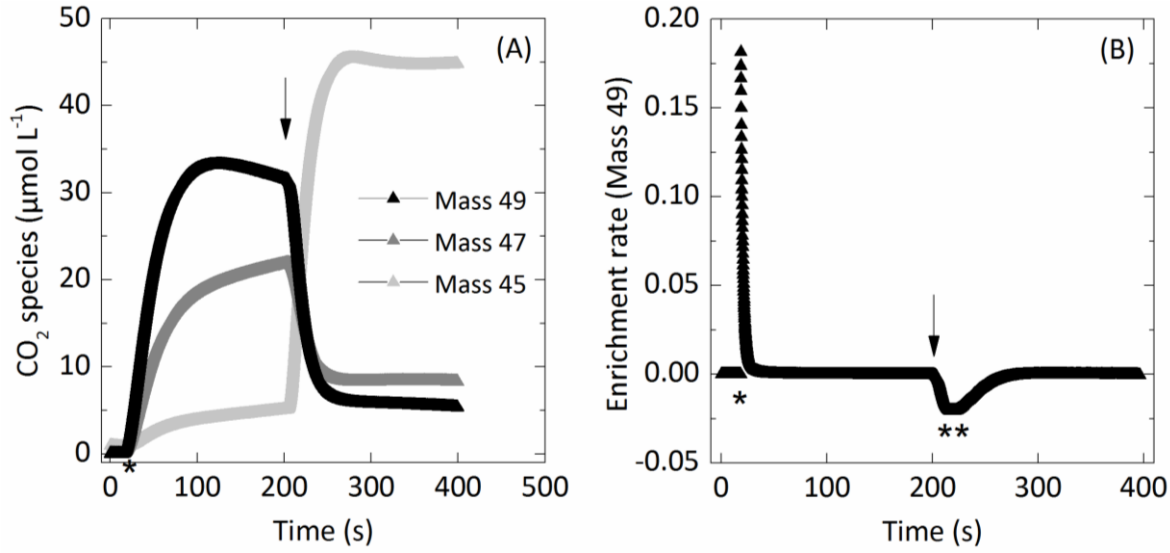

Figure 3.2: Exchange of CO_2 species monitored over time on a membrane inlet mass spectrometer (MIMS). (A) Highly enriched sodium bicarbonate ($NaH^{13}C^{18}O^{18}O^{18}O$) is added to the MIMS cuvette (*) and the movement of ^{18}O between the different CO_2 species: mass 49 ($^{13}C^{18}O^{18}O$), mass 47 ($^{13}C^{18}O^{16}O$) and mass 45 ($^{13}C^{16}O^{16}O$) is observed before and after the addition of yeast cells containing CA (arrow). (B) The enrichment rate of mass 49 is described by Equation 2. The region marked with ** is averaged over 10 sec to determine the relative CA activity.

3.2.7 Determination of CO_2 permeability

CO_2 permeability was measured on a stopped flow spectrophotometer (Bertl and Kaldenhoff, 2007; Ding *et al.*, 2013; Otto *et al.*, 2010) in collaboration with Steve Tyerman at the University of Adelaide. The principle of this assay for CO_2 triggered intracellular acidification is demonstrated in Figure 3.3. Yeast cells were grown overnight at 200 rpm at 29 °C in 10 mL SC minimal drop out media. The optical density at 600 nm (OD_{600}) of the culture was then measured and all cultures were normalised to the same OD. The OD is used as an indicator of yeast growth (Hall *et al.*, 2014). The culture was then centrifuged at 500 *g* for 5 min and supernatant removed, cells were washed in loading buffer (50 mM HEPES, pH 7), centrifuged again and resuspended in loading buffer containing 50 µM fluorescein diacetate (Sigma). Fluorescein diacetate (FDA) diffuses freely into intact cells where it is cleaved by esterases converting the non-fluorescent FDA into the green fluorescent compound fluorescein (Breeuwer *et al.*, 1995). The FDA solution was made fresh daily as a 100x stock dissolved in acetone. Cells were incubated in FDA for 30 min at 37 °C in the dark then centrifuged and the pellet resuspended in ice cold incubation buffer (75 mM NaCl, 25 mM HEPES, pH 6).

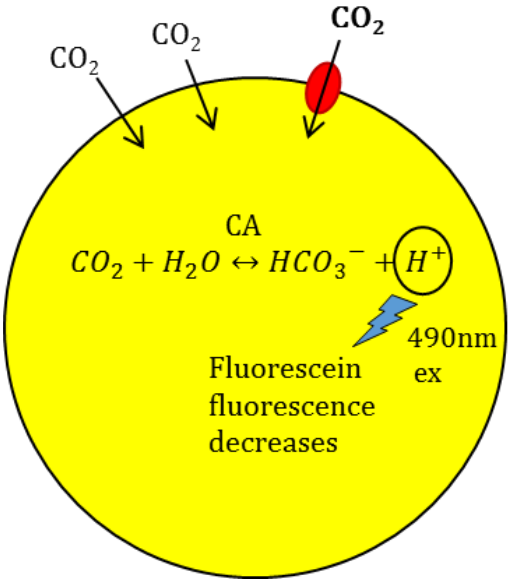

Figure 3.3: The basis of CO_2 permeability measurements. When CO_2 enters into the cell it is converted by CA into bicarbonate and protons (H^+), which decreases the intracellular pH. This change in pH is indicated by a pH sensitive dye, fluorescein. When CO_2 permeable aquaporins are present (red circle) then more CO_2 enters the cell and the decrease in pH occurs faster.

Cells loaded with FDA were then injected into the stopped flow spectrophotometer (DX.17MV, Applied Photophysics, Leatherhead, UK) alongside a buffer solution containing 75 mM $NaHCO_3$, 25 mM HEPES, pH 6 bubbled with CO_2 for 2 h (Figure 3.4). The kinetics of acidification were measured with an excitation wavelength of 490 nm and emission above 515 nm (OG515 long pass filter, Schott, supplied by Applied Photophysics, Leatherhead, UK). Data was collected over a time interval of 0.2 sec. The data presented are an average of at least 30 injections repeated 4 times. The rate constant K_{CO2} was obtained by fitting a single exponential to the decrease in fluorescence over 0.02 to 0.2 sec (Figure 3.5).

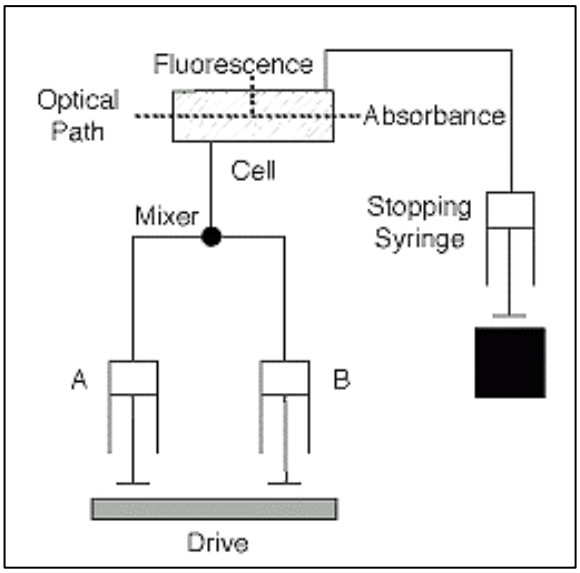

Figure 3.4: Cartoon of a stopped flow spectrophotometry instrument. Small volumes of solution are rapidly driven from syringes (A) and (B) which contain, for example, yeast loaded with FDA in one syringe and a buffer high in CO_2 in the other syringe. The volume injected into the mixer is limited by the stop syringe which provides the "stopped flow". The two solutions mix rapidly and absorbance measurements are detected with the attached spectrophotometer (Image from TgK Scientific).

The data was analysed using ProData SX viewer software provided by Applied Photophysics. The rate constant K_{CO2} was used to calculate CO_2 permeability (P_{CO2}) according to the following equation (Fang *et al.*, 2002; Yang *et al.*, 2000):

$$P_{CO2} = (V/A)K_{CO2}10^{(pHf-pKa)} \qquad \text{Equation 3}$$

Where,

P_{CO2} is the CO_2 permeability (m s^{-1});

V/A is the volume to surface area ratio (where $V = \frac{4}{3}\pi r^3$ and $A = 4\pi r^2$, therefore $\frac{V}{A} = \frac{r}{3}$ where r is the yeast cell radius);

K_{CO2} is the rate constant of the exponential kinetics of decrease in fluorescence;

pH_f is the final intracellular pH (see Section 3.2.9);

pK_a is the acid dissociation constant for HCO_3^-, given as 6.1 (Harned and Bonner, 1945; Yokota and Kitaoka, 1985).

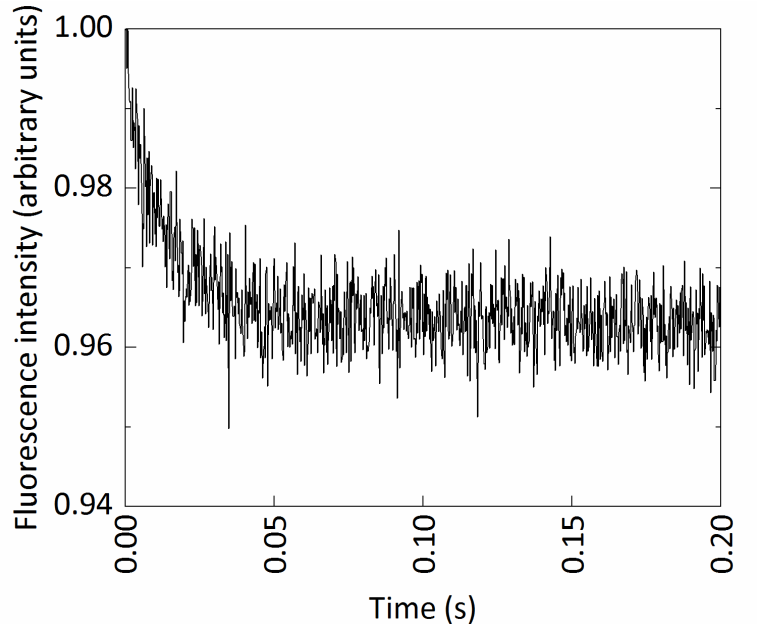

Figure 3.5: Example of data used to determine the rate constant, K_{CO2}. The decrease in fluorescence over time observed on the stopped flow spectrophotometer is fitted with a single exponential curve to obtain K_{CO2}.

3.2.8 Size estimation measurements

To determine the volume to surface area ratio (V/A) (Equation 3), overnight cultures of yeast expressing the different aquaporins were imaged on a Leica compound microscope under 40x magnification. The average cell diameter was then calculated by measuring ~100 cells using Fiji quantification software (Schindelin et al., 2012).

3.2.9 Final intracellular pH calculation

The final intracellular pH (pH_f) was determined by a fluorescent ratio technique using 100 µM fluorescein (Sigma) in 10 mM MES titrated at different pH (from pH 4 to pH 7) and measured at two different excitation wavelengths, 490 nm and 435 nm using the stopped flow spectrophotometer. The fluorescent ratios of 490/435 nm were plotted against pH to make a standard curve (Figure 3.6). The exponential fit of the trend line from the standard curve can be solved to determine the final intracellular pH. For each yeast culture injected into the stopped flow spectrophotometer the fluorescence intensities excited by both 490 and 435 nm were then also measured and the final intracellular pH calculated from the standard curve.

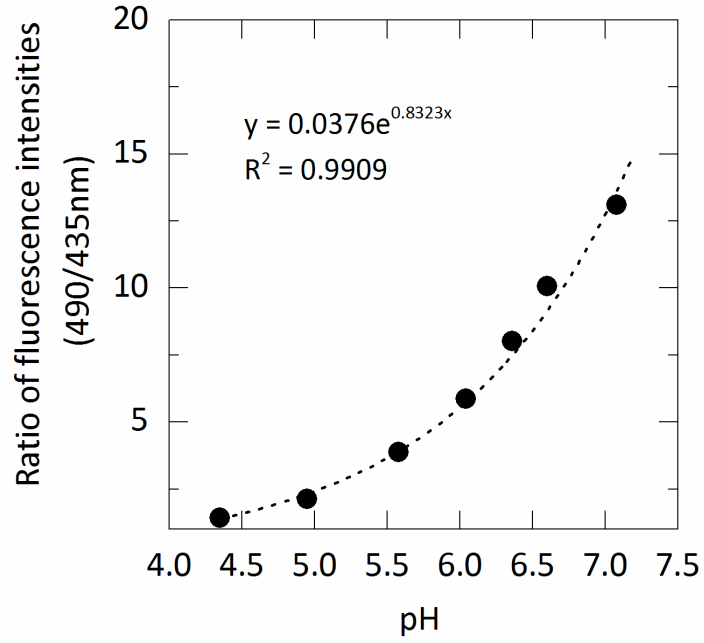

Figure 3.6: A standard curve for determining the final intracellular pH. The ratio of fluorescence intensities measured at 490 and 435 nm in MES buffer titrated to a range of different pH values (pH 4 to pH 7) is fitted with an exponential curve.

3.2.10 Confirmation of CO_2 permeability

Two negative control techniques were performed to confirm the CO_2 permeability on the stopped flow. Firstly, to confirm the decrease in FDA fluorescence was due to CO_2 permeability and not permeability of protons decreasing the intracellular pH, the fluorescence when the yeast were injected alongside a low pH solution (25 mM MES pH 4) was measured over 0.2 sec.

Secondly, the membrane permeable CA inhibitor, acetazolamide (AZ) was used to inhibit CA activity and confirm a reduction in apparent CO_2 permeability (Hempleman *et al.*, 2000). A final concentration of 50 µM acetazolamide (Sigma) dissolved in 10% (v/v) DMSO was incubated with the yeast culture (already loaded with FDA) for 15 min at room temperature. CO_2 permeability was then measured as described previously.

3.2.11 Statistical analysis

One-way ANOVAs with post-hoc Tukey test analyses were performed with P=0.05 using the IBM SPSS Statistics 22 package. Student T-test analyses were performed with Sigma Plot V11.0 with P=0.05.

3.3 Results

3.3.1 GFP localisation

Aquaporins with GFP fused to the C-terminus were expressed in yeast and GFP localisation examined (Figure 3.7). Twelve *Setaria italica* (Si) PIPs were examined along with selected *Arabidopsis thaliana* (At), *Nicotiana tabacum* (Nt) and *Sorghum bicolor* (Sb) PIPs. GFP expression varied depending on the aquaporin gene construct and localisation was observed in the plasma membrane, cytosol, endoplasmic reticulum and nucleus.

Expression of SiPIP1s showed low and punctate GFP expression in the plasma membrane with GFP also detected in the endoplasmic reticulum and cytosol, with the exception of SiPIP1;1 which showed almost no GFP expression. In general, SiPIP2s showed more GFP localised at the plasma membrane but were still varied in specificity of localisation. SiPIP2;1, SiPIP2;4, SiPIP2;5 and SiPIP2;7 clearly localised strongly to the plasma membrane, as well as the cytosol, endoplasmic reticulum and nucleus (Figure 3.7E, H, I and K). SiPIP2;2 and SiPIP2;6 showed weaker GFP expression at the plasma membrane and also GFP localisation intracellularly (Figure 3.7F and J). SiPIP2;3 (Figure 3.7G) showed strong GFP expression in the cytosol very similar in expression to the cytosolic GFP control (Figure 3.7S). SiPIP2;8 showed very weak GFP expression (Figure 3.7L).

AtPIP1;2, AtPIP2;1 and NtAQP1 were selected as positive controls as they were shown to be CO_2 permeable in previous publications (Heckwolf *et al.*, 2011; Uehlein *et al.*, 2003; Wang *et al.*, 2016), whilst AtPIP2;3 and NtPIP2;1 were selected as water permeable negative controls (Heckwolf *et al.*, 2011; Otto *et al.*, 2010). AtPIP1;2, AtPIP2;1, AtPIP2;3, NtAQP1 and NtPIP2;1 were also examined for GFP expression and showed GFP localisation to the plasma membrane, endoplasmic reticulum and nucleus (Figure 3.7M, N, O, P and Q). Sorghum SbPIP2;7 was examined for GFP localisation and expressed similarly at the plasma membrane and intracellularly (Figure 3.7R).

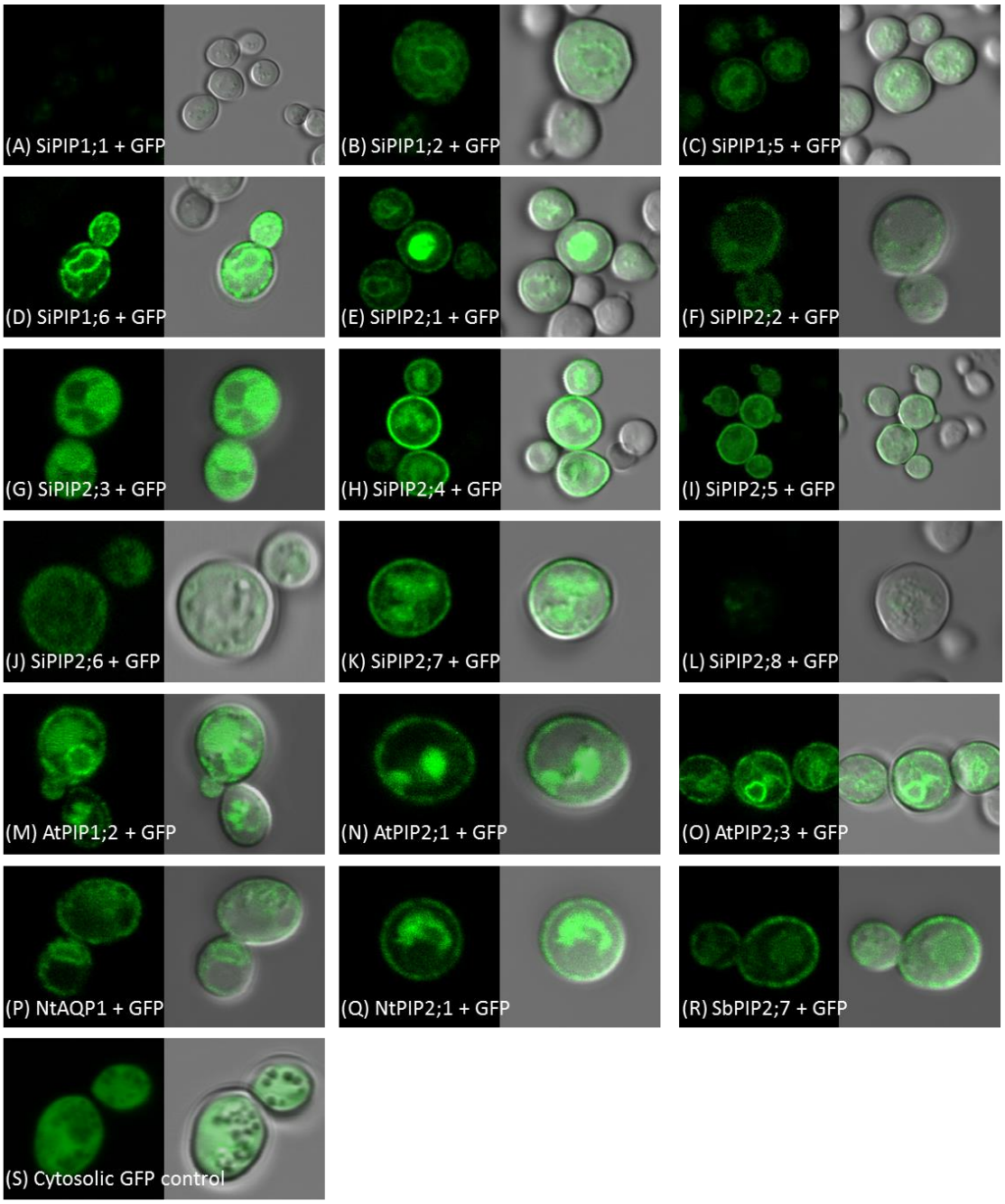

Figure 3.7: GFP localisation in yeast expressing an aquaporin with GFP fused to the C-terminus. Cells were imaged by confocal microscopy on a Zeiss 780 at 488 nm to visualise GFP and a merged bright field image is shown alongside. (A) SiPIP1;1, (B) SiPIP1;2, (C) SiPIP1;5, (D) SiPIP1;6, (E) SiPIP2;1, (F) SiPIP2;2, (G) SiPIP2;3, (H) SiPIP2;4, (I) SiPIP2;5, (J) SiPIP2;6, (K) SiPIP2;7, (L) SiPIP2;8, (M) AtPIP1;2, (N) AtPIP2;1, (O) AtPIP2;3, (P) NtAQP1, (Q) NtPIP2;1, (R) SbPIP2;7, (S) Positive control for cytosolic GFP expression.

3.3.2 CA activity

High CA activity is required to measure the CO_2 permeability of different aquaporins when expressed in yeast. To test for CA activity the movement of ^{18}O between the CO_2 species was monitored using a membrane inlet mass spectrometry (MIMS).

The relative CA activity was much higher in yeast cultures expressing hCA compared to an empty plasmid control or tobacco CA (Figure 3.8). Consequently, hCA was chosen to co-express with each aquaporin. Yeast cultures expressing both hCA and an aquaporin had CA activity comparable to the yeast expressing hCA alone.

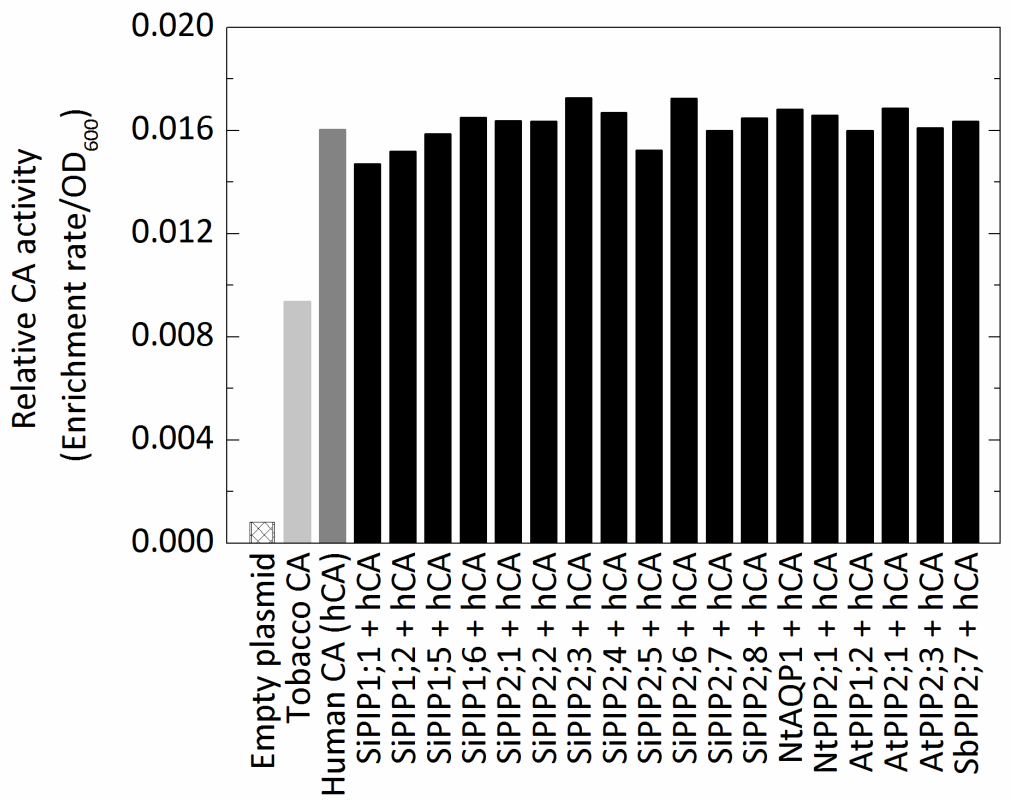

Figure 3.8: Relative CA activity of different yeast cultures. Yeast are expressing either an empty plasmid (pSF-TEF1-LEU2), tobacco CA, human CA (hCA) or an aquaporin with hCA. CA activity was measured using MIMS, and the enrichment rate is normalised to OD_{600}, n=1.

3.3.3 Size estimation

Average cell size is required to calculate CO_2 permeability (Equation 3). The average cell diameters of yeast cells expressing different aquaporins are presented in Figure 3.9. There was no statistical difference detected between the different yeast cultures as determined by one-way ANOVA using Sigma plot (P>0.05). The average cell diameter was 4.63 ± 0.02 µm.

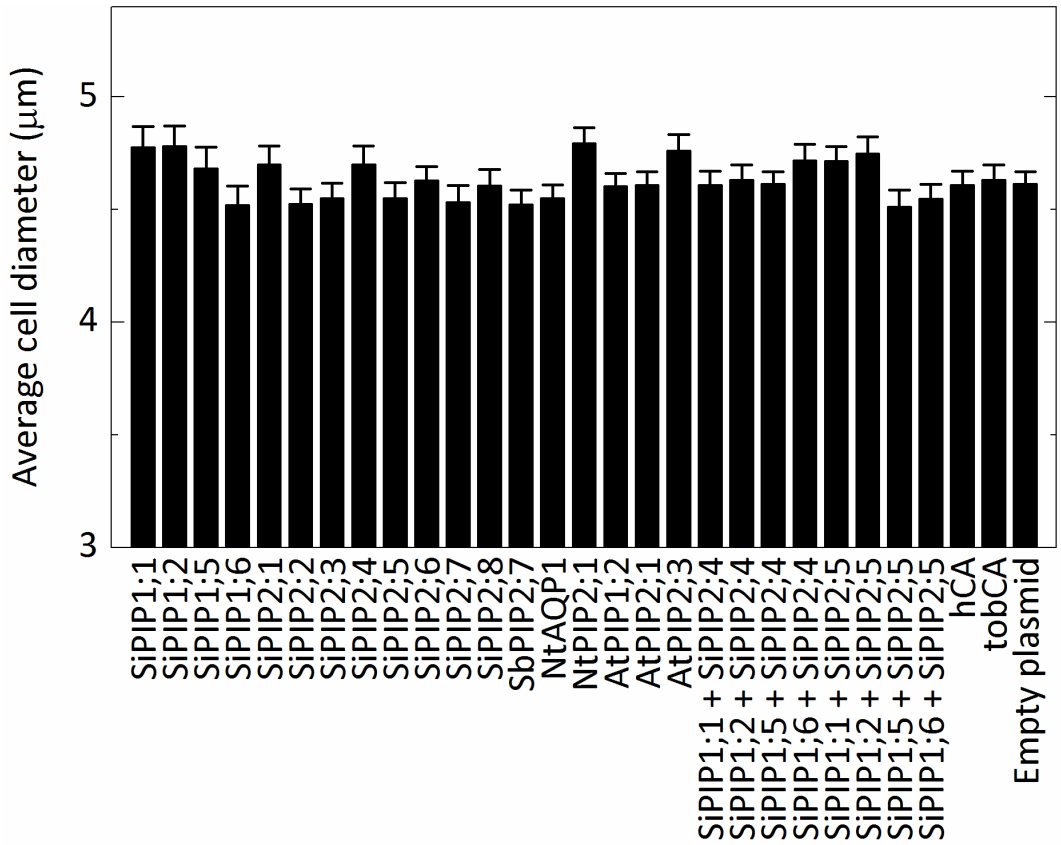

Figure 3.9: Average cell diameter of different yeast cultures. Yeast are expressing *Setaria italica* (Si), *Sorghum bicolor* (Sb), *Nicotiana tabacum* (Nt) or *Arabidopsis thaliana* (At) PIPs with human (h) CA, SiPIP1 and PIP2 co-expression with hCA and hCA, tob (tobacco) CA or an empty plasmid control (n=100). Imaged on a Leica compound microscope under 40x magnification and measured using Fiji quantification software.

3.3.4 CO_2 permeability

CO_2 permeability calculated using Equation 3 was measured in yeast expressing both an aquaporin and hCA using a stopped flow spectrophotometer (Figure 3.10). SiPIP2;7 had the highest CO_2 permeability of 1.5 x 10^{-4} ± 0.08 m s^{-1} which was significantly different to the negative control of yeast expressing hCA only (0.72 x 10^{-4} ± 0.06 m s^{-1}).

Interestingly, SiPIP2;2 was significantly lower in CO_2 permeability (0.30 x 10^{-4} ± 0.08 m s^{-1}) relative to the hCA only control. Permeability significantly lower than the control was not expected however this may be due to interaction with other proteins, low expression or weak targeting to the plasma membrane. All other Setaria PIPs were not significantly different in CO_2 permeability to the hCA only control.

The aquaporins AtPIP1;2, AtPIP2;1 and NtAQP1 were used as positive controls as they were shown to be CO_2 permeable in previous publications (Heckwolf *et al.*, 2011; Uehlein *et al.*, 2003; Wang *et al.*, 2016). However, in these assays neither of these aquaporins were observed to be CO_2 permeable (Figure 3.10). These assays were repeated over 4 different yeast cultures and an average of 30 injections were measured on the stopped flow for each culture.

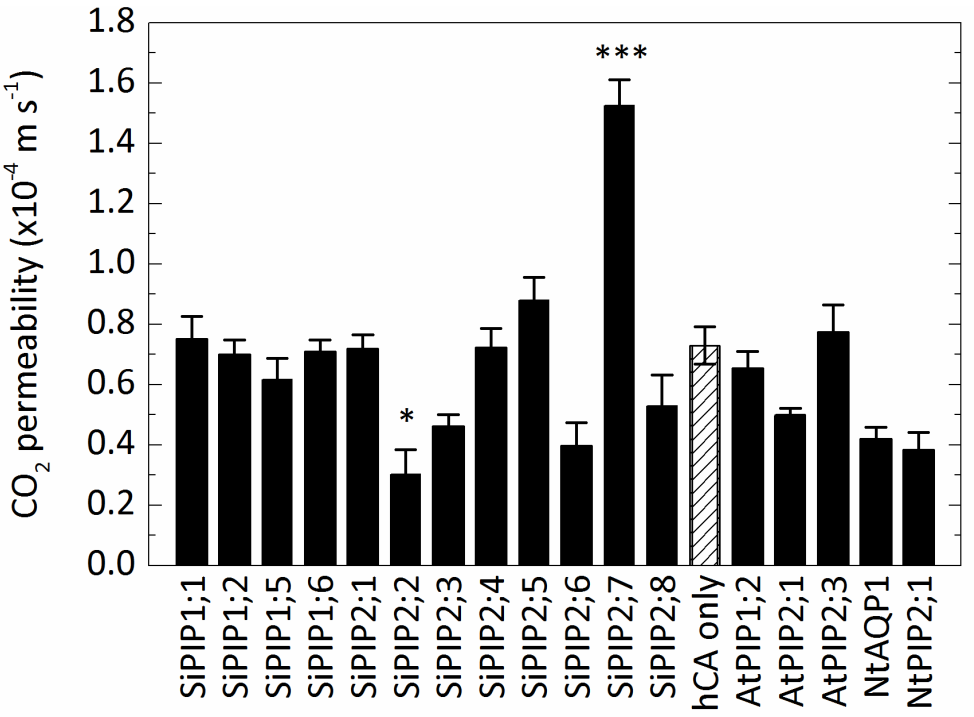

Figure 3.10: CO_2 permeability in yeast expressing PIPs and hCA. Permeability was measured on a stopped flow spectrophotometer and compared to hCA only for statistical analysis, n=4 (Sigma Plot 11.0, One-way ANOVA, * P<0.05, *** P<0.001).

Very similar results were obtained for CO_2 permeability in the Setaria aquaporins when repeated over two separate experiments, spaced one year apart. The CO_2 permeability of the aquaporins that were measured both years are shown in Figure 3.11. The results are very similar for the different Setaria PIPs and hCA only control with the exception of SiPIP2;5 and SiPIP2;8 which had significantly lower CO_2 permeability values in 2017 compared to 2016. Only SiPIP2;7 had significantly higher CO_2 permeability relative to the hCA only control for both experiments (Figure 3.11).

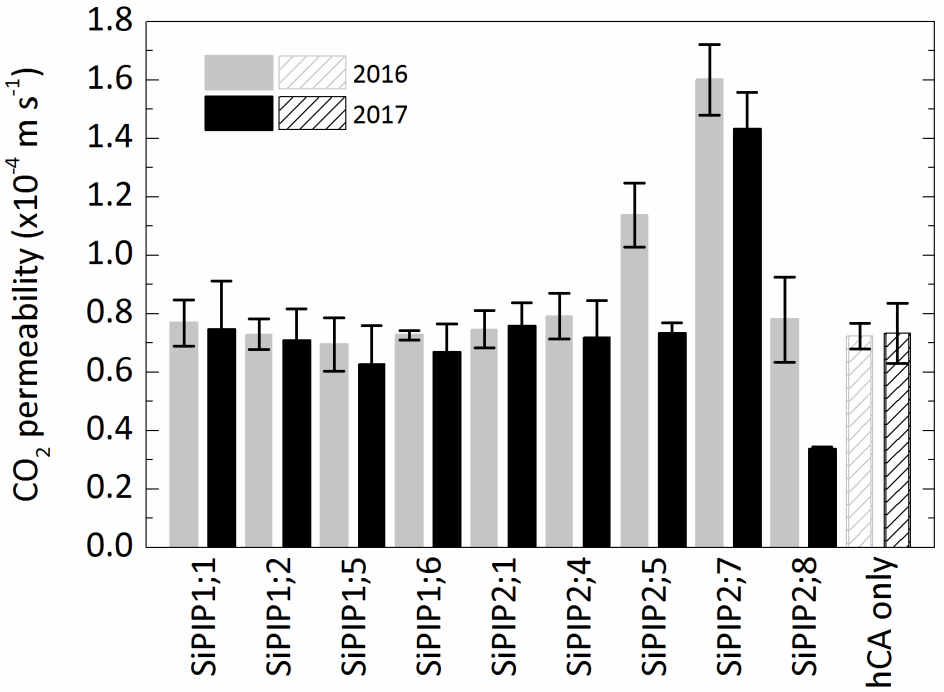

Figure 3.11: Comparison of CO_2 permeability results obtained over two separate experiments, 2016 and 2017. CO_2 permeability was measured on a stopped flow spectrophotometer in yeast expressing Setaria PIPs and hCA.

3.3.5 Assay controls: effect of low pH and CA inhibitor

The changes in CO_2 permeability, detected on the stopped flow spectrophotometer, could be confounded by other factors such as permeability to protons also causing intracellular acidification. To demonstrate the CO_2 permeability differences were caused by the expression of heterologous aquaporins an additional two assay controls were performed.

Firstly, the decrease in fluorescence intensity was compared between a buffer high in CO_2 (used normally) and a low pH solution to show proton permeability (Figure 3.12A). A decrease in fluorescence intensity was observed when yeast expressing an aquaporin and

hCA or hCA only were injected into the stopped flow spectrophotometer alongside a buffer high in CO_2. This decrease in fluorescence intensity over time was fitted with a single exponential trendline to determine K_{CO2} to calculate CO_2 permeability (Equation 3). In Figure 3.12A these traces for SiPIP2;7 (black) and hCA only (red) are compared to the effect of injecting alongside a low pH solution (MES pH 4). No decrease in fluorescence intensity was observed when SiPIP2;7 (grey) or hCA (pink) were injected alongside the low pH solution (Figure 3.12A). This demonstrates that the decrease in fluorescence was not due to movement of protons through the membrane.

Secondly, a CA inhibitor was used as an assay control to demonstrate a reduction in the apparent CO_2 permeability. The membrane permeable CA inhibitor, acetazolamide (AZ), significantly reduced CA activity which therefore reduced the CO_2 permeability detected in the yeast treated with AZ compared to the untreated culture for both yeast expressing SiPIP2;7 with hCA or hCA only (Figure 3.12B). This demonstrates that we are detecting CO_2 permeability and its interaction with CA on the stopped flow spectrophotometer.

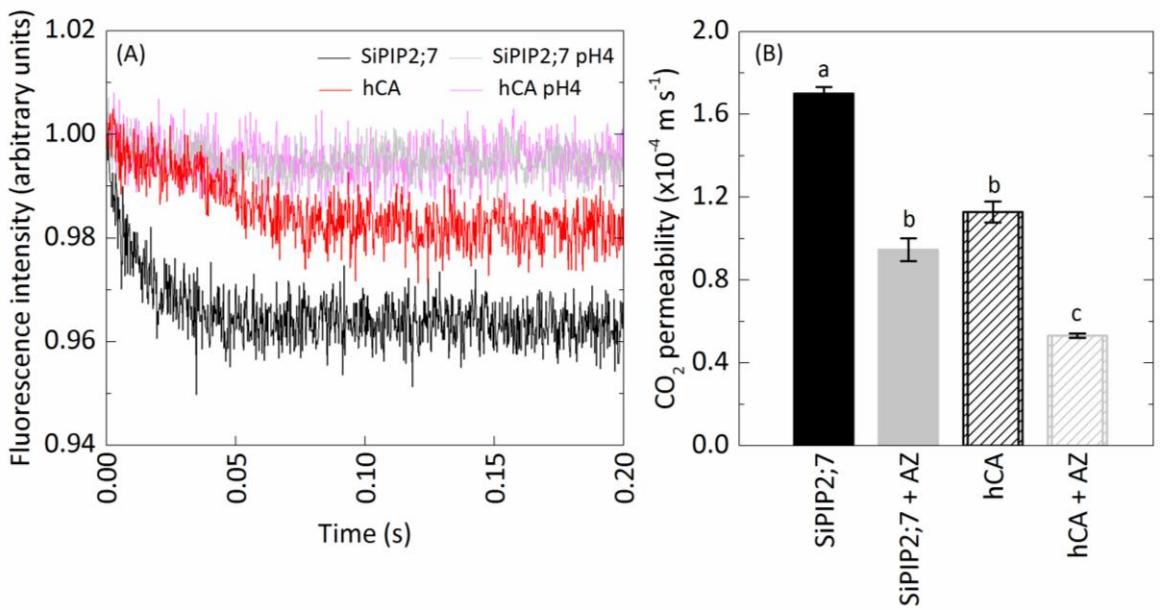

Figure 3.12: Confirmation of CO_2 permeability using assay controls. (A) CO_2 triggered intracellular acidification in yeast cells expressing either SiPIP2;7 with hCA or hCA only injected alongside a CO_2 rich buffer, compared to no acidification when injected with pH 4 buffer, n=5. (B) Effect of CA inhibitor acetazolamide (AZ) on apparent CO_2 permeability. Significant difference ($p<0.05$) is indicated by different letters as determined by one-way ANOVA.

3.3.6 Target amino acid candidates for substrate permeability

The Setaria PIP phylogeny, outlined in Chapter 2, demonstrated that SiPIP2;6 and SiPIP2;7 are very closely related and share 97% amino acid identity. Here I have shown despite this similarity, SiPIP2;6 and SiPIP2;7 have very different CO_2 permeability values: $0.39 \times 10^{-4} \pm 0.07$ m s^{-1} and $1.5 \times 10^{-4} \pm 0.08$ m s^{-1} respectively. Since both PIP constructs are driven by the same promoter, have comparable CA activity, GFP targeting to the plasma membrane and similar cell size, I hypothesised that differences in amino acid sequence could be the reason for the difference in CO_2 permeability. To investigate this I examined the amino acid alignment of these two PIPs. Figure 3.13 shows there are only eight amino acids which differ between SiPIP2;6 and SiPIP2;7. When compared to all 12 SiPIPs there are only two amino acids which are unique changes to SiPIP2;7 (Figure 3.13 boxed regions; Figure 3.14). At the N-terminus of the aquaporin at position 19 there is a change from V (valine) in SiPIP2;6 to A (alanine) in SiPIP2;7. This change results in a smaller amino acid at this position in SiPIP2;7 compared to SiPIP2;6 and all the other PIPs. The polarity of the amino acid at this position is variable throughout the other PIPs. The second unique amino acid for SiPIP2;7 is at position 165 in loop C which is located between transmembrane domains TM3 and TM4. The change from A (alanine) in SiPIP2;6 to T (threonine) in SiPIP2;7 results in a change from a nonpolar to a polar amino acid. Threonine is also a larger amino acid and has a larger R group compared to alanine. The polarity and size is variable at this position 165 in the rest of Setaria PIPs (Figure 3.14).

Since CO_2 is hypothesised to pass through the central pore of the tetramer, the key residues thought to line the central pore were also examined. These are indicated in blue and do not differ between SiPIP2;6 or SiPIP2;7 (Figure 3.13). Other amino acids involved in gating by phosphorylation such as S123 in loop B and S281 in the C-terminus or gating by pH at H201 in loop D do not differ between SiPIP2;6 and SiPIP2;7. Additionally, amino acids which are involved in stabilising loop B and D (Frick *et al.*, 2013) and those involved in stabilising tetramer formation (Yoo *et al.*, 2016) are also identical between SiPIP2;6 and SiPIP2;7. Overall these results suggest that V19A and A165T are likely amino acid changes which do not affect the aquaporin structure but may alter substrate permeability to CO_2.

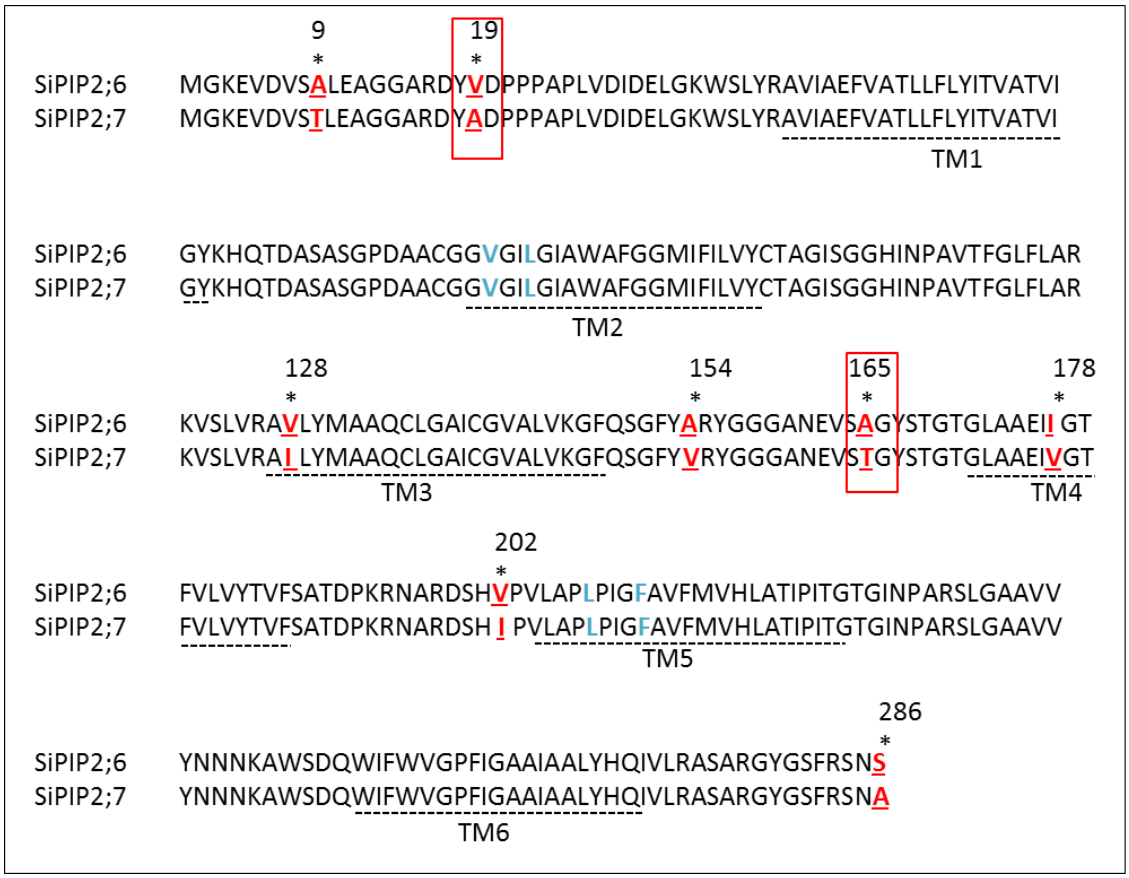

Figure 3.13: Amino acid alignment of coding sequence for SiPIP2;6 and SiPIP2;7 using ClustalW. The eight different amino acids are indicated in red with their position numbered and the transmembrane domains (TM1-6) are underlined. V19A and A165T are boxed as unique changes to SiPIP2;7 when all the SiPIPs are aligned (Figure 3.14). Key residues which line the central tetramer pore are also indicated in blue (Yu *et al.*).

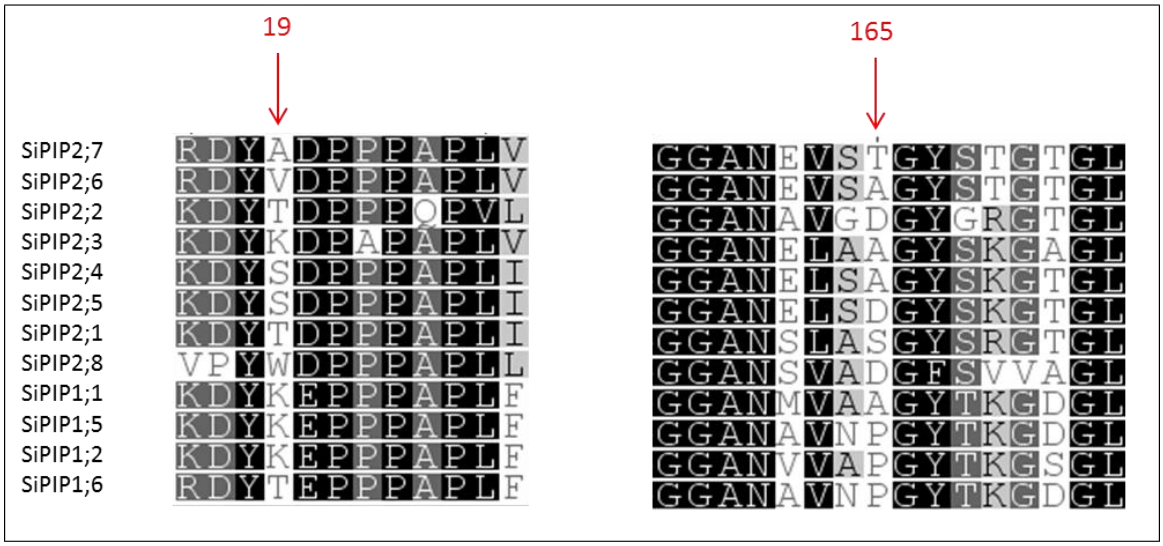

Figure 3.14: Alignment of all 12 *S. italica* PIPs at two candidate amino acid changes which are unique to only SiPIP2;7. Positions (A19 and T165) are numbered based on SiPIP2;7 sequence. Alignment performed using Clustal W in Geneious (v9.0.2), similar amino acids are shaded.

3.3.7 Effect of PIP1 and PIP2 co-expression on GFP localisation

It has been reported in the literature that co-expression of PIP1s with PIP2s can influence plasma membrane localisation (Bienert *et al.*, 2014; Fetter *et al.*, 2004; Zelazny *et al.*, 2007). To test this, SiPIP1s with a GFP tag were co-expressed with either SiPIP2;4 or SiPIP2;5. These PIP2s were chosen as they had the closest homology to the maize PIP2s, ZmPIP2;4 and ZmPIP2;5 used in the plasma membrane trafficking study of Zelazny *et al.* (2009). An N-terminal diacidic motif, DIE, was identified by Zelazny *et al.* (2009) in the ZmPIP2s to be essential for endoplasmic reticulum export. This motif is present in both SiPIP2;4 and SiPIP2;5 (Figure 3.15) but not present in the other 10 *S. italica* PIPs.

```
SiPIP2;4    ---------- MAKDIEASGP - EAGEFSAKDYSDPPPAPLIDAEELTKWS
SiPIP2;5    ---------- MAKDIEAAAAPEGGEYTAKDYSDPPPAPLIDAEELTKWS
SiPIP2;6    ---------- MGKEVDVSALEAGG- - -ARDYVDPPPAPLVDIDELGKWS
SiPIP2;7    ---------- MGKEVDVSTLEAGG- - -ARDYADPPPAPLVDIDELGKWS
SiPIP2;1    ---------- MGKDDVIESGAGGGEFAAKDYTDPPPAPLIDAAELGSWS
SiPIP2;3    ----------MNPSESMEAAGGKKD-YKDPAPAPLVNAGELGKWS
SiPIP2;8    ---------- MPIEDVSIETTEAAGPQKVPYWDPPPAPLLETSELMKWS
SiPIP2;2    ----------MAVGHEIVQQQRQRDPEHGGGGESSGKDYTDPPPQPVLTASELRRWS
SiPIP1;1    MEG -------- KEEDVRLGANKYSERQPIGTAAQGS -DDKDYKEPPPAPLFEPGELKSWS
SiPIP1;5    MEG -------- KEEDVRLGANRYSERQPIGTAAQGS -DDKDYKEPPPAPLFEAEELTSWS
SiPIP1;2    MEG -------- KEEDVRLGANKFSERQPIGTAAQGAGDDKDYKEPPPAPLFEPGELKSWS
SiPIP1;6    MAGGKLQDRFQDDEDVRVGVDRFPERHPIGATAADD-LGRDYTEPPPAPLFDAAELSSWS
```

Figure 3.15: Amino acid sequence alignment of N-terminal region of *S. italica* PIPs. The conserved diacidic signal predicted by Zelazny *et al.* (2009) to be essential for endoplasmic reticulum export is indicated in red (DIE). Only SiPIP2;4 and SiPIP2;5 contain this motif.

GFP localisation of the PIP1s tagged with GFP and co-expressed with either SiPIP2;4 or SiPIP2;5 are shown in Figure 3.16. No GFP signal was detected for SiPIP1;1 when in yeast alone or when co-expressed with either SiPIP2;4 or SiPIP2;5. Individually, SiPIP1;2 and SiPIP1;5 both showed low levels of GFP localised to the endoplasmic reticulum, the cytosol and plasma membrane. However when co-expressed with SiPIP2;4 or SiPIP2;5 a significant improvement in GFP localised to the plasma membrane was observed (Figure 3.16). GFP was still detected intracellularly in the nucleus in these co-expressed cultures. There was no improvement in GFP localisation to the plasma membrane when SiPIP1;6 was co-expressed with another PIP2, either SiPIP2;4 or SiPIP2;5. Overall, there was no difference in effect of co-expression with the different PIP2s, SiPIP2;4 or SiPIP2;5. These PIP2s are 92.7% identical at the protein level and 90.7% identical at the DNA sequence.

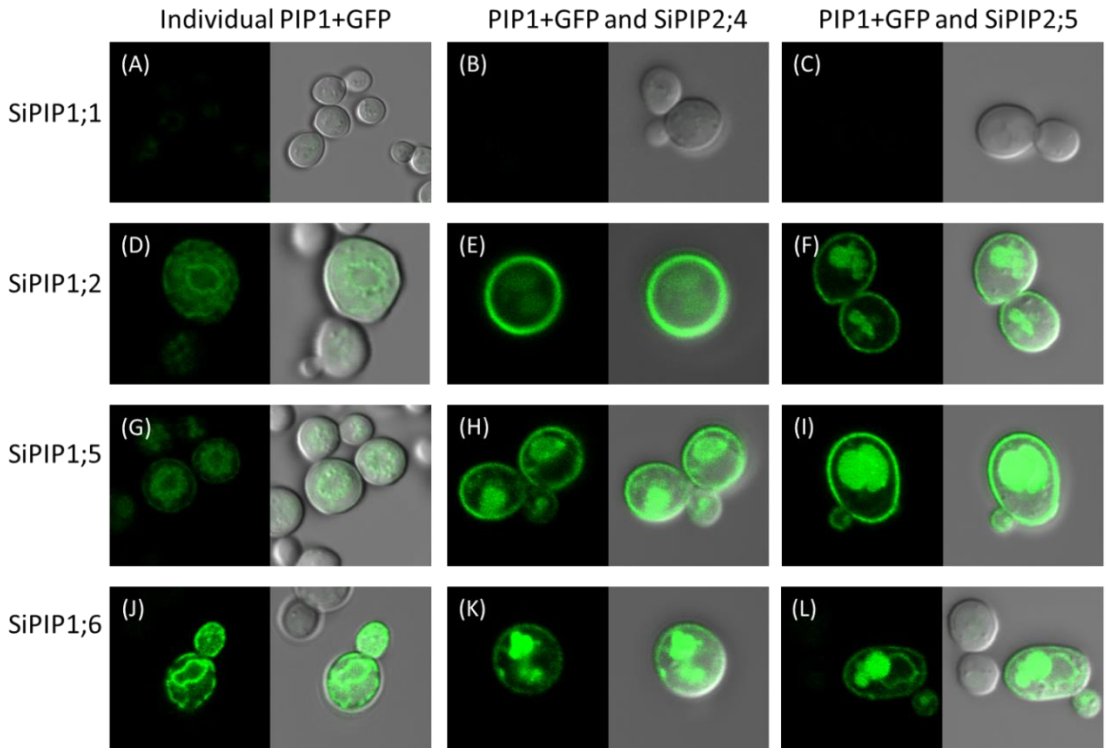

Figure 3.16: Comparison of GFP localisation in yeast co-expressing PIP1 with GFP fused to the C-terminus either alone (individual) or in combination with a PIP2 (SiPIP2;4 or SiPIP2;5).Cells were imaged by confocal microscopy on a Zeiss 780 at 488 nm to visualise GFP and a merged bright field image is shown alongside. (A) SiPIP1;1:GFP, (B) SiPIP1;1:GFP and SiPIP2;4, (C) SiPIP1;1:GFP and SiPIP2;5, (D) SiPIP1;2:GFP, (E) SiPIP1;2:GFP and SiPIP2;4, (F) SiPIP1;2:GFP and SiPIP2;5, (G) SiPIP1;5:GFP, (H) SiPIP1;5:GFP and SiPIP2;4, (I) SiPIP1;5:GFP and SiPIP2;5, (J) SiPIP1;6:GFP, (K) SiPIP1;6:GFP and SiPIP2;4, (L) SiPIP1;6:GFP and SiPIP2;5.

3.3.8 Effect of PIP1 and PIP2 co-expression on CO_2 permeability

PIP1 and PIP2 co-expression of some combinations of aquaporins seemed to increase their localisation to the plasma membrane when tagged with GFP (Figure 3.16). Thus, we tested if this effect resulted in increased CO_2 permeability. Yeast expressing these PIP1 and PIP2 combinations with hCA were tested for CO_2 permeability (Figure 3.17). CO_2 permeability was reduced in all PIP1 and PIP2 co-expression combinations compared to when expressed individually. For example, individually SiPIP1;2 had CO_2 permeability of 0.69 x 10^{-4} ± 0.04 m s^{-1} compared to 0.22 x 10^{-4} ± 0.02 m s^{-1} when SiPIP1;2 was co-expressed with SiPIP2;4. CO_2 permeability in the PIP1 and PIP2 combinations was also significantly lower than the hCA only control. The fact that CO_2 permeability is lower than the negative control when two aquaporins are co-expressed points to a pleiotropic effect of this co-expression.

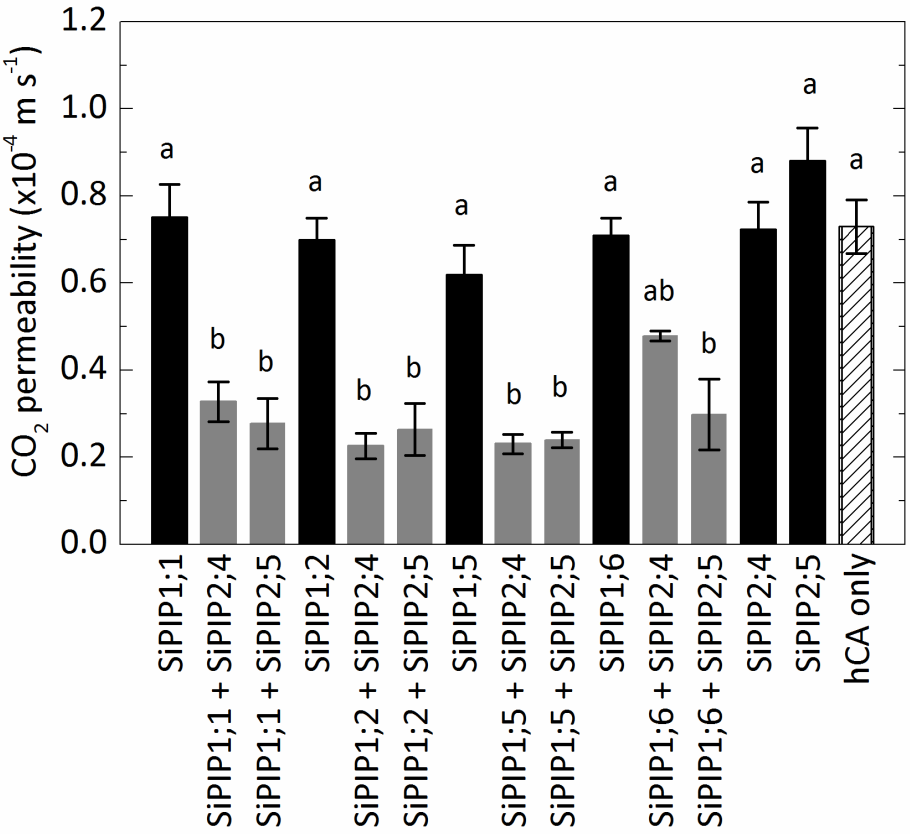

Figure 3.17: CO_2 permeability in yeast expressing individual Setaria PIPs or PIP1 and PIP2 combinations with hCA. CO_2 permeability was measured on a stopped flow spectrophotometer, different letters indicate significant difference (n=3, Sigma Plot 11.0, One-way ANOVA, $P<0.05$).

3.3.9 CA activity in PIP1 and PIP2 co-expression

To confirm CA activity was consistent between the different yeast cultures co-expressing PIP1 and PIP2 combinations with hCA (Figure 3.18) we measured CA activity as described previously for the individual PIPs (Figure 3.8). No difference was observed in relative CA activity between the hCA only control and the PIP1 and PIP2 combinations.

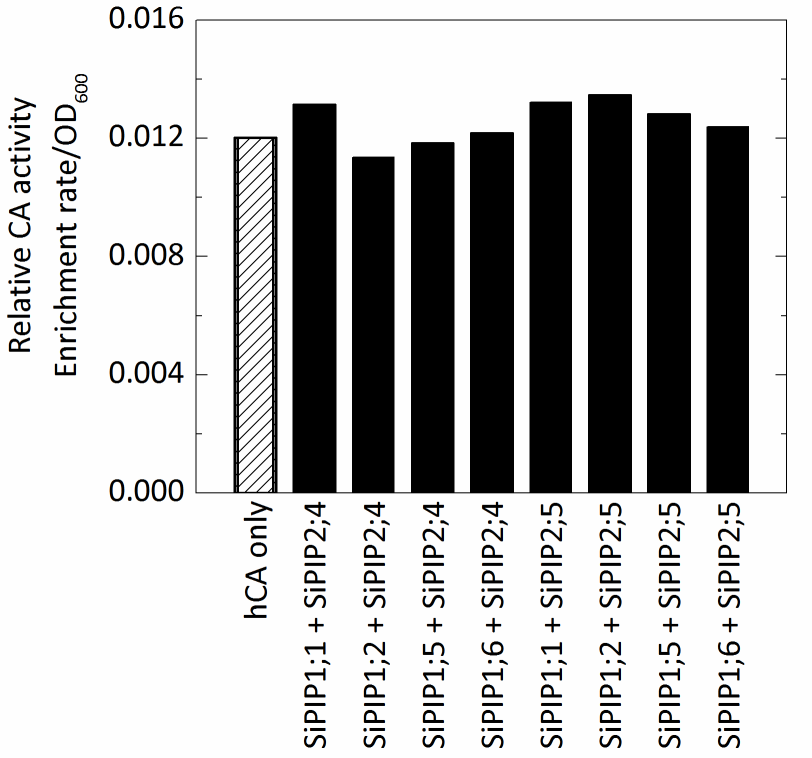

Figure 3.18: Relative CA activity of different yeast cultures expressing either hCA only or PIP1 and PIP2 co-expressed with hCA. CA activity was measured on a MIMS, and the enrichment rate is normalised to OD_{600}, n=1.

3.3.10 Sorghum aquaporin CO_2 permeability

A subset of 5 sorghum aquaporins, out of 41 aquaporins (Reddy *et al.*, 2015), were selected as possible candidates for CO_2 permeability based on co-location with putative photosynthetic quantitative trait loci (QTLs). QTL mapping is a powerful tool to uncover genetic control of complex traits. Using a set of around 1000 diverse sorghum genotypes, spanning different geographies, racial groups and end-uses, genomic regions associated with photosynthetic traits were identified (Mace et al., unpublished 2017, University of Queensland). These photosynthesis traits included chlorophyll content (as determined by

Soil-Plant Analysis Development (SPAD) measurements) and steady state chlorophyll fluorescence (as determined by Pulse Amplitude-Modulated (PAM) measurements). The diversity of the aquaporin genes in sorghum was investigated using a set of 44 diverse lines with whole genome resequencing data (Mace *et al.*, 2013b).

The selected sorghum aquaporins were expressed in aqy1/2, an aquaporin deficient strain and CO_2 permeability was measured using a stopped flow spectrophotometer. No significant difference in CO_2 permeability was found between the sorghum aquaporins with hCA and hCA only and consistent with the literature to date, no TIPs were identified as CO_2 permeable. However, some key assumptions of CA activity, cells size and correct GFP localisation to the plasma membrane have been made for the Sorghum aquaporins expressed in the yeast strain aqy1/2. Therefore, these are regarded as preliminary results which require further research.

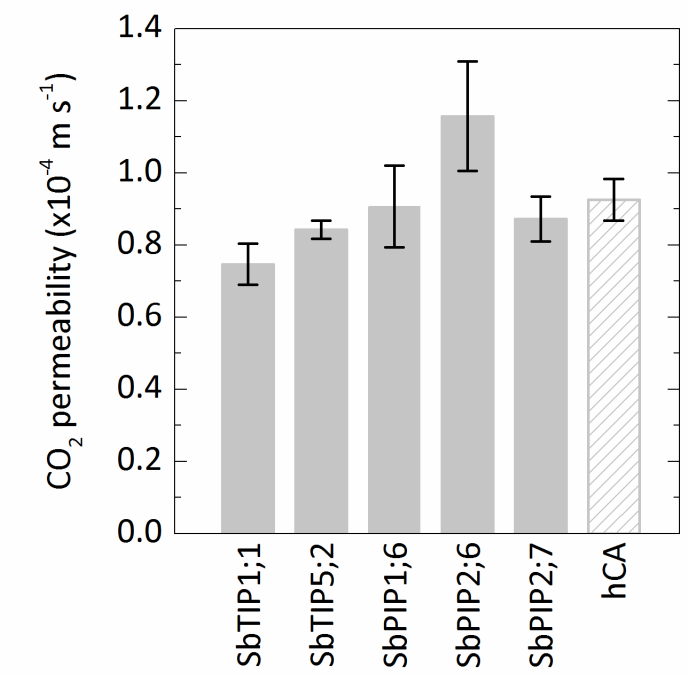

Figure 3.19: CO_2 permeability in yeast expressing sorghum aquaporins with hCA, or hCA only. CO_2 permeability was measured on a stopped flow spectrophotometer and compared to hCA only for statistical analysis, n=3.

3.4 Discussion

3.4.1 PIP2;7 is a CO_2 permeable aquaporin

In this Chapter, I have examined the permeability of Setaria PIPs to CO_2 when expressed in yeast. Using CO_2 triggered intracellular acidification I identified SiPIP2;7 as CO_2 permeable compared to the hCA only control. This result adds a third CO_2 permeable aquaporin to the limited list of C_4 plant aquaporins functionally characterised within the literature. So far only ZmPIP1;5 and ZmPIP1;6 have been demonstrated to be CO_2 permeable (Heinen *et al.*, 2014), though no effect on the C_4 photosynthetic cycle has been shown to date. The CO_2 permeability observed for SiPIP2;7 (1.5×10^{-4} m s^{-1}) is comparable to values observed in the literature using a similar technique, e.g. NtAQP1 and AtPIP1;2 measured in yeast on a stopped flow spectrophotometer had P_{CO2} of 1.9×10^{-4} m s^{-1} (Ding *et al.*, 2013; Heckwolf *et al.*, 2011).

3.4.2 Measuring CO_2 permeability

The method of detecting CO_2 permeability and the accuracy and relevance of the obtained values is an area of controversy (Endeward *et al.*, 2013). This is due to a number of factors, firstly the difficulty in determining any substrate permeability in heterologous expression systems and secondly due to the difficulty of measuring this specific substrate, CO_2.

There are two main approaches to determine CO_2 permeability, either detecting a change in pH (e.g. pH microelectrode probe or pH sensitive fluorescent dye detected using a stopped flow spectrophotometer) or by following ^{18}O isotope exchange (e.g. MIMS). Both approaches have limitations and require a number of assumptions to be made in order to calculate a permeability value (Endeward *et al.*, 2013; Tolleter *et al.*, 2017). For the stopped flow technique the limitation lies with the speed of CO_2 uptake which is much faster than the dead time of the stopped flow device. The mixing of yeast loaded with FDA and a buffer high in CO_2 occurs rapidly, however, each stopped flow device is limited by the latency of this detection of this rapid CO_2 uptake of approximately 2 ms. This can be overcome by extrapolating the fit to time zero of the acidification curve (Zhao *et al.*, 2017). With regard to the MIMS ^{18}O technique, an important assumption is that the surface area and geometric shape of the cell is accurately determined, as it heavily influences the final CO_2 permeability calculation (Tolleter *et al.*, 2017).

The possible variation in CO_2 permeability determined from the different techniques is significant and means comparison between different experiments is difficult (Endeward *et al.*, 2013). Tolleter *et al.* (2017) used my yeast construct expressing hCA (INV*Sc*1 with pSF-TEF1-LEU2+hCA) to calculate CO_2 permeability using the ^{18}O isotope exchange method on a MIMS. They calculated P_{CO2} as 1.09 x 10^{-3} m s^{-1} which is more than 10 times higher than the P_{CO2} I calculated using the stopped flow method (0.72 x 10^{-4} m s^{-1}). This is consistent with the trend reported by Endeward *et al.* (2013), whereby stopped flow assays calculate lower permeability values compared to ^{18}O isotope exchange or pH microelectrode assays (Figure 3.20).

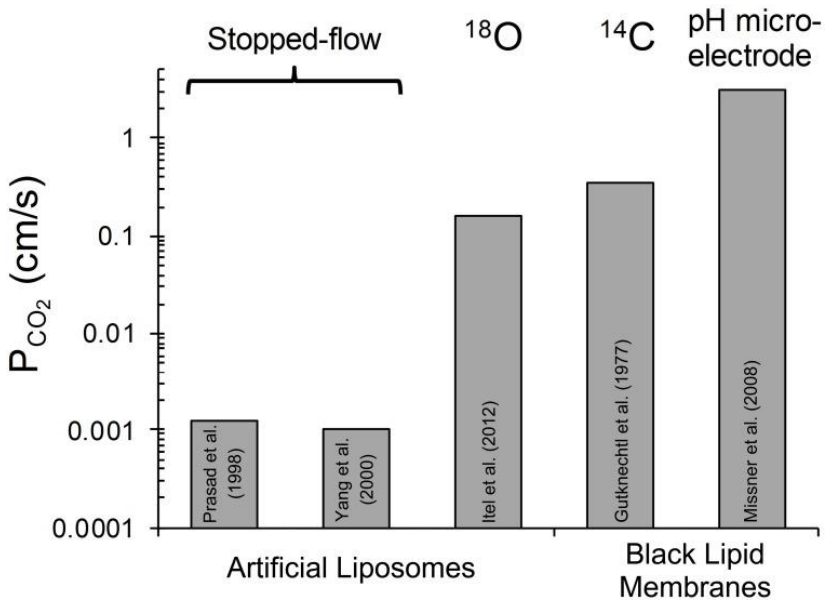

Figure 3.20: Overview of CO_2 permeability determined using various techniques including stopped flow spectrophotometry, ^{18}O isotope exchange and pH microelectrode (Image from Endeward *et al.*, 2013).

The stopped flow method is widely used in the literature to determine CO_2 permeability however it is an indirect measurement of CO_2 permeability as it relies on a change in pH. The cause of such a pH change is difficult to attribute solely to the movement of CO_2 and the following conversion of CO_2 + H_2O to HCO_3^- + H^+. Other ions may be involved and consequently false positive results may be obtained via this method. To date, no ions have been identified as permeating Setaria PIPs, however, to eliminate the movement of protons causing the decrease in intracellular pH we injected the yeast expressing SiPIP2;7 alongside a low pH buffer (Figure 3.12). No change in fluorescence intensity was observed for SiPIP2;7

or hCA only with the low pH buffer, strengthening the case that our results reflect SiPIP2;7 is CO_2 permeable.

Heterologous expression systems are great model systems in which to test individual function of aquaporins. Unfortunately, there are many variables which can influence that function including yeast growth rate, codon usage, expression level and correct localisation to the plasma membrane. In this study, we have measured permeability at the same growth stage and OD, we determined localisation with a GFP tag and used the same strong constitutive promoter for all aquaporins and codon optimised the aquaporins for expression in yeast in efforts to minimise these variables.

A major assumption in measuring CO_2 permeability is the activity of CA as it catalyses the hydration reaction between CO_2 and HCO_3^-. Prasad *et al.* (1998) and Zocher *et al.* (2012) both demonstrated that CA activity must be non-limiting in order to accurately calculate CO_2 permeability. The method of measuring CA activity on a MIMS relies on CO_2 moving into the yeast cell and following the exchange of ^{18}O in the different CO_2 species (Figure 3.2). This movement of CO_2 is influenced by the permeability of the membrane to CO_2, which in turn can be influenced by the presence of aquaporins. But CA activity has been shown to affect CO_2 movement, and thus permeability calculations, as demonstrated by Wang *et al.* (2016), CA expression alone increased the apparent CO_2 permeability to the same extent as AtPIP2;1 alone. The combination of AtPIP2;1 + AtCA4 had a significant increase in CO_2 permeability. Therefore, it was necessary in our study to compare the activity of yeast expressing an empty plasmid, tobacco β-CA or human α-CA (Figure 3.8). The human CA (hCA) was chosen since it had the highest CA activity and was considered to be sufficient to avoid any limitations and allow for complete equilibration between CO_2 and water. Previously published CO_2 permeability papers have used tobacco CA (Ding *et al.*, 2013; Heckwolf *et al.*, 2011; Otto *et al.*, 2010) or bovine CA (Itel *et al.*, 2012; Prasad *et al.*, 1998; Zhao *et al.*, 2017).

The importance of codon optimisation for determining aquaporin function has been demonstrated by Bienert *et al.* (2014) who found different H_2O_2 permeability's in native versus codon optimised sequences. The codon adaptation index (CAI) is a measure of how well the codon usage in a coding DNA sequence matches the bias of a certain host. Protein expression can be increased by having a higher CAI. Bienert *et al.* (2014) increased the CAI of maize PIP sequences from 0.5 to 0.9 by codon optimisation, and was able to detect H_2O_2 permeability in yeast only when the aquaporin sequence was codon optimised. Here, by codon optimising the Setaria PIPs for expression in yeast we increased the CAI averages from

the native sequence of 0.5 to yeast optimised of 0.76. Harmonising the codon usage is also an important consideration to have comparable translation to the native organism (Angov *et al.*, 2011). For *S. italica* PIPs, CAI is around 0.75 which is comparable to the CAI for the optimised sequences we used in yeast. The experiment by Bienert *et al.* (2014) indicates that negative permeability results need to be treated with caution and may not mean the aquaporin is not permeable to that substrate.

In addition to CAI influencing protein expression, our GFP localisation results indicate that there is a range of expression levels between different aquaporins and expression within each culture is not homogeneous, despite being under growth media selection pressure. We hypothesise that this could also influence overall permeability if one aquaporin is highly expressed relative to a lowly expressed aquaporin culture. The lack of GFP expression in every yeast cell, despite being under selection pressure, suggests that the construct may be present but the GFP and the aquaporin may not be folding and expressing correctly, adding another complication to these assays.

3.4.3 Co-expression of PIP1 and PIP2

A significant proportion of the literature characterising aquaporins have identified substrate permeability's for PIP2s, not PIP1s (Groszmann *et al.*, 2016; Yaneff *et al.*, 2015). These negative results for PIP1s are difficult to interpret however, without localisation data (Yaneff *et al.*, 2015). Likewise, our CO_2 permeability data showed no increase in permeability in individual PIP1s relative to our hCA only control which may reflect the failure of PIP1s to correctly localise to the plasma membrane (Figure 3.7). Therefore, to investigate whether permeability of the PIP1s could be improved by correctly targeting to the plasma membrane, PIP1s were co-expressed with selected PIP2s. Aquaporins assemble as tetramers in the membrane and the combination of monomers which form the tetramer can have a significant impact on both the overall permeability and correct localisation to the membrane (Otto *et al.*, 2010; Zelazny *et al.*, 2007). This has been observed widely in the literature with maize PIP1s requiring interaction with PIP2s to be correctly targeted to the plasma membrane. For example, this has been observed in oocytes with co-expression of ZmPIP1;1 with ZmPIP2;1, ZmPIP2;4 or ZmPIP2;5 increasing localisation to the plasma membrane and water permeability (Fetter *et al.*, 2004) and in yeast with co-expression of ZmPIP1;2 with ZmPIP2;5 increasing localisation to the plasma membrane and hydrogen peroxide permeability

(Bienert *et al.*, 2014). An export signal allowing the aquaporin to leave the endoplasmic reticulum and reach the plasma membrane was identified in ZmPIP2s which was absent from ZmPIP1s (Zelazny *et al.*, 2007; Zelazny *et al.*, 2009). This export signal is present in only two of the Setaria PIPs, SiPIP2;4 and SiPIP2;5, and when these PIP2s were co-expressed with the Setaria PIP1s we observed plasma membrane localisation of GFP-labelled SiPIP1;2 and SiPIP1;5 (Figure 3.16).

This improved GFP localisation in some of the PIP1 and PIP2 combinations did not, however, improve CO_2 permeability (Figure 3.17). This may be a result of a conformational change of the aquaporin tetramer, such as observed by Otto *et al.* (2010) when co-expressing NtAQP1 and NtPIP2;1. But since the CO_2 permeability is much lower than the hCA only control this decrease is difficult to interpret. We initially hypothesised it may be due to reduced overall CA activity but this was not observed when CA activity was measured (Figure 3.18). In addition to these unexpected results, AtPIP1;2, AtPIP2;1 and NtAQP1 which were used as positive controls for CO_2 permeability in this study (Heckwolf *et al.*, 2011; Uehlein *et al.*, 2003; Wang *et al.*, 2016), did not show high CO_2 permeability. Again, it is difficult to interpret since GFP localisation showed strong expression and correct localisation to the plasma membrane, CA activity was non-limiting and cell size was not significantly different. Perhaps there weren't sufficient PIPs expressed in the yeast plasma membrane. Nevertheless, we observed significant CO_2 permeability for SiPIP2;7 in two separate experiments (Figure 3.11).

3.4.4 Prediction of CO_2 permeability

Due to the very high sequence identity between SiPIP2;6 and SiPIP2;7 we hypothesised these aquaporins may perform similar roles. However, the result observed in this study showed very different permeability results, with SiPIP2;7 significantly higher in CO_2 permeability than SiPIP2;6 (Figure 3.10). The unique amino acids between these two aquaporins and the other Setaria PIPs were then investigated and we found no difference in key residues involved in gating, substrate specificity or dimerization (Groszmann *et al.*, 2016). Specifically, amino acids involved in gating by phosphorylation such as S123 in loop B and S281 in the C-terminus or gating by pH at H201 in loop D do not differ between SiPIP2;6 and SiPIP2;7. Amino acids which are involved in stabilising loop B and D (Frick *et al.*, 2013) and those involved in stabilising tetramer formation (Yoo *et al.*, 2016) are also identical between SiPIP2;6 and SiPIP2;7. A number of studies have indicated conductance of CO_2 and ions occurs though the

central pore of the aquaporin tetramer (Kruse *et al.*, 2006; Otto *et al.*, 2010). The key residues thought to line the central pore of the aquaporin tetramer are indicated in blue in Figure 3.13 (Yu *et al.*, 2006) and are identical between SiPIP2;6 and SiPIP2;7. Overall these results suggest that V19A and A165T are likely amino acid changes which do not affect the aquaporin structure but may alter substrate permeability to CO_2.

3.4.5 Translating into the field: CO_2 permeability of sorghum aquaporins

As an alternative for predicting permeability based on *in silico* analysis, we selected sorghum aquaporins based on aquaporin genes co-locating with QTLs for putative photosynthetic traits to test for CO_2 permeability. This approach screens thousands of sorghum genotypes to identify single nucleotide polymorphisms (SNPs) in genes and using association mapping are plotted against known QTLs of photosynthetic traits. Association mapping has been used previously to identify QTLs involved in sorghum seed dormancy (Li *et al.*, 2016) and flowering time (Mace *et al.*, 2013a). This link identified between photosynthetic traits and aquaporins is exciting and may indicate domestication of sorghum has been inadvertently selecting for aquaporins. One of the selected sorghum aquaporins in this study, *SbPIP1;6*, has previously been hypothesised as a possible CO_2 permeable aquaporin based on expression data when compared to drought stressed sorghum (Hasan *et al.*, 2017). High transcript expression in the morning coupled with low intercellular CO_2 concentrations and high photosynthetic rates were used to suggest a role for *SbPIP1;6* in photosynthesis and CO_2 transport. For a C_4 plant it would be expected that a CO_2 permeable aquaporin involved in photosynthesis would localise to the mesophyll plasma membrane. In Döring *et al.* (2016), cell specific expression was examined for the sorghum PIPs and both *SbPIP1;6* and *SbPIP2;6* had higher transcript expression in the mesophyll cell compared to the bundle sheath. In our study, we found no significant difference in CO_2 permeability between the Sorghum PIPs and hCA only control (Figure 3.19). These sorghum aquaporin genes co-locating with selected QTLs may instead be important for plant performance due to water permeability, rather than CO_2. Indeed, Kadam *et al.* (2017) hypothesised that a number of these aquaporins (*SbPIP2;6, SbPIP2;7* and *SbTIP5;1*) may contribute to improved sorghum performance under waterlogged stress conditions based on transcript abundance and contrasting patterns in tolerant and sensitive sorghum genotypes. This finding also supports the notion discussed in Chapter 2 that identifying novel CO_2 permeable aquaporins is not trivial.

3.4.6 Conclusions

Using yeast as a heterologous expression system I have measured CO_2 permeability of Setaria PIPs and investigated the effect of co-expressing PIP1 and PIP2s together. When comparing directly to the hCA only control we found SiPIP2;7 showed significantly higher CO_2 permeability. Although since not all PIPs correctly localised to the plasma membrane there may be more Setaria PIPs which are CO_2 permeable. I have also endeavoured to overcome and explain some of the limitations inherent in measuring CO_2 permeability.

Future studies would be best placed examining the *in planta* function of *SiPIP2;7* either through overexpression or knock out approaches to validate the high CO_2 permeability observed here using yeast. Transgenic expression in a C_3 plant which is easily transformed such as tobacco or Arabidopsis would be an excellent proof of concept study with the ultimate goal to examine the effect of *SiPIP2;7* in the C_4 photosynthetic system of Setaria. In the next Chapter, I investigate the *in planta* effect of overexpressing the CO_2 permeable PIP from Arabidopsis, *AtPIP1;2* in *S. viridis*.

CHAPTER 4: MODIFYING AQUAPORIN EXPRESSION *IN PLANTA*

4.1 Introduction

The role of CO_2 permeable aquaporins *in planta* has largely been explored through manipulation of PIP (plasma membrane intrinsic protein) expression in C_3 photosynthetic plants (as described in Chapter 1). Overexpression of known CO_2 permeable aquaporins have resulted in increased mesophyll CO_2 conductance (g_m), net photosynthetic rates and stomatal conductance (g_s) in a range of C_3 plants overexpressing either NtAQP1 in tobacco (Flexas *et al.*, 2006; Sade *et al.*, 2010), McMIPB in tobacco (Kawase *et al.*, 2013) or HvPIP2;1 in rice (Hanba *et al.*, 2004). Conversely, knockout approaches have demonstrated negative photosynthetic effects. For instance, a T-DNA insertion mutant in *AtPIP1;2* in Arabidopsis decreased g_m approximately 40% (Heckwolf *et al.*, 2011), and RNAi mediated suppression of *NtAQP1* expression (Uehlein *et al.*, 2008) and *NtAQP1* antisense (Flexas *et al.*, 2006) studies in tobacco resulted in decreased g_s and g_m as well as reduced net photosynthetic rates.

There are very few studies investigating the presence of CO_2 permeable aquaporins in C_4 species, despite the importance of optimal CO_2 transport in leaf mesophyll cells for maintaining high photosynthetic rates. The possible role of CO_2 permeable aquaporins in C_4 photosynthesis has been suggested in multiple review papers (Groszmann *et al.*, 2016; Kaldenhoff, 2012; Weber and von Caemmerer, 2010). A comparative transcriptomic study has suggested the presence of CO_2 permeable aquaporins specific to C_4 plants with a transcript encoding a putative CO_2 permeable aquaporin observed to be 20-fold higher in the C_4 leaf, *Cleome gynandra,* compared to the C_3 species, *Cleome spinosa* (Bräutigam *et al.*, 2011). There is one *in vitro* study which identified maize ZmPIP1;5 and ZmPIP1;6 as CO_2 permeable aquaporins in yeast (Heinen *et al.*, 2014) and based on expression profiles were suggested to play a role in stomatal closure. Lastly, a transcriptomic study comparing the expression of aquaporins *PIP1;5* and *PIP1;6* in two C_4 species, maize and sorghum, under drought stress suggested that PIP1;6 may play a putative role in CO_2 transport (Hasan *et al.*, 2017).

In C_4 photosynthesis, the primary enzyme of CO_2 fixation, PEPC, is located in the mesophyll cytosol. Mesophyll conductance, g_m, describes the flux of CO_2 from the intercellular airspace to its site of fixation, which defers between C_3 and C_4 photosynthetic systems and therefore impacts on how g_m is measured in the different plants (as described in Chapter 1). In C_3 photosynthesis CO_2 is fixed in the chloroplast by Rubisco and g_m can be measured easily be a number of different techniques. Whereas for C_4 plants CO_2 must be converted to HCO_3^- and then be fixed by PEPC in the mesophyll cytosol and g_m is more complex to measure.

In C_4 plants, CO_2 permeable aquaporins are predicted to be highly expressed predominately in the mesophyll plasma membrane. This is due, firstly, to the high photosynthetic rates typical of C_4 plants, which require high g_m and secondly, presence on the bundle sheath membranes would likely reduce the efficiency of the CO_2 concentrating mechanism by facilitating CO_2 leakage out of this compartment.

The aim of this study was to overexpress a known CO_2 permeable aquaporin in mesophyll cells of the model C_4 grass *S. viridis*. The Arabidopsis aquaporin *AtPIP1;2* was chosen as the CO_2 permeable aquaporin transgene to overexpress in *S. viridis* as it has been demonstrated to be CO_2 permeable in a yeast expression system and, importantly, was not water permeable (Heckwolf *et al.*, 2011). CO_2 permeability has also been confirmed *in planta* with Arabidopsis *AtPIP1;2* T-DNA insertion lines using mesophyll cells and a scanning pH microelectrode (Uehlein *et al.*, 2012) or isolated chloroplasts and an ^{18}O isotope exchange approach (Tolleter *et al.*, 2017). The *in planta* effects of modified *AtPIP1;2* expression were examined in Arabidopsis by Heckwolf *et al.* (2011) and showed differences in g_m and photosynthetic activity. The role of this aquaporin was further investigated in a transcriptomic study in Arabidopsis *AtPIP1;2* T-DNA insertion lines which compared the transcriptomic profile to wild type Arabidopsis plants grown under drought stress or low CO_2 conditions (Boudichevskaia *et al.*, 2015). The findings of this research (Boudichevskaia *et al.*, 2015), support the experimental evidence that the physiological function of AtPIP1;2 is not to facilitate water transport but to allow CO_2 diffusion.

Our hypothesis was that mesophyll conductance, and possibly CO_2 assimilation rate, in *S. viridis* would increase if correct localisation to the mesophyll plasma membrane of AtPIP1;2 occurred. In this chapter, molecular, biochemical and physiological analysis of these transgenic plants is described.

4.2 Methods

4.2.1 Construct generation

The coding sequence of *Arabidopsis thaliana* PIP1;2 (*AT2G45960.3*), *AtPIP1;2*, was synthesised by Genescript (US) including CACC motif at the 3' end for directional cloning, an AcV5 epitope tag (Lawrence et al., 2003) and GFP at the 5' end. The entry vector (pT64; kindly provided by Vivian Rolland) and *AtPIP1;2* were digested with SalI and NcoI, ligated using T4 DNA ligase (NEB) and transformed into chemically competent *E. coli* Top10 cells following the manufacturer's instructions and as described previously in Section 3.2.2.

A gateway LR recombination reaction using LR Clonase (Invitrogen) was performed to transform the gene from the entry vector, pT64/*AtPIP1;2*, into the destination overexpression vector, pSC110. pSC110 was created by Gibson Assembly (Gibson et al., 2009) from two modified pMDC164 vectors (Curtis and Grossniklaus, 2003), kindly provided to us by Udo Gowik (Heinrich-Heine University, Dusseldorf). *AtPIP1;2* expression from pSC110 was driven by the B73 *ZmPEPC* promoter (Figure 4.1A). pSC110/*AtPIP1;2* was verified by sequencing. For transient expression a different destination vector, pMDC32 (kindly provided by Vivian Rolland) was used instead, this construct contained a 2 x 35S promoter (Figure 4.1B).

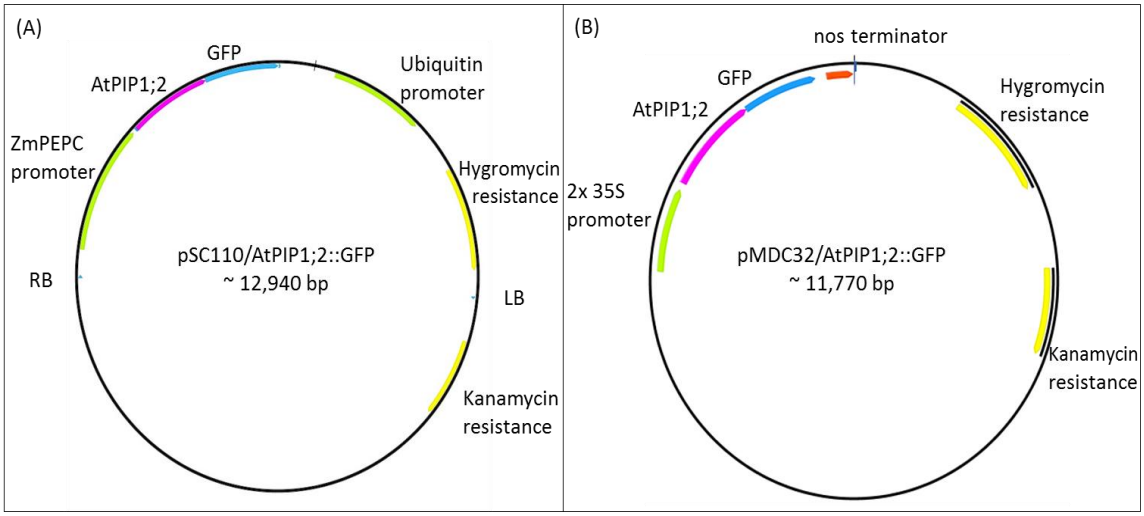

Figure 4.1: Simplified construct map for expression of AtPIP1;2 + GFP. (A) pSC110/AtPIP1;2 + GFP was used for stable transformation of *S. viridis*. The ZmPEPC promoter targets expression of the insert to the mesophyll cells. RB and LB stand for right and left border. (B) pMDC32/AtPIP1;2 + GFP was used for transient expression in tobacco protoplasts.

4.2.2 Transient expression of AtPIP1;2

The plasmid, pMDC32/*AtPIP1;2*, was transformed into *Agrobacterium tumefaciens* strain AGL1 using a freeze thaw method. Competent agrobacterium cells and 5 µL of miniprep of pMDC32/*AtPIP1;2* were placed on ice for 5 min, then in liquid nitrogen for a further 5 min and 37 °C for 5 min. 1 mL of luria broth (LB) was added to the cells and incubated at room temperature for 2 – 4 h on a rocking table. The transformation mix was then spread on LB agar plates with the appropriate antibiotic and grown at 28 °C for 2 days. The agrobacterium solution containing pMDC32/*AtPIP1;2* and P19, an RNA-silencing inhibitor which enhances the expression of transgenes (Shah *et al.*, 2013), was then infiltrated into a young *Nicotiana benthamiana* (tobacco) leaf.

Tobacco plants were grown for approximately 5 weeks as described by Rolland *et al.* (2016) in a CONVIRON growth chamber under 16 h day/ 8 h night cycle with a light intensity of 350 – 400 µmol photons m^{-2} s^{-1}. Two days post infiltration protoplasts were made as described in Breuers *et al.* (2012). Briefly, an infiltrated leaf was cut into small pieces and incubated for 1 h at room temperature in a cell wall digestion solution (0.4 M mannitol, 20 mM KCl, 10 mM $CaCl_2$, 0.1% (w/v) BSA, 20 mM MES pH 5.6 and enzymes: 1.5% (w/v) cellulose, 0.4% (w/v) macerozyme). This solution was then put on ice and allowed to settle, the supernatant was removed and replaced with cell wall digestion solution containing no enzymes. Protoplasts were then imaged on a Zeiss 780 confocal microscope at the Centre for Advanced Microscopy at the Australian National University.

4.2.3 Setaria transformation

Stable *S. viridis* transformation was in its infancy when I started my PhD (early 2014), therefore the Setaria transformation was outsourced to Joyce van Eck at the Boyce Thompson Institute at Cornell University, USA. The plasmid pSC110/*AtPIP1;2* was transformed into agrobacterium (AGL1) and then into *S. viridis* (accession A10.1).

From the transformation, 27 independent lines were generated and 7 independent lines of the T_1 plants, and subsequent T_2 plants were genotyped prior to experiments using primers against the *hygromycin phosphotransferase* gene (Table 4.2). A crude genomic DNA extraction was used (Edwards *et al.*, 1991). The progeny of a plant which went through the *S. viridis* transformation process and tested negative for the *hygromycin phosphotransferase* gene were used as null controls.

4.2.4 Setaria growth conditions

S. viridis seeds were incubated in 50% (v/v) liquid smoke (Wrights) for 30 min to promote germination, sterilised in 10% (v/v) bleach and 0.1% (v/v) Tween 20 and treated with the fungicide Thiram. The seeds were then germinated in garden soil mix fertilised with 7 g L^{-1} Osmocote (Scotts, Australia) in small containers before being transferred to individual 2 L pots. Plants were grown in a quarantine glasshouse between January and March (Canberra, Australia). The room was set to 28 °C day, 24 °C night and pots were watered daily.

4.2.5 Insertion number estimation by qRT-PCR

Leaf sections (2 cm in length) were collected from a fully expanded leaf of 5 week old *S. viridis* plants and frozen in liquid nitrogen. Leaves were then freeze dried for 48 h. This material was sent to IDNA genetics (United Kingdom) to estimate the number of transgene copies based on the number of copies of the *hygromycin phosphotransferase* reporter gene (Bartlett *et al.*, 2008). Briefly, DNA was isolated using a CTAB extraction buffer (2% (v/v) CTAB, 20 mM Tris-HCl pH 8, 1.4 M NaCl, 20 mM EDTA, 1% (w/v) PVP-40, 0.2% (v/v) β-mercaptoethanol) followed by extraction with phenol/chloroform/isoamylalcohol (25:24:1) and ethanol clean-up. DNA quality and quantity was determined using a NanoDrop spectrophotometer (Thermo Scientific). Quantitative real time PCR (qRT-PCR) was then performed and the *hygromycin phosphotransferase* gene (with a FAM reporter) and the internal positive control (IPC, with a VIC reporter) were amplified together in a multiplex reaction (15 min denaturation, then 40 cycles of 15 sec at 95 °C and 60 sec at 60 °C) in an ABI1900 real-time PCR machine. Fluorescence from the FAM and VIC fluorochromes was measured during each 60 °C step and the Ct values obtained. The difference between the Ct values for the *hygromycin phosphotransferase* gene and the IPC (the Delta Ct) was used to allocate the assayed samples into groups with the same gene copy number.

4.2.6 Microscopy

The uppermost, fully expanded leaf of 5 week old *S. viridis* plants were collected for GFP localisation and lightly fixed to meet Australian quarantine regulations. The leaf was cut into sections (10 mm x 5 mm) with a razor blade directly in the fixative solution (4% (w/v) paraformalydehyde, 0.2% (v/v) glutaraldehyde in 25 mM sodium phosphate buffer, pH 7.2). Leaf sections were allowed to sink into the fixative solution with 0.01% (v/v) Tween 20 using a speed vacuum concentrator for 1 h. The leaves which sunk were then transferred to fresh fixative solution and incubated for 4 h at room temperature. Sections were then rinsed in 25

mM phosphate buffer four times over 1 h. Very thin sections were then cut using a razor blade. Sections were mounted in 50% (v/v) glycerol and were viewed under x25 magnification using water on a Zeiss 780 confocal at the Centre for Advanced Microscopy at the Australian National University. Settings for fluorescence detection were channel 1 (ChS1) excitation 488 nm and emission 530 nm with a digital gain 750.

4.2.7 Determination of enzyme activities

For carbonic anhydrase activity, protein was extracted from frozen leaf discs (0.49 cm^2) collected from the uppermost, fully expanded leaf of 5 week old *S. viridis* plants. Soluble protein was extracted by grinding one frozen leaf disc in ice cold glass homogenizers (Tenbroek) in 500 µL of extraction buffer (50 mM HEPES, pH 7.8, 1% (w/v) polyvinylpyrrolidone, 1 mM EDTA, 10 mM dithiothreitol, 0.1% (v/v) Triton X-100, 2% (v/v) protease inhibitor cocktail (Sigma)). The crude extracts were centrifuged at 4 °C for 1 min at 13,000 x *g* and the supernatant collected for the soluble CA assay. Activity was measured on a membrane inlet mass spectrometer to measure the rates of ^{18}O exchange from labelled $^{13}C^{18}O_2$ to $H_2{}^{16}O$ at 25 °C (Badger and Price, 1989; von Caemmerer et al., 2004). The hydration rates were calculated as described by Jenkins et al. (1989).

The activities of Rubisco and PEPC were measured using a spectrophotometric technique as described previously (Pengelly et al., 2012; Sharwood et al., 2016). Buffers required for these assays are outlined in Table 4.1. Frozen leaf discs (0.49 cm^2) were ground in acid washed sand in a mortar and pestle in 490 µL of extraction buffer and 10 µL of protease inhibitor (Sigma). Crude extracts were centrifuged at 4 °C for 1 min at 13,000 x *g* and the supernatant collected for the assays. For Rubisco activity, 10 µL of leaf extract was combined with 485 µL of assay buffer and the reaction was initiated by adding 5 µl of 26.6 mM RuBP. For PEPC activity, 10 µL of leaf extract was combined with 485 µL of assay buffer and the reaction initiated by adding 10 µL of 400 mM PEP. Enzyme activities were determined spectrophotometrically (Agilent) by monitoring the decrease of NADH absorbance over time at 340 nm after initiation of the reaction.

Table 4.1: Buffers used for determination of Rubisco and PEPC activity.

Media	**Components**
Extraction buffer	50 mM HEPES-NaOH pH 7.8, 1 mM EDTA, 0.1% (v/v) Triton-X
Rubisco assay buffer	100 mM EPPS-NaOH pH 8, 20 mM $MgCl_2$, 1 mM EDTA, 1 mM ATP, 5 mM phosphocreatine, 20 mM $NaHCO_3$, 0.2 mM NADH, 50 U mL^{-1} creatine phosphokinase, 0.2 mg carbonic anhydrase, 50 U mL^{-1} 3-phosphoglycerate kinase, 40 U mL^{-1} glyceraldehyde-3-phosphate dehydrogenase, 113 U mL^{-1} Triose-phosphate isomerase, 39 U mL^{-1} glycerol 3 phosphate dehydrogenase
PEPC assay buffer	100 mM EPPS-NaOH pH 8, 20 mM $MgCl_2$, 1 mM EDTA, 1 mM $NaHCO_3$, 0.2 mM NADH, 5 mM glucose-6-phosphate, 1 U mL^{-1} malate dehydrogenase

4.2.8 Gas exchange measurements

Net photosynthesis (*A*) was measured over a range of intercellular pCO_2 (C_i) on the uppermost, fully expanded leaf of 5 week old *S. viridis* T_2 plants using a portable gas exchange system LI-COR 6400XT (LI-COR Biosciences). Measurements were made after leaves had equilibrated at 380 µbar, flow rate 500 µmol s^{-1}, leaf temperature 25 °C and irradiance 1500 µmol photons m^{-2} s^{-1}. CO_2 response curves were measured in a stepwise increase (3 min intervals) in CO_2 partial pressure 380, 0, 23.75, 47.5, 71.25, 95, 142.5, 190, 285, 380, 570, 760, 950 µbar whilst maintaining leaf temperature and irradiance conditions. Note the average atmospheric pressure in Canberra, Australia is 953 mbar.

4.2.9 RNA extraction and reverse transcriptase quantitative PCR (RT-qPCR)

Frozen leaf discs (0.49 cm^2) collected from the uppermost, fully expanded leaf of 5 week old *S. viridis* plants and stored at -80 °C were ground to a fine powder using the Qiagen TissueLyser II. RNA was extracted using the Trizol extraction method and in the presence of RNase inhibitor (Ambion). DNA was removed using the TURBO DNA free kit (Ambion) and RNA quantity and quality were determined using a NanoDrop (Thermo Scientific).

RNA (200 ng) were reverse transcribed into cDNA using Qiagen's RT^2 HT First Strand cDNA synthesis kit. RT-qPCR and melt curve analysis were performed on a Viia7 Real-time PCR system using the Power SYBR green PCR Master Mix (Thermo fisher) according to the

manufacturer's instructions. Primers were designed using Primer3 in Geneious R7.1.6, ensuring products spanned an intron (Table 4.2). Primer amplification efficiencies were determined by Ct slope method, efficiencies for all primer pairs were comparable (~95%) and no amplification was detected in the no template control. Relative fold-change was calculated by the ΔΔCt method, using the average of three nulls as reference, as described by Livak and Schmittgen (2001). The geometric mean of the Ct values for three reference genes was used for normalisation (Vandesompele *et al.*, 2002).

Table 4.2: List of primers used for RT-qPCR and genotyping.

Gene	**Description**	**Sequence 5' - 3'**	**Size (bp)**	**Use**
Sevir.1G288000	*Ubiquitin*	F: GATCTCCGCCCCAGCAAGAT	124	RT-qPCR reference gene
		R: ATGCCCTCCTTGTCCTGGAT		
Sevir.3G271600	*Elongation factor 1a*	F: GCTGCAACAAGATGGATGCC	132	RT-qPCR reference gene
		R: CCAGAGATTGGGACGAAGGC		
Sevir.9G067700	*Beta tubulin*	F: CTAAAGCTCGCCACCCCTAC	104	RT-qPCR reference gene
		R: GTCGGAGTTGAGCTGACCAG		
Sevir.2G245200	*β-CA*	F: AGATGATTCAACCTCTGGAAGCT	110	RT-qPCR
		R: TTGCACTGCATTTCAAAACTCA		
Sevir.5G247900	*β-CA*	F: AGGCCGACAAGTTCCACTTC	102	RT-qPCR
		R: CATTGGTCCTCGAAAGCAGC		
Sevir.5G248000	*β-CA*	F: GGCTGGGTTCAGGACGTTTA	112	RT-qPCR
		R: AGAGTCAGAGCACGCAAACA		
Sevir.5G247800	*β-CA*	F: CATAAATTCCCCCGCCTCGT	101	RT-qPCR
		R: CTCTTCAAGCGCTCGACGG		
Sevir.1G269400	*SvPIP1;2*	F: CCTCTCTTCACGACTGCTGC	133	RT-qPCR
		R: CTGGACGGGAACTCTTGCAA		
Sevir.1G378900	*SvPIP1;5*	F: CTGGATCTTCTGGGTTGGCC	135	RT-qPCR
		R: TGATGCATTGGTGGTTTGCT		
Sevir.2G128000	*SvPIP2;1*	F: CGGCGTTCTACCACCAGTAC	142	RT-qPCR
		R: CCATTGCTTCAACACGCACA		
Sevir.2G302500	*SvPIP2;8*	F: CGGCGAGAGAAGCTTTTGGA	123	RT-qPCR
		R: CATGCAAGGATCTGCTAGCTG		
	Hygromycin phosphotransferase	F: TGGCGTGATTTCATATGCGC	420	Genotyping
		R: CGTCAACCAAGCTCTGATAG		

4.3 Results

4.3.1 GFP localisation in a transient expression system

To test the construct and confirm AtPIP1;2 + GFP would correctly target to the plasma membrane I cloned the insert into pMDC32 for transient expression in tobacco protoplasts. Figure 4.2A shows GFP localisation to the plasma membrane of a tobacco protoplast as expected, whereas the wild type tobacco protoplast shows no GFP.

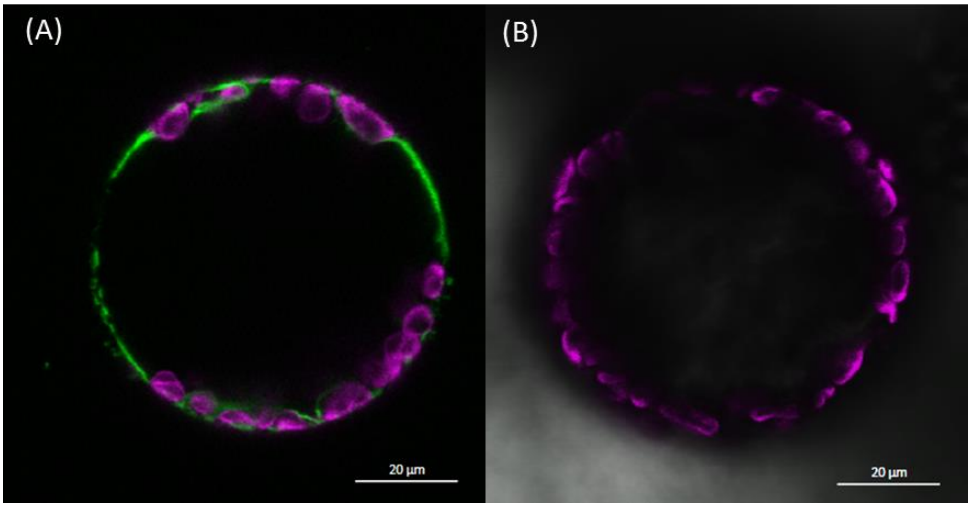

Figure 4.2: GFP localisation of *AtPIP1;2* transient expression. (A) Transient expression of pMDC32/*AtPIP1;2* + GFP in tobacco protoplast. (B) Wild type tobacco protoplast. Autofluorescence of chloroplasts are shown in magenta. Images were taken on a Zeiss 780 confocal microscope, scale bar corresponds to 20 µm.

4.3.2 Summary of AtPIP1;2 overexpression lines

The 27 independent lines of *S. viridis* expressing pSC110/*AtPIP1;2* were generated by the Boyce Thompson Institute at Cornell University, USA. Due to Australian quarantine requirements transgenic seeds must be grown in authorised quarantine facilities and, following approval, the seeds of that plant may then be released and subject to PC2 requirements. The 7 lines of T_0 seeds were grown in quarantine facilities for release (Table 4.3). 10 plants per line were initially germinated, though there was a poor survival rate in some lines. These T_1 plants were genotyped to check for the presence of the *hygromycin phosphotransferase* gene (see Table 4.2 for primers) and then samples from positive lines were sent away to be analysed by qRT-PCR to estimate the number of insertions, based on the number of copies of the *hygromycin phosphotransferase* gene (Table 4.3). Between 1 and

10 hygromycin inserts were detected. Unfortunately these plants did not pass the quarantine guidelines for release as they were infected with an unclassifiable fungal pathogen but seeds could be harvested before the plants were destroyed (T_1 seeds).

Table 4.3: Summary of pSC110/*AtPIP1;2* transformed *S. viridis* plants. T_1 plants were genotyped (PCR) to check for hygromycin resistance (✓) or not (X), and the number of hygromycin inserts (#) was detected by qRT-PCR.

T_0 line		**T_1 plant**									
		-1	-2	-3	-4	-5	-6	-7	-8	-9	-10
AtPIP1;2 -1	PCR	✓		X							
	# inserts	2									
AtPIP1;2 -2	PCR	✓	✓		✓	✓	✓	✓	✓		
	# inserts	2	1		1	1	2	1	1		
AtPIP1;2 -3	PCR		✓	✓	✓	✓	X	X	✓	✓	✓
	# inserts		10	5	10	5			5	5	10
AtPIP1;2 -4	PCR	X	X	X	✓	X	X	X	X	X	X
	# inserts				1						
AtPIP1;2 -6	PCR	X	✓		✓	✓	✓	✓	✓		
	# inserts		2		2	4	4	4	4		
AtPIP1;2 -7	PCR	X	✓	X	X	X			X	X	X
	# inserts		3								
AtPIP1;2 -8	PCR	✓		X	✓		✓		✓		✓
	# inserts	1			1		1		2		2

From the T_1 seeds, 4 lines were selected to be grown again under quarantine conditions (Table 4.4). AtPIP1;2 -8 -1, AtPIP1;2 -6 -8, AtPIP1;2 -3 -4 and AtPIP1;2 -2 -7 were selected as they were from different transformation events and had different numbers of hygromycin inserts. AtPIP1;2 -8 -3 which tested negative for the hygromycin insert was used as the null control. Unfortunately, again, these T_2 plants did not pass the quarantine guidelines for release as they were infected with an unknown bacterial strain.

The number of hygromycin inserts in these T_2 plants varied between each line from 1 – 12 (Table 4.4). In summary, the T_1 plant AtPIP1;2 -8 -1 had 1 insert and its progeny (T_2) also had a single insertion, indicating T_2 plants AtPIP1;2 -8 -1 -2 and -4 are most likely heterozygous with a single allele carrying the insert. Line AtPIP1;2 -6 -8 had 4 insertions in the T_1 generation and its progeny also had 4 insertions, indicating several linked insertions at the same locus.

The same complex insertion pattern was observed for T_1 plant AtPIP1;2 -3 -4 with 10 insertions and then 12 insertions identified in the T_2 generation. AtPIP1;2 -2 -7 had a single insertion and two plants in the T_2 generation (AtPIP1;2 -2 -7 -1 and -2) had 2 insertions indicating homozygosity with both alleles carrying the insert and one plant AtPIP1;2 -2 -7 -7 with a single insertion indicating this plant is heterozygous.

Table 4.4: Summary of T_2 plants transformed with pSC110/*AtPIP1;2*. T_2 plants were genotyped (PCR) to check for hygromycin resistance (✓) or not (X), and the number of hygromycin inserts (#) was detected by qRT-PCR.

T_1 plant		**T_2 plant**						
		-1	-2	-3	-4	-5	-6	-7
AtPIP1;2 -2 -7	PCR	✓	✓	X	X	X	X	✓
	# inserts	2	2					1
AtPIP1;2 -3 -4	PCR	✓	✓	✓	✓	✓	✓	✓
	# inserts	12	12	12	12	12	12	12
AtPIP1;2 -6 -8	PCR	✓	✓	✓	✓	✓	✓	
	# inserts	4	4	4	4	4	4	
AtPIP1;2 -8 -1	PCR	X	✓	X	✓			
	# inserts		1		1			
AtPIP1;2 -8 -3	PCR	X	X	X	X	X	X	X
	# inserts							

4.3.3 Gas exchange results

The response of CO_2 assimilation rate (A) to increasing intercellular pCO_2 (C_i) was investigated in the pSC110/*AtPIP1;2* T_2 lines. There was no difference in the AC_i curves of T_2 plants in lines 8-1, 3-4 or 2-7 in comparison to the null plants (n = 6). However, a difference was observed between T_2 plants from line 6-8 and the nulls at both low pCO_2 (initial slope) and at high pCO_2. Significantly lower initial slopes were observed in the five T_2 plants analysed in the 6-8 line (Figure 4.3 and Figure 4.4). No difference in stomatal conductance was observed (not shown).

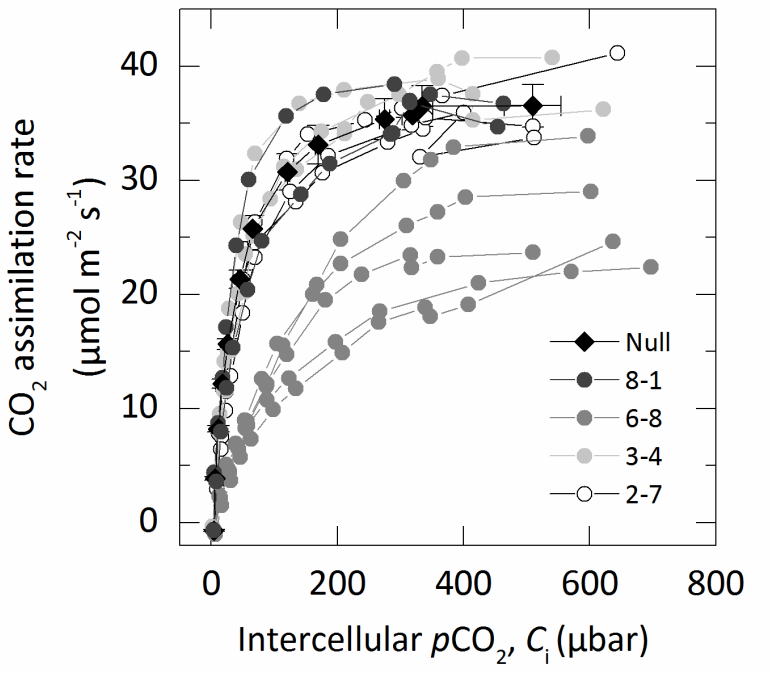

Figure 4.3: CO_2 assimilation rate over a range of intercellular pCO_2 (C_i). T_2 plants from each line were measured and an average of 6 nulls with standard error are shown. Plants were grown in glasshouse conditions over January – March, Canberra, Australia. The uppermost, fully expanded leaf of 5 week old plants were measured using a LI-6400XT at 25 °C leaf temperature and an irradiance of 1500 µmol photons m^{-2} s^{-1}.

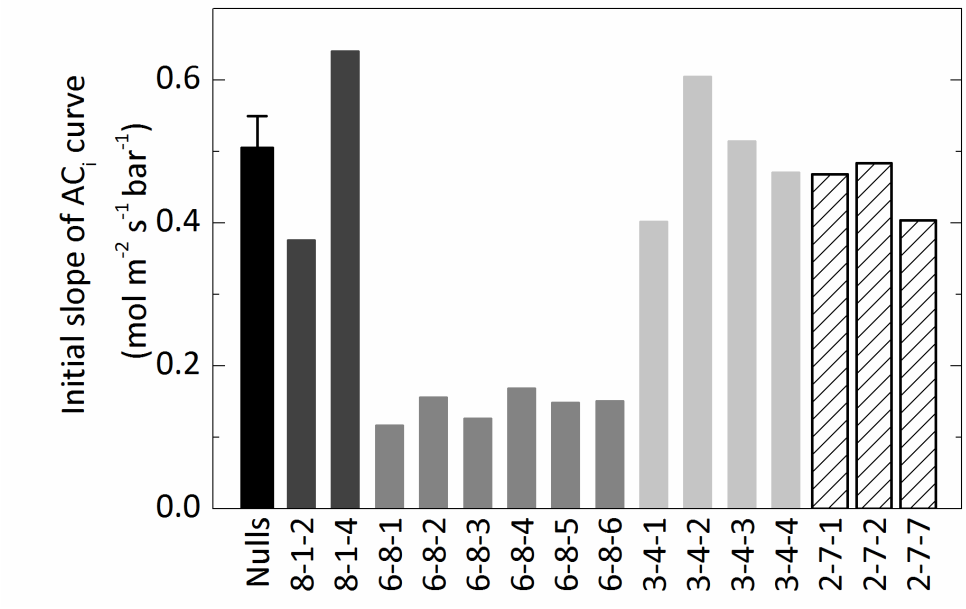

Figure 4.4: Initial slope of AC_i curve (Figure 4.3) of pSC110/*AtPIP1;2* T_2 plants. The average for the nulls is shown with standard error bar (n = 6).

4.3.4 Photosynthetic enzyme activities

Key C_4 photosynthetic enzyme activities were measured and compared to an average of four null plants. There was a significant reduction in CA activity (~93%) in the T_2 plants of line 6-8 comparative to the nulls (Figure 4.5A). CA hydration rate in the null plants was 625 ± 37 µmol m^{-2} s^{-1} as calculated at mesophyll pCO_2 (C_m) of 140 µbar (See Chapter 5 and Osborn *et al.*, 2016). There was no difference in Rubisco (Figure 4.5B) or PEPC (Figure 4.5C) activities across the different lines 8-1, 6-8, 3-4 or 2-7. Average Rubisco activity in the null plants was 18.7 ± 1.2 µmol CO_2 m^{-2} s^{-1} and the average PEPC activity was 235 ± 37 µmol CO_2 m^{-2} s^{-1}. This measured Rubisco activity does not match the *in vivo* apparent Rubisco activity (V_{cmax}) determined from the gas exchange data. We hypothesise this may be due to the difficulties of grinding C_4 leaf material and sufficiently breaking open the bundle sheath cells where Rubisco is localised.

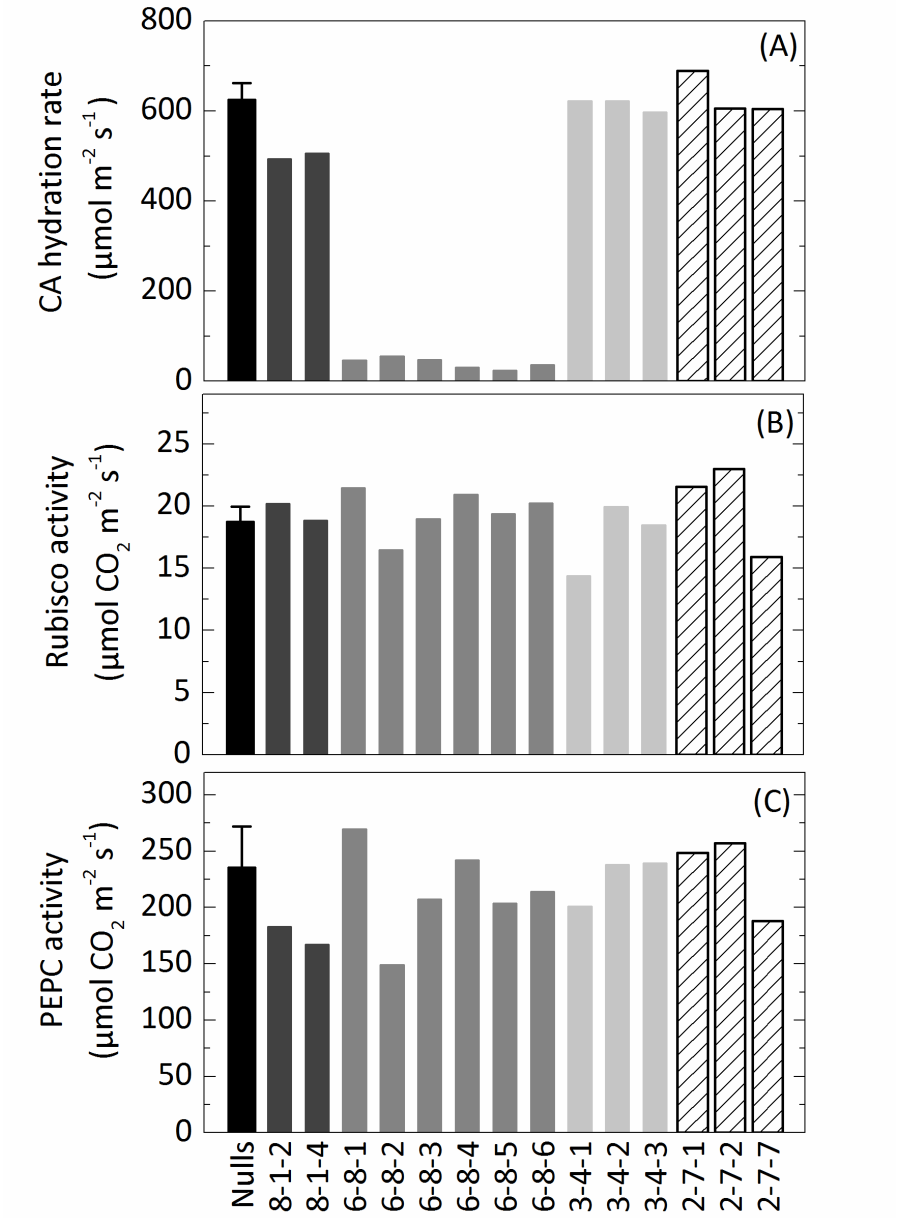

Figure 4.5: Enzyme activities in the null control plants and pSC110/*AtPIP1;2* T_2 plants in lines 8-1, 6-8, 3-4 and 2-7. (A) Range of CA hydration rates at mesophyll pCO_2 (C_m) as measured using a membrane inlet mass spectrometer. (B) Rubisco and (C) PEPC activities measured spectrophotometrically. Average null controls, n=4; error bars represent SE.

4.3.5 GFP localisation in transformed leaves

The construct pSC110 has a *ZmPEPC* promoter which was chosen to target expression of the CO_2 permeable aquaporin, *AtPIP1;2* with GFP fused to the C-terminus, specifically to the mesophyll cells. To confirm this localisation, hand sections of lightly fixed leaf tissue were examined for GFP expression (Figure 4.6). No GFP was detected in any of transformed lines AtPIP1;2- 8-1-2 (D – F), 6-8-1 (G – I), 3-4-1 (J – L) or 2-7-1 (M – O).

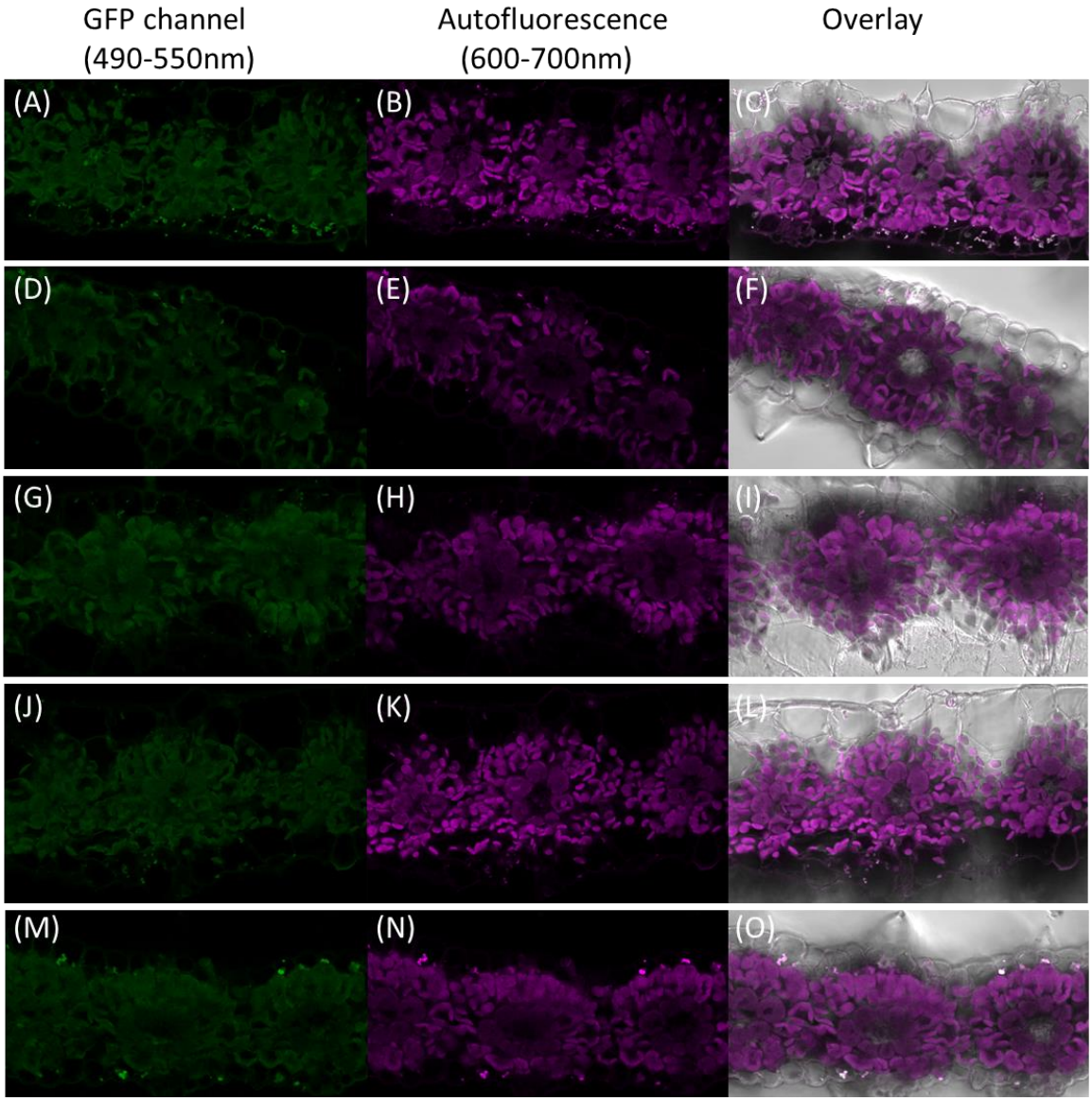

Figure 4.6: Lightly fixed, hand cut transverse sections of a fully expanded young healthy leaf from T_2 *AtPIP1;2* + GFP overexpression plants. (A – C) Null, (D – F) 8-1-2, (G – I) 6-8-1, (J – L) 3-4-1, (M – O) 2-7-1. False colour was added to show fluorescence at expected GFP emission (green), auto fluorescence of chloroplasts (magenta) and these are overlayed with a bright field image. Images were taken on a Zeiss 780 confocal microscope using x25 magnification.

4.3.6 Characterisation of inserts

Despite the presence of the selectable marker in the transgenic plants, no GFP fluorescence could be detected in leaf sections (Figure 4.6). One possible explanation is a problem with transcription or translation of the construct. To test the integrity of the insertion, I tried to amplify the complete insert from genomic DNA using different combinations of primers that annealed to different parts of the insert. Figure 4.7 illustrates that only partial fragments of the insert could be amplified in the transformed lines but the positive plasmid control, pSC110/*AtPIP1;2*, could be successfully amplified with all primer combinations. This suggests that there has not been insertion of the complete transgene during the transformation process but rather multiple, truncated insertions or rearrangements occurred. Each T_2 plant, 8-1-4, 6-8-3, 3-4-2 and 2-7-1, amplified the same partial products from the different primer combinations (T_2 plant in Figure 4.7). This suggests that the rearrangement occurred in the agrobacterium stage, however as samples of the agrobacterium used for transformation were not available, I could not determine absolutely whether the rearrangement occurred before or during transgene integration.

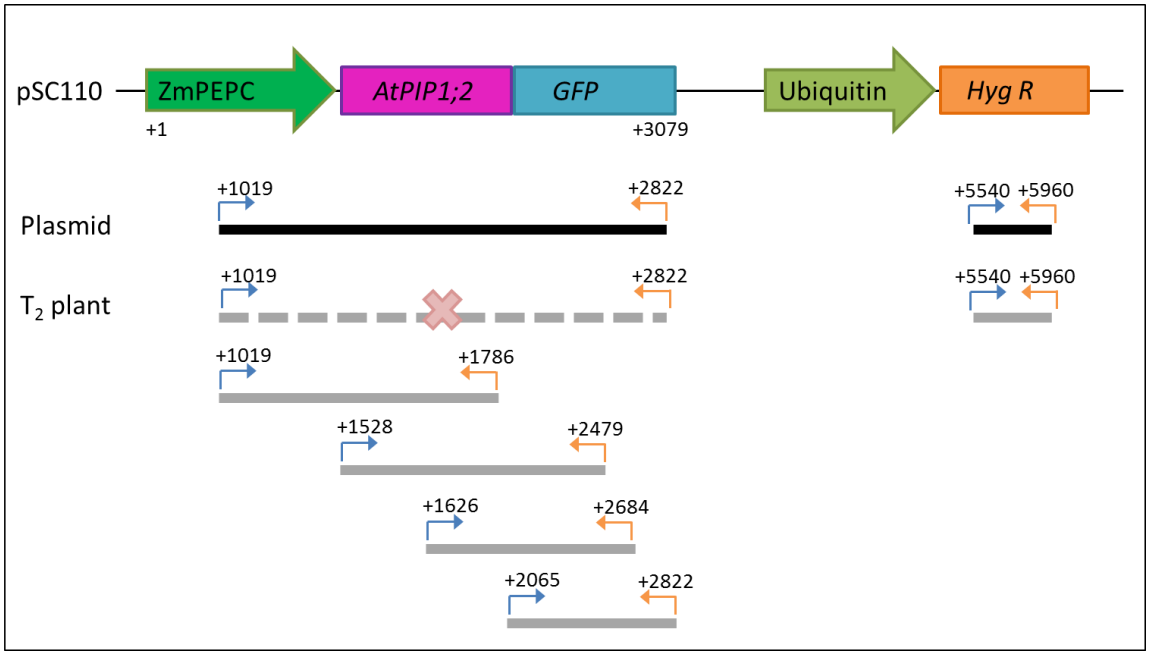

Figure 4.7: Illustration of amplifiable fragments (grey) in T_2 *S. viridis* transformed with pSC110/*AtPIP1;2*. Different primer combinations were used to PCR amplify different fragments of the transgene. The largest fragment that could be amplified is represented. The plasmid control (pSC110/*AtPIP1;2*) could be amplified from all primer combinations (black). The entire transgene could not be amplified in any of the T_2 plants (dashed line with red cross). Only partial fragments could be amplified from 8-1-4, 6-8-3, 3-4-2 or 2-7-1 (represented as T_2 plant in figure).

4.3.7 RT-qPCR

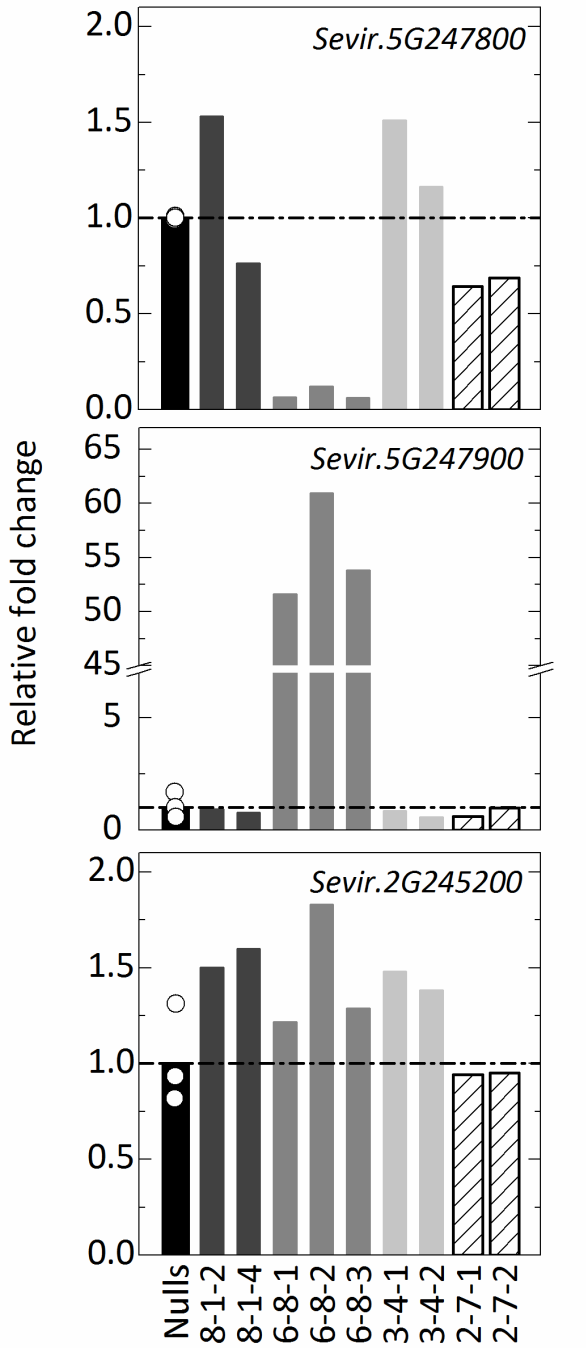

Figure 4.8: Expression level of *β-CA* transcripts: *Sevir.5G247800*, *Sevir.5G247900* and *Sevir.2G245200*.Measured by RT-qPCR in null control and overexpression *AtPIP1;2* T_2 plants in lines 8-1, 6-8, 3-4 and 2-7 and analysed by ΔΔ Ct. Fold change relative to null transformant shown, circles show data range of null plants (n = 3). Dotted line indicates average null fold change.

To determine whether the low CA enzyme activity found in line 6-8 originated at the translational or post translational level, I measured the expression level of the *β-CA* transcripts (Figure 4.8). There was a significant decrease in transcript expression for *Sevir.5G247800* and a significant increase in *Sevir.5G247900*. This suggests the multiple, partial insertions of *AtPIP1;2* + GFP have interfered with the genomic *β-CA* genes and altered their expression. No change in transcript expression was observed for the *S. viridis* aquaporins *SvPIP1;2*, *SvPIP1;5*, *SvPIP2;1* or *SvPIP2;8* (Figure 4.9).

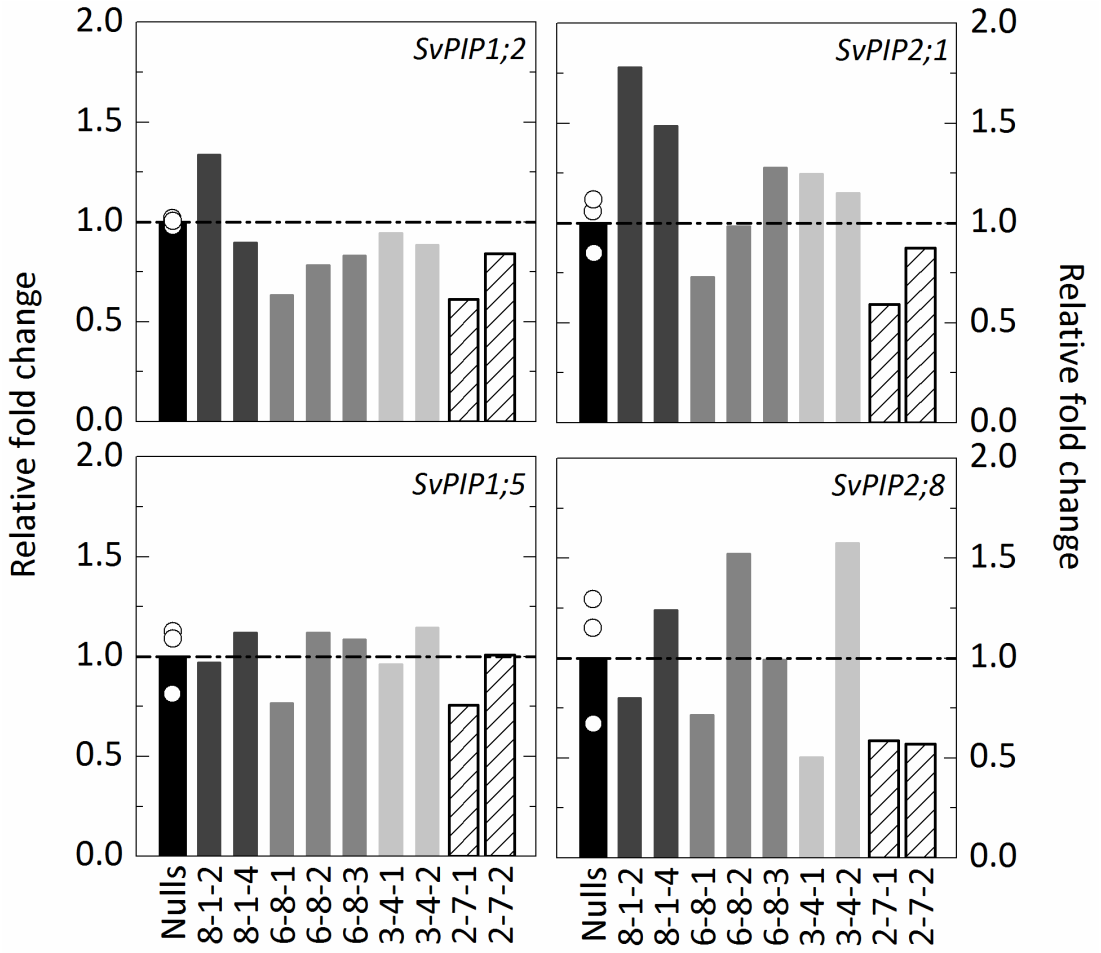

Figure 4.9: Expression level of selected *S. viridis* (Sv) PIPs. PIPs examined included: *SvPIP1;2* (*Sevir.1G269400*), *SvPIP1;5* (*Sevir.1G378900*), *SvPIP2;1* (*Sevir.2G128000*) and *SvPIP2;8* (*Sevir.2G302500*). RT-qPCR was measured in null and overexpression *AtPIP1;2* T_2 plants in lines 8-1, 6-8, 3-4 and 2-7 and analysed by ΔΔ Ct. Fold change relative to null transformant shown, circles show data range of null plants (n = 3). Dotted line indicates average null fold change.

4.4 Discussion

In this chapter, I aimed to examine the effects of overexpressing a CO_2 permeable aquaporin in a C_4 photosynthetic species. I expected to observe increased g_m and possibly increased g_s as had been reported in C_3 photosynthetic plants with modified CO_2 permeable aquaporin expression (Flexas *et al.*, 2006; Sade *et al.*, 2010; Uehlein *et al.*, 2008). Furthermore, I also expected to find differences in native PIP expression and the ultimate aim was to observe improved plant performance (such as increased net assimilation rate and increased biomass). However, in my experiments an unexpected but interesting transformation event resulted, instead, in reduced CA activity in *S. viridis*.

I have investigated *S. viridis* transformed with pSC110/*AtPIP1;2*. One transformed line, (AtPIP1;2-6-8) had a marked gas exchange phenotype, with both a lower initial slope and lower maximum CO_2 assimilation in these plants compared to the null control. These effects could be attributed to significantly lower CA activity which in turn was a result of downregulation of expression of the primary photosynthetic *β-CA* gene (*Sevir.5G247800*).

Multi-copy DNA insertions and inverted repeats are commonly reported in some agrobacterium mediated transformation systems (Jones *et al.*, 1987; Jorgensen *et al.*, 1987). Plant transformations in general are not easy or predictable and unintended phenotypes in transgenic plants are common (Latham *et al.*, 2006), though often not reported in the literature. In the case of these pSC110/*AtPIP1;2* transformed lines it appears there were multiple, partial insertions (Figure 4.7). The truncated products may have occurred during agrobacterium transformation. Performing RNA-Sequencing on the whole plant would determine where the insertion occurred, however, since the phenotype is not what we desired this is beyond the scope of this study.

One hypothesis for the low initial slope gas exchange phenotype we observed in line AtPIP1;2-6-8 T_2 plants was that a partial insert may have landed in between two *β-CA* genes on chromosome 5 (Figure 4.10). Although extremely unlikely, the insert may have disrupted *Sevir.5G247800*, the primary photosynthetic *β-CA*, resulting in gene silencing, and increased expression of *Sevir.5G247900*, a *β-CA* with unknown function, to compensate or due to the promoter region of the pSC110/*AtPIP1;*2+GFP construct causing increased transcript expression.

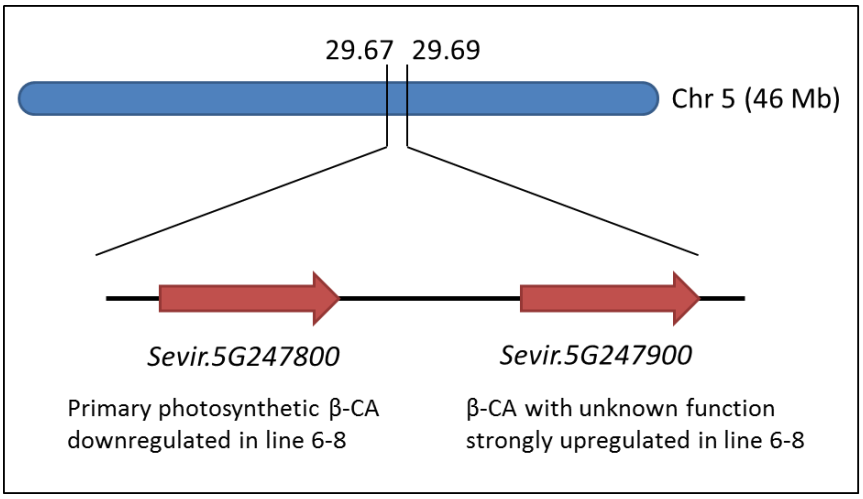

Figure 4.10: Diagram of two *β-CA* genes on *S. viridis* chromosome 5. One hypothesis for the phenotype observed in line 6-8 is a partial insert of pSC110/*AtPIP1;2* landed in between the primary photosynthetic *β-CA* gene (*Sevir.5G247800*) disrupting its expression and upregulating a second *β-CA* gene (*Sevir.5G247900*).

Another explanation for reduced CA activity in one transgenic line is possible interactions with CA which interfered with its function. In Arabidopsis, β-CA1 and β-CA4 are involved in CO_2 induced stomatal closing (Hu *et al.*, 2010; Hu *et al.*, 2015). Most recently, β-CA4 has been demonstrated to interact with the CO_2 permeable aquaporin, AtPIP2;1, in split luciferase, biomolecular fluorescence complementation and co-immunoprecipitation experiments in tobacco (Wang *et al.*, 2016). This interaction has also been observed between CAII and hAQP1 in mammalian cells (Vilas *et al.*, 2015). The interaction of CA and CO_2 permeable aquaporins may be advantageous for CO_2 diffusion in C_4 photosynthesis. CA activity converting CO_2 into HCO_3^- as soon as it enters the mesophyll cell may increase the diffusion potential for CO_2 entering through an aquaporin and result in increased intercellular CO_2. However, I found no change in PIP expression, for the subset of PIPs I tested by RT-qPCR, in the pSC110/*AtPIP1;2* transformed plants so it is very unlikely the low CA phenotype we observed is a result of an aquaporin interacting with CA in *S. viridis*. In addition, the effect appears at the RNA transcript level, not a protein level rendering this explanation implausible.

The effect of modifying the expression of a CO_2 permeable aquaporin on C_4 photosynthesis is still unknown. Future experiments may benefit from targeting native Setaria PIPs, such as PIP2;7 which we demonstrated to be CO_2 permeable when expressed in yeast in Chapter 3. Additionally, the efficiency of Setaria transformation has increased significantly since 2014,

therefore eliminating the quarantine limitations I encountered here and allowing for more experiments which alter aquaporin expression in Setaria to be examined. The effect of reduced CA activity in *S. viridis* is thoroughly investigated in the next Chapter.

CHAPTER 5: EFFECTS OF REDUCED CARBONIC ANHYDRASE ACTIVITY ON *SETARIA VIRIDIS*

Publications arising from this chapter:

Osborn HL, Alonso-Cantabrana H, Sharwood RE, Covshoff S, Evans JR, Furbank RT, von Caemmerer S. 2016. Effects of reduced carbonic anhydrase activity on CO_2 assimilation rates in *Setaria viridis*: a transgenic analysis. *Journal of Experimental Botany*. 68, 299 - 310.

5.1 Introduction

C_4 plants have evolved a CO_2 concentrating mechanism (CCM) that enables the elevation of CO_2 around the active sites of Rubisco by a combination of anatomical and biochemical specialisation (Hatch, 1987). C_4 photosynthesis has independently evolved more than 60 times, providing one of the most widespread and effective solutions for remedying the catalytic inefficiency of Rubisco (Christin and Osborne, 2013; Sage *et al.*, 2012). The key carboxylases in C_4 plants are localised to different cellular compartments. Phosphoenolpyruvate carboxylase (PEPC) is localised to the cytosol of mesophyll cells and Rubisco to the chloroplasts of bundle-sheath cells. For the CCM to operate effectively, PEPC activity must exceed Rubisco activity to balance leakage of CO_2 out of the bundle-sheath compartment, therefore maintaining a high bundle-sheath CO_2 level (von Caemmerer and Furbank, 2003). As PEPC utilises HCO_3^- and not CO_2, the first enzyme of the C_4 pathway is carbonic anhydrase (CA) which catalyses the reversible conversion of CO_2 and HCO_3^- in the cytosol of mesophyll cells. C_4 acids produced by PEPC then diffuse into the bundle-sheath cells where they are decarboxylated, supplying CO_2 for Rubisco.

Within higher plants there are multiple forms of the α-CA, β-CA and γ-CA families which share little sequence homology (Moroney *et al.*, 2001). β-CAs are the most prevalent CA family in land plants. CA is an abundant enzyme in C_3 plants, representing up to 2 % of the soluble leaf protein (Okabe *et al.*, 1984). In C_3 plants the role of CA is unclear (Badger and Price, 1994) as it does not appear to limit photosynthesis but does influence stomatal conductance, guard cell movement and amino acid biosynthesis (DiMario *et al.*, 2016; Engineer *et al.*, 2016; Hu *et al.*, 2010).

It has long been contended that the un-catalysed rate of CO_2 conversion to HCO_3^- is insufficient to support C_4 photosynthetic flux (Badger and Price, 1994; Hatch and Burnell, 1990). This hypothesis was supported by experiments in the C_4 dicot *Flaveria bidentis*, where antisense plants with less than 10% of wild type CA activity required high CO_2 for growth and showed reduced CO_2 assimilation rates (Cousins *et al.*, 2006; von Caemmerer *et al.*, 2004). However, in the C_4 monocot *Zea mays* mutant plants with reduced CA activity (3% of wild type) showed no limitation to CO_2 assimilation rates at ambient CO_2 (Studer *et al.*, 2014). CA activity has been shown to vary widely between species (Cousins *et al.*, 2008) and it is unclear whether CA activities are limiting at high CO_2 assimilation rates, as has previously been suggested (Gillon and Yakir, 2000; Hatch and Burnell, 1990).

In this chapter, we examined the role of CA in the model C_4 monocot species *S. viridis.* Here we used a stable transformation approach to examine the role of CA in *S. viridis* and could show that *S. viridis* is a useful model species that lends itself to molecular manipulation of the C_4 photosynthetic pathway. To our knowledge, this is the first publication (Osborn *et al.*, 2016) where a transgenic approach has been applied for a functional analysis in *S. viridis*. Two constructs both targeting the major leaf *β-CA* (*Sevir.5G247800*) were used to generate three independent transformed lines with reduced CA activity. A strong correlation between CO_2 assimilation rate at low pCO_2 and CA activity was observed. Our combined measurements of mesophyll conductance, g_m, and CA activity suggests that increasing mesophyll conductance may be an important way to increase the CO_2 assimilation rate at low intercellular pCO_2, as may occur under drought.

5.2 Methods

5.2.1 Phylogeny of CA

S. viridis carbonic anhydrases were identified by using maize (Studer *et al.*, 2014) and Arabidopsis (Hu *et al.*, 2010) CAs as search terms in NCBI. Protein sequences used to generate the phylogenetic tree were obtained for *S. viridis* and maize from Phytozome 11.0.5. The phylogenetic tree was generated using the neighbour-joining method in the Geneious Tree Builder program (Geneious 9.0.2).

5.2.2 Plant growth conditions

S. viridis seeds were incubated in 50% liquid smoke (Wrights) for 30 min to promote germination and were germinated in garden soil mix fertilised with Osmocote (Scotts, Australia) in small containers before being transferred to individual 2L pots. Plants were grown in controlled environmental chambers, irradiance 500 µmol photons m^{-2} s^{-1}, 16 h photoperiod, 28 °C day, 24 °C night, 2% CO_2. Pots were watered daily.

5.2.3 Construct generation

Two different constructs were used to generate three lines of reduced CA activity. Firstly, an RNAi was targeted to the primary leaf β-CA *Sevir.5G247800* which generated lines 2.1 and 5.3, this construct, pSG/*CAa* was kindly provided by Jasper Pengelly. A region of *Sevir.5G247800* was amplified by PCR using gene-specific primers (F: GAGGGCCAGGCACCCAGGTA, R: GACGGCGTACTCGATGGCGG) and reverse-transcribed RNA from *S. viridis* leaves ligated into pENTR/D-TOPO (ThermoFisher), and verified by sequencing. The fragment was inserted via a double Gateway system LR reaction (Invitrogen) into the hairpin RNAi binary vector pSTARGATE (Greenup *et al.*, 2010) to form a stem–loop region under the control of the ubiquitin promoter/intron (UBI) and octopine synthase (OCS) terminator to form the RNAi vector pSG/*CAa*.

Secondly, an overexpression approach using the maize *β-CA* gene (*GRMZM2G348512*), *ZmCA2*, which resulted in gene silencing, generated the third transformed line, 1.1, this construct, pSC110/*ZmCA2* was kindly provided by Sarah Covshoff. The coding sequence of the maize *β-CA* gene (*GRMZM2G348512*), *ZmCA2* (Studer *et al.*, 2014), was amplified by reverse transcription–PCR (RT–PCR) from total RNA extracted from B73 maize. Total RNA was isolated using hot acid phenol and chloroform, and then treated with RQ1 RNase-free DNase

(Promega). The reverse transcription and PCRs were performed as per the manufacturer's protocols with Superscript II (ThermoFisher) and Phusion High-Fidelity DNA polymerase (NEB), respectively using gene specific primers (F: CACCATGGACGACCCCGTCGAGCGCTTGAAGGAC, R: CAAGACCAGCCGCTCGCATCTTTCCAAGACGATGGCTGCTTATTGTCC). The sequence encoding an AcV5 epitope tag (Lawrence *et al.*, 2003) was added to the C-terminal end of *ZmCA2*. The resulting *ZmCA2* amplicon was cloned into pENTR/D-TOPO and verified by sequencing. LR Gateway cloning (ThermoFisher) was used to insert the *ZmCA2* coding sequence into the overexpression vector, pSC110 (described in Section 4.2.1).

Both constructs were transformed into *Agrobacterium tumefaciens* strain AGL1 for stable plant transformation.

5.2.4 Callus induction and plant transformation

T_0 lines 2 and 5 of RNAi pSG/*CAa* were kindly provided by Hugo Alonso-Cantabrana.

Stable transformation of *S. viridis* (accession A10.1) with pSC110/*ZmCA2* was carried out as described in Osborn *et al.* (2016) (Figure 5.1). Seed coats were mechanically removed from mature *S. viridis* seeds to improve germination. Seeds were sterilised before plating on callus induction medium (CIM; 4.3 g L^{-1} Murashige and Skoog (MS) salts, pH 5.8, 10 mL L^{-1} 100 x MS vitamins stock, 40 g L^{-1} maltose, 35 mg L^{-1} ZnSO4.7H2O, 0.6 mg L^{-1} CuSO4.5H2O, 4 g L^{-1} Gelzan, 0.5 mg L^{-1} kinetin, 2 mg L^{-1} 2,4-D). After 4 weeks in the dark at 24 °C any seedling structures or gelatinous calli were removed and remaining calli transferred to fresh CIM. After a further 2 weeks, calli were divided and replated onto fresh CIM. One week later transformations were performed.

AGL1 containing the construct of interest were grown in the presence of 50 µg L^{-1} kanamycin and 50 µg L^{-1} rifampicin at 28 °C to OD_{600} = 0.5 and then resuspended in CIM without Gelzan and hormones. Acetosyringone (200mM) and synperonic (0.01% (w/v)) were added to the agrobacterium solution before incubating the calli in the medium for 5 min at room temperature. The calli were blotted dry on sterile filter paper and incubated at 22 °C for 3 days in the dark. The calli were then transferred to selective CIM (CIM containing 40 mg L^{-1} hygromycin, 150 mg L^{-1} timentin) and incubated in the dark at 24 °C for 16 days. Calli were then transferred to selective plant regeneration medium (PRM) containing 4.3 g L^{-1} MS salts, pH 5.8, 10 mL L^{-1} 100 x MS vitamins, 20 g L^{-1} sucrose, 7 g L^{-1} Phytoblend, 2 mg L^{-1} kinetin, 150 mg L^{-1} timentin, 15 mg L^{-1} hygromycin. Calli were maintained at 24 °C under 16 h light: 8 h

dark photoperiod and a light intensity of 60 µmol photons m^{-2} s^{-1}. Developing shoots were transferred to selective rooting media (RM) containing 2.15 g L^{-1} MS salts, pH 5.7, 10 mL L^{-1} 100 x MS vitamins, 30 g L^{-1} sucrose, 7 g L^{-1} Phytoblend, 150 mg L^{-1} timentin, 20 mg L^{-1} hygromycin. Shoots that survived and developed roots were genotyped using primers against the *hygromycin phosphotransferase* gene (F: TGGCGTGATTTCATATGCGC, R: CGTCAACCAAGCTCTGATAG) by PCR and positive transformants were transplanted to soil.

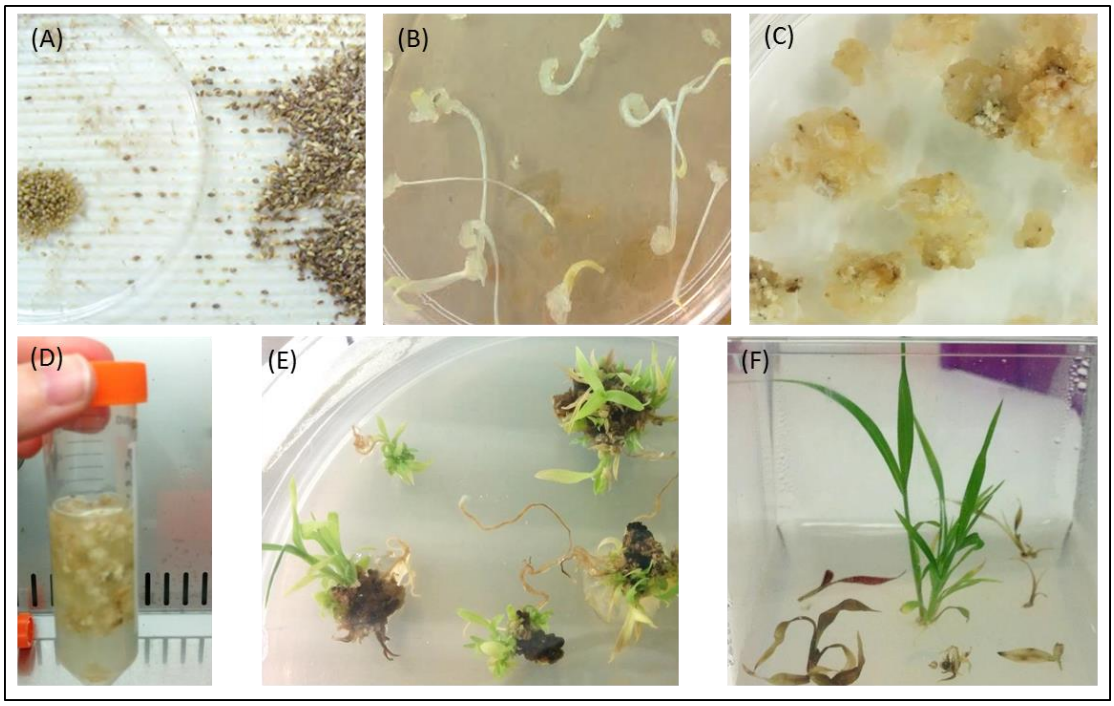

Figure 5.1: Callus production and transformation process for *S. viridis.* (A) Seed coats are removed and seeds sterilised, (B) and (C) Calli are produced on induction media for 6 – 8 weeks, (D) Calli are inoculated with agrobacterium solution, (E) Transformed calli are grown on selection media, (F) Transformed shoots are transferred to rooting media containing hygromycin selection.

5.2.5 Selection of plants for analysis

The progeny of three independent T_0 transformation events were analysed for CA hydration rates (Figure 5.2). One T_1 plant with low CA hydration rates was selected from each transformation event (labelled 5.3, 2.1 and 1.1) and its progeny (T_2) used for all future analysis. Two sets of experiments were performed on the T_2 plants. Firstly, gas exchange and biochemical analysis on lines 5.3, 2.1 and 1.1 and secondly gas exchange and oxygen

discrimination on lines 5.3 and 1.1. Each T_2 plant was genotyped prior to experiments using primers against the *hygromycin phosphotransferase* gene. The progeny of a plant which went through the *S. viridis* transformation process and tested negative for the *hygromycin phosphotransferase* gene were used as null controls.

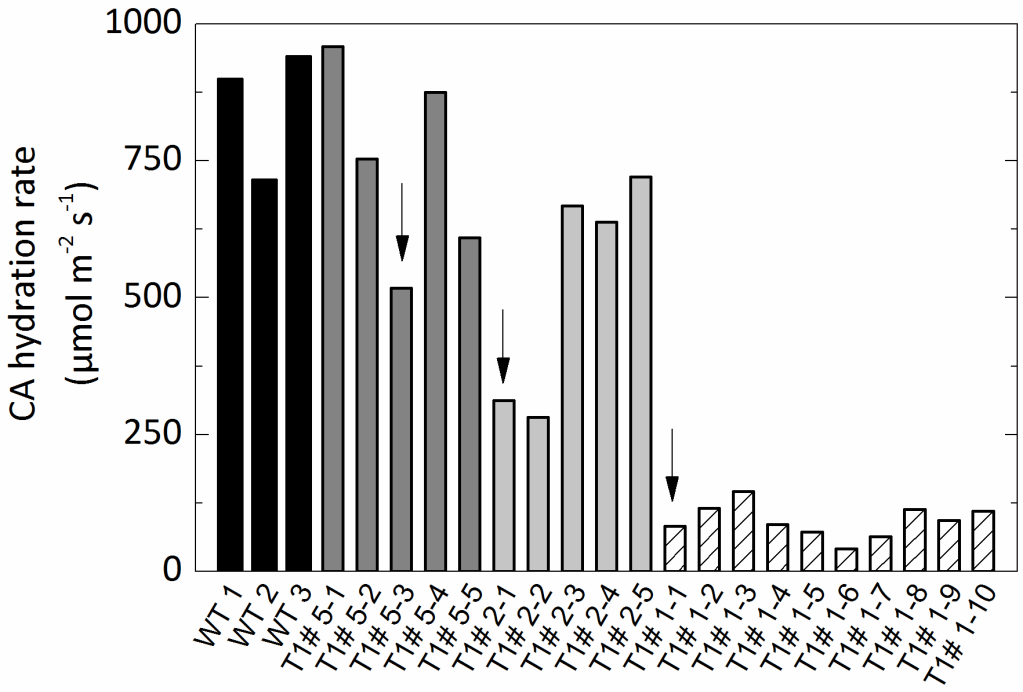

Figure 5.2: CA hydration rates at mesophyll pCO_2 in the T_1 plants from three transformation events. T_0 lines #5 and #2 were generated using the RNAi vector pSG/*CAa*. T_0 line #1 was generated by gene suppression with pSC110/*ZmCA2*. Arrows indicate the T_1 plants with low CA hydration rates whose progeny were then used for future studies and are labelled T1#5-3,T1#2-1 and T1#1-1.

5.2.6 Insertion number estimation

Freeze dried leaf material were sent to IDNA genetics (United Kingdom) to estimate the number of transgene copies in the CA transformed lines as described in Section 4.2.5 and Osborn *et al.* (2016).

5.2.7 RNA extraction and reverse transcriptase quantitative PCR (RT-qPCR)

RNA was extracted from frozen leaf discs (0.78 cm^2) and cDNA transcribed as described in Section 4.2.9. Primers (Table 4.2) were designed using Primer3 in Geneious R7.1.6, ensuring products spanned an intron. Primer amplification efficiencies were determined by Ct slope

method, efficiencies for all primer pairs were comparable (~95%) and no amplification was detected in the no template control. Relative fold-change was calculated by the ΔΔCt method, using the average of three nulls as reference, as described by Livak and Schmittgen (2001). The geometric mean of the Ct values for three reference genes was used for normalisation (Vandesompele *et al.*, 2002). Statistics were performed with Sigma Plot (version 11.0).

5.2.8 Determination of enzyme activities

CA, Rubisco, PEPC activities were determined as described in Section 4.2.7 with the exception the extractions were made from fresh leaf discs sampled directly after gas exchange and were processed in ice cold glass homogenisers (Tenbroek).

For NADP-ME activity 10 μL leaf extract was combined with 485 μL assay buffer (50 mM Trycine-KOH pH 8.3, 5 mM Malic acid, 0.5 mM NADP, 0.1 mM EDTA) and reaction initiated with 10 μL of 200 mM $MgCl_2$.

5.2.9 Gas exchange measurements

Net photosynthesis (*A*) was measured over a range of intercellular pCO_2 (C_i) on the uppermost, fully expanded leaf of 5 week old *S. viridis* plants as described in Section 4.2.8.

5.2.10 Measurements of $C^{18}O^{16}O$ discrimination ($\Delta^{18}O$)

Simultaneous measurements of exchange of CO_2, H_2O, $C^{18}O^{16}O$ and $H_2{}^{18}O$ were made by coupling two LI-6400XT gas exchange systems to a tunable diode laser (TDL: TGA200A, Campbell Scientific Inc., Logan, UT, USA) to measure $C^{18}O^{16}O$ and a Cavity Ring-Down Spectrometer (L2130-i, Picarro Inc., Sunnyvale, CA, USA) to measure the oxygen isotope composition of water vapour. The system is essentially that described by Tazoe *et al.* (2011) except that the TGA100 was replaced by a TGA200A and the additional laser for water vapour measurements has been added together with a 16 port distribution manifold. To generate gas flows to the gas exchange systems N_2 and O_2 were mixed by mass flow controllers (Omega Engineering Inc, Stamford, CT USA) to generate CO_2 free air with 2% O_2. The humidity of incoming air was adjusted by varying the temperature of water circulating around a Nafion tube (Permapure, MH-110-12P-4) but was kept constant in this set of experiments to supply water vapour of a constant ^{18}O composition. To supply flow to the TDL and the L2130-i from the sample and reference gas streams two T junctions were inserted into the match valve tubing and in the reference line of the LI-6400XT respectively. This allowed leaves of two

plants to be measured in sequence, with each LI-6400XT sampled by the TDL at 4 min intervals for 20 sec at the sample and reference line. The Picarro Cavity Ring Down spectrometer sampled for 3 min, so that leaves were sampled at 6 min intervals.

The ^{18}O isotopic composition of the CO_2 calibration gas was 22.17 ± 0.04 0/00 for Vienna mean oceanic water (VSMOW) and was checked against standards on an Isoprime mass spectrometer. We monitored daily the ^{18}O composition of water vapour of the reference air streams and the values were -6.07 ± 0.08 0/00 and -6.34 ± 0.08 0/00 (VSMOW) for LI-6400XT L1 and L2 references respectively. We attribute the small difference between the reference lines to differences in the Nafion tubing which was used for humidification of incoming air. At the end of the experiment, the calibration of the Picarro L2130-i was confirmed by collecting water vapour samples from the gas stream of the LI-6400XT reference lines going to the Picarro as described by Cousins *et al.* (2006) and assaying these water samples against standards on a Picarro 1102i, which was set up to measure ^{18}O isotopic composition of water samples.

Gas exchange was measured on the uppermost fully expanded leaf of 5 week-old *S. viridis* plants at 25 °C, and leaves were equilibrated at ambient CO_2 (380 µbar), irradiance 1500 µmol photons m^{-2} s^{-1} and 2% O_2. The flow rate was 200 µmol s^{-1}. CO_2 concentration was adjusted from 380 to 760, 570, 380 and 190 µbar at 1 h intervals. Immediately following gas exchange measurements leaf discs were collected and stored at -80 °C until measurements of enzyme activities were made.

5.2.11 Calculations of $C^{18}O^{16}O$ ($\Delta^{18}O$) discrimination and mesophyll conductance (g_m)

Discrimination against ^{18}O in CO_2 during photosynthesis $\Delta^{18}O$ was calculated from the isotopic composition of the CO_2 entering δ_{in} and exiting δ_{out} the leaf chamber and the CO_2 concentration entering C_{in} and exiting C_{out} (all measured with the TDL) (Barbour *et al.*, 2016; Evans *et al.*, 1986):

$$\Delta^{18}O = \frac{\xi(\delta_{out}-\delta_{in})}{1+\delta_{out}-\xi(\delta_{out}-\delta_{in})} \qquad \text{Equation 4}$$

where $\xi = C_{in}/(C_{in} - C_{out})$. Sample streams were passed through a nafion drying tube before entering the TDL and CO_2 values presented are all at zero water vapour concentration.

Following the derivation by Barbour *et al.* (2016) and Farquhar and Cernusak (2012) photosynthetic $\Delta^{18}O$ discrimination was used to calculate pCO_2 in the mesophyll cytosol, C_m, with the assumption that C_m is equal to the pCO_2 at the site of CO_2-H_2O exchange and assuming that cytosolic CO_2 is in full isotopic equilibrium with local cytosolic water. This allowed g_m to be calculated from

$$g_m = A/(C_i - C_m) \qquad \text{Equation 5}$$

$$C_m = C_i \left(\frac{\delta_i - a_w - \delta_A(1+a_w)}{\delta_c - a_w - \delta_A(1+a_w)}\right) \qquad \text{Equation 6}$$

Equation 6 is the same as Equation 21 of Barbour *et al.* (2016), and is a rearrangement of Equation 18 of Farquhar and Cernusak (2012) using their notation. The oxygen isotope ratios are expressed relative to the standard, Vienna Standard Mean Ocean Water (VSMOW) ($\delta_x = \frac{(^{18}O/^{16}O)_x}{(^{18}O/^{16}O)_{std}} - 1$). Intercellular pCO_2 is denoted by C_i, and a_w is the discrimination against $C^{16}O^{18}O$ during liquid phase diffusion and dissolution (0.8 ‰).

The isotopic composition of CO_2 being assimilated, δ_A, is given by

$$\delta_A = \frac{\delta_a - \Delta^{18}O}{1+\Delta^{18}O}, \qquad \text{Equation 7}$$

where δ_a is the isotopic composition of ambient air (in our case $\delta_a = \delta_{out}$).

The oxygen isotope composition of CO_2 in the intercellular airspaces, δ_i, including ternary corrections proposed by Farquhar and Cernusak (2012), is given by

$$\delta_i = \frac{\delta_{io} + t\left[\delta_A\left(\frac{C_a}{C_i}+1\right) - \delta_a\frac{C_a}{C_i}\right]}{1+t} \qquad \text{Equation 8}$$

where C_a is the pCO_2 in the ambient air. The ternary correction factor, t, is given by

$$t = \frac{\left(1+\frac{a_{18bs}}{1000}\right)E}{2g_{ac}} \qquad \text{Equation 9}$$

where g_{ac} is the total conductance to CO_2, E the transpiration rate and a_{18bs} is the weighted discrimination of $C^{16}O^{18}O$ diffusion across the boundary layer and stomata in series given by:

$$a_{18bs} = \frac{(C_a - C_s)a_{18b} - (C_s - C_i)a_{18s}}{(C_a - C_i)} \quad \text{Equation 10}$$

where C_s is the pCO_2 at the leaf surface and a_{18s} and a_{18b} are the discriminations against $C^{16}O^{18}O$ through stomata and the boundary layer (8‰ and 5.8‰ respectively).

The isotopic composition of intercellular CO_2 ignoring ternary corrections is given by

$$\delta_{io} = \delta_A \left(1 - \frac{C_a}{C_i}\right)(1 + a_{18bs}) - \frac{C_a}{C_i}(\delta_a - a_{18bs}) + a_{18bs} \quad \text{Equation 11}$$

To calculate C_m we assume that the isotopic composition of CO_2 in the cytosol, δ_c, is the isotopic composition of CO_2 equilibrated with cytosolic water, δ_{cw}, and

$$\delta_{cw} = \delta_w + \varepsilon_w \quad \text{Equation 12}$$

where δ_w is the stable oxygen isotope composition of water in the cytosol at the site of evaporation and ε_w is the isotopic equilibrium between CO_2 and water (dependent on temperature T_K in K, (Barbour *et al.*, 2016) and references therein).

$$\varepsilon_w(‰) = \frac{17604}{T_K} - 17.93 \quad \text{Equation 13}$$

5.2.12 Calculation of the isotopic composition of water at the site of evaporation from the isotopic composition of transpired water

The isotopic composition of water at the site of evaporation, δ_w, can be estimated from the Craig and Gordon model of evaporative enrichment (Craig and Gordon, 1965; Farquhar and Lloyd, 1993)

$$\delta_w = \delta_t + \varepsilon^* + \varepsilon_k + \frac{e_a}{e_i}(\delta_{wa} - \varepsilon_k - \delta_t) \quad \text{Equation 14}$$

where ε^* is the equilibrium fractionation during evaporation, ε_k is the kinetic fractionation during vapour diffusion in air and δ_t is the oxygen isotopic composition of transpired water

and e_a/ e_i is the ratio of ambient to intercellular vapour pressure and δ_a is the isotopic composition of ambient air. ε*is dependent on temperature:

$$\varepsilon^* = 2.644 - 3.206\left(\frac{10^3}{T_K}\right) + 1.534\left(\frac{10^6}{T_K^2}\right) \quad \text{Equation 15}$$

ε_k is dependent on stomatal and boundary layer conductances and associated fractionation factors (Barbour *et al.*, 2016) and references therein):

$$\varepsilon_k = \frac{28g_s^{-1}+19g_b^{-1}}{g_s^{-1}+g_b^{-1}} \quad \text{Equation 16}$$

The isotopic composition of transpired water δ_t can be calculated from mass balance knowing the isotopic composition of the water entering δ_{win} and exiting δ_{wout} the leaf chamber (measured with the Picarro) and the water vapour concentration entering w_{in} and exiting w_{out} (measured with the LI-6400XT):

$$\delta_t = \left(\delta_{wout}(1 - w_{in}) - \delta_{win}\frac{w_{in}}{w_{out}}(1 - w_{out})\right)\frac{w_{out}}{w_{out}-w_{in}} \quad \text{Equation 17}$$

5.2.13 Calculation of the proportion of mesophyll cytosolic CO_2 in equilibration with leaf water, θ

If C_m is known it is possible to calculate the isotopic composition of cytosolic CO_2 from measurements of $\Delta^{18}O$ using Equation 18 from Farquhar and Cernusak (2012):

$$\delta_c = \delta_A\left(1 - \frac{C_i}{C_m}\right)(1 + a_w) + \frac{C_i}{C_m}(\delta_i - a_w) + a_w. \quad \text{Equation 18}$$

This can then be compared to Equation 12, the isotopic composition of CO_2 in equilibrium with water at the site of evaporation. We calculated mesophyll conductance, g_m, in the *S. viridis* null plants assuming that $\delta_c = \delta_{cw}$ and then used this g_m to estimate C_m in the *S. viridis* transgenics to calculate the proportion of cytosolic CO_2 in equilibration with leaf water, θ using equations developed by Cernusak *et al.* (2004)

$$\theta = \frac{\delta_c-\delta_a+a_{18}\left(1+\frac{C_c}{C_a}\right)}{\delta_{cw}-\delta_a+a_{18}\left(1+\frac{C_c}{C_a}\right)} \quad \text{Equation 19}$$

where a_{18} is the weighted discrimination of $C^{16}O^{18}O$ diffusion across the boundary layer, stomata and the liquid phase in series given by:

$$a_{18} = \frac{a_b(C_a - C_s) + a_s(C_s - C_i) + a_w(C_i - C_m)}{(C_a - C_m)}. \qquad \text{Equation 20}$$

5.2.14 Leaf anatomical measurements and estimation of g_m from anatomical measurements

Fully expanded leaves from 5 week-old T_2 plants, null and line 1.1, were collected and cut into ~0.5 x 2 mm pieces. Leaf slices were fixed in 2.5% (v/v) glutaraldehyde, 2% (v/v) paraformaldehyde, 0.1 M phosphate buffer and 0.01% (v/v) Tween 20 under vacuum for 20 min, then replaced with buffer containing no Tween 20 and fixed overnight at 4 °C. Leaf pieces were washed in phosphate buffer and post fixed in 1% (w/v) osmium tetroxide for 2 h. Fixed leaf pieces were then dehydrated in an ethanol series (10, 30, 50, 70, 80, 95, 100%) followed by infiltration with LR white. Leaf sections were finally placed in moulds filled with resin and baked at 60 °C for 24 h. Sections of 0.5 μm thickness were cut using glass knives on a Reichert ultramicrotome, stained with toluidine blue and heat fixed to glass slides. Slides were viewed using a Zeiss Axioskop light microscope at x 400 magnification. Three images were taken from each slide for analysis, each containing a leaf cross-section in the same orientation and showing at least two vascular bundles. Fiji quantification software (Schindelin *et al.*, 2012) was used to select regions of interest. Mesophyll surface area exposed to intercellular airspace to leaf area ratio (S_m) was calculated using Equation 21 where CCF is the curvature correction factor of 1.43 (Evans *et al.*, 1994).

$$S_m = \frac{\text{Length of mesophyll cells exposed to intercellular airspace}}{\text{Interveinal distance}} \text{ x CCF} \qquad \text{Equation 21}$$

The values of S_m together with measurements of cell wall thickness and cytosol thickness were used to derive an estimate of g_m from anatomical parameters. The cell wall thickness (0.113 ± 0.005 μm) was estimated from transmission electron micrographs of *S. viridis* grown under similar conditions (Danila *et al.*, 2016). Calculations followed Equations 1-5 by von Caemmerer and Evans (2015) using the membrane permeability of Gutknecht for a lipid bilayer of 3.5 x 10^{-3} m s^{-1} since only the plasma membrane needs to be transversed for diffusion of CO_2 from intercellular airspace to mesophyll cytosol (Gutknecht *et al.*, 1977) and a cytosol thickness of 0.3 μm (von Caemmerer and Evans, 2015). These calculations give a g_m on a leaf area basis of 0.68 mol m^{-2} s^{-1} bar^{-1}.

5.3 Results

5.3.1 Phylogenetic analysis of Setaria β-CA genes

In *S. italica* we identified four *β-CA* genes: *Seita.5G240000* (*Si003882m.g*), *Seita.5G240100* (*Si002140m.g*), *Seita.5G240200* (*Si002669m.g*) and *Seita.2G35500* (*Si030616m.g*). These were then compared to *S. viridis* which has recently been sequenced and annotated (Figure 5.3). There is very high similarity between these Setaria species, with 100% amino acid sequence identity for 3 out of the 4 *β-CA* genes. Sevir.2G245200 and Seita.2G235500 share 90% amino acid sequence identity. Overall the different *β-CA* genes have low sequence identity, approximately 37% between the 4 genes.

Homology to *A. thaliana* and *Z. mays* β-CA proteins were aligned with *S. viridis* β-CA genes and a phylogenetic tree generated (Figure 5.4). *Sevir.5G247800* has been shown to be the major leaf β-CA (Christin *et al.*, 2013; John *et al.*, 2014).

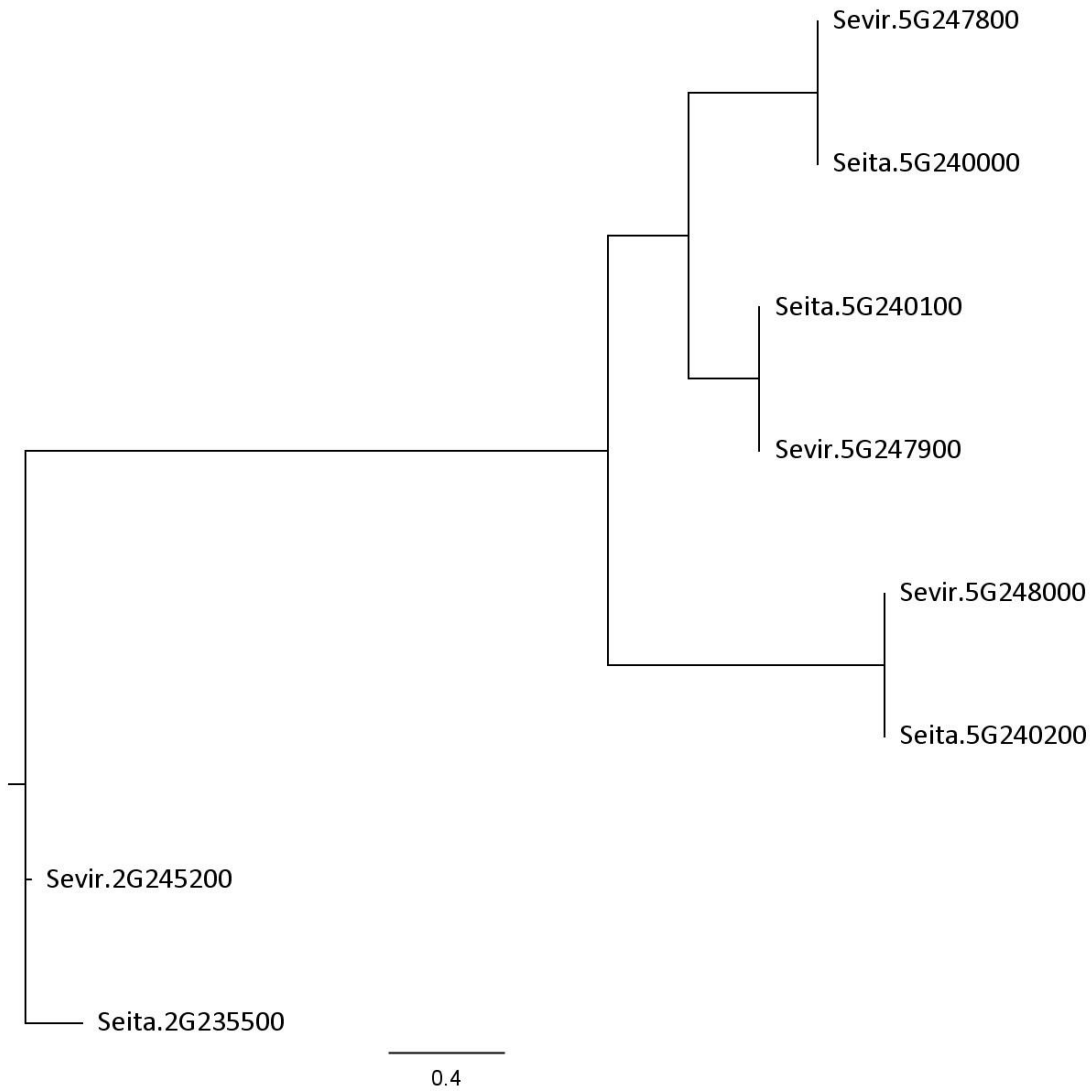

Figure 5.3: Phylogenetic tree of *β-CA* genes from *S. viridis* (Sevir) and *S. italica* (Seita). Protein sequences were aligned using Clustal W and the tree was then generated by RAxML 7.2.8. in Geneious 9.0.2. The scale bar indicates the evolutionary distance, expressed as changes per amino acid residue.

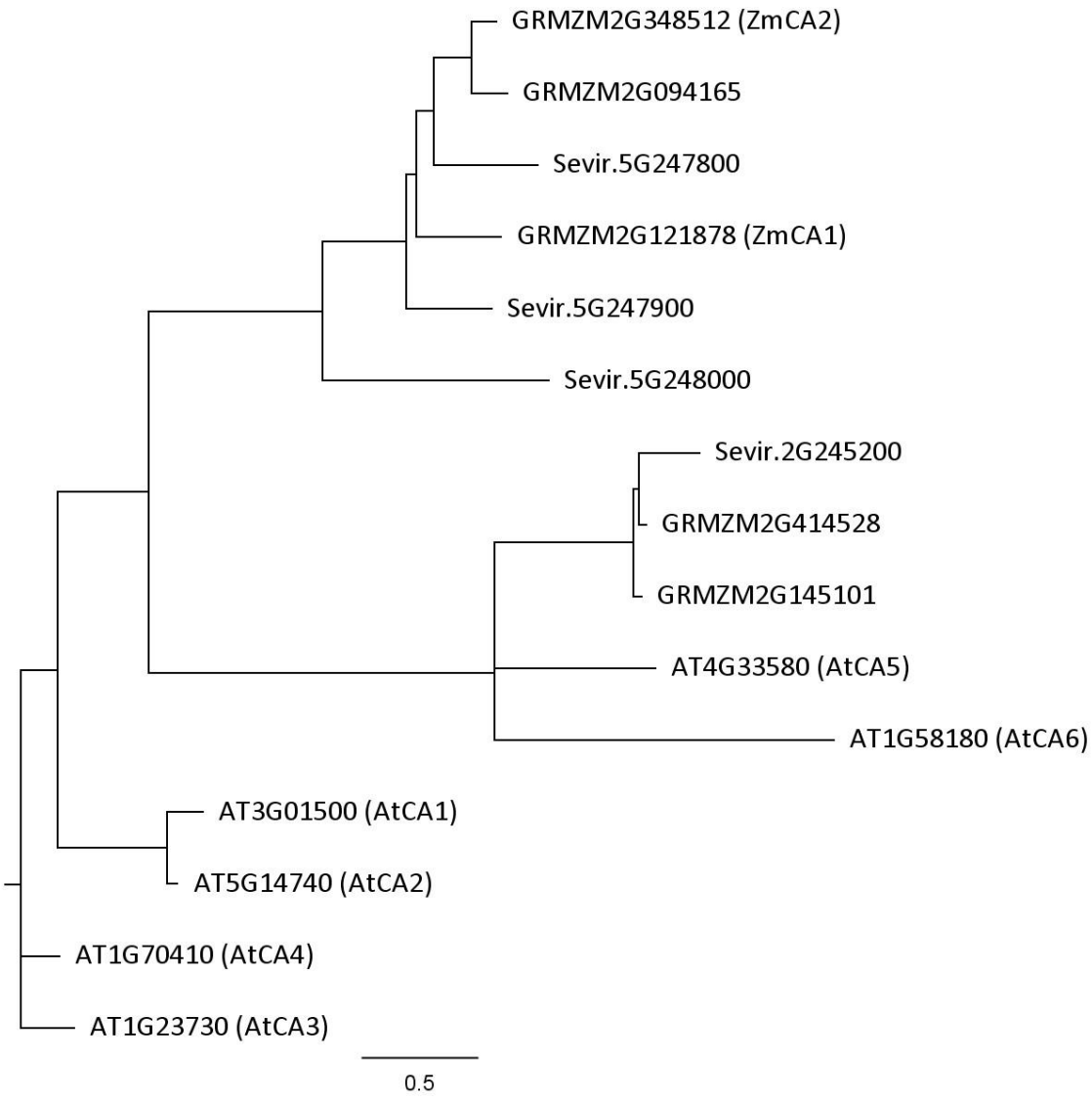

Figure 5.4: Phylogenetic tree based on protein sequences of β-CA from *A. thaliana*, *Z. mays* and *S. viridis*. Protein sequences were aligned using Clustal W and the tree was then generated by RAxML 7.2.8. in Geneious 9.0.2. The scale bar indicates the evolutionary distance, expressed as changes per amino acid residue.

5.3.2 Generation of transgenic S. viridis with reduced β-CA

Three independent transformation events resistant to hygromycin and with reduced CA activity were generated using two different approaches. Firstly, one line (1.1) was generated through gene suppression upon transformation with the overexpression construct pSC110/*ZmCA2*. The coding sequence of *ZmCA2* and *Sevir.5G247800* show 87% identity (Figure 5.5). Most likely, expression of *ZmCA2* therefore caused suppression of the primary *S. viridis β-CA* gene, resulting in reduced CA activity in line 1.1. The second approach was to target *Sevir.5G247800* using the RNAi construct pSG/*CAa* which generated stably transformed lines from two different events (2.1 and 5.3). Plants were grown at high pCO_2 for all experiments.

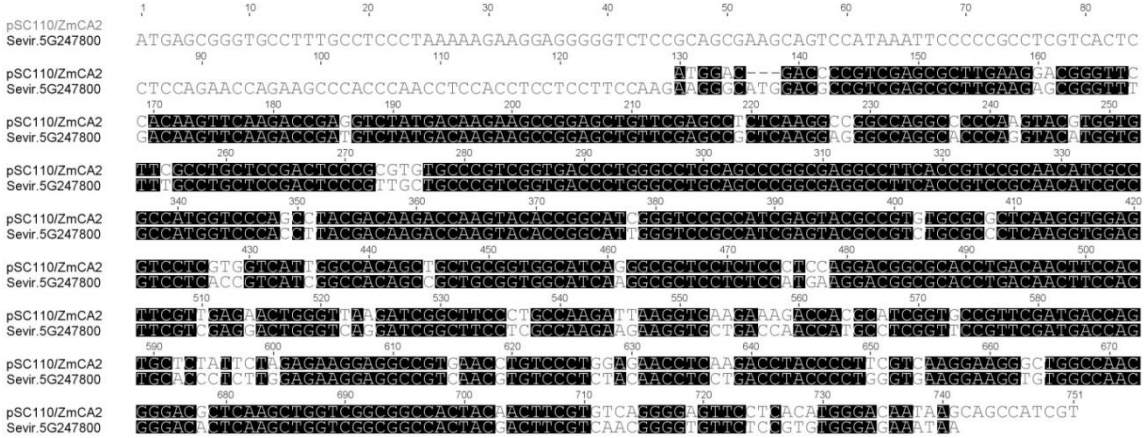

Figure 5.5: High sequence identity (87%) of *Sevir.5G247800* to the *ZmCA2* (*GRMZM2G348512*) used for transformation in overexpression construct pSC110/*ZmCA2*.Alignment using Clustal-W in Geneious 9.0.2.

To determine specificity of the RNAi construct and check which *β-CA* was suppressed in line 1.1, RT-qPCR was performed against the *β-CAs* in *S. viridis*. Expression of the primary leaf *β-CA Sevir.5G247800* was significantly down regulated, between 83 and 96%, in lines from all three transformation events (Figure 5.6A). Transcript levels of *Sevir.2G245200* and *Sevir.5G247900* were unchanged relative to expression in the null plants (Figure 5.6B, C) whilst *Sevir.5G248000* transcript was undetectable in all samples (data not shown). Therefore, expression of only the target *β-CA* gene was affected in the three transformed lines.

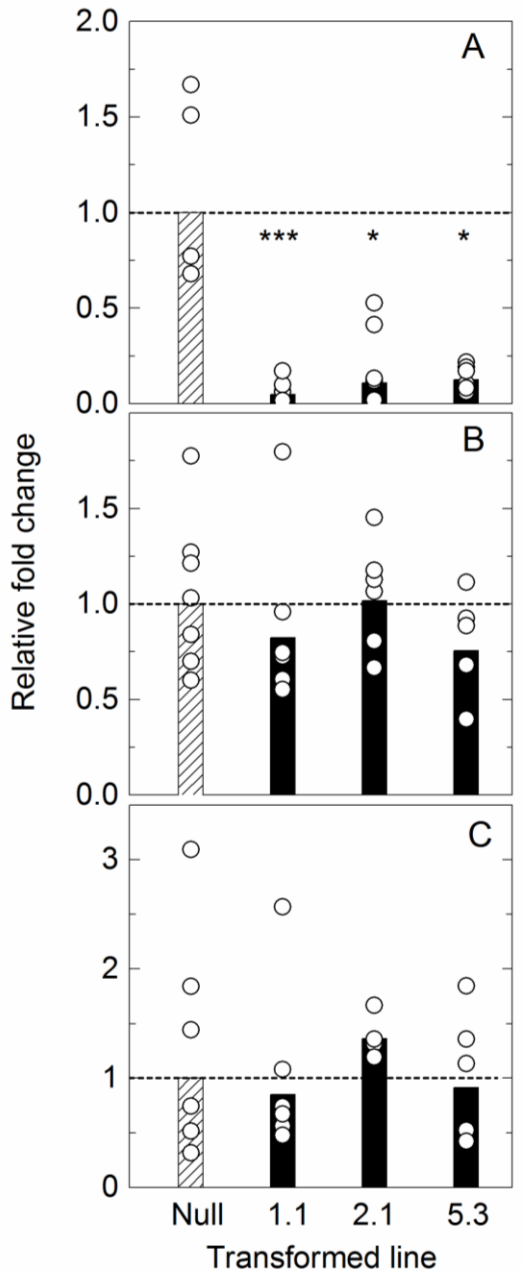

Figure 5.6: Expression level of *β-CA* transcripts. (A) *Sevir.5G247800*, (B) *Sevir.5G247900* and (C) *Sevir.2G245200* in null control and CA transformed lines 1.1, 2.1 and 5.3 as measured by RT-qPCR and analysed by ΔΔ Ct. Fold change relative to null transformant shown, bars represent mean fold change, circles show data range of T_2 plants (n = 5 to 7 plants) from each transformation event measured in triplicate. Dotted line indicates average null fold change. Expression level of the major leaf β-CA transcript *Sevir.5G247800* (A) is significantly lower compared to the null control in all three transformed lines, calculated using one-way ANOVA.

Quantitative real-time PCR was used to estimate the number of insertions in the transgenic plants, based on the number of copies of the *hygromycin phosphotransferase* gene. Three T_2 plants of the three lines were analysed and there were two, four and > four transgene insertions detected for plants of line 5.3, 2.1 and 1.1, respectively. The high copy number in the overexpressing line of 1.1 is the likely cause of the suppression of transcript accumulation.

5.3.3 CA and photosynthetic enzyme activity and leaf anatomy

T_1 progeny of the three independent transformation events showed a range of CA hydration rates as measured on the soluble leaf fraction on a membrane inlet mass spectrometer. Compared to the null control, lines 1.1, 2.1 and 5.3 had on average (n = 7 T_2 plants) an 87, 70 and 50% reduction of CA activity, respectively (Figure 5.7). CA hydration rate in the null plants was 934 ± 92 µmol m^{-2} s^{-1} as calculated at mesophyll pCO_2 (C_m) of 140 µbar (Equation 5).

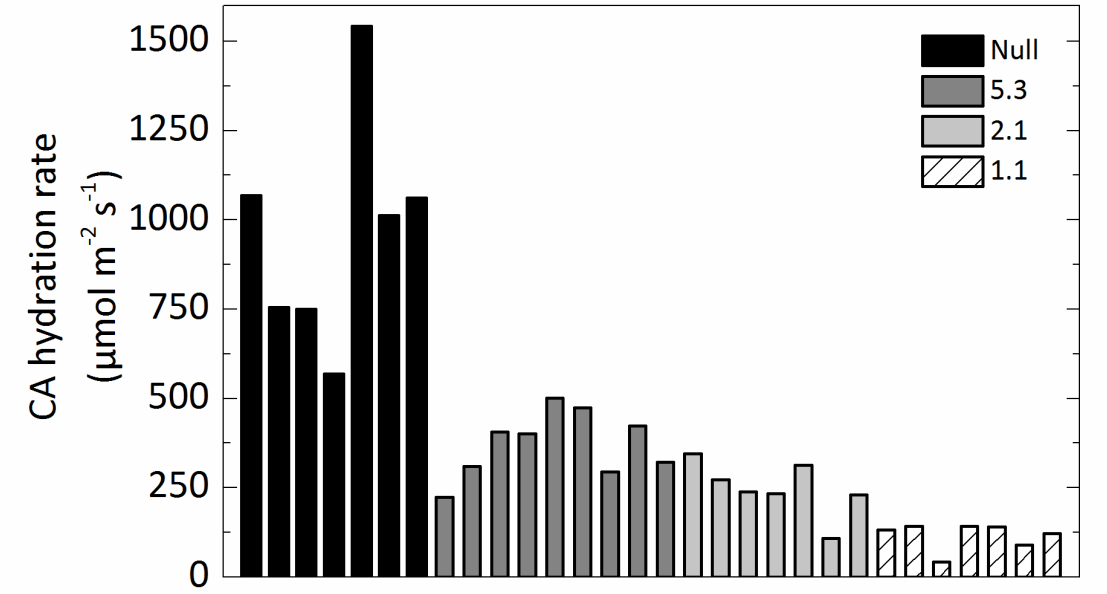

Figure 5.7: Range of CA hydration rates at mesophyll pCO_2 (C_m). Measured using a membrane inlet mass spectrometer in the null control and three T_2 plants from lines 5.3, 2.1 and 1.1.

The activities of the photosynthetic enzymes Rubisco, PEPC and NADP-ME were unchanged in lines 5.3, 2.1, and 1.1 compared to the nulls and showed no correlation with CA hydration rates (one-way ANOVA and Tukey post hoc analysis (SPSS statistics version 22; p = 0.05).

No significant differences were observed for the surface area of mesophyll cells exposed to intercellular airspace per unit leaf area (S_m) in embedded leaf sections of nulls (10.22 $\pm$ 0.35 $m^2\,m^{-2}$) and plants from line 1.1 (10.18 $\pm$ 0.95 $m^2\,m^{-2}$). These anatomical measurements were used to estimate an anatomical g_m of 0.68 mol $m^{-2}\,s^{-1}\,bar^{-1}$ (Section 5.2.14).

Table 5.1: Physiological and biochemical characteristics of CA transformants under ambient CO_2 conditions. Net CO_2 assimilation rate (*A*), stomatal conductance (g_s), mesophyll pCO_2 (C_m), the rate constant of CA hydration (k_{CA}) and enzyme activities were measured from the uppermost, fully expanded leaf of 5 week-old plants grown at 2% CO_2. Gas exchange measurements were made at 25 °C leaf temperature, flow rate at 500 µmol m^{-2} s^{-1}, irradiance of 1500 µmol photons m^{-2} s^{-1}. Three T_2 plants from three different transformation events were measured, significant difference based on one way ANOVA and Tukey post hoc analysis (SPSS statistics version 22; p = 0.05).

	A µmol m^{-2} s^{-1}	g_s mol m^{-2} s^{-1}	C_m µbar	k_{CA} mol m^{-2} s^{-1} bar^{-1}	**Rubisco** µmol m^{-2} s^{-1}	**PEPC** µmol m^{-2} s^{-1}	**NADP ME** µmol m^{-2} s^{-1}
Null	22.5 ± 0.6[a]	0.19 ± 0.01[a]	132.4 ± 3.3[a]	6.1 ± 0.8[a]	18.7 ± 1.5[a]	229.6 ± 19.3[a]	59.8 ± 4.3[a]
5.3	21.7 ± 2.6[a]	0.2 ± 0.02[a]	118.9 ± 13.1[a]	3.3 ± 0.2[b]	18.8 ± 1.8[a]	249.3 ±24.6[a]	54.5 ± 5.8[a]
2.1	18.5 ± 1.9[a]	0.16 ± 0.01[a]	152.9 ± 15.2[a]	2.0 ± 0.2[bc]	20.9 ± 2.9[a]	181.5 ± 25.4[a]	47.3 ± 2.6[a]
1.1	19.1 ± 1.2[a]	0.19 ± 0.02[a]	153.9 ± 4.4[a]	0.8 ± 0.1[c]	19.7 ± 1.8[a]	180.3 ± 18.4[a]	43.6 ± 3.9[a]

5.3.4 CO_2 assimilation rates

The response of CO_2 assimilation rate (*A*) to increasing intercellular pCO_2 (C_i) was investigated to examine the effect of reduced CA activity on CO_2 assimilation rates (Figure 5.8A). There were no statistical differences in the maximum rate of CO_2 assimilation under ambient or high CO_2 conditions between null control and progeny of transformant lines. At low pCO_2, CO_2 assimilation rates were reduced to varying degrees in the progeny of the transformed lines compared to the null control. Individuals of line 1.1 with the lowest CA hydration rate had the lowest initial slopes of the AC_i curves. The initial slopes of the AC_i and AC_m curve were plotted against the CA hydration rate constant (k_{CA}; Figure 5.9). Mesophyll cytosolic pCO_2, C_m was calculated from Equation 5, using the average null g_m (0.9 mol m^{-2} s^{-1} bar^{-1}) since there was no difference in S_m. A strong correlation between the initial slope from the AC_m curve and k_{CA} was observed with initial slope increasing as CA hydration rates increase (R^2 = 0.845; Figure 5.9). There was a curvilinear response between the initial slope of the AC_i curves indicating other limitations. No difference in stomatal conductance (g_s) was observed across a range of intercellular pCO_2 between null controls and any of the transformed lines during the rapid measurements of CO_2 responses (Figure 5.8B).

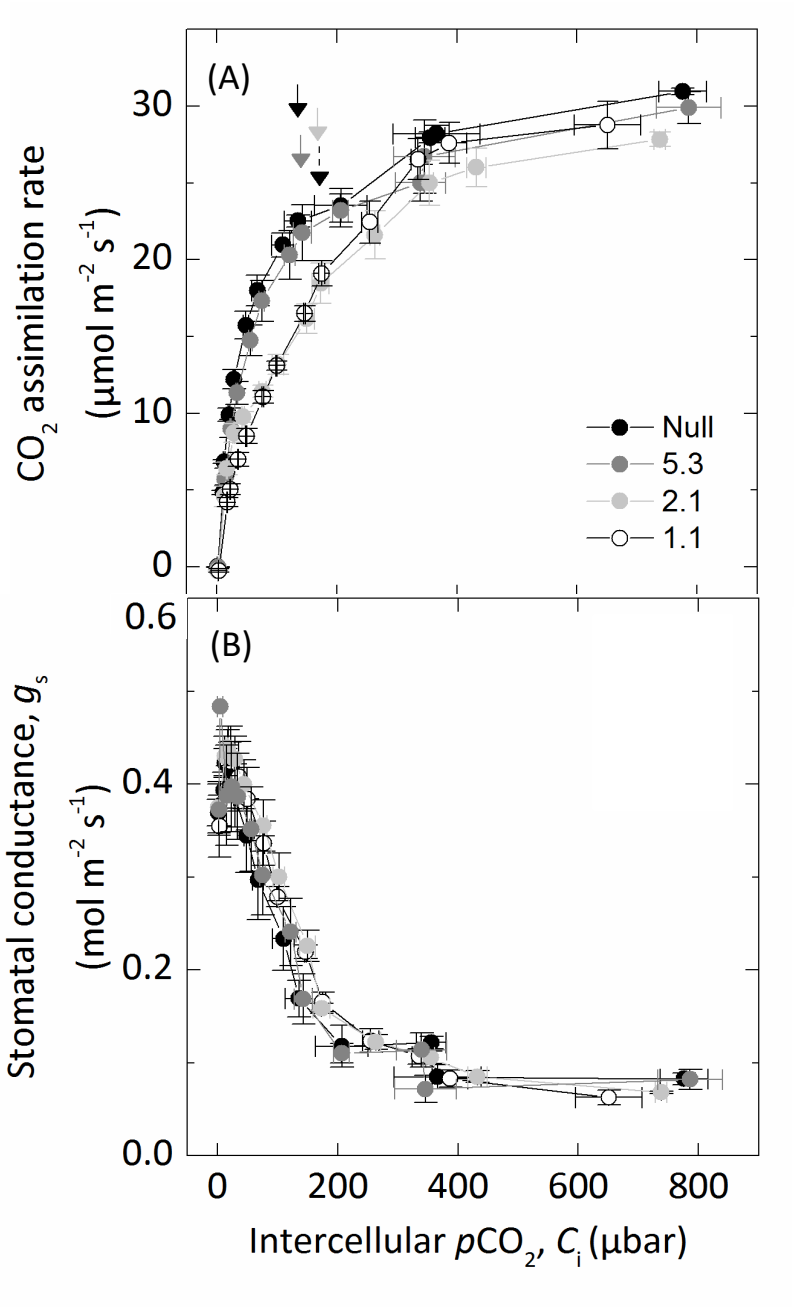

Figure 5.8: (A) CO_2 assimilation rate and (B) Stomatal conductance (g_s) over a range of intercellular pCO_2 (C_i). Average of three T_2 plants from each line. Plants were grown at 2% CO_2 and the uppermost, fully expanded leaf of 5 week-old plants were measured using a LI-6400XT at 25 °C leaf temperature at an irradiance of 1500 µmol photons m^{-2} s^{-1}. Arrows (A) mark ambient pCO_2 for each line, note dotted arrow is line 1.1.

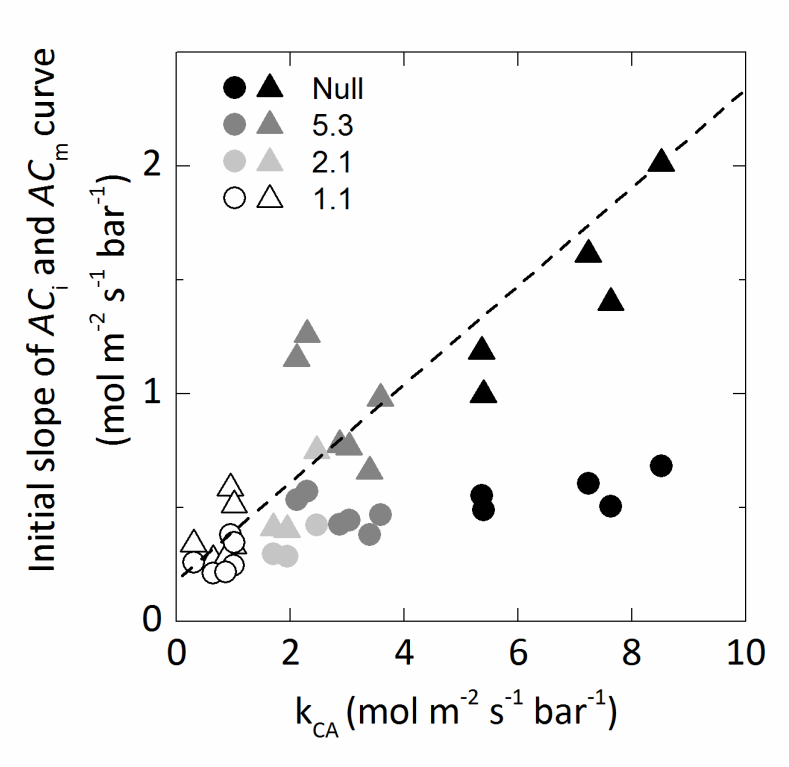

Figure 5.9: Relationship between the initial slope of the AC_m (triangles) or AC_i (circles) curves and the rate constant of CA hydration rates (k_{CA}). AC_m R^2 = 0.846. Each point represents a measurement made on an individual leaf of a T_2 plant.

5.3.5 Oxygen isotope discrimination measurements

Oxygen ($\Delta^{18}O$) isotope discrimination and CO_2 assimilation rates were measured in response to changes in pCO_2 using a LI-6400XT coupled to a tunable diode laser trace gas analyser to measure $C^{18}O^{16}O$ and a Cavity Ring-Down Spectrometer to measure the oxygen isotope composition of water vapour. Transformed plants with reduced CA hydration rates had lower $\Delta^{18}O$ compared to the nulls, but only line 1.1 was significantly lower (Table 5.2).

Table 5.2: Physiological characteristics of CA transformants at ambient CO_2 measured using LI-6400XT coupled to a tunable diode laser. Net CO_2 assimilation rate (A), stomatal conductance (g_s), mesophyll pCO_2 (C_m), the ratio of intercellular to ambient pCO_2 (C_i/C_a), the rate constant of CA hydration (k_{CA}), online $\Delta^{18}O$ discrimination and the length of mesophyll cells exposed to intercellular airspace (S_m) were measured on the uppermost, fully expanded leaf of 5 week-old plants grown at 2% CO_2. Gas exchange measurements were made at 2% O_2, 25 °C leaf temperature, flow rate at 500 µmol m^{-2} s^{-1}, irradiance of 1500 µmol photons m^{-2} s^{-1}. Three T_2 plants from two different transformation events were measured, significant difference based on one way ANOVA and Tukey post hoc analysis (SPSS statistics version 22; p = 0.05).

	A µmol m^{-2} s^{-1}	g_s mol m^{-2} s^{-1}	C_m µbar	C_i/C_a µbar	k_{CA} mol m^{-2} s^{-1} bar^{-1}	$\Delta^{18}O$ ‰	S_m m^2 m^{-2}
Null	30.0 ± 1.4[a]	0.30 ± 0.03[a]	144.6 ± 5.9[a]	0.39 ± 0.03[a]	8.4 ± 0.7[a]	18.0 ± 1.4[a]	10.2 ± 0.4[a]
5.3	29.2 ± 0.9[a]	0.29 ± 0.02[a]	157.9 ± 10.5[a]	0.34 ± 0.01[a]	2.5 ± 0.3[b]	13.6 ± 0.7[ab]	-
1.1	24.5 ± 1.6[a]	0.26 ± 0.03[a]	178.1 ± 13.5[a]	0.43 ± 0.02[a]	0.8 ± 0.2[b]	10.9 ± 0.6[b]	10.2 ± 0.9[a]

In the null controls, measurements of $\Delta^{18}O$ were used to estimate conductance of CO_2 from the intercellular airspace to the sites of CO_2 and H_2O exchange in the cytosol (g_m) with the assumption that CO_2 was in full isotopic equilibrium with leaf water in the cytosol (Equation 5, Figure 5.10). Although g_m appeared to increase with decreasing C_i there were no significant differences between g_m estimated at the different C_i and the average value was 0.94 $\pm$ 0.06 mol m^{-2} s^{-1} bar^{-1} (Figure 5.10B). $C_i - C_m$ indicates the drawdown of CO_2 from the intercellular airspace to the site of fixation and for the null controls there is an increasing gradient of pCO_2 as C_i increases (Figure 5.10C).

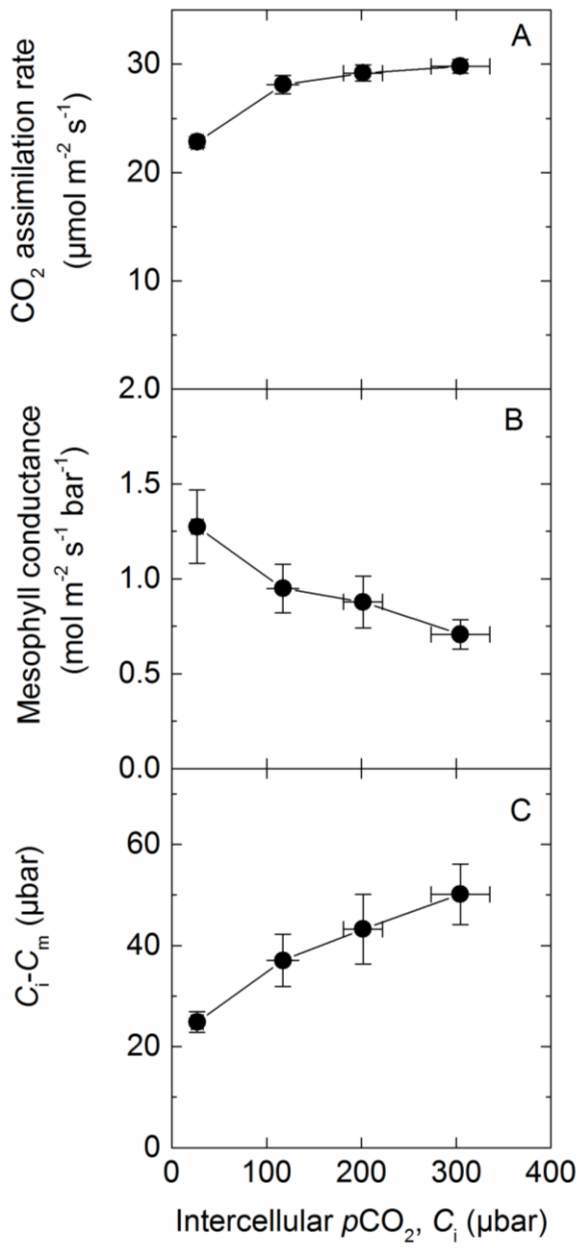

Figure 5.10: Physiological characteristics of null controls measured over a range of intercellular pCO_2 using a LI-6400XT coupled to a tunable diode laser. (A) CO_2 assimilation rate, (B) mesophyll conductance (g_m: Equation 5) and (C) C_i – C_m. Plants were grown at 2% CO_2 and the uppermost, fully expanded leaf of 5 week-old plants were measured at 25 °C leaf temperature, flow rate 200 µmol m^{-2} s^{-1}, 2% O_2 at an irradiance of 1500 µmol photons m^{-2} s^{-1}.

$\Delta^{18}O$ at ambient pCO_2 showed statistically significant differences between line 1.1 (with the lowest CA activity) and null plants (Table 5.2). When plotted against C_m/C_a, $\Delta^{18}O$ measurements closely correspond with theoretical curves representing θ (Equation 19) under different scenarios either where cytosolic CO_2 is at full isotopic equilibrium with the cytosolic water (null lines) or where there is only partial equilibrium (such as line 1.1; Figure 5.11). Calculated values for line 5.3 which showed a 50% reduction in CA activity relative to the null controls fell in between these two theoretical lines. This is illustrated again with theta (θ) of lines 1.1 and 5.3 over a range of C_m (Figure 5.12). When CO_2 is at full isotopic equilibrium with the cytosolic water θ would be 1, whereas in lines 1.1 and 5.3 (with reduced CA hydration rates relative to the null control) θ is less than 1. There was no CO_2 dependence of θ over the range of pCO_2 measured.

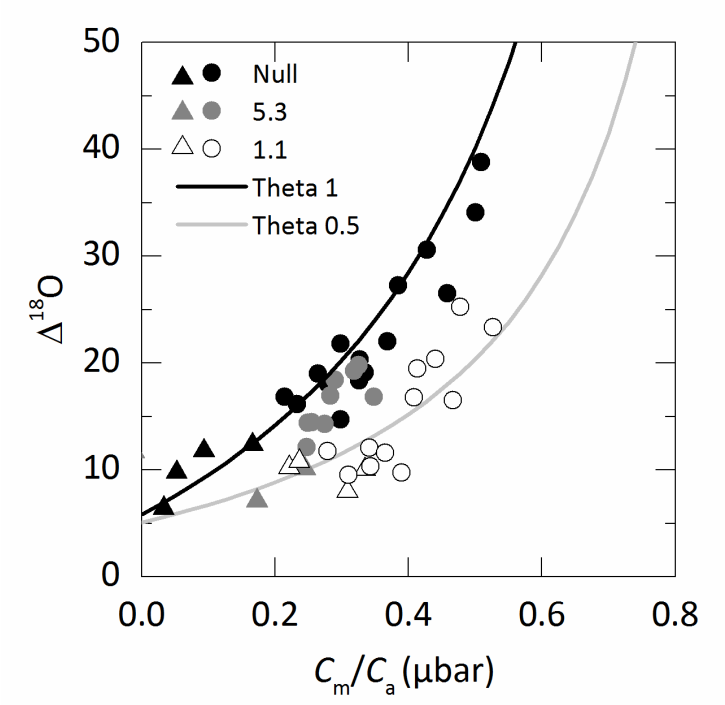

Figure 5.11: Oxygen isotope discrimination ($\Delta^{18}O$) as a function of the ratio of mesophyll pCO_2 to ambient pCO_2 (C_m/C_a) in null and lines 5.3 and 1.1. Each point represents a measurement made on an individual leaf of a T_2 plant. Triangle symbols represent measurements made at low pCO_2. Theoretical curves represent the scenario where cytosolic CO_2 is at full isotopic equilibrium with cytosolic water (Theta = 1, black) or under partial equilibrium (Theta = 0.5, grey) of ^{18}O in the leaf. The equations for the curves are given by $\Delta^{18}O = a_{18} + \frac{C_m}{C_a - C_m}(\delta_c - \delta_a)$ and a_{18}=5.85‰ and $\delta_c - \delta_a$=33‰ at full equilibration or a_{18}=5.1‰ and $\delta_c - \delta_a$=15‰ (Farquhar and Lloyd, 1993).

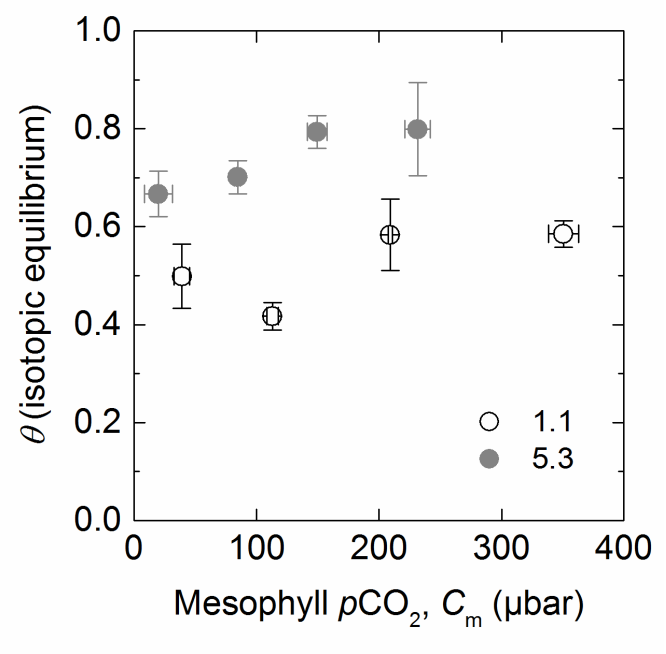

Figure 5.12: Average isotopic equilibrium (theta, θ) over a range of mesophyll pCO_2 in two reduced CA lines 5.3 (grey) and 1.1 (white). Measured values of θ were determined from $\Delta^{18}O$ using Equation 19. Each point represents the average measurement of three T_2 plants.

5.4 Discussion

5.4.1 S. viridis as a model species to study photosynthetic physiology in a C_4 monocot

Flaveria bidentis, a readily transformable model C_4 dicot, has been successfully used to study the regulation of C_4 photosynthesis using antisense and RNAi technology (Furbank *et al.*, 1997; Matsuoka *et al.*, 2001; Pengelly *et al.*, 2012; von Caemmerer *et al.*, 2004). This work has been crucial in quantifying the rate limiting steps in the C_4 pathway by "titrating" out levels of target enzymes by gene suppression and observing the effects on physiological characteristics of the resultant transgenics (Furbank *et al.*, 1997). There are however important differences between C_4 dicots and the C_4 monocots which make up the majority of agriculturally important C_4 species. *S. viridis* has emerged as a new model grass to study C_4 photosynthesis in crops and related bioenergy species. *S. viridis* is an appropriate biochemical model species for *Z. mays* and *S. bicolor* as all three use NADP-ME as the primary decarboxylation enzyme. We generated transgenic *S. viridis* plants with reduced CA activity to compare the effect to previous results obtained with *F. bidentis* and *Z. mays* (Studer *et al.*, 2014; von Caemmerer *et al.*, 2004) and to explore the effect of a reduction in CA activity has on the initial slope of the AC_i and AC_m curves. In these lines, only the major leaf isoform of β-CA was reduced (Figure 5.6). The transgenic plants had a range of different CA activities (Figure 5.7), but showed no changes in PEPC and Rubisco activity (Table 5.1) or anatomical parameters (Table 5.2) making these plants ideal for exploring the role of CA activity in *S. viridis*.

5.4.2 Initial slope of AC_i curves in C_4 plants

Models of C_4 photosynthesis suggest that the initial slope of the AC_i curve is determined by three possible limitations: a) the mesophyll conductance to CO_2 diffusion from intercellular airspace to the mesophyll cytosol (g_m), b) the rate of CO_2 hydration by CA and c) the rate of PEP carboxylation (von Caemmerer, 2000). However, it is not readily known which is the major limitation in C_4 species. Studies with PEPC mutants from the C_4 dicot, *Amaranthus edulis* indicate that PEPC activity may not be the major limitation as a 60% reduction in PEPC leads to only a 20% reduction in CO_2 assimilation rate at ambient pCO_2 accompanied by a small reduction in initial slope for the AC_i curves (Cousins *et al.*, 2007; Dever *et al.*, 1997). This study with *S. viridis* confirms that substantial reductions in CA activity are possible before a reduction in steady state CO_2 assimilation rate and initial slope of the AC_i curve are observed.

This is in accordance with previous observations in *F. bidentis* and *Z. mays* (Studer *et al.*, 2014; von Caemmerer *et al.*, 2004).

The Michaelis Menten constant for CO_2 for CA is above 2 mM (~5% CO_2) which makes it appropriate to quantify CA activity by its first order rate constant (Hatch and Burnell, 1990; Jenkins *et al.*, 1989) and simplifies species comparisons. In *S. viridis*, the lowest rate constant recorded was 0.8 mol m^{-2} s^{-1} bar^{-1} compared to values of 0.1 for the Ca1Ca2 double mutant in *Z. mays* and 0.47 for transgenic *F. bidentis* (Studer *et al.*, 2014; von Caemmerer *et al.*, 2004). With this low rate constant, *F. bidentis* had very low CO_2 assimilation rates and the CO_2 response curves did not saturate at high CO_2. By contrast, for both *S. viridis* transgenics and *Z. mays* mutants CO_2 assimilation rates were only slightly less than the controls, suggesting that *S. viridis* is more similar to *Z. mays* in its CA requirements. This suggests that these two monocot species can make better use of leaf CA activity or that *in vivo* CA activity is greater than that estimated *in vitro*.

5.4.3 Mesophyll conductance and the initial slope of AC_m curves

Next, we used recently established techniques that utilise ^{18}O discrimination measurements to quantify g_m in our null controls (Figure 5.10B; Barbour *et al.*, 2016). This estimates the diffusion of CO_2 from the intercellular airspace through the cell wall, plasma membrane and cytosol to the sites of CA activity. At ambient pCO_2, the g_m observed for the null plants were similar to those reported by Barbour *et al.* (2016) and Ubierna *et al.* (2017). A key assumption for the calculation of g_m is that CA activity is not limiting and that CO_2 is in isotopic equilibrium with HCO_3^-, consequently g_m was not measured in the transgenic lines with reduced CA activity. In C_3 species g_m (in this instance from intercellular airspace to the chloroplast stroma) has been shown to be proportional to the chloroplast surface area appressing intercellular airspace per unit leaf area (Evans *et al.*, 1994). Evans and von Caemmerer (1996) hypothesized that in C_4 species g_m may correlate with the mesophyll surface area exposed to intercellular airspace per unit leaf area (S_m). Since S_m was similar between the nulls and line 1.1 plants we assumed g_m may also be similar between the plants. In C_3 species, g_m has been shown to, in some instances, increase with decreasing pCO_2 (Alonso-Cantabrana and von Caemmerer, 2016; Flexas *et al.*, 2007; Tazoe *et al.*, 2011). These changes to g_m which may be important in regulating and maintaining photosynthesis were also observed here in the *S. viridis* null plants with g_m increasing slightly at low pCO_2. However, because the differences in g_m at different pCO_2 were not significant we used the average g_m estimated for the null plants to calculate mesophyll cytosolic pCO_2 (C_m) in the transgenics.

As shown in Figure 5.9, a strong almost linear relationship was found between AC_m vs k_{CA} whereas a saturating relationship was observed with AC_i. This indicates that CO_2 assimilation rate is limited by cytosolic CA activity, with the relationship becoming clearer after accounting for g_m. It is tempting to speculate that the differences between the two monocot species and *F. bidentis* relate to differences in limitations imposed by g_m which affects cytosolic pCO_2 and hence *in vivo* CA activity, but this is not borne out by comparative measurements of g_m made by Barbour *et al.* (2016). CA activity increases with increasing pH, so variation in cytosolic pH can also contribute to variations in *in vivo* CA activity, however these effects are not large (Jenkins *et al.*, 1989). The interaction of β-CA and a CO_2 permeable aquaporin in *A. thaliana* has indicated that CA can be localised near the plasma membrane rather than dispersed throughout the mesophyll cytosol (Wang *et al.*, 2016). This may also impact on CA activity and result in another difference between the C_4 species. Other possibilities pertain to differences in anatomical characteristics of leaves. Both CA and PEPC are cytosolic enzymes and differences in S_m may affect the efficiency with which CA is used. Our results suggest that increasing g_m may be an important way to increase CO_2 assimilation rate at low intercellular pCO_2, a scenario that may, for example, occur under drought.

5.4.4 Oxygen isotope discrimination and the CO_2 dependence of isotopic equilibrium

As had previously been observed, $\Delta^{18}O$ decreased with reductions in CA activity as CA facilitates the exchange of O_2 between cytosolic water and CO_2 (Figure 5.11; Cousins *et al.*, 2006; Williams *et al.*, 1996). Previous reports, which have estimated the proportion of cytosolic CO_2 in equilibrium with leaf water (θ) in C_4 species, have generally assumed a relatively large g_m value and this then led to lower estimates of θ (Cousins *et al.*, 2006; Cousins *et al.*, 2008). Here we assumed that in the *S. viridis* null plants there is sufficient CA for isotopic equilibrium to be reached as discussed by Barbour *et al.* (2016). For comparison we also estimated g_m from anatomical estimates of S_m, cell wall and cytosolic thickness following calculations outlined by von Caemmerer and Evans (2015). This gives a g_m value of 0.68 mol m^{-2} s^{-1} bar^{-1} which is less than the value of 0.9 mol m^{-2} s^{-1} bar^{-1} calculated from $\Delta^{18}O$ measurements and highlights the anatomical constraints for CO_2 diffusion dictated by the photosynthetic pathway in leaves of C_4 plants (von Caemmerer *et al.*, 2007).

Reduction in CA activity led to significant reductions in θ but it is interesting to note that θ did not vary significantly with pCO_2. This is explained by the fact that CA activity increases linearly with pCO_2 so that although there is more CO_2 that needs to equilibrate with leaf water there is also proportionally more CA activity. The fact that neither transgenic line showed a

CO_2 dependence suggests that the decrease in ratio of CA hydrations to PEP carboxylations is not affecting the isotopic equilibration of CO_2 with leaf water. These results have important implications for the interpretation of ^{18}O signature of atmospheric CO_2 (Gillon and Yakir, 2000; Wingate *et al.*, 2009; Yakir and Sternberg, 2000).

5.4.5 Reduction in CA in S. viridis does not alter the stomatal response to CO_2

The CO_2 regulation of stomatal conductance remains an open question (Engineer *et al.*, 2016). It has been previously shown that in the ca1/ca4 double mutant of *A. thaliana*, the degree of stomatal closure in response to increasing pCO_2 was reduced (Hu *et al.*, 2010; Wang *et al.*, 2016). It is clear that CA is part of a complex signal transduction network. However, nothing is currently known about the role of CA in stomatal CO_2 responses in C_4 species. In our study, where only one β-CA isoform was reduced, we found no change in the response of stomatal conductance to CO_2. The *S. viridis* β-CA reduced here (*Sevir.5G247800*) has low sequence identity (< 50%) to all of the Arabidopsis β-CAs but we would predict that multiple reductions in β-CA isoforms would be required to observe a similar stomatal phenotype in *S. viridis*.

5.4.6 Conclusion

Under current atmospheric conditions, CA activity was not rate limiting for C_4 photosynthesis in *S. viridis.* At lower C_i, which may, for example, occur under conditions of drought, our results suggest that g_m may pose a greater limitation than CA activity. However, it is important to investigate the role of CA on C_4 photosynthesis under a range of environmental conditions such as high temperatures which have recently been suggested to deactivate CA activity in *S. viridis* (Boyd *et al.*, 2015; Ubierna *et al.*, 2017). Here we have shown that *S. viridis* is a useful model monocot C_4 species that lends itself to molecular manipulation of the C_4 photosynthetic pathway.

CHAPTER 6: GENERAL DISCUSSION AND CONCLUSIONS

6.1 Overview

There is strong evidence that high rates of photosynthesis require high rates of CO_2 diffusion within leaves (Evans and von Caemmerer, 1996). Consequently, improving CO_2 diffusion is a major target in efforts to improve photosynthesis and overall crop productivity. To this end, I have investigated CO_2 permeable aquaporins and carbonic anhydrase activity in the C_4 grass *S. viridis.*

Firstly, I investigated the phylogeny and expression pattern of PIPs, plasma membrane intrinsic proteins, in Setaria (Chapter 2). There are 41 aquaporins in *S. viridis* which are divided into four different groups based on localisation and amino acid homology. The group localising to the plasma membrane, PIPs, are the only group identified to date which can permeate CO_2. There are 12 PIPs which share very high sequence similarity between *S. viridis* and *S. italica*, 10 out of the 12 share 100% identity between the different species. In Chapter 2 I used publically available transcriptomic data to examine the expression pattern of these PIPs. I observed higher expression for most of the PIPs in the roots compared to the leaves, and much higher expression when exposed to drought stress in the roots. *SvPIP2;8* had the highest expression in the leaves out of all the PIPs, and along with *SvPIP2;4* were the only 2 PIPs with higher expression in the mesophyll cell relative to the bundle sheath cells. This location is an important factor for CO_2 permeable aquaporins in a C_4 photosynthetic leaf to support the unique CO_2 concentrating mechanism.

Despite the increasing information available on aquaporins it is still very difficult to predict specific substrate permeability based on sequence homology or transcript expression profiles. Therefore I used yeast as a heterologous expression system to test for CO_2 permeability in all 12 Setaria PIPs (Chapter 3). Using separate GFP tagged versions of each aquaporin I determined the localisation of each aquaporin within the yeast cell and then tested for permeability using CO_2 triggered intracellular acidification detected using stopped flow spectrophotometry. The majority of the PIP2s localised to the plasma membrane. However, as reported in the literature, PIP1s required co-expression with a PIP2 for correct localisation. To calculate a final CO_2 permeability value I also determined the final intracellular pH, the average cell size and ensured CA activity was non-limiting. Using this approach I identified SiPIP2;7 as a CO_2 permeable aquaporin, adding a third CO_2 pore to the list of C_4 plant aquaporins characterised to date.

Testing the role of aquaporins *in planta* is vital to confirm permeability determined from an isolated expression system and to determine if interactions with native PIPs and plant

proteins influence this permeability. I attempted to examine the effects of overexpressing a known CO_2 permeable aquaporin, *AtPIP1;2*, in *S. viridis* (Chapter 4). To date, there has been no information on the role of CO_2 permeable aquaporins in C_4 photosynthesis and the impact on modifying their expression within this photosynthetic mechanism. Unfortunately our experiments did not meet this aim as an incomplete, truncated transgene was incorporated, resulting only in reduced CA in one transformed line and no effects on PIP expression. The von Caemmerer lab has since significantly developed and improved *S. viridis* transformation efficiency and is now following up this research aim to understand CO_2 permeable aquaporins in C_4 plants.

In Chapter 5 I explored the role of CA in CO_2 diffusion further by modifying the expression of CA in Setaria. I used a stable transformation approach to modify CA in this model grass. Reduced CA activity altered the gas exchange phenotype, specifically resulting in a lower CO_2 assimilation rates at low CO_2. Along with mesophyll conductance, we hypothesised that CA activity was a major limiting factor for photosynthesis under low CO_2 conditions.

6.2 Modelled effects of altered mesophyll conductance

Together with stomatal conductance (g_s) and biochemical capacity, mesophyll conductance (g_m) is a major factor influencing C_3 photosynthesis (Flexas *et al.*, 2012). Comparative to C_3 photosynthesis, very little research has been done in C_4 photosynthesis; however, with advances in technology more measurements are being made to demonstrate the importance of g_m. Indeed, a strong relationship between CO_2 assimilation rate and g_m has been observed for maize, Setaria and miscanthus (Ubierna *et al.*, 2017) and *Flaveria bidentis* (Barbour *et al.*, 2016). Here, I have modelled the effect of increasing g_m in C_4 photosynthesis to highlight the role of CO_2 diffusion pertaining to my investigations of CO_2 permeable aquaporins and CA.

In C_4 photosynthesis, CO_2 moves from the atmosphere (C_a), through the stomata of the leaf to the intercellular space (C_i) and across the mesophyll plasma membrane (C_m) to its site of hydration with CA (Figure 6.1). As CO_2 diffuses from the air to the site of fixation there are a number of resistances, including g_s and g_m, which decrease the CO_2 partial pressure along the diffusion pathway so that $C_a > C_i > C_m$ (Figure 6.1A). Under suboptimal conditions such as drought stress, stomata close to reduce water loss, and as a consequence this also reduces CO_2 diffusion. I hypothesised that, in these situations where C_i is low, overexpression of CO_2 permeable aquaporins would increase g_m resulting in elevated C_m (Figure 6.1B). CO_2

permeable aquaporins have been demonstrated to influence g_m within C_3 photosynthetic systems; however the effect on a C_4 photosynthetic system is unknown. I modelled the predicted effect of increasing CO_2 diffusion on a C_4 crop by increasing g_m on an individual leaf level and also on the crop canopy level and then compared the effect of altering g_m under low CO_2 conditions.

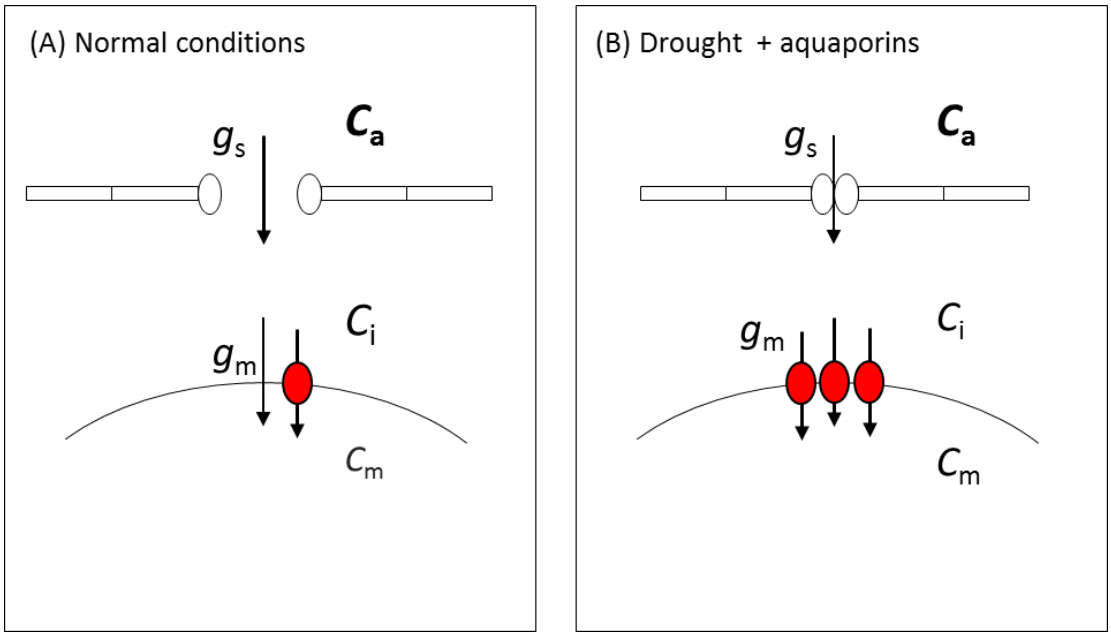

Figure 6.1: Diagram of CO_2 diffusion under different conditions. (A) Under normal conditions CO_2 moves through the stomata and into the mesophyll cell. (B) Under drought conditions stomata close to reduce water loss and consequently there is less CO_2 diffusion. I hypothesise that this may be overcome by overexpressing CO_2 permeable aquaporins (red circles). Note g_s and g_m are stomatal and mesophyll conductance respectively; C_a, C_i and C_m are the ambient, intercellular and mesophyll CO_2 partial pressures respectively.

Using comparable variables to that observed for Setaria in Chapter 5 (Table 6.1), I modelled an AC_i curve with the average g_m of 0.9 mol m^{-2} s^{-1} bar^{-1} on an individual leaf in Figure 6.2A using equations from von Caemmerer (2000). This g_m was calculated for wild type *S. viridis* using a tunable diode laser system measuring $\Delta^{18}O$ to estimate conductance of CO_2 from the intercellular airspace to the sites of CO_2 and H_2O exchange in the cytosol, with the assumption that CO_2 was in full isotopic equilibrium with leaf water in the cytosol (see Section 5.2.11). I then modelled the effect of halving this g_m to 0.45 which showed a lower initial slope of the AC_i curve whereas doubling g_m to 1.8 mol m^{-2} s^{-1} bar^{-1} showed only a modest increase in initial

slope above normal g_m (Figure 6.2A). The effect of increasing g_m on CO_2 assimilation rate is modelled in Figure 6.2B. This demonstrates that the impact of increasing g_m starts to plateau beyond a g_m of 0.5 mol m^{-2} s^{-1} bar^{-1} under normal conditions with C_i of 150 µbar and increasing g_m no longer has an impact on the assimilation rate. Under low C_i of 0.75 µbar, such as might occur under drought conditions when stomata close to conserve water (Figure 6.1), increasing g_m continues to increase assimilation rate, though this increase slows beyond g_m of 1 mol m^{-2} s^{-1} bar^{-1}.

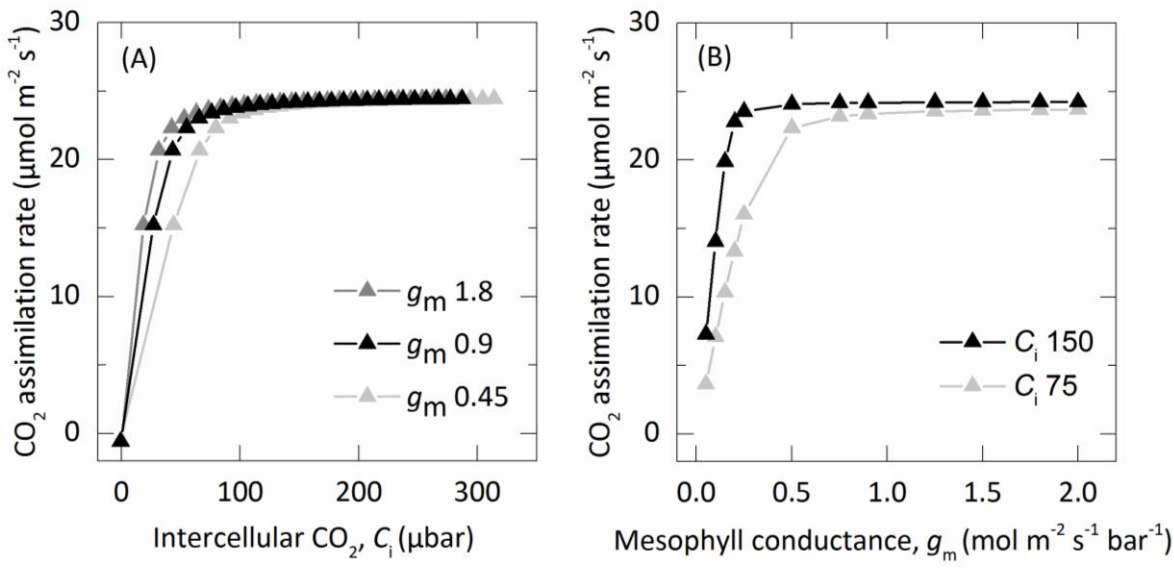

Figure 6.2: Modelled effects of altering g_m on a leaf level (von Caemmerer, 2000).(A) CO_2 assimilation rate over a range of C_i (intercellular CO_2 partial pressures) at different g_m including low, normal and high g_m (0.45, 0.9 and 1.8 mol m^{-2} s^{-1} bar^{-1} respectively). (B) The effect of changing g_m on CO_2 assimilation rate under different C_i: normal C_i at 150 µbar or low C_i at 75 µbar.

Table 6.1: Variables used in modelling the effect of altered g_m on a leaf level or canopy level basis. Canopy level V_{cmax} and V_{pmax} are calculated per m^2 ground level but are equivalent to leaf level values.

Variable	Description	Value on leaf level	Value on canopy level
V_{cmax}	Maximum Rubisco carboxylation rate	25.94 µmol leaf m^{-2} s^{-1}	155.64 µmol ground m^{-2} s^{-1}
V_{pmax}	Maximum PEP carboxylation rate	341.07 µmol leaf m^{-2} s^{-1}	2046.47 µmol ground m^{-2} s^{-1}
g_{bs} CO_2	Bundle sheath conductance to CO_2	0.003 mol m^{-2} s^{-1}	0.003 mol m^{-2} s^{-1}
$T_{max/min}$	Maximum and minimum temperature	25 °C	28/21 °C
C_i/C_a	Ratio of the intercellular to ambient CO_2 partial pressures	0.39 or 0.2	0.39 or 0.2
C_i/C_a vs VPD	Slope of linear relationship between C_i/C_a and air vapour pressure deficient		0

Note: C_i/C_a vs VPD is set to 0 in DCaPS to simulate a constant C_i/C_a and eliminate g_s as a factor.

I used the Daily Canopy Photosynthesis Simulator (DCaPS; www.dcaps.net.au) developed by Wu *et al.* (2016) to model the effect of increasing g_m at the crop canopy level. Upscaling from the biochemical models of C_4 leaf photosynthesis to canopy level requires modelling of key environmental factors (i.e. light, CO_2 and temperature), canopy nitrogen status, and canopy architecture (i.e. leaf area index and leaf angle). The modelling framework of DCaPS is shown in Figure 6.3 which combines biochemical leaf level photosynthesis with canopy/crop level growth and development factors. A number of the DCaPS parameters were altered to reflect the growth conditions and responses observed previously for Setaria (Chapter 5; Table 6.1). Using these variables and assuming the DCaPS settings for diurnal temperature and sunlight to shaded leaves ratio are appropriate for Setaria, I examined the response of crop biomass to g_m of 0.45, 0.9 and 1.8 mol m^{-2} s^{-1} bar^{-1}. I observed a similar response to the leaf level modelling, specifically under optimal conditions; total crop biomass was predicted to

increase by 0.07% when g_m increased from 0.45 to 0.9 mol m^{-2} s^{-1} bar^{-1} compared to a more modest increase of 0.04% if g_m was doubled from 0.9 to 1.8 mol m^{-2} s^{-1} bar^{-1}. Consistent with the leaf level modelling this increase is larger if we simulate drought stress, such as a low CO_2 environment due to stomatal closure by reducing the intercellular CO_2 concentration, as described by the ratio of C_i/C_a, to 0.2. Under these drought conditions and increasing g_m from 0.45 to 0.9 mol m^{-2} s^{-1} bar^{-1} then a 5.5% increase in crop biomass is predicted with DCaPS. The improvement in biomass under drought conditions, when g_m is doubled from 0.9 to 1.8 mol m^{-2} s^{-1} bar^{-1}, is comparable to the increase in biomass predicted under normal condition of 0.04%. Again, this small increase at higher g_m predicted by DCaPS is reflected in the leaf level model (Figure 6.2B).

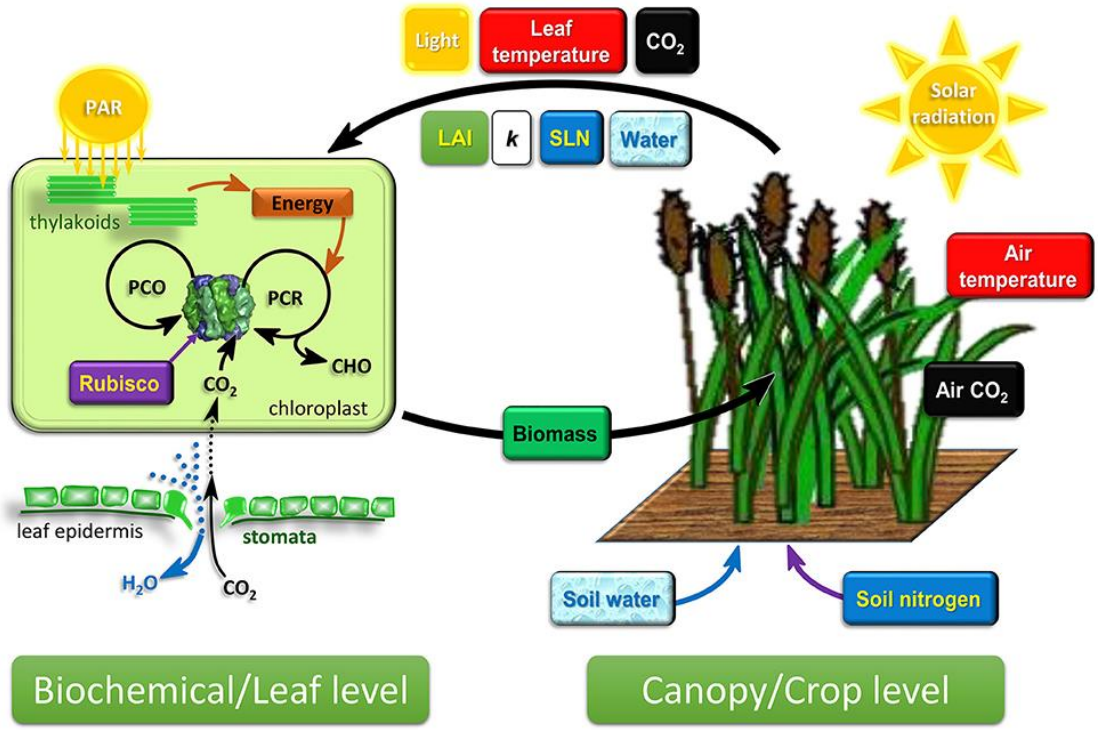

Figure 6.3: The cross-scale modelling framework considered in the Daily Canopy Photosynthesis Simulator (DCaPS). The canopy model can be used for both C_3 (shown in this figure) and C_4 photosynthetic crops. It connects both biochemical/leaf level photosynthesis with canopy/crop level growth and development factors. Note: PAR, photosynthetic active radiation; LAI, leaf area index; k, canopy light extinction coefficient; SLN, specific leaf nitrogen; PCR, photosynthetic carbon reduction cycle; PCO, photorespiratory carbon oxidation cycle; CHO, carbohydrates synthesized by photosynthesis. Image from Wu *et al.* (2016).

In both instances: leaf level and canopy level, modelling the effects of altered g_m indicates there are only modest increases in assimilation rate and biomass available by improving g_m alone under normal conditions. These predictions are consistent with previous findings using free air concentration enrichment (FACE) experiments that C_4 photosynthesis, specifically maize assimilation rate, biomass and yield, are not significantly affected by elevated ambient CO_2 conditions (Leakey *et al.*, 2006). A greater effect is predicted under drought conditions where stomata close to reduce water loss and thereby reduce C_i. Indeed, Ubierna *et al.* (2017) observed a strong temperature response for g_m in Setaria with g_m sharply decreasing with temperatures over 35 °C. Improving g_m by overexpressing CO_2 permeable aquaporins in plants exposed to extreme environments such high temperatures or drought stress may have a greater impact and be a valuable area for further research.

These simulations demonstrate the increases possible by changing just one photosynthetic parameter and the increases available under extreme conditions if g_m can be increased by overexpressing a CO_2 permeable aquaporin. Of course, this is an indication only and field trials and *in planta* experiments would be required, as have occurred for the impact of altered CA activity under low CO_2 conditions in maize (Studer *et al.*, 2014). Modifying multiple aspects of C_4 photosynthesis will ultimately have a larger impact on overall yield improvement. Indeed overall strategies for improving C_4 photosynthesis (von Caemmerer and Furbank, 2016) are aiming to increase not only CO_2 delivery but PEPC activity, Rubisco function, substrate regeneration, metabolite exchange and chloroplast electron transport.

6.3 Improvements to CO_2 permeability measurements

In order to improve g_m through manipulation of aquaporins, a better understanding of CO_2 permeable aquaporins is required. However, identifying and characterising aquaporins which are permeable to CO_2 is challenging. As discussed in Chapter 3, there are a number of limitations and difficulties involved in measuring CO_2 permeability, including specialised equipment, false positives due to proton permeability, aquaporin expression level, protein interactions and limited CA activity.

Heterologous expression systems such as yeast are commonly used to test for substrate permeability with a growth/death assay approach. This allows for high throughput and an indication of substrate permeability. This is routinely used for substrates which can be supplemented or depleted from the growth media such as sugars, metals or salts. From a CO_2

perspective, Ding *et al.* (2013) used a spot plate approach with cyanobacteria grown under different CO_2 conditions and compared a wild type strain to a knockout cyanobacteria aquaporin strain. They observed that the knockout aquaporin strain could not grow as well as the wild type in high CO_2 conditions and there was no difference in growth under low CO_2 conditions.

In a similar vein, an alternative and perhaps more thorough approach to measuring CO_2 permeability includes using an easily transformed plant such as tobacco to screen for altered g_m by complementation or overexpression which would indicate whether the aquaporin is involved in CO_2 diffusion *in planta*. Indeed, detecting changes in g_m in the C_3 model plant tobacco would be readily achievable compared to Arabidopsis which has low a g_m and any changes would be difficult to detect. This *in planta* approach has been used by a number of researchers to indicate CO_2 permeability of an aquaporin on the basis of altered g_m including for *AtPIP2;1* in Arabidopsis (Wang *et al.*, 2016) and *HvPIP2;1* in rice (Hanba *et al.*, 2004). However, since C_4 photosynthesis is anatomically and biochemically specialised compared to C_3 photosynthetic plants it would be advantageous and more complete to study C_4 aquaporins using C_4 model plants. This is increasingly achievable as the efficiency of stable *S. viridis* transformations increases.

6.4 Suggested areas for further research

6.4.1 Directed mutagenesis assay

It is very difficult to predict aquaporin function based on amino acid sequence, expected motifs or homology to known substrate permeable aquaporins identified in other species. Nor have expression patterns or co-location of key aquaporins with certain characteristics shed light on specificity of aquaporins for particular substrates. It appears that the only definitive approach to discovering the permeability of an aquaporin is to test it in a heterologous expression system or *in planta*. Here I found one aquaporin, SiPIP2;7, which was highly permeable to CO_2 relative to our control by heterologous expression in yeast. Interestingly, this aquaporin is very similar to SiPIP2;6 with only eight amino acids differing between the two aquaporins. Yet, SiPIP2;6 was not CO_2 permeable in yeast. Investigating these amino acid changes further revealed only two changes were unique to SiPIP2;7 compared to all other Setaria PIPs. We suggest that these would be ideal candidates to test

what determines CO_2 permeability, in a similar approach to that used to identify a CO_2 motif in barley PIPs (Mori *et al.*, 2014). A directed mutagenesis assay of SiPIP2;6 whereby each individual amino acid and combination of these changes is tested in a heterologous expression system would be key to furthering this research. Likewise, to further the preliminary work on PIP1 and PIP2 co-expression in Chapter 3, experimenting with a non-functional PIP2 co-expressed with the PIP1 would help elucidate the permeability, specifically, of the PIP1 when correctly localised to the plasma membrane.

Simulations of CO_2 permeation through aquaporins have been explored for human AQP1, highlighting the likelihood of CO_2 movement through the central pore of a tetramer due to lower activation energies than the individual monomer pores (Hub *et al.*, 2009). However, the key residues lining the central pore, identified by Yu *et al.* (2006), are identical in all 12 Setaria PIPs. More research is needed on CO_2 movement through this central pore to help predict substrate permeability. In addition, very little is known about gating in relation to CO_2 movement. It is likely important to control, but there is no empirical evidence for gating of CO_2 diffusion through PIPs to date.

6.4.2 Manipulating expression in planta

In Chapter 4 I attempted to examine the effects of overexpressing a CO_2 permeable aquaporin within the C_4 photosynthetic pathway, but I was unsuccessful due to technical issues. It is important to examine the *in planta* effects within a C_4 system to firstly validate modelling and test if improvements to g_m can be achieved within this photosynthetic mechanism and, secondly, to observe what other impacts may occur, such as increased assimilation rate, increased biomass or altered g_s. I attempted to overexpress a foreign CO_2 permeable aquaporin in Setaria, however, another approach would be to overexpress or knockout the native *SiPIP2;7* which I demonstrated in yeast to be a CO_2 permeable aquaporin. Interestingly, based on publicly available transcriptomic data, *PIP2;7* is highly expressed in the root compared to the leaf (Chapter 2, Phytomine). Which raises the question of whether PIP2;7 is CO_2 permeable *in planta* and playing a physiological role in CO_2 diffusion or rather is permeable to a number of substrates. This is the case for the dual function aquaporin NtAQP1 which is permeable to both H_2O and CO_2 and has different roles depending on where it is expressed in the plant (Sade *et al.*, 2010). Alternatively, SiPIP2;7 may still function as CO_2 permeable in the roots, as for example PEPC which is expressed in roots in C_3 plants where it

fixes bicarbonate and sends the C_4 acid up to the leaf for decarboxylation. More information is required on the expression of *SiPIP2;7* in the leaf, as it was not identified in the cell specific, mesophyll versus bundle sheath, transcriptomic profile by John *et al.* (2014). Basic research is also required to understand CO_2 permeable aquaporins in C_4 plants, specifically regarding their localisation, such as are they present on the chloroplast membrane and where do aquaporin promoters target.

In addition to examining the photosynthetic responses to overexpressing a CO_2 permeable aquaporin in a C_4 plant it would be interesting to observe the response of native aquaporins to environmental cues and expression patterns with different PIPs. The interactions of different aquaporins and other proteins are suggested to play a significant role in influencing substrate permeability by altering tetramer formation (Otto *et al.*, 2010). I have demonstrated this for some of the Setaria PIPs in yeast with improved plasma membrane targeting occurring when *SiPIP1;2* or *SiPIP1;5* were co-expressed with *SiPIP2;4* or *SiPIP2;5*. Would overexpression of one particular aquaporin affect expression levels or function of the remaining PIPs *in planta*? This has not been investigated in other experimental papers modifying the expression of one aquaporin and is worthy of future research for both C_3 and C_4 photosynthetic plants.

In Chapter 5 I attempted to overexpress CA in Setaria. However, potentially due to co-suppression, I significantly reduced CA activity. It would be interesting to overexpress CA in Setaria again using either a highly heterologous transgene or one codon modified to avoid co-suppression to achieve this aim. The *ZmCA* gene I tried to overexpress in Setaria in Chapter 5 was 87% identical to the primary photosynthetic CA in Setaria. To avoid gene suppression in future experiments I suggest ensuring sequence similarity is low and there is no stretch of similar nucleotides greater than ~21bp, the length typically used for RNAi mediated suppression. It would also be interesting to trial a bacterial CA gene or even an α or γ CA which are very different in sequence to the βCAs but perform the same hydration reaction and check if they function and localise correctly to supplement the high CA activity in Setaria. Overexpression of CA in a C_4 plant has been demonstrated in *Flaveria bidentis* using a tobacco CA under a constitutive 35S promoter (Ludwig *et al.*, 1998; von Caemmerer *et al.*, 1997). This resulted in increased expression of CA in the cytosol of both the mesophyll and bundle sheath cells and in increased leakiness to the bundle sheath and disruption of the CO_2 concentrating mechanism. If CA overexpression was localised specifically to the mesophyll cytosol I would

expect to see improved assimilation rates, increased g_m and perhaps increased PEPC activity. This may be challenging, however, since CA activity is already very high in Setaria and overexpression of CA may only result in a small change. Growth under different stress conditions, such as low CO_2 as discussed previously, may be one way to observe a significant change.

6.5 Final outlook

Improving C_4 photosynthesis is an ambitious aim since it is already highly efficient with both anatomical and biochemical specialisation. However, if global supply and demand for food continues on its current trajectory then improvements to all crops, both C_3 and C_4, will be required.

Ultimately, this improvement to C_4 photosynthesis will be delivered by stacking multiple enhancements at each key step of the photosynthetic cycle (von Caemmerer and Furbank, 2016). As modelled earlier, improving just g_m has only modest impacts on CO_2 assimilation rates or total crop biomass. By increasing each key step of the photosynthetic pathway it is envisioned that, especially under extreme environments, a substantial improvement to C_4 crop yield could be achieved.

REFERENCES

Ainsworth EA, Long SP. 2005. What have we learned from 15 years of free-air CO_2 enrichment (FACE)? A meta-analytic review of the responses of photosynthesis, canopy properties and plant production to rising CO_2. *New Phytologist* **165**, 351-372.

Alberti S, Gitler AD, Lindquist S. 2007. A suite of Gateway cloning vectors for high-throughput genetic analysis in *Saccharomyces cerevisiae*. *Yeast* **24**, 913-919.

Alonso-Cantabrana H, von Caemmerer S. 2016. Carbon isotope discrimination as a diagnostic tool for C_4 photosynthesis in C_3-C_4 intermediate species. *Journal of Experimental Botany* **67**, 3109-3121.

Anderberg H, Danielson J, Johanson U. 2011. Algal MIPs, high diversity and conserved motifs. *BMC Evolutionary Biology* **11**, 1-15.

Angov E, Legler PM, Mease RM. 2011. Adjustment of codon usage frequencies by codon harmonization improves protein expression and folding. *Methods in Molecular Biology* **705**, 1-13.

Azad AK, Ahmed J, Alum MA, Hasan MM, Ishikawa T, Sawa Y, Katsuhara M. 2016. Genome-Wide Characterization of Major Intrinsic Proteins in Four Grass Plants and Their Non-Aqua Transport Selectivity Profiles with Comparative Perspective. *PloS one* **11**, 1-30.

Badger MR, Price GD. 1989. Carbonic anhydrase activity associated with the cyanobacterium Synechococcus PCC7942. *Plant physiology* **89**, 51-60.

Badger MR, Price GD. 1994. The role of carbonic anhydrase in photosynthesis. *Annual review of plant biology* **45**, 369-392.

Barbour MM, Evans JR, Simonin KA, von Caemmerer S. 2016. Online CO_2 and H_2O oxygen isotope fractionation allows estimation of mesophyll conductance in C_4 plants, and reveals that mesophyll conductance decreases as leaves age in both C_4 and C_3 plants. *New Phytologist* **210**, 875-889

Bartlett JG, Alves SC, Smedley M, Snape JW, Harwood WA. 2008. High-throughput Agrobacterium-mediated barley transformation. *Plant Methods* **4**, 1-12.

Bennetzen JL, Schmutz J, Wang H, Percifield R, Hawkins J, Pontaroli AC, Estep M, Feng L, Vaughn JN, Grimwood J, Jenkins J, Barry K, Lindquist E, Hellsten U, Deshpande S, Wang X, Wu X, Mitros T, Triplett J, Yang X, Ye C-Y, Mauro-Herrera M, Wang L, Li P, Sharma M, Sharma R, Ronald PC, Panaud O, Kellogg EA, Brutnell TP, Doust AN, Tuskan GA, Rokhsar D, Devos KM. 2012. Reference genome sequence of the model plant Setaria. *Nature Biotechnology* **30**, 555-561.

Bertl A, Kaldenhoff R. 2007. Function of a separate NH_3-pore in Aquaporin TIP2;2 from wheat. *FEBS letters* **581**, 5413-5417.

Biela A, Grote K, Otto B, Hoth S, Hedrich R, Kaldenhoff R. 1999. The *Nicotiana tabacum* plasma membrane aquaporin NtAQP1 is mercury-insensitive and permeable for glycerol. *The Plant Journal* **18**, 565-570.

Bienert GP, Heinen RB, Berny MC, Chaumont F. 2014. Maize plasma membrane aquaporin ZmPIP2;5, but not ZmPIP1;2, facilitates transmembrane diffusion of hydrogen peroxide. *Biochimica et Biophysica Acta (BBA) - Biomembranes* **1838**, 216-222.

Boron WF. 2010. Sharpey-Schafer Lecture: Gas channels. *Experimental physiology* **95**, 1107-1130.

Boudichevskaia A, Heckwolf M, Kaldenhoff R. 2015. T-DNA insertion in aquaporin gene AtPIP1;2 generates transcription profiles reminiscent of a low CO_2 response. *Plant, Cell and Environment* **38**, 2286-2298.

Boyd RA, Gandin A, Cousins AB. 2015. Temperature response of C_4 photosynthesis: Biochemical analysis of Rubisco, Phosphoenolpyruvate Carboxylase and Carbonic Anhydrase in *Setaria viridis*. *Plant physiology* **169**, 1850-1861.

Bräutigam A, Kajala K, Wullenweber J, Sommer M, Gagneul D, Weber KL, Carr KM, Gowik U, Maß J, Lercher MJ. 2011. An mRNA blueprint for C_4 photosynthesis derived from comparative transcriptomics of closely related C_3 and C_4 species. *Plant physiology* **155**, 142-156.

Breeuwer P, Drocourt JL, Bunschoten N, Zwietering MH, Rombouts FM, Abee T. 1995. Characterization of uptake and hydrolysis of fluorescein diacetate and carboxyfluorescein diacetate by intracellular esterases in *Saccharomyces cerevisiae*, which result in accumulation of fluorescent product. *Applied and Environmental Microbiology* **61**, 1614-1619.

Breuers FKH, Bräutigam A, Geimer S, Welzel UY, Stefano G, Renna L, Brandizzi F, Weber APM. 2012. Dynamic Remodeling of the Plastid Envelope Membranes – A Tool for Chloroplast Envelope in vivo Localizations. *Frontiers in Plant Science* **3**, 1-10.

Brutnell TP, Wang L, Swartwood K, Goldschmidt A, Jackson D, Zhu X-G, Kellogg E, Van Eck J. 2010. *Setaria viridis*: a model for C_4 photosynthesis. *The Plant Cell Online* **22**, 2537-2544.

Burnell JN, Hatch MD. 1988. Low bundle sheath carbonic anhydrase is apparently essential for effective C_4 pathway operation. *Plant physiology* **86**, 1252-1256.

Carbrey JM, Bonhivers M, Boeke JD, Agre P. 2001. Aquaporins in Saccharomyces: Characterization of a second functional water channel protein. *Proceedings of the National Academy of Sciences* **98**, 1000-1005.

Cernusak LA, Farquhar GD, Wong SC, Stuart-Williams H. 2004. Measurement and Interpretation of the Oxygen Isotope Composition of Carbon Dioxide Respired by Leaves in the Dark. *Plant physiology* **136**, 3350-3363.

Chaumont F, Barrieu F, Jung R, Chrispeels MJ. 2000. Plasma membrane intrinsic proteins from maize cluster in two sequence subgroups with differential aquaporin activity. *Plant physiology* **122**, 1025-1034.

Chaumont F, Barrieu F, Wojcik E, Chrispeels MJ, Jung R. 2001. Aquaporins constitute a large and highly divergent protein family in maize. *Plant physiology* **125**, 1206-1215.

Chaumont F, Tyerman SD. 2014. Aquaporins: Highly Regulated Channels Controlling Plant Water Relations. *Plant physiology* **164**, 1600-1618.

Chevalier AS, Bienert GP, Chaumont F. 2014. A new LxxxA motif in the transmembrane helix 3 of maize PIP2 aquaporins is required for their trafficking to the plasma membrane. *Plant physiology* **166**, 125-138.

Christin P-A, Boxall SF, Gregory R, Edwards EJ, Hartwell J, Osborne CP. 2013. Parallel Recruitment of Multiple Genes into C_4 Photosynthesis. *Genome Biology and Evolution* **5**, 2174-2187.

Christin PA, Osborne CP. 2013. The recurrent assembly of C_4 photosynthesis, an evolutionary tale. *Photosynthesis Research* **117**, 163-175.

Cousins AB, Badger MR, von Caemmerer S. 2006. A Transgenic Approach to Understanding the Influence of Carbonic Anhydrase on $C^{18}OO$ Discrimination during C_4 Photosynthesis. *Plant physiology* **142**, 662-672.

Cousins AB, Badger MR, von Caemmerer S. 2008. C_4 photosynthetic isotope exchange in NAD-ME-and NADP-ME-type grasses. *Journal of Experimental Botany* **59**, 1695-1703.

Cousins AB, Baroli I, Badger MR, Ivakov A, Lea PJ, Leegood RC, von Caemmerer S. 2007. The Role of Phosphoenolpyruvate Carboxylase during C_4 Photosynthetic Isotope Exchange and Stomatal Conductance. *Plant physiology* **145**, 1006-1017.

Craig H, Gordon LI. 1965. *Deuterium and oxygen 18 variations in the ocean and the marine atmosphere*. Pisa, Italy: Lischi and Figli.

Curtis MD, Grossniklaus U. 2003. A gateway cloning vector set for high-throughput functional analysis of genes *in planta*. *Plant physiology* **133,** 462-469.

Danielson JÅ, Johanson U. 2008. Unexpected complexity of the Aquaporin gene family in the moss Physcomitrella patens. *BMC Plant Biology* **8**, 45-60.
Danila FR, Quick WP, White RG, Furbank RT, von Caemmerer S. 2016. The metabolite pathway between bundle sheath and mesophyll: quantification of plasmodesmata in leaves of C_3 and C_4 monocots. *The Plant Cell* **28**, 1461-1471.
de Andrade LM, Nobile PM, Ribeiro RV, de Oliveira JFNC, de Oliveira Figueira AV, Frigel LTM, Nunes D, Perecin D, dos Santos Brito M, de Matos Pires RC. 2016. Characterization of PIP2 aquaporins in Saccharum hybrids. *Plant Gene* **5**, 31-37.
Defelice MS. 2002. Green Foxtail, *Setaria viridis* (L.) P. Beauv 1. *Weed technology* **16**, 253-257.
Dengler NG, Dengler RE, Donnelly PM, Hattersley PW. 1994. Quantitative leaf anatomy of C_3 and C_4 grasses (Poaceae): bundle sheath and mesophyll surface area relationships. *Annals of Botany* **73**, 241-255.
Dever LV, Bailey KJ, Leegood RC, Lea PJ. 1997. Control of photosynthesis in *Amaranthus edulis* mutants with reduced amounts of PEP carboxylase. *Functional Plant Biology* **24**, 469-476.
DiMario RJ, Clayton H, Mukherjee A, Ludwig M, Moroney JV. 2017. Plant Carbonic Anhydrases: Structures, Locations, Evolution, and Physiological Roles. *Molecular Plant* **10**, 30-46.
DiMario RJ, Quebedeaux JC, Longstreth D, Dassanayake M, Hartman MM, Moroney JV. 2016. The cytoplasmic carbonic anhydrases βCA2 and βCA4 are required for optimal plant growth at low CO_2. *Plant physiology* **171**, 280-293.
Ding X, Matsumoto T, Gena P, Liu C, Pellegrini-Calace M, Zhong S, Sun X, Zhu Y, Katsuhara M, Iwasaki I, Kitagawa Y, Calamita G. 2013. Water and CO_2 permeability of SsAqpZ, the cyanobacterium Synechococcus sp. PCC7942 aquaporin. *Biology of the Cell* **105**, 118-128.
Ding Z, Weissmann S, Wang M, Du B, Huang L, Wang L, Tu X, Zhong S, Myers C, Brutnell TP, Sun Q, Li P. 2015. Identification of Photosynthesis-Associated C_4 Candidate Genes through Comparative Leaf Gradient Transcriptome in Multiple Lineages of C_3 and C_4 Species. *PloS one* **10**, 1-19.
Döring F, Streubel M, Bräutigam A, Gowik U. 2016. Most photorespiratory genes are preferentially expressed in the bundle sheath cells of the C_4 grass *Sorghum bicolor*. *Journal of Experimental Botany* **67**, 3053-3064.
Doust AN, Kellogg EA, Devos KM, Bennetzen JL. 2009. Foxtail millet: a sequence-driven grass model system. *Plant physiology* **149**, 137-141.
Edwards K, Johnstone C, Thompson C. 1991. A simple and rapid method for the preparation of plant genomic DNA for PCR analysis. *Nucleic acids research* **19**, 1349.
Ehleringer JR, Sage RF, Flanagan LB, Pearcy RW. 1991. Climate change and the evolution of C_4 photosynthesis. *Trends in Ecology & Evolution* **6**, 95-99.
Endeward V, Al-Samir S, Itel F, Gros G. 2013. How does carbon dioxide permeate cell membranes? A discussion of concepts, results and methods. *Frontiers in Physiology* **4**, 382-403.
Endeward V, Musa-Aziz R, Cooper G, Chen L-M, Pelletier M, Virkki L, Supuran C, King L, Boron W, Gros G. 2006. Evidence that aquaporin 1 is a major pathway for CO_2 transport across the human erythrocyte membrane. *The FASEB Journal* **20**, 1974-1981.
Engineer CB, Hashimoto-Sugimoto M, Negi J, Israelsson-Nordström M, Azoulay-Shemer T, Rappel W-J, Iba K, Schroeder JI. 2016. CO_2 Sensing and CO_2 Regulation of Stomatal Conductance: Advances and Open Questions. *Trends in Plant Science* **21**, 16-30.
Evans J, Sharkey T, Berry J, Farquhar G. 1986. Carbon Isotope Discrimination measured Concurrently with Gas Exchange to Investigate CO_2 Diffusion in Leaves of Higher Plants. *Functional Plant Biology* **13**, 281-292.

Evans JR, Caemmerer S, Setchell BA, Hudson GS. 1994. The relationship between CO_2 transfer conductance and leaf anatomy in transgenic tobacco with a reduced content of Rubisco. *Functional Plant Biology* **21**, 475-495.
Evans JR, Kaldenhoff R, Genty B, Terashima I. 2009. Resistances along the CO_2 diffusion pathway inside leaves. *Journal of Experimental Botany* **60**, 2235-2248.
Evans JR, von Caemmerer S. 1996. Carbon dioxide diffusion inside leaves. *Plant physiology* **110**, 339-346.
Fang X, Yang B, Matthay MA, Verkman AS. 2002. Evidence against aquaporin-1-dependent CO_2 permeability in lung and kidney. *The Journal of Physiology* **542**, 63-69.
Farquhar G, Lloyd J. 1993. Carbon and oxygen isotope effects in the exchange of carbon dioxide between terrestrial plants and the atmosphere. *Stable isotopes and plant carbon-water relations* **40**, 47-70.
Farquhar GD, Cernusak LA. 2012. Ternary effects on the gas exchange of isotopologues of carbon dioxide. *Plant, Cell & Environment* **35**, 1221-1231.
Fetter K, Van Wilder V, Moshelion M, Chaumont F. 2004. Interactions between Plasma Membrane Aquaporins Modulate Their Water Channel Activity. *The Plant Cell* **16**, 215-228.
Finn RD, Clements J, Arndt W, Miller BL, Wheeler TJ, Schreiber F, Bateman A, Eddy SR. 2015. HMMER web server: 2015 update. *Nucleic acids research*, **43,** 397.
Flexas J, Barbour MM, Brendel O, Cabrera HM, Carriquí M, Díaz-Espejo A, Douthe C, Dreyer E, Ferrio JP, Gago J, Gallé A, Galmés J, Kodama N, Medrano H, Niinemets Ü, Peguero-Pina JJ, Pou A, Ribas-Carbó M, Tomás M, Tosens T, Warren CR. 2012. Mesophyll diffusion conductance to CO_2: An unappreciated central player in photosynthesis. *Plant Science* **193–194**, 70-84.
Flexas J, Diaz-Espejo A, GalmES J, Kaldenhoff R, Medrano H, Ribas-Carbo M. 2007. Rapid variations of mesophyll conductance in response to changes in CO_2 concentration around leaves. *Plant, Cell and Environment* **30**, 1284-1298.
Flexas J, Ribas-CarbÓ M, Diaz-Espejo A, GalmÉS J, Medrano H. 2008. Mesophyll conductance to CO_2: current knowledge and future prospects. *Plant, Cell & Environment* **31**, 602-621.
Flexas J, Ribas-Carbó M, Hanson DT, Bota J, Otto B, Cifre J, McDowell N, Medrano H, Kaldenhoff R. 2006. Tobacco aquaporin NtAQP1 is involved in mesophyll conductance to CO_2 in vivo. *The Plant Journal* **48**, 427-439.
Frick A, Jarva M, Tornroth-Horsefield S. 2013. Structural basis for pH gating of plant aquaporins. *FEBS letters* **587**, 989-993.
Froger A, Tallur B, Thomas D, Delamarche C. 1998. Prediction of functional residues in water channels and related proteins. *Protein Science* **7**, 1458-1468.
Furbank RT. 2011. Evolution of the C_4 photosynthetic mechanism: are there really three C_4 acid decarboxylation types? *Journal of Experimental Botany* **62**, 3103-3108.
Furbank RT, Chitty JA, Jenkins CL, Taylor WC, Trevanion SJ, von Caemmerer S, Ashton AR. 1997. Genetic manipulation of key photosynthetic enzymes in the C_4 plant *Flaveria bidentis*. *Functional Plant Biology* **24**, 477-485.
Furbank RT, Hatch MD. 1987. Mechanism of C_4 photosynthesis- The size and composition of the inorganic carbon pool in bundle sheath cells. *Plant physiology* **85**, 958-964.
Furbank RT, Quick WP, Sirault XRR. 2015. Improving photosynthesis and yield potential in cereal crops by targeted genetic manipulation: Prospects, progress and challenges. *Field Crops Research* **182**, 19-29.
Gibson DG, Young L, Chuang RY, Venter JC, Hutchison CA, Smith HO. 2009. Enzymatic assembly of DNA molecules up to several hundred kilobases. *Nature Methods* **6,** 343-345.
Gillon JS, Yakir D. 2000. Naturally low carbonic anhydrase activity in C_4 and C_3 plants limits discrimination against $C^{18}OO$ during photosynthesis. *Plant, Cell & Environment* **23**, 903-915.
Gomes D, Agasse A, Thiébaud P, Delrot S, Gerós H, Chaumont F. 2009. Aquaporins are multifunctional water and solute transporters highly divergent in living organisms. *Biochimica et Biophysica Acta (BBA) - Biomembranes* **1788**, 1213-1228.

Greenup AG, Sasani S, Oliver SN, Talbot MJ, Dennis ES, Hemming MN, Trevaskis B. 2010. ODDSOC2 Is a MADS Box Floral Repressor That Is Down-Regulated by Vernalization in Temperate Cereals. *Plant physiology* **153**, 1062-1073.
Groszmann M, Osborn HL, Evans JR. 2016. Carbon dioxide and water transport through plant aquaporins. *Plant, Cell and Environment* **40**, 938-961.
Guan XG, Su WH, Yi F, Zhang D, Hao F, Zhang HG, Liu YJ, Feng XC, Ma TH. 2010. NPA motifs play a key role in plasma membrane targeting of aquaporin-4. *IUBMB Life* **62**, 222-226.
Gutknecht J, Bisson MA, Tosteson FC. 1977. Diffusion of carbon dioxide through lipid bilayer membranes. Effects of carbonic anhydrase, bicarbonate, and unstirred layers. *The Journal of General Physiology* **69**, 779-794.
Hachez C, Heinen RB, Draye X, Chaumont F. 2008. The expression pattern of plasma membrane aquaporins in maize leaf highlights their role in hydraulic regulation. *Plant Mol Biol* **68**, 337-353.
Hachez C, Zelazny E, Chaumont F. 2006. Modulating the expression of aquaporin genes in planta: A key to understand their physiological functions? *Biochimica et Biophysica Acta (BBA) - Biomembranes* **1758**, 1142-1156.
Hall BG, Acar H, Nandipati A, Barlow M. 2014. Growth Rates Made Easy. *Molecular Biology and Evolution* **31**, 232-238.
Hanba YT, Shibasaka M, Hayashi Y, Hayakawa T, Kasamo K, Terashima I, Katsuhara M. 2004. Overexpression of the barley aquaporin HvPIP2; 1 increases internal CO_2 conductance and CO_2 assimilation in the leaves of transgenic rice plants. *Plant and Cell Physiology* **45**, 521-529.
Harley PC, Loreto F, Di Marco G, Sharkey TD. 1992. Theoretical Considerations when Estimating the Mesophyll Conductance to CO2 Flux by Analysis of the Response of Photosynthesis to CO2. *Plant physiology* **98**, 1429-1436.
Harned HS, Bonner FT. 1945. The First Ionization of Carbonic Acid in Aqueous Solutions of Sodium Chloride. *Journal of the American Chemical Society* **67**, 1026-1031.
Hasan S, Rabei S, Nada R, Abogadallah G. 2017. Water use efficiency in the drought-stressed sorghum and maize in relation to expression of aquaporin genes. *Biologia Plantarum*, **61,** 127-137.
Hatch MD. 1987. C_4 photosynthesis: a unique elend of modified biochemistry, anatomy and ultrastructure. *Biochimica et Biophysica Acta (BBA) - Reviews on Bioenergetics* **895**, 81-106.
Hatch MD, Burnell JN. 1990. Carbonic anhydrase activity in leaves and its role in the first step of C_4 photosynthesis. *Plant physiology* **93**, 825-828.
Hatch MD, Slack CR. 1966. Photosynthesis by sugarcane leaves. *Biochemical Journal* **101**, 103-111.
Heckwolf M, Pater D, Hanson DT, Kaldenhoff R. 2011. The *Arabidopsis thaliana* aquaporin AtPIP1;2 is a physiologically relevant CO_2 transport facilitator. *The Plant Journal* **67**, 795-804.
Heinen RB, Bienert GP, Cohen D, Chevalier AS, Uehlein N, Hachez C, Kaldenhoff R, Le Thiec D, Chaumont F. 2014. Expression and characterization of plasma membrane aquaporins in stomatal complexes of *Zea mays*. *Plant Mol Biol* **86**, 335-350.
Hempleman SC, Rodriguez TA, Bhagat YA, Begay RS. 2000. Benzolamide, acetazolamide, and signal transduction in avian intrapulmonary chemoreceptors. *American Journal of Physiology Regulatory, Integrative and Comparative Physiology* **279**, 1988-1995.
Heymann JB, Agre P, Engel A. 1998. Progress on the Structure and Function of Aquaporin 1. *Journal of Structural Biology* **121**, 191-206.
Hofmann K, Stoffel W. 1993. TMbase-a database of membrane spanning proteins segments. *Biological Chemistry. Hoppe Seyler* **347**, 166.
Hove RM, Bhave M. 2011. Plant aquaporins with non-aqua functions: deciphering the signature sequences. *Plant Mol Biol* **75**, 413-430.
Hove RM, Ziemann M, Bhave M. 2015. Identification and expression analysis of the barley *(Hordeum vulgare* L.) aquaporin gene family. *PloS one* **10**, 1-21.

Hu H, Boisson-Dernier A, Israelsson-Nordstrom M, Bohmer M, Xue S, Ries A, Godoski J, Kuhn JM, Schroeder JI. 2010. Carbonic anhydrases are upstream regulators of CO_2-controlled stomatal movements in guard cells. *Nature Cell Biology* **12**, 87-93.
Hu H, Rappel WJ, Occhipinti R, Ries A, Bohmer M, You L, Xiao C, Engineer CB, Boron WF, Schroeder JI. 2015. Distinct Cellular Locations of Carbonic Anhydrases Mediate Carbon Dioxide Control of Stomatal Movements. *Plant physiology* **169**, 1168-1178.
Hub JS, De Groot BL. 2008. Mechanism of selectivity in aquaporins and aquaglyceroporins. *Proceedings of the National Academy of Sciences* **105**, 1198-1203.
Hub JS, Grubmuller H, de Groot BL. 2009. Dynamics and energetics of permeation through aquaporins. What do we learn from molecular dynamics simulations? *Handb Exp Pharmacol*, 57-76.
Itel F, Al-Samir S, Oberg F, Chami M, Kumar M, Supuran CT, Deen PM, Meier W, Hedfalk K, Gros G, Endeward V. 2012. CO_2 permeability of cell membranes is regulated by membrane cholesterol and protein gas channels. *Faseb journal* **26**, 5182-5191.
Jenkins CLD, Furbank RT, Hatch MD. 1989. Mechanism of C_4 Photosynthesis: A Model Describing the Inorganic Carbon Pool in Bundle Sheath Cells. *Plant physiology* **91**, 1372-1381.
Johanson U, Karlsson M, Johansson I, Gustavsson S, Sjövall S, Fraysse L, Weig AR, Kjellbom P. 2001. The complete set of genes encoding major intrinsic proteins in Arabidopsis provides a framework for a new nomenclature for major intrinsic proteins in plants. *Plant physiology* **126**, 1358-1369.
John CR, Smith-Unna RD, Woodfield H, Covshoff S, Hibberd JM. 2014. Evolutionary convergence of cell-specific gene expression in independent lineages of C_4 grasses. *Plant physiology* **165**, 62-75.
Jones JDG, Gilbert DE, Grady KL, Jorgensen RA. 1987. T-DNA structure and gene expression in petunia plants transformed by Agrobacterium tumefaciens C58 derivatives. *Molecular and General Genetics MGG* **207**, 478-485.
Jorgensen R, Snyder C, Jones JDG. 1987. T-DNA is organized predominantly in inverted repeat structures in plants transformed with Agrobacterium tumefaciens C58 derivatives. *Molecular and General Genetics MGG* **207**, 471-477.
Kadam S, Abril A, Dhanapal AP, Koester RP, Vermerris W, Jose S, Fritschi FB. 2017. Characterization and Regulation of Aquaporin Genes of Sorghum [*Sorghum bicolor* (L.) Moench] in Response to Waterlogging Stress. *Frontiers in Plant Science* **8**, 1-14.
Kaldenhoff R. 2012. Mechanisms underlying CO_2 diffusion in leaves. *Current opinion in plant biology* **15**, 276-281.
Kaldenhoff R, Grote K, Zhu JJ, Zimmermann U. 1998. Significance of plasmalemma aquaporins for water-transport in Arabidopsis thaliana. *The Plant Journal* **14**, 121-128.
Karnovsky A, Weymouth T, Hull T, Tarcea VG, Scardoni G, Laudanna C, Sartor MA, Stringer KA, Jagadish HV, Burant C, Athey B, Omenn GS. 2012. Metscape 2 bioinformatics tool for the analysis and visualization of metabolomics and gene expression data. *Bioinformatics* **28**, 373-380.
Kawase M, Hanba YT, Katsuhara M. 2013. The photosynthetic response of tobacco plants overexpressing ice plant aquaporin McMIPB to a soil water deficit and high vapor pressure deficit. *Journal of plant research* **126**, 517-527.
Kelly G, Sade N, Attia Z, Secchi F, Zwieniecki M, Holbrook NM, Levi A, Alchanatis V, Moshelion M, Granot D. 2014. Relationship between Hexokinase and the Aquaporin PIP1 in the Regulation of Photosynthesis and Plant Growth. *PloS one* **9**, 1-9.
Kromdijk J, Głowacka K, Leonelli L, Gabilly ST, Iwai M, Niyogi KK, Long SP. 2016. Improving photosynthesis and crop productivity by accelerating recovery from photoprotection. *Science* **354**, 857-861.
Kruse E, Uehlein N, Kaldenhoff R. 2006. The aquaporins. *Genome Biol* **7**, 1-206.
Latham JR, Wilson AK, Steinbrecher RA. 2006. The mutational consequences of plant transformation. *BioMed Research International* **25376**, 1-7.

Lawrence SD, Novak NG, Slack JM. 2003. Epitope tagging: a monoclonal antibody specific for recombinant fusion proteins in plants. *Biotechniques* **35**, 488-492.
Leakey AD, Uribelarrea M, Ainsworth EA, Naidu SL, Rogers A, Ort DR, Long SP. 2006. Photosynthesis, productivity, and yield of maize are not affected by open-air elevation of CO_2 concentration in the absence of drought. *Plant physiology* **140**, 779-790.
Li G, Santoni V, Maurel C. 2014. Plant aquaporins: Roles in plant physiology. *Biochimica et Biophysica Acta (BBA) - General Subjects* **1840**, 1574-1582.
Li L, Wang H, Gago J, Cui H, Qian Z, Kodama N, Ji H, Tian S, Shen D, Chen Y, Sun F, Xia Z, Ye Q, Sun W, Flexas J, Dong H. 2015. Harpin Hpa1 Interacts with Aquaporin PIP1;4 to Promote the Substrate Transport and Photosynthesis in Arabidopsis. *Scientific reports* **5**, 1-17.
Li P, Brutnell TP. 2011. *Setaria viridis* and *Setaria italica*, model genetic systems for the Panicoid grasses. *Journal of Experimental Botany* **62**, 3031-3037.
Li P, Mace ES, Guo Y, Han L, Wang M, He Y, Chen J, Yuyama N, Jordan DR, Cai H. 2016. Fine Mapping of qDor7, a Major QTL Affecting Seed Dormancy in Sorghum (*Sorghum bicolor* (L.) Moench). *Tropical Plant Biology* **9**, 109-116.
Li P, Ponnala L, Gandotra N, Wang L, Si Y, Tausta SL, Kebrom TH, Provart N, Patel R, Myers CR, Reidel EJ, Turgeon R, Liu P, Sun Q, Nelson T, Brutnell TP. 2010. The developmental dynamics of the maize leaf transcriptome. *Nat Genet* **42**, 1060-1067.
Lin X, Hong T, Mu Y, Torres J. 2012. Identification of residues involved in water versus glycerol selectivity in aquaporins by differential residue pair co-evolution. *Biochimica et Biophysica Acta (BBA) - Biomembranes* **1818**, 907-914.
Livak KJ, Schmittgen TD. 2001. Analysis of relative gene expression data using real-time Quantitative PCR and the 2–ΔΔCt method. *Methods* **25**, 402-408.
Lloyd J, Farquhar GD. 1994. ^{13}C Discrimination during CO_2 Assimilation by the Terrestrial Biosphere. *Oecologia* **99**, 201-215.
Long SP, Zhu X-G, Naidu SL, Ort DR. 2006. Can improvement in photosynthesis increase crop yields? *Plant, Cell & Environment* **29**, 315-330.
Ludwig M. 2012. Carbonic anhydrase and the molecular evolution of C_4 photosynthesis. *Plant, Cell & Environment* **35**, 22-37.
Ludwig M, von Caemmerer S, Price GD, Badger MR, Furbank RT. 1998. Expression of Tobacco Carbonic Anhydrase in the C_4 Dicot Flaveria bidentis Leads to Increased Leakiness of the Bundle Sheath and a Defective CO_2-Concentrating Mechanism. *Plant physiology* **117**, 1071-1081.
Mace ES, Hunt CH, Jordan DR. 2013a. Supermodels: sorghum and maize provide mutual insight into the genetics of flowering time. *Theoretical and Applied Genetics* **126**, 1377-1395.
Mace ES, Tai S, Gilding EK, Li Y, Prentis PJ, Bian L, Campbell BC, Hu W, Innes DJ, Han X, Cruickshank A, Dai C, Frère C, Zhang H, Hunt CH, Wang X, Shatte T, Wang M, Su Z, Li J, Lin X, Godwin ID, Jordan DR, Wang J. 2013b. Whole-genome sequencing reveals untapped genetic potential in Africa's indigenous cereal crop sorghum. *Nature Communications* **4**, 2320-2329.
Martin AP, Palmer WM, Brown C, Abel C, Lunn JE, Furbank RT, Grof CP. 2016. A developing *Setaria viridis* internode: an experimental system for the study of biomass generation in a C_4 model species. *Biotechnology for biofuels* **9**, 1-12.
Matsuoka M, Furbank RT, Fukayama H, Miyao M. 2001. Molecular engineering of C_4 photosynthesis. *Annual review of plant biology* **52**, 297-314.
Maurel C, Boursiac Y, Luu D-T, Santoni V, Shahzad Z, Verdoucq L. 2015. Aquaporins in Plants. *Physiological Reviews* **95**, 1321-1358.
Maurel C, Reizer J, Schroeder JI, Chrispeels MJ. 1993. The vacuolar membrane protein gamma-TIP creates water specific channels in *Xenopus* oocytes. *The EMBO Journal* **12**, 2241-2247.
Maurel C, Verdoucq L, Luu D-T, Santoni V. 2008. Plant aquaporins: membrane channels with multiple integrated functions. *Annual Reviews of Plant Biology* **59**, 595-624.

McGaughey SA, Osborn HL, Chen L, Pegler JL, Tyerman SD, Furbank RT, Byrt CS, Grof CPL. 2016. Roles of Aquaporins in *Setaria viridis* Stem Development and Sugar Storage. *Frontiers in Plant Science* **7**, 1-13.
Meinild A-K, Klaerke DA, Zeuthen T. 1998. Bidirectional water fluxes and specificity for small hydrophilic molecules in aquaporins 0–5. *Journal of Biological Chemistry* **273**, 32446-32451.
Metsalu T, Vilo J. 2015. ClustVis: a web tool for visualizing clustering of multivariate data using Principal Component Analysis and heatmap. *Nucleic acids research* **43**, W566-570.
Missner A, Kügler P, Saparov SM, Sommer K, Mathai JC, Zeidel ML, Pohl P. 2008. Carbon dioxide transport through membranes. *Journal of Biological Chemistry* **283**, 25340-25347.
Missner A, Pohl P. 2009. 110 Years of the Meyer–Overton rule: predicting membrane permeability of gases and other small compounds. *ChemPhysChem* **10**, 1405-1414.
Mori IC, Rhee J, Shibasaka M, Sasano S, Kaneko T, Horie T, Katsuhara M. 2014. CO_2 Transport by PIP2 Aquaporins of Barley. *Plant and Cell Physiology* **55**, 251-257.
Moroney JV, Bartlett SG, Samuelsson G. 2001. Carbonic anhydrases in plants and algae. *Plant, Cell & Environment* **24**, 141-153.
Moshelion M, Halperin O, Wallach R, Oren RAM, Way DA. 2015. Role of aquaporins in determining transpiration and photosynthesis in water-stressed plants: crop water-use efficiency, growth and yield. *Plant, Cell & Environment* **38**, 1785-1793.
Murata K, Mitsuoka K, Hirai T, Walz T, Agre P, Heymann JB, Engel A, Fujiyoshi Y. 2000. Structural determinants of water permeation through aquaporin-1. *Nature* **407**, 599-605.
Nakagawa S, Niimura Y, Gojobori T, Tanaka H, Miura K-i. 2008. Diversity of preferred nucleotide sequences around the translation initiation codon in eukaryote genomes. *Nucleic acids research* **36**, 861-871.
Nakhoul NL, Davis BA, Romero MF, Boron WF. 1998. Effect of expressing the water channel aquaporin-1 on the CO_2 permeability of Xenopus oocytes. *American Journal of Physiology-Cell Physiology* **274**, C543-C548.
Navarro-Rodenas A, Ruiz-Lozano JM, Kaldenhoff R, Morte A. 2012. The aquaporin TcAQP1 of the desert truffle *Terfezia claveryi* is a membrane pore for water and CO_2 transport. *Molecular Plant Microbe Interact* **25**, 259-266.
Niinemets Ü, Reichstein M. 2003. Controls on the emission of plant volatiles through stomata: a sensitivity analysis. *Journal of Geophysical Research: Atmospheres* **108**, 1-10.
Okabe K, Yang S-Y, Tsuzuki M, Miyachi S. 1984. Carbonic anhydrase: its content in spinach leaves and its taxonomic diversity studied with anti-spinach leaf carbonic anhydrase antibody. *Plant science letters* **33**, 145-153.
Ort DR, Merchant SS, Alric J, Barkan A, Blankenship RE, Bock R, Croce R, Hanson MR, Hibberd JM, Long SP, Moore TA, Moroney J, Niyogi KK, Parry MAJ, Peralta-Yahya PP, Prince RC, Redding KE, Spalding MH, van Wijk KJ, Vermaas WFJ, von Caemmerer S, Weber APM, Yeates TO, Yuan JS, Zhu XG. 2015. Redesigning photosynthesis to sustainably meet global food and bioenergy demand. *Proceedings of the National Academy of Sciences* **112**, 8529-8536.
Osborn HL, Alonso-Cantabrana H, Sharwood RE, Covshoff S, Evans JR, Furbank RT, von Caemmerer S. 2016. Effects of reduced carbonic anhydrase activity on CO_2 assimilation rates in *Setaria viridis*: a transgenic analysis. *Journal of Experimental Botany* **68**, 299 - 310.
Otto B, Uehlein N, Sdorra S, Fischer M, Ayaz M, Belastegui-Macadam X, Heckwolf M, Lachnit M, Pede N, Priem N. 2010. Aquaporin tetramer composition modifies the function of tobacco aquaporins. *Journal of Biological Chemistry* **285**, 31253-31260.
Parry MAJ, Hawkesford MJ. 2010. Food security: increasing yield and improving resource use efficiency. *Proceedings of the Nutrition Society* **69**, 592-600.
Pengelly JJL, Sirault XRR, Tazoe Y, Evans JR, Furbank RT, von Caemmerer S. 2010. Growth of the C_4 dicot *Flaveria bidentis*: photosynthetic acclimation to low light through shifts in leaf anatomy and biochemistry. *Journal of Experimental Botany* **61**, 4109-4122.

Pengelly JJL, Tan J, Furbank RT, von Caemmerer S. 2012. Antisense Reduction of NADP-Malic Enzyme in *Flaveria bidentis* Reduces Flow of CO_2 through the C_4 Cycle. *Plant physiology* **160**, 1070-1080.
Pfeffer M, Peisker M. 1998. CO_2 gas exchange and phosphoenolpyruvate carboxylase activity in leaves of *Zea mays* L. *Photosynthesis Research* **58**, 281-291.
Prasad GVR, Coury LA, Finn F, Zeidel ML. 1998. Reconstituted Aquaporin 1 Water Channels Transport CO_2 across Membranes. *Journal of Biological Chemistry* **273**, 33123-33126.
Price GD, Badger MR. 1989. Expression of Human Carbonic Anhydrase in the Cyanobacterium Synechococcus PCC7942 Creates a High CO_2-Requiring Phenotype: Evidence for a Central Role for Carboxysomes in the CO_2 Concentrating Mechanism. *Plant physiology* **91**, 505-513.
Raines CA. 2011. Increasing Photosynthetic Carbon Assimilation in C_3 Plants to Improve Crop Yield: Current and Future Strategies. *Plant physiology* **155**, 36-42.
Ray DK, Mueller ND, West PC, Foley JA. 2013. Yield Trends Are Insufficient to Double Global Crop Production by 2050. *PloS one* **8**, 1-8.
Reddy PS, Rao TSRB, Sharma KK, Vadez V. 2015. Genome-wide identification and characterization of the aquaporin gene family in *Sorghum bicolor* (L.). *Plant Gene* **1**, 18-28.
Richards RA. 2000. Selectable traits to increase crop photosynthesis and yield of grain crops. *Journal of Experimental Botany* **51**, 447-458.
Rolland V, Badger MR, Price GD. 2016. Redirecting the cyanobacterial bicarbonate transporters BicA and SbtA to the chloroplast envelope: soluble and membrane cargos need different chloroplast targeting signals in plants. *Frontiers in Plant Science* **7**, 1-19.
Sade N, Gallé A, Flexas J, Lerner S, Peleg G, Yaaran A, Moshelion M. 2014. Differential tissue-specific expression of NtAQP1 in Arabidopsis thaliana reveals a role for this protein in stomatal and mesophyll conductance of CO_2 under standard and salt-stress conditions. *Planta* **239**, 357-366.
Sade N, Gebretsadik M, Seligmann R, Schwartz A, Wallach R, Moshelion M. 2010. The role of tobacco Aquaporin1 in improving water use efficiency, hydraulic conductivity, and yield production under salt stress. *Plant physiology* **152**, 245-254.
Sage RF. 2004. The evolution of C_4 photosynthesis. *New Phytologist* **161**, 341-370.
Sage RF, Christin PA, Edwards EJ. 2011. The C_4 plant lineages of planet Earth. *Journal of Experimental Botany* **62**, 3155-3169.
Sage RF, Li M, Monson RK. 1999. The Taxonomic Distribution of C_4 Photosynthesis. In: Sage RF, Monson RK, eds. *C_4 Plant Biology*. San Diego: Academic Press, 551-584.
Sage RF, Sage TL, Kocacinar F. 2012. Photorespiration and the evolution of C_4 photosynthesis. *Annual review of plant biology* **63**, 19-47.
Sakurai J, Ishikawa F, Yamaguchi T, Uemura M, Maeshima M. 2005. Identification of 33 rice aquaporin genes and analysis of their expression and function. *Plant and Cell Physiology* **46**, 1568-1577.
Savage DF, O'Connell JD, Miercke LJW, Finer-Moore J, Stroud RM. 2010. Structural context shapes the aquaporin selectivity filter. *Proceedings of the National Academy of Sciences* **107**, 17164-17169.
Schindelin J, Arganda-Carreras I, Frise E, Kaynig V, Longair M, Pietzsch T, Preibisch S, Rueden C, Saalfeld S, Schmid B, Tinevez J-Y, White DJ, Hartenstein V, Eliceiri K, Tomancak P, Cardona A. 2012. Fiji: an open-source platform for biological-image analysis. *Nat Methods* **9**, 676-682.
Secchi F, Schubert A, Lovisolo C. 2016. Changes in Air CO_2 Concentration Differentially Alter Transcript Levels of NtAQP1 and NtPIP2;1 Aquaporin Genes in Tobacco Leaves. *International Journal of Molecular Sciences* **17**, 1-12.
Shah KH, Almaghrabi B, Bohlmann H. 2013. Comparison of Expression Vectors for Transient Expression of Recombinant Proteins in Plants. *Plant Molecular Biology Reporter / Ispmb* **31**, 1529-1538.

Sharwood RE. 2017. Engineering chloroplasts to improve Rubisco catalysis: prospects for translating improvements into food and fiber crops. *New Phytologist* **213**, 494-510.
Silvera K, Neubig KM, Whitten WM, Williams NH, Winter K, Cushman JC. 2010. Evolution along the crassulacean acid metabolism continuum. *Functional Plant Biology* **37**, 995-1010.
Studer AJ, Gandin A, Kolbe AR, Wang L, Cousins AB, Brutnell TP. 2014. A limited role for carbonic anhydrase in C_4 photosynthesis as revealed by a ca1ca2 double mutant in maize. *Plant physiology* **165**, 608-617.
Suga S, Maeshima M. 2004. Water channel activity of radish plasma membrane aquaporins heterologously expressed in yeast and their modification by site-directed mutagenesis. *Plant Cell Physiology* **45**, 823-830.
Tazoe Y, Von Caemmerer S, Estavillo GM, Evans JR. 2011. Using tunable diode laser spectroscopy to measure carbon isotope discrimination and mesophyll conductance to CO_2 diffusion dynamically at different CO_2 concentrations. *Plant, Cell & Environment* **34**, 580-591.
Terashima I, Ono K. 2002. Effects of $HgCl_2$ on CO_2 dependence of leaf photosynthesis: evidence indicating involvement of aquaporins in CO_2 diffusion across the plasma membrane. *Plant and Cell Physiology* **43**, 70-78.
Tolleter D, Chochois V, Poire R, Price GD, Badger MR. 2017. Measuring CO_2 and HCO_3^- permeabilities of isolated chloroplasts using a MIMS-^{18}O approach. *Journal of Experimental Botany* **68**, 3915-3924.
Tu CK, Acevedo-Duncan M, Wynns GC, Silverman DN. 1986. Oxygen-18 Exchange as a Measure of Accessibility of CO_2 and HCO_3^- to Carbonic Anhydrase in Chlorella vulgaris (UTEX 263). *Plant physiology* **80**, 997-1001.
Tyerman SD, Niemietz CM, Bramley H. 2002. Plant aquaporins: multifunctional water and solute channels with expanding roles. *Plant, Cell & Environment* **25**, 173-194.
Ubierna N, Gandin A, Boyd RA, Cousins AB. 2017. Temperature response of mesophyll conductance in three C_4 species calculated with two methods: ^{18}O discrimination and *in vitro* V_{pmax}. *New Phytologist* **214**, 66-80.
Uehlein N, Lovisolo C, Siefritz F, Kaldenhoff R. 2003. The tobacco aquaporin NtAQP1 is a membrane CO_2 pore with physiological functions. *Nature* **425**, 734-737.
Uehlein N, Otto B, Eilingsfeld A, Itel F, Meier W, Kaldenhoff R. 2012. Gas tight triblock copolymer membranes are converted to CO2 permeable by insertion of plant aquaporins. *Scientific reports* 2, 538.
Uehlein N, Otto B, Hanson DT, Fischer M, McDowell N, Kaldenhoff R. 2008. Function of *Nicotiana tabacum* aquaporins as chloroplast gas pores challenges the concept of membrane CO_2 permeability. *The Plant Cell Online* **20**, 648-657.**Uehlein N, Sperling H, Heckwolf M, Kaldenhoff R**. 2012. The Arabidopsis aquaporin PIP1;2 rules cellular CO_2 uptake. *Plant, Cell & Environment* **35**, 1077-1083. **Vandesompele J, De Preter K, Pattyn F, Poppe B, Van Roy N, De Paepe A, Speleman F**. 2002. Accurate normalization of real-time quantitative RT-PCR data by geometric averaging of multiple internal control genes. *Genome Biol* **3**, 1-12.

Verkman AS, Anderson MO, Papadopoulos MC. 2014. Aquaporins: important but elusive drug targets. *Nature Reviews Drug Discovery* **13**, 259-277.
Vilas G, Krishnan D, Loganathan SK, Malhotra D, Liu L, Beggs MR, Gena P, Calamita G, Jung M, Zimmermann R, Tamma G, Casey JR, Alexander RT. 2015. Increased water flux induced by an aquaporin-1/carbonic anhydrase II interaction. *Molecular Biology of the Cell* **26**, 1106-1118.
von Caemmerer S. 2000. *Biochemical models of leaf photosynthesis*. Collingwood, Australia: CSIRO Publishing.
von Caemmerer S, Evans J, Cousins A, Badger M, Furbank R. 2007. C_4 photosynthesis and CO_2 diffusion. *Charting New Pathways to C4 rice* **4**, 95-115.
von Caemmerer S, Evans JR. 2015. Temperature responses of mesophyll conductance differ greatly between species. *Plant, Cell & Environment* **38**, 629-637.

von Caemmerer S, Furbank RT. 2003. The C_4 pathway: an efficient CO_2 pump. *Photosynthesis Research* **77**, 191-207.
von Caemmerer S, Furbank RT. 2016. Strategies for improving C_4 photosynthesis. *Current opinion in plant biology* **31**, 125-134.
von Caemmerer S, Ludwig M, Millgate A, Farquhar GD, Price D, Badger M, Furbank RT. 1997. Carbon Isotope Discrimination during C_4 Photosynthesis: Insights from Transgenic Plants. *Functional Plant Biology* **24**, 487-494.
von Caemmerer S, Quick WP, Furbank RT. 2012. The development of C_4 rice: current progress and future challenges. *Science* **336**, 1671-1672.
von Caemmerer S, Quinn V, Hancock N, Price G, Furbank R, Ludwig M. 2004. Carbonic anhydrase and C_4 photosynthesis: a transgenic analysis. *Plant, Cell & Environment* **27**, 697-703.
Wang C, Hu H, Qin X, Zeise B, Xu D, Rappel W-J, Boron WF, Schroeder JI. 2016. Reconstitution of CO_2 Regulation of SLAC1 Anion Channel and Function of CO_2-Permeable PIP2;1 Aquaporin as CARBONIC ANHYDRASE4 Interactor. *The Plant Cell* **28**, 568-582.
Wang L, Peterson RB, Brutnell TP. 2011. Regulatory mechanisms underlying C_4 photosynthesis. *New Phytology* **190**, 9-20.
Weber AP, von Caemmerer S. 2010. Plastid transport and metabolism of C_3 and C_4 plants—comparative analysis and possible biotechnological exploitation. *Current opinion in plant biology* **13**, 256-264.
Williams TG, Flanagan LB, Coleman JR. 1996. Photosynthetic gas exchange and discrimination against $^{13}CO_2$ and $C^{18}O^{16}O$ in tobacco plants modified by an antisense construct to have low chloroplastic carbonic anhydrase. *Plant physiology* **112**, 319-326.
Wingate L, Ogée J, Cuntz M, Genty B, Reiter I, Seibt U, Yakir D, Maseyk K, Pendall EG, Barbour MM. 2009. The impact of soil microorganisms on the global budget of $\delta^{18}O$ in atmospheric CO_2. *Proceedings of the National Academy of Sciences* **106**, 22411-22415.
Wu A, Song Y, van Oosterom EJ, Hammer GL. 2016. Connecting Biochemical Photosynthesis Models with Crop Models to Support Crop Improvement. *Frontiers in Plant Science* **7**, 1-16.
Wu B, Beitz E. 2007. Aquaporins with selectivity for unconventional permeants. *Cellular and Molecular Life Sciences* **64**, 2413-2421.
Wunder M, Böllert P, Gros G. 1997. Mathematical Modelling of the Role of Intra- and Extracellular Activity of Carbonic Anhydrase and Membrane Permeabilities of HCO_3, H_2O and CO_2 in ^{18}O Exchange. *Isotopes in Environmental and Health Studies* **33**, 197-205.
Yakir D, Sternberg L. 2000. The use of stable isotopes to study ecosystem gas exchange. *Oecologia* **123**, 297-311.
Yaneff A, Vitali V, Amodeo G. 2015. PIP1 aquaporins: Intrinsic water channels or PIP2 aquaporin modulators? *FEBS letters* **589**, 3508-3515.
Yang B, Fukuda N, van Hoek A, Matthay MA, Ma T, Verkman AS. 2000. Carbon Dioxide Permeability of Aquaporin-1 Measured in Erythrocytes and Lung of Aquaporin-1 Null Mice and in Reconstituted Proteoliposomes. *Journal of Biological Chemistry* **275**, 2686-2692.
Yokota A, Kitaoka S. 1985. Correct pK values for dissociation constant of carbonic acid lower the reported Km values of ribulose bisphosphate carboxylase to half. Presentation of a nomograph and an equation for determining the pK values. *Biochemical and Biophysical Research Communications* **131**, 1075-1079.
Yoo Y-J, Lee Hyun K, Han W, Kim Dae H, Lee MH, Jeon J, Lee Dong W, Lee J, Lee Y, Lee J, Kim Jin S, Cho Y, Han J-K, Hwang I. 2016. Interactions between Transmembrane Helices within Monomers of the Aquaporin AtPIP2;1 Play a Crucial Role in Tetramer Formation. *Molecular Plant* **9**, 1004-1017.
Yoshida S, Uemura M. 1986. Lipid Composition of Plasma Membranes and Tonoplasts Isolated from Etiolated Seedlings of Mung Bean (*Vigna radiata* L.). *Plant physiology* **82**, 807-812.

Yu J, Yool AJ, Schulten K, Tajkhorshid E. 2006. Mechanism of Gating and Ion Conductivity of a Possible Tetrameric Pore in Aquaporin-1. *Structure* **14**, 1411-1423.
Zelazny E, Borst JW, Muylaert M, Batoko H, Hemminga MA, Chaumont F. 2007. FRET imaging in living maize cells reveals that plasma membrane aquaporins interact to regulate their subcellular localization. *Proceedings of the National Academy of Science USA* **104**, 12359-12364.
Zelazny E, Miecielica U, Borst JW, Hemminga MA, Chaumont F. 2009. An N-terminal diacidic motif is required for the trafficking of maize aquaporins ZmPIP2;4 and ZmPIP2;5 to the plasma membrane. *The Plant Journal* **57**, 346-355.
Zhang G, Liu X, Quan Z, Cheng S, Xu X, Pan S, Xie M, Zeng P, Yue Z, Wang W, Tao Y, Bian C, Han C, Xia Q, Peng X, Cao R, Yang X, Zhan D, Hu J, Zhang Y, Li H, Li H, Li N, Wang J, Wang C, Wang R, Guo T, Cai Y, Liu C, Xiang H, Shi Q, Huang P, Chen Q, Li Y, Wang J, Zhao Z, Wang J. 2012. Genome sequence of foxtail millet (*Setaria italica*) provides insights into grass evolution and biofuel potential. *Nature Biotechnology* **30**, 549-554.
Zhao M, Tan H-T, Scharwies J, Levin K, Evans JR, Tyerman SD. 2017. Association between water and carbon dioxide transport in leaf plasma membranes: assessing the role of aquaporins. *Plant, Cell & Environment* **40**, 789-801.
Zocher F, Zeidel ML, Missner A, Sun T-T, Zhou G, Liao Y, von Bodungen M, Hill WG, Meyers S, Pohl P. 2012. Uroplakins do not restrict CO_2 transport through urothelium. *Journal of Biological Chemistry* **287**, 11011-11017.
Zwiazek JJ, Xu H, Tan X, Navarro-Ródenas A, Morte A. 2017. Significance of oxygen transport through aquaporins. *Scientific reports* **7**, 1-11.

APPENDIX

Papers published throughout PhD:

Groszmann M., Osborn H.L., Evans J.R. 2016. Carbon dioxide and water transport through plant aquaporins. *Plant Cell and Environment*, 40, 938-961.

McGaughey S.A., Osborn H.L., Chen L., Pegler J.L., Tyerman S.D., Furbank R.T., Byrt C.S., Grof C.P.L. 2016. Roles of Aquaporins in *Setaria viridis* Stem Development and Sugar Storage. *Frontiers in Plant Science* 7, 1-13.

Osborn HL, Alonso-Cantabrana H, Sharwood RE, Covshoff S, Evans JR, Furbank RT, von Caemmerer S. 2016. Effects of reduced carbonic anhydrase activity on CO_2 assimilation rates in *Setaria viridis*: a transgenic analysis. *Journal of Experimental Botany*. 68, 299 - 310.

Plant, Cell & Environment

Plant, Cell and Environment (2016) doi: 10.1111/pce.12844

Review

Carbon dioxide and water transport through plant aquaporins

Michael Groszmann, Hannah L Osborn & John R Evans

Australian Research Council Centre of Excellence for Translational Photosynthesis, Division of Plant Sciences, Research School of BiologyThe Australian National University, Acton, ACT 2601, Australia

ABSTRACT

Aquaporins are channel proteins that function to increase the permeability of biological membranes. In plants, aquaporins are encoded by multigene families that have undergone substantial diversification in land plants. The plasma membrane intrinsic proteins (PIPs) subfamily of aquaporins is of particular interest given their potential to improve plant water relations and photosynthesis. Flowering plants have between 7 and 28 *PIP* genes. Their expression varies with tissue and cell type, through development and in response to a variety of factors, contributing to the dynamic and tissue specific control of permeability. There are a growing number of PIPs shown to act as water channels, but those altering membrane permeability to CO_2 are more limited. The structural basis for selective substrate specificities has not yet been resolved, although a few key amino acid positions have been identified. Several regions important for dimerization, gating and trafficking are also known. PIP aquaporins assemble as tetramers and their properties depend on the monomeric composition. PIPs control water flux into and out of veins and stomatal guard cells and also increase membrane permeability to CO_2 in mesophyll and stomatal guard cells. The latter increases the effectiveness of Rubisco and can potentially influence transpiration efficiency.

INTRODUCTION

During photosynthesis, CO_2 assimilation reduces the partial pressure of CO_2 inside chloroplasts relative to that in the surrounding atmosphere. As a result, there is a net diffusion of CO_2 into the leaf. At the same time, water diffuses from wet mesophyll cell wall surfaces out to the drier atmosphere. Plants control this diffusive exchange of water and CO_2 by enclosing leaves with an impermeable barrier perforated by dynamic pores called stomata. CO_2 uptake from the atmosphere is inevitably linked to transpirational water loss because water and CO_2 share the same diffusional path across the epidermis through stomata. A wall surrounds each plant cell that defines its shape and allows hydraulic pressure to build up within it. The porous matrix of the wall contains an aqueous solution that allows water and gases to pass between the inside of the cell and the atmosphere. Behind each cell wall lies the plasma membrane. This lipid bilayer contains almost equal proportions of phospholipids and sterols while proteins account for about 40% of the mass (Yoshida & Uemura 1986). The plasma membrane provides cells with a barrier that limits the exchange of water, solutes and gases between the external and internal solution. Exchange across the membrane is then controlled by protein pores and transporters that are integrated into it.

In mammalian red blood cells, there is an abundant 28 kD integral membrane protein (CHIP28, now called AQP1) which was firstly cloned in 1991 (Preston & Agre 1991). The function of this protein as a water channel was discovered by expressing it in *Xenopus* oocytes (Preston *et al.* 1992). Oocyte membrane water permeability containing CHIP28 could be inhibited by $HgCl_2$. Using the same expression system, two other proteins homologous to CHIP28 were found to be water channels, one from the collecting duct of the rat kidney (Fushimi *et al.* 1993) and the other a tonoplast intrinsic protein (TIP) from *Arabidopsis thaliana* (Maurel *et al.* 1993). Given that these proteins came from a large family of integral membrane proteins identified in diverse organisms and the demonstration that all three acted as water channels, the term aquaporin (AQP) was coined (Agre *et al.* 1993). Since then, there has been an explosion of research on AQPs and numerous reviews on their role in plants (Javot & Maurel 2002; Tyerman *et al.* 2002; Kaldenhoff & Fischer 2006; Katsuhara *et al.* 2008; Maurel *et al.* 2008; Heinen *et al.* 2009; Prado & Maurel 2013; Chaumont & Tyerman 2014; Maurel *et al.* 2015; Moshelion *et al.* 2015).

This review focuses on AQPs in the plasma membrane that alter permeability to water and CO_2. We firstly introduce the phylogenetic origins of major intrinsic proteins (MIPs) before considering the evidence that they are water channels. The role of AQPs varies depending on the location in the plant. Evidence for AQPs altering the membrane permeability to CO_2 is more limited than for water, but there is evidence that CO_2 permeable AQPs function in leaves both in mesophyll cells and stomatal guard cells. We consider the functionally significant amino acids and end with a brief summary of attempts to engineer improved plants by manipulating AQPs.

PHYLOGENETIC BACKGROUND TO MAJOR INTRINSIC PROTEINS

MIPs are an ancient superfamily of proteins found essentially throughout all taxonomic kingdoms. Their classic six transmembrane structure consisting of two repeated halves evolved through a tandem intragenic duplication of a three transmembrane domain protein that may have functioned as a homodimer (Park & Saier 1996). The first major phylogenetic division of MIPs is considered to be the separation into water channel AQPs and glycerol transporting aquaglyceroporins

Correspondence: J. R. Evans. e-mail: john.evans@anu.edu.au

(GLPs) within bacteria and archaea. An increased availability of genomic sequences has advanced this view showing a more complex diversification in bacteria and archaea involving four major grades; GLP, AQPM, AQPZ and the newly identified AQPN (Finn *et al.* 2014). Since then, these groups have undergone an explosion in sequence and functional diversification resulting in many types (subfamilies) and variants (groups and isoforms therein) of MIPs across all kingdoms (Abascal *et al.* 2014; Finn & Cerda 2015). AQPs are most diverse in green plants (Viridiplantae), with 12 distinct subfamilies acknowledged thus far (Fig. 1); MIPsA-E, GlpF-like intrinsic proteins (GIPs), hybrid intrinsic proteins (HIPs), plasma membrane intrinsic proteins (PIPs), TIPs, NOD26-like intrinsic proteins (NIPs), small basic intrinsic proteins (SIPs) and uncharacterized X intrinsic proteins (XIPs).

Nomenclature of the subfamilies is somewhat arbitrary being based on a combination of main cellular localization (PIPs, TIPs), first identified tissue expression (NIPs,(Heymann & Engel 1999)), protein structure (SIPs, (Johanson & Gustavsson 2002); HIPs, (Danielson & Johanson 2008)), phylogenetic relationships with earlier identified AQPs (GIPs, (Gustavsson *et al.* 2005); MIPsA-E, (Anderberg *et al.* 2011)) or simply uncharacterized (XIPs – (Danielson & Johanson 2008)). Little is known about the localization and functions of MIPsA-E or HIPs, but the other subfamilies have been well characterized. GIPs localize to the plasma membrane and

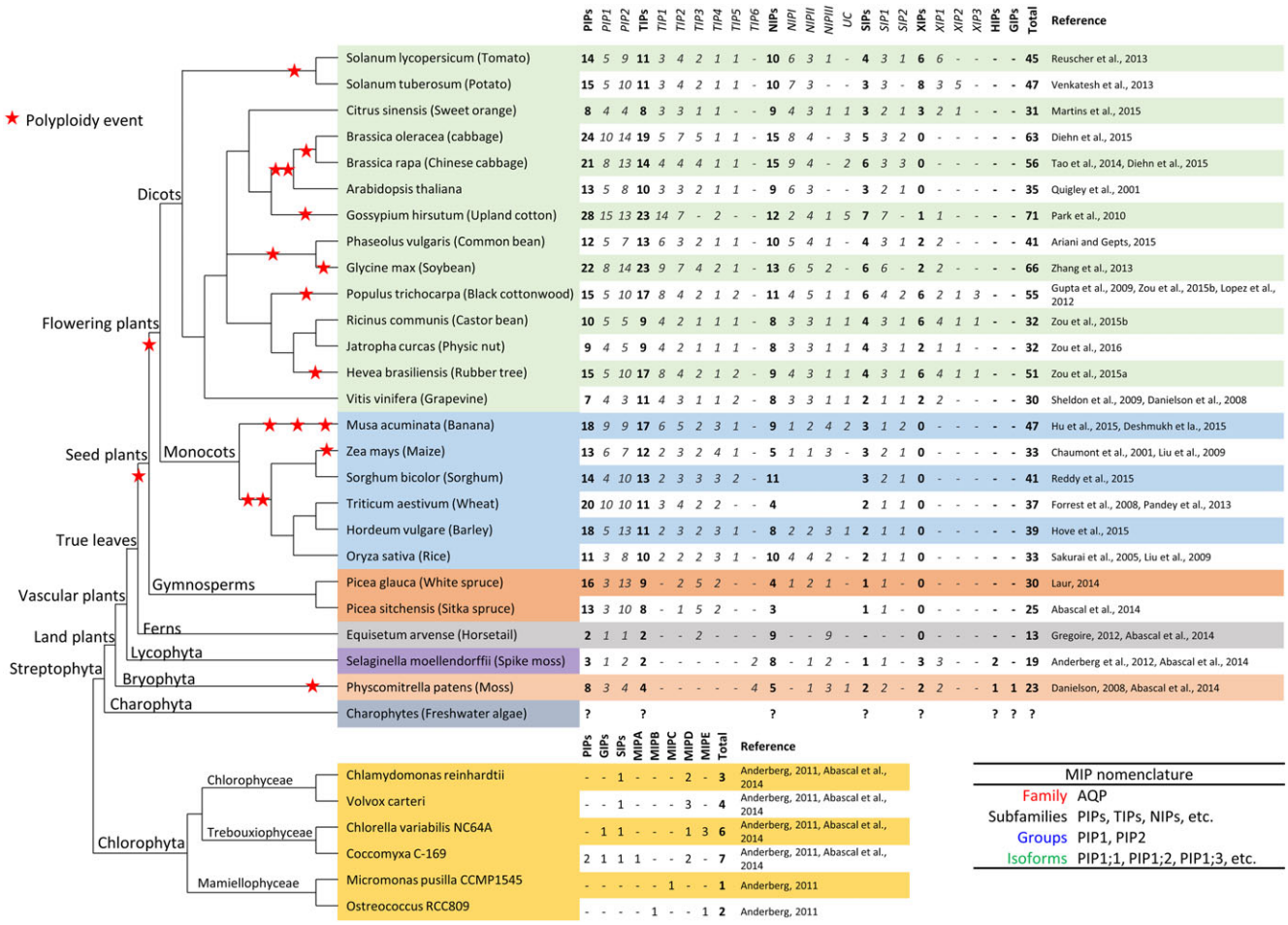

	PIPs	PIP1	PIP2	TIPs	TIP1	TIP2	TIP3	TIP4	TIP5	TIP6	NIPs	NIPI	NIPII	NIPIII	UC	SIPs	SIP1	SIP2	XIPs	XIP1	XIP2	XIP3	HIPs	GIPs	Total	Reference
Solanum lycopersicum (Tomato)	14	5	9	11	3	4	2	1	1	-	10	6	3	1	-	4	3	1	6	6	-	-	-	-	45	Reuscher et al., 2013
Solanum tuberosum (Potato)	15	5	10	11	3	4	2	1	1	-	10	7	3	-	-	3	3	-	8	3	5	-	-	-	47	Venkatesh et al., 2013
Citrus sinensis (Sweet orange)	8	4	4	8	3	3	1	1	-	-	9	4	3	1	1	3	2	1	3	2	1	-	-	-	31	Martins et al., 2015
Brassica oleracea (cabbage)	24	10	14	19	5	7	5	1	1	-	15	8	4	-	3	5	3	2	0	-	-	-	-	-	63	Diehn et al., 2015
Brassica rapa (Chinese cabbage)	21	8	13	14	4	4	4	1	1	-	15	9	4	-	2	6	3	3	0	-	-	-	-	-	56	Tao et al., 2014, Diehn et al., 2015
Arabidopsis thaliana	13	5	8	10	3	3	2	1	1	-	9	6	3	-	-	3	2	1	0	-	-	-	-	-	35	Quigley et al., 2001
Gossypium hirsutum (Upland cotton)	28	15	13	23	14	7	-	2	-	-	12	2	4	1	5	7	7	-	1	1	-	-	-	-	71	Park et al., 2010
Phaseolus vulgaris (Common bean)	12	5	7	13	6	3	2	1	1	-	10	5	4	1	-	4	3	1	2	2	-	-	-	-	41	Ariani and Gepts, 2015
Glycine max (Soybean)	22	8	14	23	9	7	4	2	1	-	13	6	5	2	-	6	6	-	2	2	-	-	-	-	66	Zhang et al., 2013
Populus trichocarpa (Black cottonwood)	15	5	10	17	8	4	2	1	2	-	11	4	5	1	1	6	4	2	6	2	1	3	-	-	55	Gupta et al., 2009, Zou et al., 2015b, Lopez et al., 2012
Ricinus communis (Castor bean)	10	5	5	9	4	2	1	1	1	-	8	3	3	1	1	4	3	1	6	4	1	1	-	-	32	Zou et al., 2015b
Jatropha curcas (Physic nut)	9	4	5	9	4	2	1	1	1	-	8	3	3	1	1	4	3	1	2	1	1	-	-	-	32	Zou et al., 2016
Hevea brasiliensis (Rubber tree)	15	5	10	17	8	4	2	1	2	-	9	4	3	1	1	4	3	1	6	4	1	1	-	-	51	Zou et al., 2015a
Vitis vinifera (Grapevine)	7	4	3	11	4	3	1	1	2	-	8	3	3	1	1	2	1	1	2	2	-	-	-	-	30	Sheldon et al., 2009, Danielson et al., 2008
Musa acuminata (Banana)	18	9	9	17	6	5	2	3	1	-	9	1	2	4	2	3	1	2	0	-	-	-	-	-	47	Hu et al., 2015, Deshmukh et la., 2015
Zea mays (Maize)	13	6	7	12	2	3	2	4	1	-	5	1	1	3	-	3	2	1	0	-	-	-	-	-	33	Chaumont et al., 2001, Liu et al., 2009
Sorghum bicolor (Sorghum)	14	4	10	13	2	3	3	3	2	-	11					3	2	1	0	-	-	-	-	-	41	Reddy et al., 2015
Triticum aestivum (Wheat)	20	10	10	11	3	4	2	2	-	-	4					2	1	1	0	-	-	-	-	-	37	Forrest et al., 2008, Pandey et al., 2013
Hordeum vulgare (Barley)	18	5	13	11	2	3	2	3	1	-	8	2	2	3	1	2	1	1	0	-	-	-	-	-	39	Hove et al., 2015
Oryza sativa (Rice)	11	3	8	10	2	2	2	3	1	-	10	4	4	2	-	2	1	1	0	-	-	-	-	-	33	Sakurai et al., 2005, Liu et al., 2009
Picea glauca (White spruce)	16	3	13	9	-	2	5	2	-	-	4	1	2	1	-	1	1	-	0	-	-	-	-	-	30	Laur, 2014
Picea sitchensis (Sitka spruce)	13	3	10	8	-	1	5	2	-	-	3					1	1	-	0	-	-	-	-	-	25	Abascal et al., 2014
Equisetum arvense (Horsetail)	2	1	1	2	-	-	2	-	-	-	9	-	-	9	-	-	-	-	0	-	-	-	-	-	13	Gregoire, 2012, Abascal et al., 2014
Selaginella moellendorffii (Spike moss)	3	1	2	2	-	-	-	-	-	2	8	-	1	2	-	1	1	-	3	3	-	-	2	-	19	Anderberg et al., 2012, Abascal et al., 2014
Physcomitrella patens (Moss)	8	3	4	4	-	-	-	-	-	4	5	-	1	3	1	2	2	-	2	2	-	-	1	1	23	Danielson, 2008, Abascal et al., 2014
Charophytes (Freshwater algae)	?			?							?					?			?				?	?	?	

	PIPs	GIPs	SIPs	MIPA	MIPB	MIPC	MIPD	MIPE	Total	Reference
Chlamydomonas reinhardtii	-	-	1	-	-	-	2	-	3	Anderberg, 2011, Abascal et al., 2014
Volvox carteri	-	-	1	-	-	-	3	-	4	Anderberg, 2011, Abascal et al., 2014
Chlorella variabilis NC64A	-	1	1	-	-	-	1	3	6	Anderberg, 2011, Abascal et al., 2014
Coccomyxa C-169	2	1	1	1	-	-	2	-	7	Anderberg, 2011, Abascal et al., 2014
Micromonas pusilla CCMP1545	-	-	-	-	-	1	-	-	1	Anderberg, 2011
Ostreococcus RCC809	-	-	-	-	1	-	-	1	2	Anderberg, 2011

Figure 1. Aquaporin diversity across the green plant (Viridiplantae) kingdom. The phylogenetic tree is based on reconstructions from Leliaert *et al.* (2012) and Ruhfel *et al.* (2014), with major divisions listed at their respective evolutionary points. Polyploidy events (red stars) were obtained from summaries provided in Mühlhausen & Kollmar (2013) and CoGepedia https://genomevolution.org/wiki/index.php/Plant_paleopolyploidy. Suspected genome doubling in Rubber tree (Zou *et al.* 2015a; Zou *et al.* 2016), consistent with the higher frequency of aquaporin genes compared to close relatives of Physic nut and Castor bean. Modifications from initial classification: *Physcomitrella patens*; removed unlikely third PIP group (PIP3) as PpPIP3;1 is likely non-functional (Danielson & Johanson 2008). *Citrus sinensis*; removed CsTIP1;3, CsTIP5;1 and CsTIP6;1 as these were all substantially truncated proteins. *Equisetum arvense*; reassigned EaTIP1;1 and EaTIP2;1 to EaTIP3;1 and EaTIP3;2 in accordance with (Abascal *et al.* 2014). *Picea glauca*; reassigned PgTIP1s as PgTIP3s in accordance with (Abascal *et al.* 2014). *Populus trichocarpa*; reassigned PtXIPs in accordance with (Lopez *et al.* 2012) and PtNIPs in accordance with (Zou *et al.* 2015b). *Solanum lycopersicum*; removed two SlNIPs because of substantial deletions. Noted limitations in data: *Equisetum arvense* information derived from root transcriptome only (Gregoire *et al.* 2012). *Triticum aestivum*; unlikely to be an exhaustive search (Forrest & Bhave 2008; Pandey *et al.* 2013). Currently there is a lack of aquaporin family data in the charophyta. Aquaporin data in this primitive evolutionary important plant lineage could contribute significantly to our understanding of early plant aquaporin evolution.

transport glycerol but not water (Gustavsson *et al.* 2005). PIPs generally localize to the plasma membrane but have been found to co-localize to the chloroplast envelope (Uehlein *et al.* 2008; Beebo *et al.* 2013) and are highly water permeable, but can also transport hydrogen peroxide and uniquely carbon dioxide (Bienert *et al.* 2007; Hooijmaijers *et al.* 2012; Prado & Maurel 2013; Kaldenhoff *et al.* 2014; Tian *et al.* 2016). TIPs are mainly localized in the tonoplast (vacuole membrane), but have been found in the plasma, chloroplast and thylakoid membranes (Ferro *et al.* 2010; Beebo *et al.* 2013) and are permeable to water and other solutes such as urea, ammonia and hydrogen peroxide (Liu *et al.* 2003; Loque *et al.* 2005; Dynowski *et al.* 2008; Mao & Sun 2015). The co-localization of PIPs and TIPs to the chloroplast and thylakoid membranes maybe particularly important in supplying water and CO_2 for photosynthetic reactions (discussed later). XIPs are plasma membrane localized and permeable to various solutes but only moderately to water (Bienert *et al.* 2011; Lopez *et al.* 2012). SIPs are localized to the endoplasmic reticulum (ER) and have moderate water permeability (Ishikawa *et al.* 2005; Noronha *et al.* 2014). NIPs are found in the plasma membrane and ER and are permeable to numerous substrates including both beneficial and toxic metalloids, but generally show poor water permeability (Pommerrenig *et al.* 2015).

The most basal of green plants, the green algae (chlorophytes), have seven AQP subfamilies; MIPsA-E, which are specific to algae, in addition to PIP, GIP and SIP homologs (Anderberg *et al.* 2011; Abascal *et al.* 2014). These AQPs are found in sparse and assorted complements among species which may reflect redundant functions or specific lifestyle requirements given the remarkable variation in green algal ecology (Anderberg *et al.* 2011; Leliaert *et al.* 2012). In land plants (Embryophyta), the number of AQP subfamilies has contracted from seven in primitive land plants to five in seed plants (Spermatophyta). However, the number of groups and isoforms therein has undergone substantial expansion and diversification (Fig. 1). Gone from higher plants are the HIPs and GIPs, presumably because of functional redundancy with the TIPs and NIPs, respectively (Anderberg *et al.* 2012; Abascal *et al.* 2014). XIPs persist in higher plants to an extent, having been lost in the Brassicaceae, monocots and possibly the gymnosperms, but diversified in the Malpighiales. The SIPs split into two groups with the emergence of angiosperms, but in general show little diversification compared to the other subfamilies. The TIPs, may have ancestral ties with the algal MIPA, but emerged as a distinct subfamily in land plants (Anderberg *et al.* 2011). An independent diversification in primitive plants gave rise to the TIP6 group, while the major expansion seemingly originates in the ancestor of seed plants after divergence from the ferns. TIP2, TIP3 and TIP4 represent the basal groups, with TIP1 and TIP5 emerging in angiosperms as sister groups to TIP3 and TIP2, respectively (Abascal *et al.* 2014; Laur & Hacke 2014). Coinciding with their wide substrate specificities, NIP isoforms are the most divergent among higher plant AQP subfamilies. This makes it difficult to fully resolve the relationships between groups of distantly related species using subgrouping normally applied to other AQP subfamilies (Pommerrenig *et al.* 2015). Using the alternative ar/R filter classification shows that the ancestral NIPs belong to groups II and III, with the latter having proliferated in monocots and been lost in the brassica genus. Group I NIPs are seed plant specific. The PIP subfamily has the longest clearly discernible lineage among plant AQPs. PIP isoforms exist in the chlorophytes and have key similarities to algal MIPEs suggesting a paralogous and possibly redundant relationship, consistent with PIPs and MIPEs not being found in the same extant algal species (Anderberg *et al.* 2011). PIPs diverge into two highly conserved groups (PIP1 and PIP2) prior to the emergence of land plants and although there has been no further expansion of group types, there has been a substantial proliferation in the number of PIP1 and PIP2 isoforms coinciding with the appearance of seed plants.

Horizontal gene transfer (HGT) has been important in the acquisition of AQPs into the plant kingdom. The origin of GIPs reside in a HGT event with bacteria Glp (Gustavsson *et al.* 2005), while the ancestral NIP arose through a HGT event involving bacterial AQPN (Finn & Cerda 2015). HGT events would also, in part, account for the assorted complements of MIP types found in different chlorophytes (Fig. 1; (Anderberg *et al.* 2011)). In land plants, the impressive diversification of AQPs has likely been facilitated by a propensity for gene duplication events, especially prevalent in the angiosperms. Major diversification of land plant AQPs coincide with ancient polyploidization events occurring prior to the divergence of spermatophytes and another before angiosperms arose (Fig. 1; (Jiao *et al.* 2011)). This association with events that heralded today's diverse plant life supports AQPs being important in higher plant evolution. Later lineage-specific polyploidization events likely facilitated further diversification and expansion apparent between angiosperm lineages (Abascal *et al.* 2014). Reflecting this concept, AQP numbers are often higher in species that have experienced a more recent polyploidy event (e.g. Soybean versus Common bean; *Arabidopsis* versus *Brassica rapa*; Poplar versus Castor bean; Fig. 1). In addition to whole genome duplications, single gene replication events locally (i.e. tandem or proximal duplication) or between different regions of the genome (transposition or retrotransposition) have contributed to lineage and species specific expansion of AQPs.

As with most genes, the AQP duplicates (homeologs or paralogs) would be deleted over time. Progress of such gene loss is evident in the numerous AQP pseudogenes present in soybean, cotton and cabbage which have undergone relatively recent polyploidization (Park *et al.* 2010; Zhang *et al.* 2013; Diehn *et al.* 2015). Retention of a paralog relies on the duplicate gene acquiring a novel role (neo-functionalization) or the two duplicate genes dividing the original function (subfunctionalization) (Rensing 2014). Given the high homology of AQP isoforms in a given species, it is likely that paralog retention has largely been driven through divergence in gene regulation. Consistent with this, AQP isoforms within a species show differences in expression patterns even at the broad level of whole tissues (e.g. leaf, roots, fruit, seed etc.) (Quigley *et al.* 2001; Sakurai *et al.* 2005; Gupta & Sankararamakrishnan 2009; Cohen *et al.* 2013; Reuscher *et al.* 2013; Venkatesh *et al.* 2013; Abascal *et al.* 2014; Tao *et al.* 2014; Ariani & Gepts 2015; Diehn *et al.* 2015; Hu *et al.* 2015; Martins *et al.* 2015; Reddy *et al.* 2015;

Zou *et al.* 2015b; Zou *et al.* 2016), with differences becoming more distinct at the level of cell types within a tissue (Bots *et al.* 2005; Fraysse *et al.* 2005; Hachez *et al.* 2006; Sakurai *et al.* 2008; Gomes *et al.* 2009; Alexandersson *et al.* 2010; Lopez *et al.* 2012; Prado *et al.* 2013). Divergence in AQP isoform expression also extends to differential responses to abiotic stresses and environmental stimuli (see later section on regulation of AQP expression). Presumably, this refined transcriptional regulation offers plants an intricate control over hydraulic properties and transport of the various solutes and gases that permeate AQPs.

With roles in water transport and nutrient acquisition, it is not surprising that the evolution of AQPs and plants appear strongly intertwined. AQP diversity in bryophytes compared to algal species may represent an additional need for AQPs to transition from an aquatic to a terrestrial environment (Danielson & Johanson 2008; Anderberg *et al.* 2011; Hanson & Rice 2014). Subsequent AQP diversification in land plants likely stems from an increasing complexity of organ structures and cell types, involved in migration from low growth habits in moist environments to taller growth and more arid conditions. The association of TIPs with the metabolically important vacuole and ability of NIPs to transport nutritionally beneficial metalloids (e.g. boron and silicon) (Martinoia *et al.* 2007; Pommerrenig *et al.* 2015), likely drove their diversification during land plant evolution. Early evolution of PIPs in plants reflects the primary importance of water transport. PIPs in free living aquatic algae may regulate water content for buoyancy, aiding in nutrient acquisition and transport (Anderberg *et al.* 2011; Komsic-Buchmann *et al.* 2014; Raven & Doblin 2014), while in the earliest land plants, PIP proteins provide osmoprotection (Lienard *et al.* 2008). In higher plants, water permeability has continued as a key selected trait evident by strong PIP gene expression in tissues with large water fluxes (e.g. vasculature, stomata, flowers). Uniquely, among plant AQPs, PIPs also transport CO_2, the substrate for carbohydrate production via photosynthesis. In animals, AQP 0, 1, 4, 5 and 6 and bacterial AQPZ in cyanobacteria PCC7942 have also been shown capable of transporting CO_2 to varying levels (Musa-Aziz *et al.* 2009; Ding *et al.* 2013; Geyer *et al.* 2013). These animal AQPs, AQPZ and plant PIPs appear to have a deep rooted phylogenetic connection (Abascal *et al.* 2014), which temptingly points to an ancient origin for CO_2 specificity. However, this would require assuming many independent functional losses of CO_2 specificity given its infrequency compared to water permeability. It is more likely that CO_2 specificity arose through convergent evolution, with the water permeable AQP archetype reasonably amenable to sequence variation leading to significant CO_2 permeability that is selected upon if the need arises.

In aquatic environments, CO_2 diffusion is much slower than in terrestrial environments and bicarbonate (HCO_3^-) is frequently the dominant inorganic carbon species (Wang *et al.* 2015). Consequently, algae have evolved both active CO_2 and HCO_3^- uptake systems (Wang *et al.* 2015), making CO_2 permeable MIP/PIP unnecessary or even undesirable. A niche role may still exist as *Chlamydomonas* possess a plasma membrane localized passive CO_2 channel in the form of Rhesus proteins that reportedly aid carbon uptake under elevated CO_2 conditions (Soupene *et al.* 2002; Soupene *et al.* 2004). However, the absence of Rhesus proteins in land plants and their existence in algae (Peng & Huang 2006) may yet represent a further preclusion for an algal CO_2 MIP/PIP. A role for a CO_2 permeable PIP would presumably be most favoured in a terrestrial environment. Mesophyll CO_2 conductance in land plants generally scales with their phylogenetic ranking (Flexas *et al.* 2012; Raven & Beardall 2016; Tosens *et al.* 2016). Low values for bryophytes through to ferns are predominantly linked with sub-optimal anatomical traits and requirements for external moisture coatings (Flexas *et al.* 2012; Royles *et al.* 2013; Kubásek *et al.* 2014; Field *et al.* 2015; Raven & Beardall 2016; Tosens *et al.* 2016). For a given cell wall thickness, ferns have a mesophyll conductance per unit of chloroplast surface area exposed to intercellular airspace that is similar to angiosperms. This suggests that the extent of PIP facilitated CO_2 diffusion in ferns is similar to that in angiosperms despite having an apparently more limited number of PIP genes. The diversification of PIPs in seed plants enabled temporal and spatial specialization of expression, coinciding with greater photosynthetic energy demands, more complex leaf structures and decreasing atmospheric CO_2 concentrations (Beerling 2005). A better understanding of PIP (or AQPs in general) evolution could be achieved by complementing protein sequence phylogenetic reconstructions with substrate specificities from more AQPs across the plant kingdom.

EVIDENCE THAT PLANT AQUAPORINS ENHANCE MEMBRANE PERMEABILITY TO WATER

The demonstration that a plant TIP acted as a water channel (Maurel *et al.* 1993) spurred a search for other candidate genes encoding AQPs in the plasma membrane. Using a mammalian COS cell line and an antibody raised against plasma membrane proteins, five genes from *Arabidopsis* representing two families of PIPs were identified (Kammerloher *et al.* 1994). These were expressed in *Xenopus* oocytes to demonstrate that they were water channels. The PIP2 type showed greater water permeability than the PIP1 type, but both types could be inhibited by $HgCl_2$. Because plasma membrane composition is likely to vary between organisms, the function of an AQP in one cell type does not necessarily mean that it will function in the same way in another cell. Thus, it is important to demonstrate that AQPs alter water permeability *in planta*. To do this, an antisense line was created against PIP1b in *Arabidopsis* (now AtPIP1;2) driven by the cauliflower mosaic virus 35S promoter (Kaldenhoff *et al.* 1998). Protoplasts prepared from leaf mesophyll tissue were found to have greatly reduced permeability to water compared to protoplasts isolated from control plants. Antisense-pip1b plants also developed a five-fold greater root mass than control plants that presumably compensated for their impaired water uptake capability.

An antisense construct against NtAQP1 with a cauliflower mosaic virus 35S promoter was introduced into *Nicotiana tabacum* (Siefritz *et al.* 2002). Protoplasts isolated from the roots of these plants showed reduced permeability to water. Hydraulic conductivity of intact roots was also reduced by

55%. In contrast to *Arabidopsis* antisense-AtPIP1b plants, no change in the relative size of the root system was observed for tobacco, but the antisense plants were more prone to wilting compared to wild type.

Membrane permeability depends on temperature, and the response can be described by the Arrhenius activation energy, E_a. When water is diffusing through the lipid bilayer, a high E_a is expected and when flow occurs through a channel, a low E_a is expected. When human AQP1 was expressed in *Xenopus* oocytes, E_a decreased from $>>10\,kcal\,mol^{-1}$ for control oocytes to $<3\,kcal\,mol^{-1}$ for oocytes injected with AQP1 (Preston *et al.* 1992). Similarly, the E_a for tonoplast enriched vesicles isolated from suspension cultured *N. tabacum* containing active AQPs (i.e. sensitive to $HgCl_2$ inhibition) was $2.5\,kcal\,mol^{-1}$ compared to $13.5\,kcal\,mol^{-1}$ for plasma membrane enriched vesicles (Maurel *et al.* 1997). The water permeability of purified plasma membrane vesicles isolated from *Arabidopsis* grown in suspension culture could be substantially reduced by the presence of Ca^{2+} (Gerbeau *et al.* 2002). At the same time, the permeability was rendered much more responsive to temperature, consistent with lipid mediated water diffusion brought about by the closure of a channel. In the absence of Ca^{2+}, the permeability was sensitive to pH, declining to minimal values below pH 7. These findings demonstrated that plant AQPs could be gated and their permeability could be altered by changes in Ca^{2+} and pH (see later section on gating).

PIP AQUAPORINS AS WATER CHANNELS

The relative ease of expressing specific AQPs in *Xenopus* oocytes to assess their function has led to a growing list of genes from a range of plant species that are capable of increasing membrane water permeability when expressed in *Xenopus* oocytes. For some species, multiple isoforms have been shown to function as water channels (Table 1). In the case of *Arabidopsis*, the impact on water permeability was initially reported as being greater for PIP2s compared to PIP1s (Kammerloher *et al.* 1994). Weaker effects were also observed for PIP1s compared to PIP2s from *Hordeum vulgare* (Katsuhara & Shibasaka 2007), *Oryza sativa* (Li *et al.* 2000; Lian *et al.* 2004) and *Raphanus sativa* (Suga & Maeshima 2004). However, the observation that PIP1s were apparently less effective than PIP2s came into question following the discovery that co-expression of PIP1 with PIP2 genes in *Xenopus* oocytes increased water permeability (Fetter *et al.* 2004). Oocytes with co-expression of PIP1 and PIP2 genes had greater water permeability than oocytes injected with the same amount of PIP2 genes but no PIP1 genes, and PIP1 genes by themselves had no effect. Previously, it had been established that PIP1 proteins could be recovered from the plasma membrane fraction of *Xenopus* oocytes when just PIP1 genes were injected, but these did not alter membrane permeability to water (Chaumont *et al.* 2000). Thus, to become functional in the plasma membrane of *Xenopus* oocytes, PIP1 needed to assemble in a hetero-tetrameric association with PIP2 (Fetter *et al.* 2004). Subsequently, when PIP1 genes have been co-expressed with PIP2 genes, increased water permeability has been associated with PIP1s from a range of species (Table 2). For both *Zea mays* (Fetter *et al.* 2004) and *H. vulgare* (Horie *et al.* 2011), multiple forms of PIP2 were capable of conferring functionality to the PIP1 protein. ZmPIP1;2 was also capable of gaining functionality through association with a PIP2 from another species: AtPIP2;3 (Fetter *et al.* 2004). Perhaps, even more surprising was the observation that co-expression of ZmPIP1;1 with ZmPIP1;2 also resulted in increased permeability of *Xenopus* oocytes to water (Fetter *et al.* 2004). In this case, functionality was presumably enabled through the formation of a hetero-tetramer between ZmPIP1;1 and ZmPIP1;2. Not all forms of PIP1 increase water permeability when co-expressed with PIP2. For HvPIP1;3, co-expression with any one of HvPIP2;1–5 could not influence permeability whereas water permeability could be further increased when HvPIP2;1–5 was co-expressed with either HvPIP1;2 or HvPIP1;4 (Horie *et al.* 2011).

Different AQP monomers can dimerize through a disulphide linkage in loop A before forming into tetramers (Bienert *et al.* 2012). The functional and regulatory properties of heterotetramers reflect their composition and may provide an additional level of control (Yaneff *et al.* 2014). Expression profiling has revealed that certain combinations of PIP1 and PIP2 genes occur in *Arabidopsis*, maize and rice (Yaneff *et al.* 2015). An F220A mutation in the transmembrane domain 5 of ZmPIP1;2 activated its water activity while inactivating its dimeric partner ZmPIP2;5 within a heterotetramer (Berny *et al.* 2016).

Finally, it is worth repeating that water permeability associated with a given PIP gene depends on the membrane system it is tested in. For some species, PIP1 can form tetramers and reach the plasma membrane in yeast (Sabir *et al.* 2014) or *Xenopus* oocytes (Chaumont *et al.* 2000; Berny *et al.* 2016) without requiring an association with PIP2. AQP1 from tobacco was shown to enhance water permeability in *Xenopus* oocytes (Biela *et al.* 1999) but not when expressed in yeast (Otto *et al.* 2010). For HvPIP1;2 expressed in *Xenopus* oocytes, water permeability was only observed when it was co-expressed with PIP2 (Horie *et al.* 2011) whereas it conferred increased water permeability by itself when expressed in yeast (Besse *et al.* 2011). A PIP1 from *Lilium longiflorum* increased water permeability weakly when expressed in *Xenopus* oocytes, whereas when expressed in *N. tabacum* under a cauliflower mosaic virus 35S promoter, it greatly increased mesophyll protoplast permeability to water (Ding *et al.* 2004). The large number of AQP genes and the tissue specificity of their expression make it a challenge to conclusively attribute function *in planta*.

PATH OF WATER MOVEMENT THROUGH THE PLANT

The majority of water used by plants is extracted from the soil by roots and transported to the shoot where it is lost to the atmosphere by transpiration from leaves. Long distance water transport occurs through dead xylem vessels. These are surrounded by a sheath of living cells that control the flow of water into and out of the xylem (Fig. 2). Movement of water through and along the wall outside of a cell's plasma

Table 1. Functional properties of PIP1 and PIP2 aquaporins. Aquaporins conferring increased permeability to water (cells highlighted in blue) when expressed in *Xenopus* oocytes are marked as strong (✓), weak (w), or requires co-expression with another PIP (+, see Table 2). Aquaporins conferring increased permeability to water when expressed in yeast are marked as (Y), or (✗) if expression in yeast increased CO_2 permeability but did not alter water permeability. Aquaporins conferring increased permeability to CO_2 (cells highlighted in red) when expressed in *Xenopus* oocytes (✓) or when expressed in yeast (Y) or incorporated into a triblock copolymer membrane (P). Instances marked by a red (●) are where increased water permeability was observed when expressed in yeast, but no change to CO_2 permeability was observed. For *N. tabacum*, AQP1 is assigned to PIP1;2. Multiple symbols show instances where there are conflicting reports. The assignment of the same PIP number between species does not necessarily imply that the genes are orthologous.

			PIP1						PIP2							
Plant	Reference	Substrate	1;1	1;2	1;3	1;4	1;5	1;6	2;1	2;2	2;3	2;4	2;5	2;6	2;7	2;8
Arabidopsis thaliana	1	H_2O	✓	w,✗	✓				✓	✓	✓				✓	
	2	CO_2		Y					✓		●					
Beta vulgaris	3	H_2O	+						✓	✓						
Fragaria ananassa	4	H_2O	+						✓							
Helianthemum almeriense	5	H_2O	✗						Y							
		CO_2	Y						●							
Hevea brasiliensis	6	H_2O							✓		✓					
Hordeum vulgare	7	H_2O		+,Y	w	+			✓	✓	✓	✓	✓		✓	✓
	8	CO_2							✓	✓	✓	●	✓			
Juglans regia	9	H_2O							✓							
Lilium longiflorum	10	H_2O	✓													
Mimosa pudica	11	H_2O	+						✓							
Nicotiana tabacum	12	H_2O	+	w,✗,✓					✓							
	13	CO_2		Y,P, ✓					P							
Oryza sativa	14	H_2O	w		w				✓	✓	✓	✓	✓		✓	
	15	CO_2							●							
Phaseolus vulgaris	16	H_2O									✓					
Rosa hybrida	17	H_2O	+						✓							
Raphanus sativa	18	H_2O		w	w				✓	✓	✓					
Spinacia oleracea	19	H_2O							✓							
Samanea saman	20	H_2O							✓							
Tulipa gesneriana	21	H_2O								✓						
Vitis vinifera	22	H_2O	+			✗		+	✓	✓	✓,✗	✓				
Zea mays	23	H_2O	+	+			+	Y	✓				✓			
	24	CO_2					Y	Y								

References

1. (Daniels *et al.*, 1994, Heckwolf *et al.*, 2011, Kammerloher *et al.*, 1994, Soto *et al.*, 2008, Weig *et al.*, 1997); 2. (Heckwolf *et al.*, 2011, Uehlein *et al.*, 2012b, Wang *et al.*, 2016); 3. (Bellati *et al.*, 2010, Jozefkowicz *et al.*, 2013); 4. (Alleva *et al.*, 2010); 5. (Navarro-Rodenas *et al.*, 2013); 6. (An *et al.*, 2015); 7. (Besse *et al.*, 2011, Horie *et al.*, 2011, Katsuhara *et al.*, 2002, Shibasaka *et al.*, 2012); 8. (Mori *et al.*, 2014); 9. (Sakr *et al.*, 2003); 10. (Ding *et al.*, 2004); 11. (Temmei *et al.*, 2005); 12. (Biela *et al.*, 1999, Mahdieh *et al.*, 2008, Otto *et al.*, 2010, Sade *et al.*, 2010, Siefritz *et al.*, 2002); 13. (Ding *et al.*, 2013, Otto *et al.*, 2010, Uehlein *et al.*, 2003, Uehlein *et al.*, 2012a); 14. (Ding *et al.*, 2016, Ding *et al.*, 2013, Li *et al.*, 2008, Li *et al.*, 2000, Lian *et al.*, 2004, Sakurai *et al.*, 2008, Sakurai *et al.*, 2005, Zhang *et al.*, 2010); 15. (Ding *et al.*, 2013); 16. (Zhou *et al.*, 2007); 17. (Chen *et al.*, 2013, Ma *et al.*, 2008, Postaire *et al.*, 2010); 18. (Suga & Maeshima, 2004); 19. (Johansson *et al.*, 1998); 20. (Moshelion *et al.*, 2002); 21. (Azad *et al.*, 2008); 22. (Sabir *et al.*, 2014, Shelden *et al.*, 2009, Vandeleur *et al.*, 2009); 23. (Bienert *et al.*, 2012, Chaumont *et al.*, 2000, Fetter *et al.*, 2004, Heinen *et al.*, 2014); 24. (Heinen *et al.*, 2014)

membrane is called apoplastic flow. Water can pass along many connected cells via apoplastic flow, for example, in the root cortex or leaf mesophyll, bundle sheath extension or epidermis. However, there are barriers that interrupt this path in the root endodermis (Steudle 2000; Zimmermann *et al.* 2000) and the bundle sheath surrounding veins in the shoot and leaf (Canny 1988; Canny 1995; Hachez *et al.* 2008) (Fig. 2). At such points, water needs to move inside the cells to pass the barrier. To enter and exit cells, water must cross the plasma membrane, called the transcellular path. As the plasma membrane is rather impermeable to water, AQPs provide the channel through which most water moves. It is also possible for water to move between cells while remaining in the cytosol through plasmodesmatal pores between adjacent cells, and this is called symplastic flow.

Localization of PIPs using GUS reporter constructs, mRNA expression or antibodies reveal widespread PIP expression. There is particularly high expression in root tips, the stele of the root and leaf veins (Frangne *et al.* 2001; Javot *et al.* 2003; Kaldenhoff *et al.* 2008; Postaire *et al.* 2010). The locations surrounding water entry in the xylem where apoplastic flow is blocked are exactly where a high density of AQPs would be needed to enable transcellular water flow. This simplified scheme for water movement in roots which applies to wheat, has exceptions both between species, for example, lupin (Bramley *et al.* 2009) and with distance from the root tip (Steudle 2000). A measure of the ease with which water can flow through roots is hydraulic conductance. This can be determined either by a gradient in hydrostatic pressure or osmotic potential, with the latter reflecting the influence of a plasma

Table 2. Increased permeability of *Xenopus* oocytes to water when particular PIP1s (+) are co-expressed together with PIP2s (✓). The sole exception so far is ZmPIP1;1, where co-expression with ZmPIP1;2 (c) rendered the PIP1 active. Where several different PIP1 genes have been investigated for a given species, a separate line is used to identify interactions for each PIP1

Plant	Reference	PIP1						PIP2							
		1;1	1;2	1;3	1;4	1;5	1;6	2;1	2;2	2;3	2;4	2;5	2;6	2;7	2;8
Beta vulgaris	(Bellati *et al.* 2010; Jozefkowicz *et al.* 2013)	+							✓						
Fragaria ananassa	(Alleva *et al.* 2010)	+						✓							
Hordeum vulgare	(Horie *et al.* 2011)		+					✓	✓	✓	✓	✓			
					+			✓	✓	✓	✓	✓			
Mimosa pudica	(Temmei *et al.* 2005)	+						✓							
Nicotiana tabacum	(Mahdieh *et al.* 2008)	+						✓							
Rosa hybrida	(Chen *et al.* 2013)	+						✓							
Vitis vinifera	(Vandeleur *et al.* 2009)	+							✓						
Zea mays	(Fetter *et al.* 2004)	c	c												
			+					✓		At	✓	✓			
	(Bienert *et al.* 2012)		+									✓			
	(Heinen *et al.* 2014)					+		✓							
							+	✓							

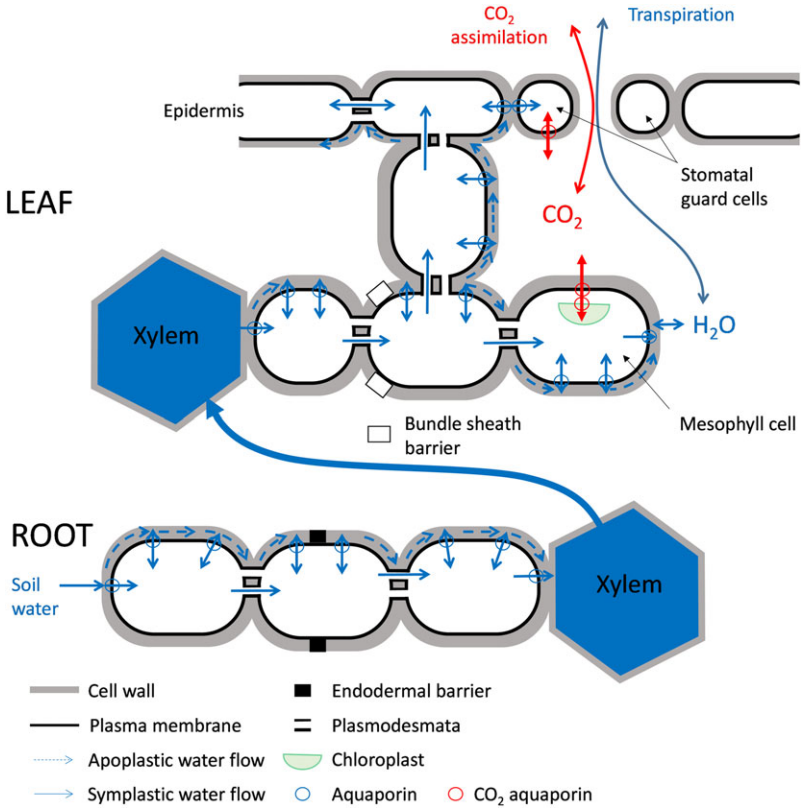

Figure 2. Diagrammatic illustration of water flow from the soil through the plant to the atmosphere and CO_2 diffusion between the leaf and atmosphere. Water can flow either along cell walls via the apoplast or through cells via plasmodesmata in the symplast. Water needs to cross plasma membranes at several points along the way through aquaporins, which allow bidirectional flow. The combination of apoplastic and symplastic flow enabled by entry and exit via aquaporins is termed transcellular flow. Water entry and exit from the vascular system are isolated from apoplastic flow by the endodermis in roots and the bundle sheath in leaves. Mature guard cells have no symplastic connection to adjacent epidermal cells. Not shown is the cuticle that lines the external surface of the epidermis making it impermeable to water and CO_2. Leaf mesophyll and stomatal guard cells have aquaporins that enhance the permeability of the plasma membrane and chloroplast envelope to CO_2

membrane barrier (Chaumont & Tyerman 2014). In wheat, root hydraulic conductivity was rapidly decreased upon exposure to $HgCl_2$ and could be restored with DTT which is consistent with AQPs controlling water uptake (Clarkson *et al.* 2000). *Arabidopsis* plants with antisense reductions to PIP1, PIP2 or a combination of these genes were found to have root hydraulic conductance decreased by 50–70% compared to wildtype controls (Martre *et al.* 2002). In rice, a strong diurnal change in root hydraulic conductance which rises and falls early each day is also seen in the expression of PIP genes (Ishikawa-Sakurai *et al.* 2014). The transpirational pull of water through the xylem is a consequence of a gradient in water potential between leaves and roots. If transpiration exceeds the ability of resupply from the soil, then there is increased risk of hydraulic failure associated with embolisms forming in the xylem. PIP1s have been found to influence both the vulnerability to embolism as well as the capacity to repair embolism in poplar (Secchi & Zwieniecki 2014). Thus, there are multiple lines of evidence linking AQPs to the function of water transport in a plant.

In the leaf there are three places where AQPs are likely to play a significant role in the path of water movement (Fig. 2). As with roots, there are multiple solutions to how water moves through leaves (Zwieniecki *et al.* 2007). A barrier to apoplastic water movement exists at the bundle sheath surrounding the vein which restricts movement to the symplasm and requires transcellular flow for water to enter the mesophyll. AQPs surrounding leaf veins have been shown to influence leaf hydraulic conductance in *Arabidopsis* (Shatil-Cohen *et al.* 2011; Prado *et al.* 2013). As with roots, diurnal changes in leaf hydraulic conductivity are also correlated to changes in PIP expression in walnut (Cochard *et al.* 2007) and poplar (Lopez *et al.* 2013). Flow through the mesophyll can occur either via symplastic, apoplastic or a combination (transcellular) paths, and theoretical arguments have been made in support of apoplastic flow dominating the flow of water through the mesophyll (Buckley 2015). AQPs in the plasma membrane of mesophyll cells permit exchange of water between these two pools. When stomatal guard cells mature, their plasmodesmata cease to function (Willmer & Sexton 1979; Oparka & Roberts 2001) (Fig. 2). Consequently, the hydraulic flow necessary for stomata to open and close requires dynamic control over the permeability of the plasma membrane to water. The function of AQPs in stomata will be dealt with in more detail subsequently.

Using T-DNA insertion lines of *Arabidopsis*, both PIP1 and PIP2 AQPs were shown to influence the flux of water into leaves, although it was not possible to separate the contributions from root and shoot (Da Ines *et al.* 2010). Water leaving leaf veins needs to pass across the plasma membrane to get around the apoplastic barrier to flow at the bundle sheath. Evidence for this comes from plants with miRNA directed at PIP1s. Protoplasts from cells isolated from either the bundle sheath or mesophyll of leaves from constitutively expressed miRNA plants had reduced osmotic water permeability (Sade *et al.* 2014b). In addition, leaf hydraulic conductance was reduced by the miRNA construct. A second construct was made using the SCARECROW promoter to reduce PIP1 expression specifically within bundle sheath tissue. Intriguingly, this still reduced osmotic water permeability of both bundle sheath and mesophyll protoplasts. However, it is clear that AQPs are involved in the pathway of water movement through leaves.

SOME PLANT PIPS ARE CO_2 CHANNELS

The diffusion of CO_2 across biological membranes was thought to be non-limiting because of the high solubility of CO_2 in the lipid bilayer. It was surprising, therefore, that expression of human AQP1 together with carbonic anhydrase in *Xenopus* oocytes increased their permeability to CO_2 (Nakhoul *et al.* 1998). Terashima & Ono (2002) reasoned that if AQPs functioned as a CO_2 channel through the plasma membranes in leaf mesophyll cells, photosynthetic CO_2 uptake should be sensitive to inhibition by $HgCl_2$. Reductions in the rate of CO_2 assimilation at low intercellular CO_2 concentrations following the application of $HgCl_2$ were observed in both *Vicia faba* and *Phaseolus vulgaris*, and it was inferred from this that AQPs increase the permeability of mesophyll cells to CO_2. However, as $HgCl_2$ is a non-specific inhibitor, no precise explanation of these observations was possible. By expressing NtAQP1, a tobacco homologue to human AQP1, in *Xenopus* oocytes, the first demonstration of a plant AQP increasing permeability to CO_2 was made (Uehlein *et al.* 2003). It was argued that improved supply of CO_2 leads to increases in the rate of CO_2 assimilation and subsequent growth of tobacco plants with antisense suppression or overexpression of NtAQP1.

A debate developed over whether AQPs could indeed enhance membrane permeability to CO_2. Arguments in favour of AQPs increasing CO_2 permeability (Boron 2010) and arguments against (Missner *et al.* 2008b; Missner *et al.* 2008a; Missner & Pohl 2009) were clarified in a joint letter (Boron *et al.* 2011). A CO_2 permeable membrane would not benefit from the inclusion of AQPs. However, biological membranes in plants are protein rich which reduces the amount of lipid bilayer available for direct diffusion (Kaldenhoff 2012; Uehlein *et al.* 2012b; Kaldenhoff *et al.* 2014). They also have a high sterol content (Uemura *et al.* 1995) which reduces CO_2 permeability in artificial membranes (Hub & de Groot 2006; Ludewig & Dynowski 2009; Kai & Kaldenhoff 2014; Tsiavaliaris *et al.* 2015) and biological membranes (Itel *et al.* 2012). Both of these features suggest that plant plasma membranes may not be very permeable to CO_2, and therefore the inclusion of AQPs could have an impact on overall permeability (Endeward *et al.* 2014). There is sufficient functional evidence to justify showing AQPs enhancing CO_2 diffusion into mesophyll and stomatal guard cells (Fig. 2).

By comparison to the numerous examples of PIPs acting as water channels, demonstrations of PIPs enhancing membrane permeability to CO_2 are more limited. This is partly a reflection of the greater difficulty in assaying for CO_2 permeability. One assay method is to isolate membrane vesicles and introduce carbonic anhydrase and a pH sensitive fluorofor into them (Uehlein *et al.* 2008). The vesicles are then rapidly mixed into a new external solution saturated with CO_2. CO_2 diffusing into the vesicles is converted to bicarbonate by carbonic anhydrase

leading to internal acidification which is detected by a change in fluorescence. The derived permeability values appear much less than expected from calculations of mesophyll conductance for intact leaves (Evans *et al.* 2009). This may reflect the fact that the speed with which CO_2 equilibrates between a new external solution and that inside a vesicle is much faster than the mixing time of stopped flow devices. However, the observed pH change following mixing can be readily fitted with an exponential curve. Concerns about the limitations imposed by unstirred boundary layers (Missner *et al.* 2008b) have been countered (Endeward *et al.* 2014; Tsiavaliaris *et al.* 2015). Alternative methods to detect CO_2 permeability have utilized pH microelectrodes inserted into Xenopus oocytes (Nakhoul *et al.* 1998), scanning pH near the membrane surface (Uehlein *et al.* 2012b), expression in yeast cells and following intracellular acidification (Otto *et al.* 2010) or following the loss of ^{18}O labelled CO_2 from the bathing solution containing cells expressing AQPs and containing carbonic anhydrase (Itel *et al.* 2012). Methods for determining permeability currently have an upper limit around $0.1\,cm\,s^{-1}$ (Itel *et al.* 2012; Tsiavaliaris *et al.* 2015). As this is less than the permeability required to account for CO_2 assimilation rates (Evans *et al.* 2009), it is still a challenge to exactly relate functional performance in assays to that in leaves.

PIPs that have been demonstrated to enhance membrane permeability to CO_2 are shown in red in Table 1. Members of both PIP1 and PIP2 families appear capable of facilitating CO_2 diffusion, but not all are capable. Four cases are shown where expression of a PIP gene did not alter membrane permeability to CO_2. In each of these instances, the PIP had been shown to increase membrane permeability to water thus confirming that it was present as a functional protein in the plasma membrane of either the *Xenopus* oocyte or yeast cell. From the limited number of PIPs where function has been demonstrated unambiguously in *Xenopus* or yeast expression assays, three classes of functional type have been found: water only (PIP2s), CO_2 only (PIP1s) or both water and CO_2 (PIP1s and PIP2s). As already mentioned for water permeability, the expression system influences the function of a given PIP gene. In the case of *Arabidopsis*, the ability to enhance membrane CO_2 permeability when expressed in yeast cells (Heckwolf *et al.* 2011) was confirmed *in planta* (Uehlein *et al.* 2012b). However, for NtPIP2;1, no enhancement of CO_2 permeability was detected when expressed in yeast (Otto *et al.* 2010), and it was only evident when inserted into a CO_2 impermeable triblock copolymer membrane (Uehlein *et al.* 2012a).

Importantly, when NtAQP1 was expressed in yeast as linked hetero-tetramers with NtPIP2;1, enhancement of CO_2 permeability was most effective when all four of the monomers in the tetramers were NtAQP1 (Otto *et al.* 2010). By contrast, maximum water permeability was achieved with two NtPIP2;1 in a tetramer and increasing this to three or four did not lead to any further increase in permeability to water. These results lead to the suggestion that CO_2 may follow a different path than water through AQPs. Molecular dynamic simulation has identified that there are three possible routes for CO_2 to cross the tetrameric complex in a membrane (Wang *et al.* 2007) whereas water moves through the central pore of the monomer (Hub & de Groot 2006).

EXTENT OF AQUAPORIN INFLUENCE ON MESOPHYLL CONDUCTANCE

It is possible to infer changes to membrane permeability towards CO_2 in leaf mesophyll cells from measurements of mesophyll conductance, the ease with which CO_2 can diffuse between intercellular airspaces and mesophyll chloroplasts. Rice plants transformed with HvPIP2;1 driven by a cauliflower mosaic virus 35S promoter could be separated into two groups (Hanba *et al.* 2004). In one group, the insertion leads to overexpression of HvPIP2;1 (135%) which was associated with an increase in mesophyll conductance (40%) and increased mesophyll cell wall thickness. In the other group which arose from the same transformation event, transgenic co-suppression leads to a reduction of PIP2;1 (12–33%) and a decrease in mesophyll conductance (15–26%). The changes in mesophyll conductance in relation to the amount of HvPIP2;1 lend *in planta* support to the finding in *Xenopus* oocytes that these PIP proteins influence membrane permeability to CO_2 (Mori *et al.* 2014). A comparison between a wild type rice and *ospip1;1* rice mutant which knocked out *PIP1;1* but also reduced *PIP1;3*, *PIP2;1* and *PIP2;7* expression revealed that the mutation decreased stomatal (30%) and mesophyll (50%) conductances which reduced the CO_2 assimilation rate (Ding *et al.* 2016). This implies that OsPIP1;1 is also likely to alter membrane permeability to CO_2.

In tobacco, the expression of *NtAQP1* was varied by antisense reduction or overexpression to investigate its function *in planta* (Flexas *et al.* 2006). NtAQP1 content was reduced by 85% or increased two-fold which was associated with a 30% decrease or 34% increase, respectively, in mesophyll conductance in tobacco. When membranes were isolated from the RNAi plants, it was shown that the decrease in NtAQP1 reduced the CO_2 permeability of the chloroplast envelope but did not alter that of the plasma membrane (Uehlein *et al.* 2008). As was found with rice, expressing a foreign AQP gene in tobacco led to an increase in mesophyll conductance (Kawase *et al.* 2013). However, the expression of the PIP1 type AQP from *Mesembryanthemum crystallinum*, *McMIPB*, increased the rate of CO_2 assimilation by far more than could be expected from simply increasing access to CO_2. Even though the authors observed no change in Rubisco content, an increase in Rubisco activity of nearly 50% would be required to account for the observed increase in CO_2 assimilation rate.

For *A. thaliana*, it was found that knocking out *AtPIP1;2* reduced mesophyll conductance by 40% while knocking out *AtPIP2;3* did not alter mesophyll conductance relative to wildtype (Heckwolf *et al.* 2011). The reduction in mesophyll conductance increased the draw-down in CO_2 partial pressure from the intercellular airspaces to the sites of carboxylation ($C_i - C_c$) from 83 to 102 μbar. These results were consistent with the effects on CO_2 and water permeability they observed when the two genes were expressed in yeast. However, two other reports with *Arabidopsis* using miRNA suppression of PIPs or knockout and overexpression of *PIP1;4* are less clear.

PIP1s were suppressed to slightly different degrees in two lines using miRNA and reductions in mesophyll conductance of 10 and 20% were presented (Sade *et al.* 2014b). The veracity of these mesophyll conductance estimates seems unlikely as the mesophyll drawdown $C_i - C_c$ that can be calculated (200 μbar) is double that normally seen. In the other paper where *PIP1*;*4* was altered (Li *et al.* 2015b), the changes reported for CO_2 assimilation rate greatly exceed that expected from the reported change in mesophyll conductance. The results imply that a large increase or decrease in Rubisco activity accompanied the changes in mesophyll conductance. Another concern is apparent in the decline in mesophyll drawdown for the *Atpip1*;*4* plants from 64 to 43 μbar when it should have increased to 90 μbar.

When RNAi against *PIP1* was engineered into *Populus tremula* × *alba*, large reductions in *PIP1*;*1* and *PIP1*;*3* were observed with no change to *PIP2* genes (Secchi & Zwieniecki 2013). While mesophyll conductance was reported to have decreased by 50%, the mesophyll drawdown for the wild type can be calculated to be only 10 μbar. This is highly unlikely and means that the magnitude of the change in mesophyll conductance is probably very different. In another experiment with *Populus*, RNAi was used to reduce *PIP* expression (Bi *et al.* 2015). Although both lines had similar reductions in several PIP1 and PIP2 proteins, the phenotypes differed with mesophyll conductance increasing in one and not changing in the other compared to wild type controls. Despite this inconsistent pattern, the authors drew attention to the increase in mesophyll conductance.

Unfortunately, for several of the papers mentioned above implying causal links between changes in AQPs and mesophyll conductance, there are serious doubts. Mesophyll conductance is a complex trait that depends upon the surface area of chloroplasts adjacent to intercellular airspace per unit leaf area, cell wall thickness and membrane permeability (Evans *et al.* 2009). To assess what might be expected from altering PIP expression, we have modelled the effect of changing membrane permeability on photosynthetic characteristics by assuming that altered *PIP* expression only changes mesophyll conductance (Fig. 3). Two scenarios are illustrated where either stomatal conductance or intercellular CO_2 partial pressure is held constant as mesophyll conductance varies. For these curves, the normal leaf is assumed to have a Rubisco activity of 100 μmol m^{-2} s^{-1} and a mesophyll conductance of 0.3 mol m^{-2} s^{-1} bar^{-1} which results in a mesophyll drawdown of 72 μbar under ambient CO_2 conditions. Decreasing mesophyll conductance results in a reduction in CO_2 assimilation rate and an increase in mesophyll drawdown ($C_i - C_c$) or vice versa if mesophyll conductance increases (Fig. 3a,b). Data from three papers are added in Fig. 3b to illustrate when it is consistent with expectations (Hanba *et al.* 2004; Flexas *et al.* 2006) or when the mesophyll conductance information seems unreliable (Li *et al.* 2015b).

SHORT-TERM RESPONSES TO TEMPERATURE

Temperature directly affects the permeability of membranes. In the short term, this reflects the properties of the lipids and proteins that comprise the membrane. Over the longer term, the composition can be altered which can adjust the response of membrane permeability to temperature. The activation energy from the Arrhenius equation, E_a, is useful for describing how responsive membrane permeability is to a change in temperature. E_a values associated with diffusion through the lipid bilayer are high whereas those through AQPs are low and are similar to that associated with simply the viscosity of water. Consequently, the activation energy provides an indication of the relative influence of these two pathways (lipid bilayer and pores) to the overall diffusion across a membrane.

Additional information discriminating between pathways is obtained by assaying permeability in the presence or absence of transporter inhibitors. For red blood cells, permeability to water was greatly reduced by the inhibitor p-chloromercuribenzoate while concomitantly leading to an increase in E_a from 20 to 60 kJ mol^{-1} (Brahm 1982). When tonoplast membranes were compared against plasma membranes, it was found that tonoplast membranes were much more permeable to water and had much lower E_a than plasma membranes (10.5 versus 57 for tobacco, 23 versus 48 kJ mol^{-1} for wheat (Maurel *et al.* 1997; Niemietz & Tyerman 1997). Tonoplast membrane permeability could be inhibited by mercury indicating that AQPs normally contributed substantially to the overall flux of water across the membrane. By contrast, plasma membrane permeability was insensitive to mercury. However, in the case of plasma membranes isolated from wheat roots, a ratio of osmotic to diffusive permeability of 3 indicated that there must have been mercury insensitive AQPs still contributing to the flow of water (Niemietz & Tyerman 1997). Over-expression of *AtPIP1*;*4* or *AtPIP2*;*5* genes in Arabidopsis (Lee *et al.* 2012) and *PtdPIP2*;*5* in poplar (Ranganathan *et al.* 2016) dramatically reduced the E_a for root hydraulic conductivity without affecting the value at 20 °C. Sensitivity to mercury inhibition was also reduced for Arabidopsis over expressing these PIP genes (Lee *et al.* 2012), consistent with the properties of plasma membranes isolated from wheat roots.

AQPs can be switched in a gating mechanism that responds to divalent cations such as Ca^{2+} or low pH which reduces membrane permeability to water and subsequently increases E_a (Gerbeau *et al.* 2002; Tournaire-Roux *et al.* 2003). Gating complicates the interpretation of permeability assays because closure of AQPs during membrane isolation could lead to an underestimation of membrane permeability. It is also possible that gating changes with temperature which could confound the estimation of E_a, particularly in assays involving whole tissue rather than isolated membranes, such as root hydraulic conductivity.

There is limited experimental data available for the temperature response of membrane permeability to CO_2. For plasma membranes isolated from pea leaves, E_a varied between 32 and 36 kJ mol^{-1} in the presence of sufficient carbonic anhydrase to catalyse the detection system (carbonic anhydrase itself has an E_a of 51.5 kJ mol^{-1}) (Zhao *et al.* 2016). The addition of either silver sulfadiazine (a potent inhibitor of water permeability (Niemietz & Tyerman 2002) or 4,4′-diisothiocyano-2,2′-stilbenedisulfonic acid (which inhibits CO_2 permeability associated with human AQP1 (Endeward *et al.* 2006)) reduced

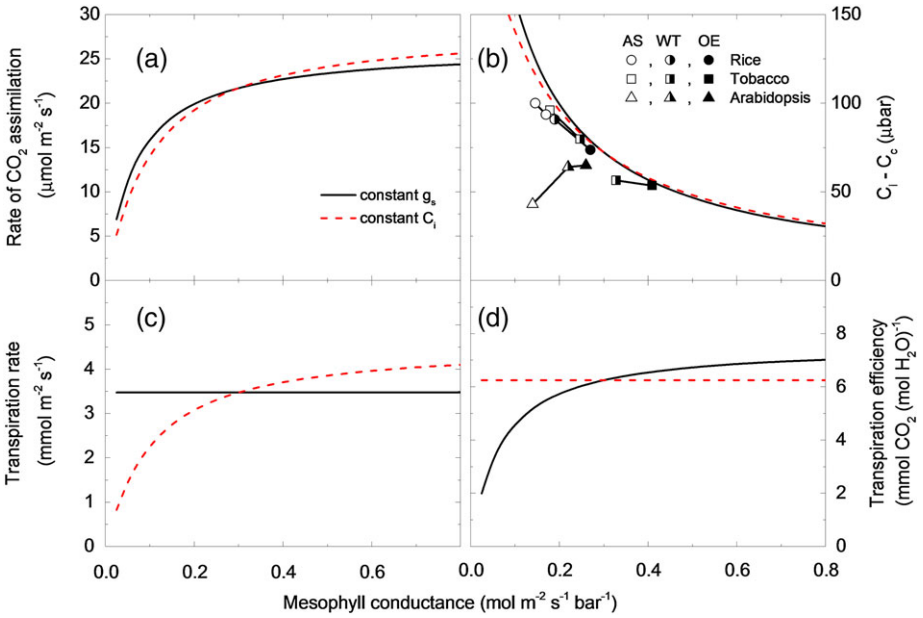

Figure 3. Impact of varying mesophyll conductance on CO_2 assimilation rate and transpiration efficiency. Two scenarios are modelled: constant stomatal conductance (0.3 mol H_2O m^{-2} s^{-1}, solid curves), or constant C_i (280 μbar, dashed red curves). (a) Rate of CO_2 assimilation, (b) drawdown in CO_2 partial pressure between the intercellular airspaces (C_i) and the sites of carboxylation in the chloroplast (C_c), (c) transpiration rate and (d) transpiration efficiency (rate of CO_2 assimilation/transpiration rate). Model curves assume Rubisco activity of 100 μmol m^{-2} s^{-1}, respiration rate 1 μmol m^{-2} s^{-1}, Γ* 35.5 μbar, K_{21} 550 μbar, leaf to air vapour pressure difference 12 mbar (von Caemmerer & Farquhar 1981; von Caemmerer *et al.* 1994). Shown in (b) are three examples where mesophyll conductance has been altered by antisense/knockout (AS) or overexpression (OE), respectively, of an aquaporin compared to their respective wild type (WT): rice (Hanba *et al.* 2004), tobacco (Flexas *et al.* 2006) and *Arabidopsis* (Li *et al.* 2015b). Mesophyll conductance (0.05 – 0.6 mol m^{-2} s^{-1} bar^{-1}) typically scales with photosynthetic capacity which results in similar CO_2 drawdowns across the mesophyll (C_i – C_c, typically between 50 and 150 μbar under high irradiance).

permeability to water but did not affect permeability to CO_2 of plasma membranes isolated from pea leaves.

The temperature response of mesophyll conductance to CO_2 in part reflects changing membrane permeability. When Bernacchi *et al.* (2002) observed a strong temperature dependence of mesophyll conductance, they suggested that as this did not conform to what was expected by simple diffusion, it was likely that an enzyme or protein-facilitated process was involved. Subsequently, a simple model for the temperature response was proposed which considered liquid diffusion and membrane permeability as the two components (Evans & von Caemmerer 2013). To account for variation in temperature responses of mesophyll conductance between species in the model, both the liquid path-length and activation energies had to be varied between species (E_a 36–76 kJ mol^{-1} (von Caemmerer & Evans 2015). However, because carbonic anhydrase facilitates CO_2 diffusion within mesophyll cells, it is also possible that the apparent E_a represents a combination of changes in membrane permeability and carbonic anhydrase activity. There is an obvious need to compare the temperature response of mesophyll conductance in a manner analogous to the inhibitor studies for water permeability. Because inhibitor specificity is problematic with intact plant tissue, a practical alternative would be to compare wildtype plants against plants where AQP expression had been either increased or reduced. A reduction in CO_2 permeable AQP contribution should increase the apparent activation energy of mesophyll conductance, whereas an increase in CO_2 permeable AQP activity should decrease the activation energy values.

ROLE OF CO_2 PERMEABLE AQUAPORINS IN C_4 PHOTOSYNTHESIS

Despite increasing research on CO_2 permeable AQPs in C_3 photosynthetic plants, their role in CO_2 diffusion in C_4 plants is largely unknown (von Caemmerer & Furbank 2016). Given the high rates of CO_2 fixation characteristic of the C_4 pathway, a large mesophyll conductance is needed to minimize the drawdown between intercellular airspaces and the cytosol of mesophyll cells where carbonic anhydrase catalyses the conversion of CO_2 into bicarbonate, the substrate for PEP carboxylase. Consequently, attention should be focussed on AQPs in the plasma membrane of mesophyll cells. The absence of Rubisco from mesophyll chloroplasts may mean that CO_2 permeable AQPs are not needed in the chloroplast envelope membranes. A comparison between the proteomes of chloroplast envelopes from bundle sheath and mesophyll chloroplasts in maize revealed only one AQP (Majeran *et al.* 2008). PIP2;4 was present in bundle sheath but not mesophyll chloroplasts, but as yet there is no evidence indicating whether ZmPIP2;4 enhances permeability to CO_2 and/or water. The specialized Kranz anatomy of C_4 plants, where mesophyll cells are tightly packed around bundle sheath cells, means that there is limited surface area available for direct CO_2 diffusion between intercellular airspace and bundle

sheath cells (von Caemmerer *et al.* 2007). However, a high permeability of the plasma membrane of bundle sheath cells would be undesirable as it could increase the escape of CO_2 from the bundle sheath and reduce the efficiency of the C_4 pump. Analysis of a leaf transcriptome comparison between two *Cleome* species with C_3 or C_4 photosynthesis revealed a 20-fold increase in the abundance of an mRNA coding for a PIP1;2 homolog in the C_4 plant (Braeutigam *et al.* 2011). A homolog of this gene in maize (ZmPIP1;2, Table 1) has been shown to increase water permeability (Fetter *et al.* 2004; Bienert *et al.* 2012) while its homolog in *Arabidopsis* (AtPIP1;2) increases permeability to CO_2 (Heckwolf *et al.* 2011). It remains to be shown whether this PIP increases permeability to CO_2 in C_4 species.

The number of PIPs in C_4 species is comparable to their C_3 counterparts (see Fig. 1): 14 PIPs in *Sorghum bicolor* (Reddy *et al.* 2015) and 13 PIPs in *Z. mays* (Chaumont *et al.* 2001). Within C_4 plants, only two PIPs (ZmPIP1;5 and ZmPIP1;6) have been identified as CO_2 permeable (Heinen *et al.* 2014). When co-expressed with a PIP2, both also conferred water permeability. Interestingly, these PIPs had significantly higher expression in the leaf epidermis suggesting a role in stomatal complexes (Heinen *et al.* 2014). A key area for future studies is identifying which PIPs are permeable to CO_2 in C_4 plants and examining their effects on mesophyll CO_2 conductance.

REGULATION OF AQUAPORIN EXPRESSION

AQPs have varied transcriptional regulation. Their expression has been shown to be tissue specific and strongly influenced by environmental factors including drought (Smart *et al.* 2001; Jang *et al.* 2004; Alexandersson *et al.* 2005; Alexandersson *et al.* 2010), salinity (Zhu *et al.* 2005; Qian *et al.* 2015), temperature (Lee *et al.* 2012; Ranganathan *et al.* 2016) and humidity (Laur & Hacke 2013) as well as diurnal (Moshelion *et al.* 2002; Lopez *et al.* 2003) and circadian clock (Harmer *et al.* 2000; Takase *et al.* 2011) regulation.

Expression studies have revealed developmental and tissue specific profiles of AQP abundance in leaves and roots. Changes in AQP abundance over leaf developmental gradients have been observed in maize (Hachez *et al.* 2008) and barley (Besse *et al.* 2011) with expression highest in the elongating zone of the leaf. Detailed cell specific localization of rice AQPs with different water transport activities implies that there are distinct roles for each AQP within the rice root (Sakurai *et al.* 2008; Grondin *et al.* 2016). The preferential expression profile of individual AQPs within the leaf or root organ may provide a clue towards their putative role. For instance in the *Arabidopsis* leaf, *AtPIP1;2* has high gene expression in mesophyll cells and has been shown to enhance membrane permeability to CO_2 (Heckwolf *et al.* 2011) whereas PIPs expressed solely in the leaf vasculature (e.g. *AtPIP2;1*, *AtPIP2;6*) are more likely to be involved in water permeability (Prado *et al.* 2013). AQPs may also have dual roles as several have been found to influence membrane permeability towards both water and CO_2 (Table 1). The actual role may also depend on the composition of heterotetramers (Otto *et al.* 2010; Berny *et al.* 2016).

In response to drought stress, plants close their stomata to reduce transpiration and down-regulate AQP gene expression. As a consequence of stomatal closure, intercellular CO_2 partial pressure (C_i) decreases which also reduces photosynthesis. Whilst the majority of PIPs are down-regulated during drought stress, certain PIP isoforms are up-regulated. This could increase mesophyll conductance to compensate for the declining availability of CO_2 in the intercellular airspaces. Interestingly, AtPIP1;4 which increases membrane CO_2 permeability (Li *et al.* 2015b), was one of only a few AQPs to be consistently up-regulated in drought stress experiments in *Arabidopsis* (Jang *et al.* 2004; Alexandersson *et al.* 2005; Alexandersson *et al.* 2010). Similarly, in tobacco, while the water permeable AQPs NtPIP1;1 and NtPIP2;1 were down-regulated in response to drought, the CO_2 permeable but weakly water permeable NtAQP1 was up-regulated (Mahdieh *et al.* 2008). In *Nicotiana plumbaginifolia*, ABA induced by drought or applied to a detached leaf decreased both stomata and mesophyll conductances but whether the mechanism(s) involved AQPs or carbonic anhydrase remains to be demonstrated (Mizokami *et al.* 2015).

Distinct AQP transcript responses to changes in CO_2 concentrations have been observed in tobacco leaves (Secchi *et al.* 2016). Growth in low atmospheric CO_2 concentrations increased the expression of the CO_2 permeable NtAQP1, whereas the water permeable NtPIP2;1 did not change. This fits with the argument that CO_2 permeable AQPs are up-regulated under drought in order to maintain photosynthetic rates when CO_2 becomes limiting because of stomatal closure. Because different PIP genes confer different functions, it could be possible to reduce water permeability in response to drought by down-regulating one gene while increasing CO_2 permeability by up-regulating another.

AQUAPORIN PROTEIN STRUCTURE AND TRAFFICKING

The AQP protein forms a helical bundle consisting of six membrane spanning domains (H1 to H6) connected by five loops (LA to LE). LA, LC and LE reside on the apoplastic side of the membrane, while LB and LD along with both terminal tails are exposed to the cytoplasm (Tornroth-Horsefield *et al.* 2006) (Fig. 4). LB and LE each form half helices that insert into the membrane and meet in the middle to form the pore. Situated at the meeting point are two highly conserved NPA domains that together with four residues located on the apoplastic sides of H2 (F81) and H5 (H210) and within LE (T, R) (referred to as the ar/R filter) govern to a large extent the substrate specificity of the pore.

AQP monomers form homo- and hetero-dimers and subsequently tetramers in the ER before being transported and integrated into the membrane. Subcellular trafficking of AQPs to their respective membranes is complex and represents another significant control over membrane permeability by controlling channel density within the membrane. Several recent reviews detail AQP trafficking in plants (Hachez *et al.* 2013; Luu & Maurel 2013; Chaumont & Tyerman 2014; Chevalier &

Chaumont 2015). Briefly, the majority of our understanding of AQP trafficking has been obtained by studying Arabidopsis and maize PIPs. Maize PIPs have a distinctive feature whereby ZmPIP2s can reach the plasma membrane when expressed alone while ZmPIP1s are retained in the ER and require hetero-oligomerization with ZmPIP2s to exit the ER. This distinction is observed both in plants and heterologous expression systems in oocytes and yeast (Fetter *et al.* 2004; Zelazny *et al.* 2007; Bienert *et al.* 2014). Similar relationships between PIP1s and PIP2s also occur in other species (Mahdieh *et al.* 2008; Mori *et al.* 2014; Yaneff *et al.* 2014; Jozefkowicz *et al.* 2016). However, this relationship is not absolute as some PIP1s appear capable of reaching the plasma membrane alone as determined directly by PIP fusions with fluorescent proteins or implicitly via increased membrane permeability when expressed in oocytes or yeast (Ding *et al.* 2004; Fitzpatrick & Reid 2009; Otto *et al.* 2010; Zhang *et al.* 2010; Heckwolf *et al.* 2011; Navarro-Rodenas *et al.* 2013; Sabir *et al.* 2014; Berny *et al.* 2016; Mosa *et al.* 2016).

Several Arabidopsis and maize PIP2 isoforms contain a so-called diacidic motif, more precisely a DxE configuration (X; underdetermined), in the N-terminal region which facilitates exiting from the ER into the secretory pathway (Zelazny *et al.* 2009; Sorieul *et al.* 2011). Additionally, a LxxxA motif in the third transmembrane domain, which is highly conserved among PIP2 proteins, also assists exit out of the ER and correct sorting in the Golgi (Chevalier *et al.* 2014). However, both motifs alone or in combination are incapable of translocating a ZmPIP1 to the plasma membrane, indicating the existence of other yet to be identified export or retention signals. More recently, a F220A mutation within the fifth transmembrane domain of ZmPIP1;2 was found to effectively increase ZmPIP1;2 localization to the membrane of oocytes and subsequently increase water permeability (Berny *et al.* 2016). Post-Golgi transport and insertion of PIPs into the plasma membrane involve SNARE (soluble *N*-ethylmaleimide-sensitive factor protein attachment protein receptor) proteins, which are well known vesicle traffickers in eukaryotes. Two SNARE proteins in SYNTAXIN OF PLANTS 121 and 67 (SYP121 and SYP67) have been shown to physically interact and ensure proper delivery of AtPIP2;7 and ZmPIP2;5 into the plasma membrane (Besserer *et al.* 2012; Hachez *et al.* 2014). It is speculated that different

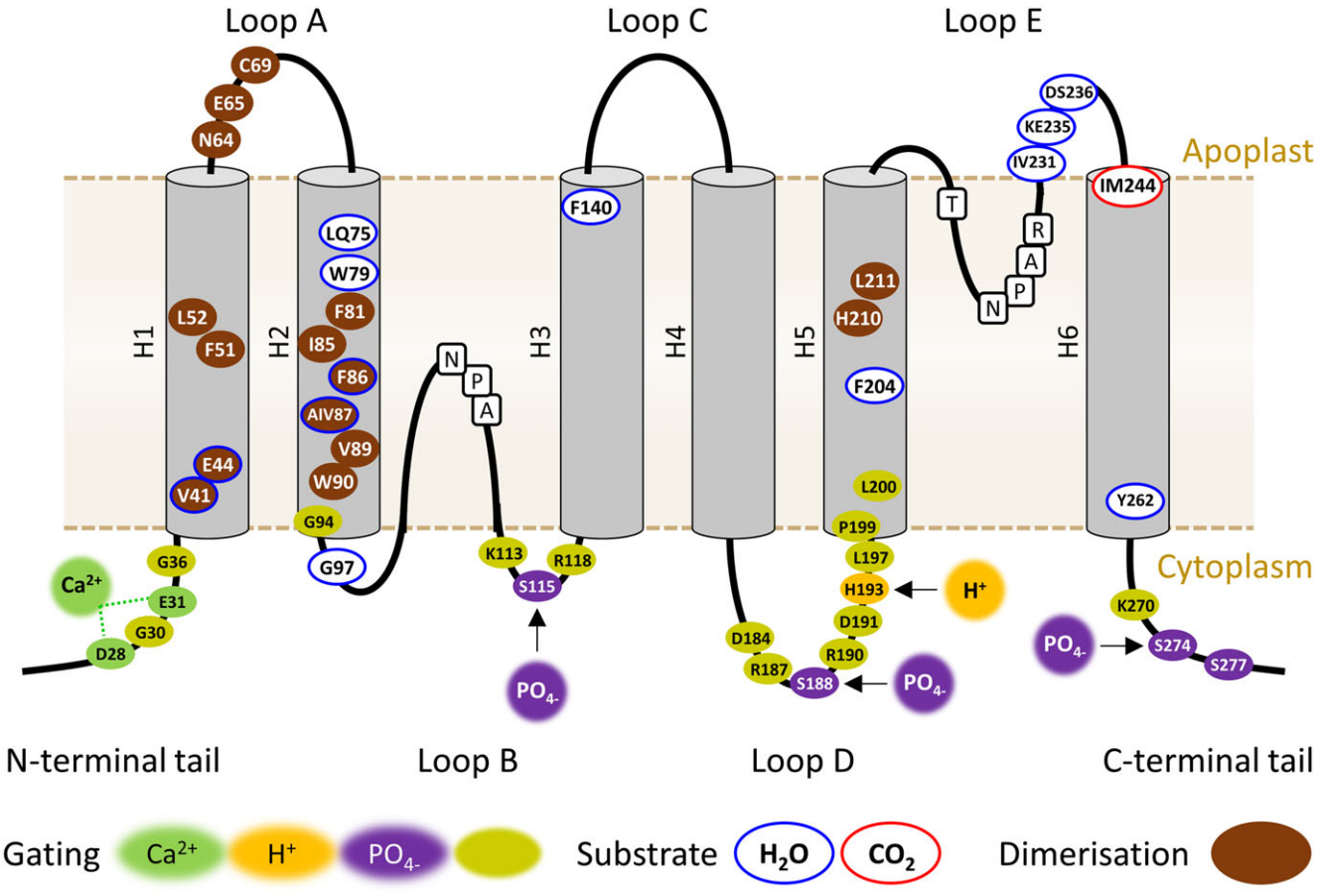

Figure 4. Diagram of a PIP aquaporin showing key amino acid residues involved in gating, substrate specificity and dimerization. Amino acids are numbered in reference to an alignment with SoPIP2;1; the numbering of the equivalent residues in the actual tested PIPs can be found in Supplementary Tables S1 and S2. Supplementary Tables S1 and S2 also provide summaries of the functional role of these residues. Further details of the interactions between residues involved in gating can be found in Supplementary Fig. 1. Dimerization of two monomers occurs through a disulphide bridge at C69 (Bienert *et al.* 2012) and other interactions associated with Loop A and the transmembrane helices (Jozefkowicz *et al.* 2013; Yoo *et al.* 2016). The mutation I244M at the end of helix 6 stops permeability to CO_2 without affecting permeability to water for HvPIP2;3 and HvPIP2;4 (Mori *et al.* 2014).

SNARE isoforms may control subcellular routing of PIPs and possibly more broadly AQPs at different stages of delivery to respective membranes (Hachez *et al.* 2013).

Once in the membrane, each AQP monomer of the tetramer complex constitutes an independent pore, the activity of which is determined by its amino acid composition, interactions with accompanying monomers, post-translational modification and interactions with signalling molecules and other proteins (detailed below). AQPs appear to be continually cycled in and out of membranes which may aid in maintaining a homogeneous distribution within the membranes. There are also PIPs and NIPs that are directionally distributed within the plasma membrane of leaf and root cells, but the mechanism and its physiological implication are unknown (Chevalier & Chaumont 2015). In addition to resting state cycling, AQPs can also be rapidly removed from their respective membranes in response to osmotic and salt stress subsequently reducing membrane water permeability (Boursiac *et al.* 2005; Dhonukshe *et al.* 2007; Li *et al.* 2011). This rapid response is partly governed by the phosphorylation status of the C-terminal tail (Prak *et al.* 2008).

GATING

Through conformational changes of the tertiary protein structure, membrane channels can switch between open and closed states (gating). Gating is a general mechanism of many types of membrane channels for controlling permeability (Verma *et al.* 2015b). Three-dimensional structures of about a dozen unique AQP proteins from species across the major phylogenetic kingdoms have facilitated our understanding of AQP gating (Gonen & Walz 2006; Sachdeva & Singh 2014; Kreida & Tornroth-Horsefield 2015; Verma *et al.* 2015a). Differences exist in the structural moieties and residue topology involved in gating between these divergent AQPs (Sachdeva & Singh 2014; Kreida & Tornroth-Horsefield 2015). Several resolved structures of spinach PIP2;1 (SoPIP2;1) in an open and closed state, phosphorylated mutant forms and at high and low pH (pH 6 versus pH8), together with molecular dynamic simulations have been instrumental in understanding plant AQP gating (Kukulski *et al.* 2005; Tornroth-Horsefield *et al.* 2006; Khandelia *et al.* 2009; Nyblom *et al.* 2009; Frick *et al.* 2013).

Inferred from these structural studies is that gating is in a dynamic equilibrium mediated through different combinations of interactions in response to changing environmental cues. The physical blockage of PIPs occurs through capping of the cytosolic entrance by loop D, causing insertion of a hydrophobic leucine residue into the channel entrance (L197, Fig. 4). Anchoring of loop D in a closed state is accomplished through interactions between residues of loop D and residues in the N-terminal tail, loop B, transmembrane helix 2 (H2) and C-terminal tail (Fig. 4; Supplementary Fig. S1). Disruption of these interactions displaces loop D resulting in removal of L197 and opening of the channel. Phosphorylation, divalent cations (Ca^{2+}) and cytosolic pH mediate the interactions between the open and closed positioning of loop D, and subsequently affect membrane permeability (Supplementary Fig. 1; Supplementary Table S1) (Johansson *et al.* 1998; Gerbeau *et al.* 2002; Tournaire-Roux *et al.* 2003; Fischer & Kaldenhoff 2008; Verdoucq *et al.* 2008; Nyblom *et al.* 2009; Di Pietro *et al.* 2013; Grondin *et al.* 2015). AQPs gate shut in response to elevated cytosolic Ca^{2+} concentrations and lower cytosolic pH. Such conditions are commonly observed under flooding stress, mechanical stimulation, pathogen attack and ROS accumulation (Tournaire-Roux *et al.* 2003; Monshausen & Gilroy 2009; Monshausen & Haswell 2013; Chaumont & Tyerman 2014). Ca^{2+} triggers pore closure by ligating to N28 and G30 inducing a series of interactions, involving loop B, that draws loop D into a closed configuration (Fig. 4; Supplementary Fig. S1). Low pH causes channel closure through protonation of H193. In the absence of a bound cation, the protonated H193 (denoted as $H193^+$) draws loop D into a closed state through interaction with loop B. In the presence of a bound cation, the repositioned N-terminal tail allows $H193^+$ to bind D28 (Supplementary Fig. S1). These networks of interactions are further governed by three cytoplasmically exposed serine residues that are targets for phosphorylation (S115, S188 and S274) (Hsu *et al.* 2009; Nyblom *et al.* 2009; Kline *et al.* 2010; Di Pietro *et al.* 2013). In an unphosphorylated state, such as drought conditions (Kline *et al.* 2010), these serine residues stabilize the closed loop D structure through interactions with the N-terminal tail (S115), within loop D (S188) and by creating a steric hindrance for the open loop position (S274) (Fig. 4; Supplementary Fig. S1). Phosphorylation, on the other hand (symbolized with $-PO_4$), swings loop D away from the channel entrance by repulsion forces that dislodge Ca^{2+} from E31 (S115-PO_4), promotes interactions between loop D and the C-terminal tail (S188-PO_4) and provides room for the open state repositioning of loop D (S274-PO_4).

Complementing the structural analysis is functional testing of AQP gating using mimetic mutations (Supplementary Table S1). Mimetic mutants do not necessarily exert the same level of effect as the modelled response (Nyblom *et al.* 2009) and can show variability between experiments. This could be because of discrepancies in the properties of the mimetic residues, inherent variation between expression systems or the fact that some components of the network exert an overriding influence over other components (e.g. $H193^+ > S\text{-}PO_4$ (Frick *et al.* 2013; Nyblom *et al.* 2009). Interestingly, the characteristics of pH gating are present in PIPs across the entire plant kingdom, whereas motifs associated with Ca^{2+} gating appear specific to land plants (Anderberg *et al.* 2011). The evolution of a more intricate gating mechanism likely reflects the need for greater control over hydraulic and other substrate transport in a terrestrial environment.

BEYOND GATING

Beyond gating, the analysis of APQ tertiary structures and mutagenic approaches has also identified residues mediating

channel activity. These have been summarized in Fig. 4 and Supplementary Table S2 (for consistency all references of residue positions are in accordance to SoPIP2;1 in Fig. 4; positioning of the equivalent residue within the actual tested AQPs are listed in Supplementary Table S2). Substitutions at some of these positions (W79, F86 and G97) cause a complete loss in channel activity in multiple PIP variants, indicating a core role in channel integrity. Others, such as position 87, are variable between PIP1s and PIP2s and contribute to the differences in water permeability between these groups in rice (Zhang *et al.* 2010). Loop E, which forms the apoplastic entrance half of the channel, has a number of important positions. In addition to the NPA motif and half of the ar/R filter, three other residues influence water transport activity (Suga & Maeshima 2004). Modelling of G228A mutations in loop E has predicted a potential doubling of water permeability. Although this was modelled with mammalian AQP1, G228 shows a high degree of conservation and the inference may be applicable to plant AQPs. So far at least one third of the residues in loop E have been identified as influencing permeability.

In addition to pore lining residues, the functional relevance of a number of transmembrane helix residues has recently been elucidated. Sequence conservation of 1500 MIPs across the major kingdoms has identified up to 40 positions within the transmembrane helices that show a high degree (avg. 92%) of conservation (Verma *et al.* 2015b). Two thirds of these positions are occupied by small and weakly polar residues that are speculated to facilitate condensed helical packing, allowing for a tight union between interacting transmembrane helices. Larger predominantly bulky hydrophobic residues have been identified, using alanine scanning combined with structure based modelling, as facilitating intra-monomer and inter-monomer interactions that establish and stabilize tetramer formation and subsequently functionality of the *Arabidopsis* PIP2;1 homo-tetramer (Yoo *et al.* 2016). Structural modelling combined with mutagenesis was used to identify residues important in water channel activity, subcellular localization, protein abundance and physical interaction between maize PIP1;2 and PIP2;5 (Berny *et al.* 2016). Interestingly, certain mutant forms can increase water activity in one monomer while hindering activity of the adjacent monomer. Together, these two reports extend on previous knowledge (Fetter *et al.* 2004; Otto *et al.* 2010; Bienert *et al.* 2012; Jozefkowicz *et al.* 2013; Heinen *et al.* 2014) of the importance and interplay of individual monomers to the collective functionality of the tetrameric complex. Beyond the transmembrane helices, residues in loop A are important in tetrameric organization. C69 of each monomer interacts to stabilize the tetramer (Kukulski *et al.* 2005; Bienert *et al.* 2012), while residues 64 and 65 are implicated in influencing interactions between PIP1 and PIP2 of *Beta vulgaris* (Jozefkowicz *et al.* 2013).

Most of these studies have examined effects on water permeability. Single amino acid substitutions (e.g. SoPIP2;1 positions G97W, S115A and H193K; Supplementary Tables S1 and S2) have been shown to block CO_2 and H_2O_2 in conjunction with water transport through PIPs (Shelden *et al.* 2009; Bienert *et al.* 2014; Wang *et al.* 2016). But these induce channel closure and are therefore general in effect. However, a single amino acid change has been found that confers different CO_2 permeability between HvPIP2;3 and HvPIP2;4 (Mori *et al.* 2014). Each of the six amino acids that differed between these two AQPs was mutated, but only the I to M switch at the apoplastic end of helix 6 affected CO_2 permeability (Fig. 4). Having I opposed to M conferred CO_2 permeability in both HvPIP2;3 and HvPIP2;4. However, both AQPs remained permeable to water regardless of which two amino acids were present.

INTERACTIONS WITH OTHER PROTEINS

Besides interactions amongst each other, AQPs also form protein–protein interactions with other protein types (reviewed in (Maurel *et al.* 2015; Sjohamn & Hedfalk 2014)). Many of these are involved in trafficking of AQPs to and from membranes (Chevalier & Chaumont 2015). But evidence is emerging of interactions that directly influence transport efficiency when membrane bound. AtPIP2;1 has been recently shown to interact with the carbonic anhydrase enzyme, βCA4, as part of a transport metabolon regulating stomatal closure in response to internal leaf CO_2 concentrations (Wang *et al.* 2016). Although not established, this interaction likely occurs via the cytoplasmic located C-terminal tail of AtPIP2;1, as has been shown for mammalian AQP1 and CARBONIC ANHYDRASE II (CAII) (Vilas *et al.* 2015). The C-terminal tail of AQPs appears a common site for interactions with non-AQP cytosolic partners (Masalkar *et al.* 2010; Sjohamn & Hedfalk 2014). Because CAs catalyse the conversion of CO_2 and water into bicarbonate and hydrogen ions, we can speculate that the coupling of AtPIP2;1 and βCA4 could enhance transport by depleting CO_2 and creating a concentration gradient immediately adjacent to the pore. A similar process is proposed to account for the enhanced water flux through mammalian AQP1 when associated with CAII (Vilas *et al.* 2015). CAII is also connected with the Rh CO_2 transporter as part of a CO_2 metabolon in the erythrocyte membrane (discussed in (Kustu & Inwood 2006)). CAII interacts and enhances the activity of numerous mammalian membrane transporters (Pushkin *et al.* 2004; Li *et al.* 2006; Becker & Deitmer 2007; Becker & Deitmer 2008; Becker *et al.* 2010; Krishnan *et al.* 2015), suggesting a need to further explore plant PIP–CA interactions in modulating both water and CO_2 transport. An analogous AQP involved metabolon occurs with the interaction between the ammonia transporter Nodulin 26 (a NIP AQP) and Glutamine Synthase, the catalytic substrate of which is ammonia (Masalkar *et al.* 2010).

Because AQPs span the membrane, interactions with non-AQP partners are not limited to cytosolic side. Recently, AtPIP1;4 has been reported to interact with the plant pathogen bacterial protein Harpin 1 (Hpa1) on the apoplastic side of the plasma membrane (Li *et al.* 2015b). This interaction was associated with enhancement in plant growth upon the exogenous treatment with Hpa1. The PM localized AtPIP1;4-Hpa1 interaction increases the activity of AtPIP1;4

in mediating transmembrane CO_2 transport and leaf photosynthesis. This result extends the biological role of AQP beyond simply transport and into sensing biotic signals (Li *et al.* 2015b).

AQUAPORINS AND STOMATAL FUNCTION

Stomata are the gatekeepers for water and CO_2 diffusing between the atmosphere and the inside of the leaf. Guard cells respond to many signals and can change the aperture of the pore by swelling and shrinking to open or close (Kim *et al.* 2010). Because mature guard cells have non-functional plasmodesmata (Oparka & Roberts 2001), the flux of water into and out of guard cells depends upon AQPs. Detailed analysis of the expression pattern for AQP genes has been made for maize guard cells (Heinen *et al.* 2014). Each of the six genes for PIP1 and PIP2 was expressed with PIP1;1 (66% of total PIP transcripts) and PIP1;3 (12%) being the most abundant. Five PIPs (PIP1;4 and PIP2;3–6) were in low abundance. Expression of all of the abundant PIP genes was found to show strong diurnal variation. ZmPIP1;5 and ZmPIP1;6 which each represented about 2.5% of the total PIP expression, were shown to enhance water and CO_2 permeability when expressed in *Xenopus* oocytes or yeast, respectively.

Two recent discoveries have revealed how AQPs fit into the stomatal signalling response pathway network. For *Arabidopsis* plants lacking AtPIP2;1, ABA is unable to trigger stomatal closure. This pathway involves Open Stomata 1 protein kinase which has been shown to phosphorylate AtPIP2;1 at S121 (S115 in Fig. 4) which increases membrane permeability to water (Grondin *et al.* 2015). AtPIP2;1 has also been shown to increase CO_2 permeability of *Xenopus* oocytes and interacts with the carbonic anhydrase βCA4 (Wang *et al.* 2016). Four independent methods were used to demonstrate interactions between βCA4 and AtPIP2;1 in plasma membranes. When co-expressed with a βCA4, a slow anion channel (SLAC1) and a Ca^{2+}-dependent protein kinase (CPK6 or CPK23), AtPIP2;1 conferred CO_2 sensitivity to SLAC anion channel activity. Introducing a single point mutation G103W disrupted the ability of AtPIP2;1 to increase CO_2 permeability (Wang *et al.* 2016). Thus, the presence of AtPIP2;1 in the plasma membrane of guard cells enables the sensing of external CO_2 and this or ABA can trigger phosphorylation at S121 which enhances permeability to water in association with SLAC1 activity to drive stomatal closure.

ENGINEERING AQUAPORINS TO IMPROVE PLANT PERFORMANCE

Abiotic stress, such as drought, salinity and extreme temperature, can reduce the average yield of major crops by more than 50% (Wang *et al.* 2003). The dynamic nature of AQPs means that they can adjust their transcript level in response to drought and other abiotic stresses (Alexandersson *et al.* 2005; Moshelion *et al.* 2015). Their role in response to different environmental stresses has been reviewed comprehensively by Afzal *et al.* (2016). Here we have summarized research which has modified AQP expression with the aim of engineering plants with improved growth and tolerance to different abiotic stresses (Table 3).

Depending on the desired outcome, some researchers have selected an AQP from a species which is naturally tolerant to a given stress and transferred it to another species. For instance, AcPIP2 (Li *et al.* 2015b) from the saltbush *Atriplex canescens* was used for salt tolerance and FaPIP2;1 (Zhuang *et al.* 2015) from the grass *Festuca arundinacea* and JcPIP2;7 or JcTIP1;3 from *Jatropha curcas* (Khan *et al.* 2015) were used for drought tolerance. Others have used an AQP with a known permeability function to engineer an improved plant. Overexpression of *NtAQP1* has resulted in enhanced plant performance under normal as well as salt stress conditions in a range of plants including *Arabidopsis* (Sade *et al.* 2014a), tomato (Sade *et al.* 2010; Kelly *et al.* 2014) and tobacco (Uehlein *et al.* 2003). Specifically, increases in biomass and yield, photosynthetic rate, mesophyll and stomatal conductance and root hydraulic conductivity have been observed when NtAQP1 expression was manipulated.

Significant improvements in plant growth in banana have been found when overexpressing either the native *MusaPIP1;2* or *MusaPIP2;6* over a range of stress conditions including drought, salt and cold treatment (Sreedharan *et al.* 2013; Sreedharan *et al.* 2015). Overexpression of endogenous AQP genes has also been shown to improve plant growth in a range of species including *SlTIP2;2* in *Solanum lycopersicum* under drought and salt stress (Sade *et al.* 2009) and improved tolerance to boron when the native *AtTIP5;1* was overexpressed in *Arabidopsis* (Pang *et al.* 2010). Benefits to plant performance also extend to improved immunity with a recent report showing that overexpression of *AtPIP1;4* enhances resistance of Arabidopsis to infection by the biotrophic bacterial pathogen, *Pseudomonas syringae* (Tian *et al.* 2016). However, broad improvement to stress tolerance is uncommon and generally increasing expression of one AQP to improve tolerance to one stress has a detrimental effect under a different stress. This is the case for a range of *Arabidopsis* PIPs where overexpression has resulted in improved growth under normal conditions (Aharon *et al.* 2003) or cold stress (Jang *et al.* 2007) but increased the plant's susceptibility to drought.

Engineering better plants by modifying AQP expression is a complex and difficult task but expression can be made tissue specific (Sade *et al.* 2014a). Monomer function and trafficking could also be modified depending on the heterodimerization with different PIPs (Fetter *et al.* 2004; Berny *et al.* 2016). If mesophyll conductance could be increased, there is potential to improve both photosynthetic rate and transpiration efficiency (Fig. 3). The improvement in transpiration efficiency would depend on feedback controls in the leaf that could either keep stomatal conductance constant (which would mean transpiration efficiency would increase as mesophyll conductance increased), or intercellular CO_2 partial pressure constant (there would be no change in transpiration efficiency). Stomatal guard cell functioning could also be targeted to alter sensitivity to ABA or CO_2, or influence the time constant for changing aperture. Any of these would impact on transpiration and transpiration efficiency.

Table 3. Summary of aquaporins that have been used in attempts to engineer plants with improved responses to different abiotic conditions including drought, salt or cold stress and tolerance when exposed to heavy metals or pathogen infection. Symbols represent improved growth (✓), no difference to WT (=) or negative effects on growth (X)

			Condition					
Gene	Promoter	Host	Normal	Drought	Salt	Cold	Other	Reference
AcNIP5;1	35S	Arabidopsis		✓	X			(Yu *et al.* 2015)
AcPIP2	35S	Arabidopsis	✓	X	✓			(Li *et al.* 2015a)
AtPIP1;2	35S	Tobacco	✓	X	=			(Aharon *et al.* 2003)
AtPIP1;4	35S	Tobacco		X		✓		(Jang *et al.* 2007)
AtPIP1;4	35S	Arabidopsis	✓	X		=	✓Bacterial infection	(Jang *et al.* 2007; Li *et al.* 2015b; Tian *et al.* 2016)
AtPIP2;5	35S	Tobacco		X		✓		(Jang *et al.* 2007)
AtPIP2;5	35S	Arabidopsis		X		=		(Jang *et al.* 2007)
AtTIP5;1	35S	Arabidopsis					✓Boron	(Pang *et al.* 2010)
BjPIP1	35S	Tobacco		✓			✓Cadmium	(Zhang *et al.* 2008)
BnPIP1	35S	Tobacco		✓				(Yu *et al.* 2005)
FaPIP2;1		Arabidopsis		✓				(Zhuang *et al.* 2015)
GmPIP1;6	35S	Tobacco	=		✓			(Zhou *et al.* 2014)
HvPIP2;1	35S	Rice	✓					(Hanba *et al.* 2004)
HvPIP2;1	35S	Rice			X			(Katsuhara *et al.* 2003)
JcPIP2;7	35S	Arabidopsis	=	✓	✓			(Khan *et al.* 2015)
JcTIP1;3	35S	Arabidopsis	=	✓	✓			(Khan *et al.* 2015)
MaPIP1;1	35S	Arabidopsis		✓	✓			(Xu *et al.* 2014)
McMIPB	35S	Tobacco	✓					(Kawase *et al.* 2013)
MusaPIP1;2	Ubiquitin	Banana		✓	✓	✓		(Sreedharan *et al.* 2013)
MusaPIP2;6	Ubiquitin	Tobacco	=		✓			(Sreedharan *et al.* 2015)
NtAQP1	35S	Arabidopsis	✓		✓			(Sade *et al.* 2010; Sade *et al.* 2014a)
NtAQP1	35S	Tomato	✓					(Kelly *et al.* 2014)
NtAQP1	35S	Tomato	✓		✓			(Sade *et al.* 2010)
NtAQP1	35S	Tobacco	✓					(Uehlein *et al.* 2003)
OsPIP1;1/2;2	35S	Arabidopsis	=		✓			(Guo *et al.* 2006)
OsPIP2;4/2;6/2;7	actin2	Arabidopsis					✓Arsenic	(Mosa *et al.* 2012)
PgTIP1	35S	Arabidopsis	✓	✓	✓	X		(Peng *et al.* 2007)
PtdPIP2;5	Ubiquitin	Poplar	=			✓		(Ranganathan *et al.* 2016)
RsPIP2;1	35S	Eucalyptus	✓		=			(Tsuchihira *et al.* 2010)
SlTIP2;2	EVO205	Tomato		✓	✓			(Sade *et al.* 2009)
SpAQP1	35S	Tobacco	=		✓			(Chang *et al.* 2016)
TaAQP7	35S	Tobacco		✓				(Zhou *et al.* 2012)
TaAQP7	35S	Tobacco				✓		(Huang *et al.* 2014)
TaAQP8	35S	Tobacco			✓			(Hu *et al.* 2012)
TaNIP	35S	Arabidopsis			✓			(Gao *et al.* 2010)
TdPIP1;1/2;1	35S	Tobacco	✓		✓			(Ayadi *et al.* 2011)
TsTIP1;2	35S	Arabidopsis		✓	✓			(Wang *et al.* 2014)
VfPIP1	35S	Arabidopsis		✓				(Cui *et al.* 2008)

CONCLUSIONS

PIP AQP diversity exists at many levels, and the functional roles of many of the PIP genes still remain to be demonstrated. There are more PIP genes known to affect membrane permeability to water than CO_2, and this limits our ability to identify amino acids that confer substrate specificity. The dynamic changes in gene expression and abundance of tetramers in the plasma membrane, together with the rapid regulation through gating, provide plant cells with highly responsive mechanisms to control the flux of water into cells and through the plant. Despite the challenge of assaying for CO_2 permeability, there is a need to characterize many more of the PIP genes for their effect on CO_2 permeability, particularly in C_4 species. Functional screens should also look at other substrates to enhance the possibility of revealing key motifs. There is also a need to consider what other molecules interact with the PIP AQPs as they are ideally placed to act as sensors. How plants gain and use both water and CO_2 is crucial for plant productivity and growth under stressful conditions, so AQPs are sensible targets when trying to increase our mechanistic understanding or seeking ways to improve plants.

ACKNOWLEDGEMENTS

We thank the Australian Research Council for the financial support to the Centre of Excellence for Translational Photosynthesis CE140100015.

REFERENCES

Abascal F., Irisarri I. & Zardoya R. (2014) Diversity and evolution of membrane intrinsic proteins. *Biochimica Et Biophysica Acta-General Subjects* **1840**, 1468–1481.

Afzal Z., Howton T., Sun Y. & Mukhtar M. (2016) The roles of aquaporins in plant stress responses. *Journal of Developmental Biology* **4**, 9.

Agre P., Sasaki S. & Chrispeels M.J. (1993) Aquaporins: a family of water channel proteins. *American Journal of Physiology* **F461**.

Aharon R., Shahak Y., Wininger S., Bendov R., Kapulnik Y. & Galili G. (2003) Overexpression of a plasma membrane aquaporin in transgenic tobacco improves plant vigor under favorable growth conditions but not under drought or salt stress. *Plant Cell* **15**, 439–447.

Alexandersson E., Danielson J.A., Rade J., Moparthi V.K., Fontes M., Kjellbom P. & Johanson U. (2010) Transcriptional regulation of aquaporins in accessions of Arabidopsis in response to drought stress. *Plant Journal* **61**, 650–660.

Alexandersson E., Fraysse L., Sjovall-Larsen S., Gustavsson S., Fellert M., Karlsson M., Johanson U. & Kjellbom P. (2005) Whole gene family expression and drought stress regulation of aquaporins. *Plant Molecular Biology* **59**, 469–484.

Alleva K., Marquez M., Villarreal N., Mut P., Bustamante C., Bellati J., … Amodeo G. (2010) Cloning, functional characterization, and co-expression studies of a novel aquaporin (FaPIP2;1) of strawberry fruit. *Journal of Experimental Botany* **61**, 3935–3945.

An F., Zou Z., Cai X.Q., Wang J., Rookes J., Lin W.F., … Kong L. (2015) Regulation of HbPIP2;3, a latex-abundant water transporter, is associated with latex dilution and yield in the rubber tree (*Hevea brasiliensis* Muell. Arg.). *Plos One* **10**, e0125595.

Anderberg H.I., Danielson J.A. & Johanson U. (2011) Algal MIPs, high diversity and conserved motifs. *BMC Evolutionary Biology* **11**, 110.

Anderberg H.I., Kjellbom P. & Johanson U. (2012) Annotation of *Selaginella moellendorffi* major intrinsic proteins and the evolution of the protein family in terrestrial plants. *Frontiers in Plant Science* **3**, 33.

Ariani A. & Gepts P. (2015) Genome-wide identification and characterization of aquaporin gene family in common bean (*Phaseolus vulgaris* L.). *Molecular Genetics and Genomics* **290**, 1771–1785.

Ayadi M., Cavez D., Miled N., Chaumont F. & Masmoudi K. (2011) Identification and characterization of two plasma membrane aquaporins in durum wheat (*Triticum turgidum* L. subsp. durum) and their role in abiotic stress tolerance. *Plant Physiology and Biochemistry* **49**, 1029–1039.

Azad A.K., Katsuhara M., Sawa Y., Ishikawa T. & Shibata H. (2008) Characterization of four plasma membrane aquaporins in tulip petals: a putative homolog is regulated by phosphorylation. *Plant and Cell Physiology* **49**, 1196–1208.

Becker H.M. & Deitmer J.W. (2007) Carbonic anhydrase II increases the activity of the human electrogenic Na+/HCO_3^- cotransporter. *Journal of Biological Chemistry* **282**, 13508–13521.

Becker H.M. & Deitmer J.W. (2008) Nonenzymatic proton handling by carbonic anhydrase II during H + -lactate cotransport via monocarboxylate transporter 1. *Journal of Biological Chemistry* **283**, 21655–21667.

Becker H.M., Klier M. & Deitmer J.W. (2010) Nonenzymatic augmentation of lactate transport via monocarboxylate transporter isoform 4 by carbonic anhydrase II. *Journal of Membrane Biology* **234**, 125–135.

Beebo A., Mathai J.C., Schoefs B. & Spetea C. (2013) Assessment of the requirement for aquaporins in the thylakoid membrane of plant chloroplasts to sustain photosynthetic water oxidation. *FEBS Letters* **587**, 2083–2089.

Beerling D.J. (2005) Leaf evolution: gases, genes and geochemistry. *Annals of Botany* **96**, 345–352.

Bellati J., Alleva K., Soto G., Vitali V., Jozefkowicz C. & Amodeo G. (2010) Intracellular pH sensing is altered by plasma membrane PIP aquaporin co-expression. *Plant Molecular Biology* **74**, 105–118.

Bernacchi C.J., Portis A.R., Nakano H., von Caemmerer S. & Long S.P. (2002) Temperature response of mesophyll conductance. Implications for the determination of Rubisco enzyme kinetics and for limitations to photosynthesis in vivo. *Plant Physiology* **130**, 1992–1998.

Berny M.C., Gilis D., Rooman M. & Chaumont F. (2016) Single mutations in the transmembrane domains of maize plasma membrane aquaporins affect the activity of the monomers within a heterotetramer. *Molecular Plant* **9**, 986–1003.

Besse M., Knipfer T., Miller A.J., Verdeil J.L., Jahn T.P. & Fricke W. (2011) Developmental pattern of aquaporin expression in barley (*Hordeum vulgare* L.) leaves. *Journal of Experimental Botany* **62**, 4127–4142.

Besserer A., Burnotte E., Bienert G.P., Chevalier A.S., Errachid A., Grefen C., … Chaumont F. (2012) Selective regulation of maize plasma membrane aquaporin trafficking and activity by the SNARE SYP121. *Plant Cell* **24**, 3463–3481.

Bi Z., Merl-Pham J., Uehlein N., Zimmer I., Muehlhans S., Aichler M., … Block K. (2015) RNAi-mediated downregulation of poplar plasma membrane intrinsic proteins (PIPs) changes plasma membrane proteome composition and affects leaf physiology. *Journal of Proteomics* **128**, 321–332.

Biela A., Grote K., Otto B., Hoth S., Hedrich R. & Kaldenhoff R. (1999) The *Nicotiana tabacum* plasma membrane aquaporin NtAQP1 is mercury-insensitive and permeable for glycerol. *Plant Journal* **18**, 565–570.

Bienert G.P., Bienert M.D., Jahn T.P., Boutry M. & Chaumont F. (2011) Solanaceae XIPs are plasma membrane aquaporins that facilitate the transport of many uncharged substrates. *Plant Journal* **66**, 306–317.

Bienert G.P., Cavez D., Besserer A., Berny M.C., Gilis D., Rooman M. & Chaumont F. (2012) A conserved cysteine residue is involved in disulfide bond formation between plant plasma membrane aquaporin monomers. *Biochemical Journal* **445**, 101–111.

Bienert G.P., Heinen R.B., Berny M.C. & Chaumont F. (2014) Maize plasma membrane aquaporin ZmPIP2;5, but not ZmPIP1;2, facilitates transmembrane diffusion of hydrogen peroxide. *Biochimica et Biophysica Acta* **1838**, 216–222.

Bienert G.P., Moller A.L., Kristiansen K.A., Schulz A., Moller I.M., Schjoerring J. K. & Jahn T.P. (2007) Specific aquaporins facilitate the diffusion of hydrogen peroxide across membranes. *Journal of Biological Chemistry* **282**, 1183–1192.

Boron W.F. (2010) Sharpey–Schafer lecture: gas channels. *Experimental Physiology* **95**, 1107–1130.

Boron W.F., Endeward V., Gros G., Musa-Aziz R. & Pohl P. (2011) Intrinsic CO_2 permeability of cell membranes and potential biological relevance of CO_2 channels. *Chemphyschem* **12**, 1017–1019.

Bots M., Feron R., Uehlein N., Weterings K., Kaldenhoff R. & Mariani T. (2005) PIP1 and PIP2 aquaporins are differentially expressed during tobacco anther and stigma development. *Journal of Experimental Botany* **56**, 113–121.

Boursiac Y., Chen S., Luu D.T., Sorieul M., van den Dries N. & Maurel C. (2005) Early effects of salinity on water transport in Arabidopsis roots. Molecular and cellular features of aquaporin expression. *Plant Physiology* **139**, 790–805.

Braeutigam A., Kajala K., Wullenweber J., Sommer M., Gagneul D., Weber K.L., … Weber A.P.M. (2011) An mRNA blueprint for C_4 photosynthesis derived from comparative transcriptomics of closely related C_3 and C_4 species. *Plant Physiology* **155**, 142–156.

Brahm J. (1982) Diffusional water permeability of human-erythrocytes and their ghosts. *Journal of General Physiology* **79**, 791–819.

Bramley H., Turner N.C., Turner D.W. & Tyerman S.D. (2009) Roles of morphology, anatomy, and aquaporins in determining contrasting hydraulic behavior of roots. *Plant Physiology* **150**, 348–364.

Buckley T.N. (2015) The contributions of apoplastic, symplastic and gas phase pathways for water transport outside the bundle sheath in leaves. *Plant, Cell and Environment* **38**, 7–22.

Canny M.J. (1988) Water pathways in wheat leaves. 4. The interpretation of images of a fluorescent apoplastic tracer. *Australian Journal of Plant Physiology* **15**, 541–555.

Canny M.J. (1995) Apoplastic water and solute movement – new rules for an old space. *Annual Review of Plant Physiology and Plant Molecular Biology* **46**, 215–236.

Chang W., Liu X., Zhu J., Fan W. & Zhang Z. (2016) An aquaporin gene from halophyte *Sesuvium portulacastrum*, SpAQP1, increases salt tolerance in transgenic tobacco. *Plant Cell Reports* **35**, 385–395.

Chaumont F., Barrieu F., Jung R. & Chrispeels M.J. (2000) Plasma membrane intrinsic proteins from maize cluster in two sequence subgroups with differential aquaporin activity. *Plant Physiology* **122**, 1025–1034.

Chaumont F., Barrieu F., Wojcik E., Chrispeels M.J. & Jung R. (2001) Aquaporins constitute a large and highly divergent protein family in maize. *Plant Physiology* **125**, 1206–1215.

Chaumont F. & Tyerman S.D. (2014) Aquaporins: highly regulated channels controlling plant water relations. *Plant Physiology* **164**, 1600–1618.

Chen W., Yin X., Wang L., Tian J., Yang R., Liu D., … Gao J. (2013) Involvement of rose aquaporin RhPIP1;1 in ethylene-regulated petal expansion through interaction with RhPIP2;1. *Plant Molecular Biology* **83**, 219–233.

Chevalier A.S., Bienert G.P. & Chaumont F. (2014) A new LxxxA motif in the transmembrane Helix3 of maize aquaporins belonging to the plasma membrane intrinsic protein PIP2 group is required for their trafficking to the plasma membrane. *Plant Physiology* **166**, 125–138.

Chevalier A.S. & Chaumont F. (2015) Trafficking of plant plasma membrane aquaporins: multiple regulation levels and complex sorting signals. *Plant and Cell Physiology* **56**, 819–829.

Clarkson D.T., Carvajal M., Henzler T., Waterhouse R.N., Smyth A.J., Cooke D. T. & Steudle E. (2000) Root hydraulic conductance: diurnal aquaporin expression and the effects of nutrient stress. *Journal of Experimental Botany* **51**, 61–70.

Cochard H., Venisse J.S., Barigah T.S., Brunel N., Herbette S., Guilliot A., … Sakr S. (2007) Putative role of aquaporins in variable hydraulic conductance of leaves in response to light. *Plant Physiology* **143**, 122–133.

Cohen D., Bogeat-Triboulot M.B., Vialet-Chabrand S., Merret R., Courty P.E., Moretti S., … Hummel I. (2013) Developmental and environmental regulation of Aquaporin gene expression across Populus species: divergence or redundancy? *PLoS One* **8**e55506.

Cui X.-H., Hao F.-S., Chen H., Chen J. & Wang X.-C. (2008) Expression of the *Vicia faba* VfPIP1 gene in *Arabidopsis thaliana* plants improves their drought resistance. *Journal of Plant Research* **121**, 207–214.

Da Ines O., Graf W., Franck K.I., Albert A., Winkler J.B., Scherb H., … Schaffner A.R. (2010) Kinetic analyses of plant water relocation using deuterium as tracer – reduced water flux of Arabidopsis pip2 aquaporin knockout mutants. *Plant Biology* **12**, 129–139.

Daniels M.J., Mirkov T.E. & Chrispeels M.J. (1994) The plasma-membrane of *Arabidopsis thaliana* contains a mercury-insensitive aquaporin that is a homolog of the tonoplast water channel protein TIP. *Plant Physiology* **106**, 1325–1333.

Danielson J.A. & Johanson U. (2008) Unexpected complexity of the aquaporin gene family in the moss *Physcomitrella patens*. *BMC Plant Biology* **8**, 45.

Dhonukshe P., Aniento F., Hwang I., Robinson D.G., Mravec J., Stierhof Y.D. & Friml J. (2007) Clathrin-mediated constitutive endocytosis of PIN auxin efflux carriers in Arabidopsis. *Current Biology* **17**, 520–527.

Di Pietro M., Vialaret J., Li G.-W., Hem S., Prado K., Rossignol M., … Santoni V. (2013) Coordinated post-translational responses of aquaporins to abiotic and nutritional stimuli in Arabidopsis roots. *Molecular & Cellular Proteomics* **12**, 3886–3897.

Diehn T.A., Pommerrenig B., Bernhardt N., Hartmann A. & Bienert G.P. (2015) Genome-wide identification of aquaporin encoding genes in *Brassica oleracea* and their phylogenetic sequence comparison to Brassica crops and Arabidopsis. *Frontiers in Plant Science* **6**, 166.

Ding L., Gao L., Liu W., Wang M., Gu M., Ren B., … Guo S. (2016) Aquaporin plays an important role in mediating chloroplastic CO_2 concentration under high-N supply in rice (*Oryza sativa*) plants. *Physiologia Plantarum* **156**, 215–226.

Ding X., Iwasaki I. & Kitagawa Y. (2004) Overexpression of a lily PIP1 gene in tobacco increased the osmotic water permeability of leaf cells. *Plant, Cell and Environment* **27**, 177–186.

Ding X., Matsumoto T., Gena P., Liu C., Pellegrini-Calace M., Zhong S., … Calamita G. (2013) Water and CO_2 permeability of SsAqpZ, the cyanobacterium Synechococcus sp PCC7942 aquaporin. *Biology of the Cell* **105**, 118–128.

Dynowski M., Mayer M., Moran O. & Ludewig U. (2008) Molecular determinants of ammonia and urea conductance in plant aquaporin homologs. *FEBS Letters* **582**, 2458–2462.

Endeward V., Al-Samir S., Itel F. & Gros G. (2014) How does carbon dioxide permeate cell membranes? A discussion of concepts, results and methods. *Frontiers in Physiology* **4**, 382.

Endeward V., Musa-Aziz R., Cooper G.J., Chen L.-M., Pelletier M.F., Virkki L. V., … Gros G. (2006) Evidence that aquaporin 1 is a major pathway for CO_2 transport across the human erythrocyte membrane. *FASEB Journal* **20**, 1974–1981.

Evans J.R., Kaldenhoff R., Genty B. & Terashima I. (2009) Resistances along the CO_2 diffusion pathway inside leaves. *Journal of Experimental Botany* **60**, 2235–2248.

Evans J.R. & von Caemmerer S. (2013) Temperature response of carbon isotope discrimination and mesophyll conductance in tobacco. *Plant, Cell and Environment* **36**, 745–756.

Ferro M., Brugière S., Salvi D., Seigneurin-Berny D., Moyet L., Ramus C., … Kieffer-Jaquinod S. (2010) AT_CHLORO, a comprehensive chloroplast proteome database with subplastidial localization and curated information on envelope proteins. *Molecular & Cellular Proteomics* **9**, 1063–1084.

Fetter K., Van Wilder V., Moshelion M. & Chaumont F. (2004) Interactions between plasma membrane aquaporins modulate their water channel activity. *Plant Cell* **16**, 215–228.

Field K.J., Duckett J.G., Cameron D.D. & Pressel S. (2015) Stomatal density and aperture in non-vascular land plants are non-responsive to above-ambient atmospheric CO_2 concentrations. *Annals of Botany* **115**, 915–922.

Finn R.N. & Cerda J. (2015) Evolution and functional diversity of aquaporins. *Biological Bulletin* **229**, 6–23.

Finn R.N., Chauvigne F., Hlidberg J.B., Cutler C.P. & Cerda J. (2014) The lineage-specific evolution of aquaporin gene clusters facilitated tetrapod terrestrial adaptation. *PLoS One* **9**e113686.

Fischer M. & Kaldenhoff R. (2008) On the pH regulation of plant aquaporins. *Journal of Biological Chemistry* **283**, 33889–33892.

Fitzpatrick K.L. & Reid R.J. (2009) The involvement of aquaglyceroporins in transport of boron in barley roots. *Plant, Cell and Environment* **32**, 1357–1365.

Flexas J., Barbour M.M., Brendel O., Cabrera H.M., Carriqui M., Diaz-Espejo A., … Warren C.R. (2012) Mesophyll diffusion conductance to CO_2: an unappreciated central player in photosynthesis. *Plant Science* **193**, 70–84.

Flexas J., Ribas-Carbo M., Hanson D.T., Bota J., Otto B., Cifre J., … Kaldenhoff R. (2006) Tobacco aquaporin NtAQP1 is involved in mesophyll conductance to CO_2 *in vivo*. *The Plant Journal* **48**, 427–439.

Forrest K.L. & Bhave M. (2008) The PIP and TIP aquaporins in wheat form a large and diverse family with unique gene structures and functionally important features. *Functional & Integrative Genomics* **8**, 115–133.

Frangne N., Maeshima M., Schaffner A.R., Mandel T., Martinoia E. & Bonnemain J.L. (2001) Expression and distribution of a vacuolar aquaporin in young and mature leaf tissues of *Brassica napus* in relation to water fluxes. *Planta* **212**, 270–278.

Fraysse L.C., Wells B., McCann M.C. & Kjellbom P. (2005) Specific plasma membrane aquaporins of the PIP1 subfamily are expressed in sieve elements and guard cells. *Biology of the Cell* **97**, 519–534.

Frick A., Jarva M. & Tornroth-Horsefield S. (2013) Structural basis for pH gating of plant aquaporins. *FEBS Letters* **587**, 989–993.

Fushimi K., Uchida S., Hara Y., Hirata Y., Marumo F. & Sasaki S. (1993) Cloning and expression of apical membrane water channel of rat-kidney collecting tubule. *Nature* **361**, 549–552.

Gao Z., He X., Zhao B., Zhou C., Liang Y., Ge R., … Huang Z. (2010) Overexpressing a putative aquaporin gene from wheat, TaNIP, enhances salt tolerance in transgenic Arabidopsis. *Plant and Cell Physiology* **51**, 767–775.

Gerbeau P., Amodeo G., Henzler T., Santoni V., Ripoche P. & Maurel C. (2002) The water permeability of Arabidopsis plasma membrane is regulated by divalent cations and pH. *Plant Journal* **30**, 71–81.

Geyer R.R., Musa-Aziz R., Qin X. & Boron W.F. (2013) Relative CO(2)/NH(3) selectivities of mammalian aquaporins 0–9. *American Journal of Physiology – Cell Physiology* **304**, C985–994.

Gomes D., Agasse A., Thiebaud P., Delrot S., Geros H. & Chaumont F. (2009) Aquaporins are multifunctional water and solute transporters highly divergent in living organisms. *Biochimica Et Biophysica Acta-Biomembranes* **1788**, 1213–1228.

Gonen T. & Walz T. (2006) The structure of aquaporins. *Quarterly Reviews of Biophysics* **39**, 361–396.

Gregoire C., Remus-Borel W., Vivancos J., Labbe C., Belzile F. & Belanger R.R. (2012) Discovery of a multigene family of aquaporin silicon transporters in the primitive plant *Equisetum arvense*. *Plant Journal* **72**, 320–330.

Grondin A., Mauleon R., Vadez V. & Henry A. (2016) Root aquaporins contribute to whole plant water fluxes under drought stress in rice (*Oryza sativa* L.). *Plant, Cell & Environment* **39**, 347–365.

Grondin A., Rodrigues O., Verdoucq L., Merlot S., Leonhardt N. & Maurel C. (2015) Aquaporins contribute to ABA-triggered stomatal closure through OST1-mediated phosphorylation. *Plant Cell* **27**, 1945–1954.

Guo L., Wang Z.Y., Lin H., Cui W.E., Chen J., Liu M., … Gu H. (2006) Expression and functional analysis of the rice plasma-membrane intrinsic protein gene family. *Cell Research* **16**, 277–286.

Gupta A.B. & Sankararamakrishnan R. (2009) Genome-wide analysis of major intrinsic proteins in the tree plant *Populus trichocarpa*: characterization of XIP subfamily of aquaporins from evolutionary perspective. *BMC Plant Biology* **9**, 134.

Gustavsson S., Lebrun A.S., Norden K., Chaumont F. & Johanson U. (2005) A novel plant major intrinsic protein in *Physcomitrella patens* most similar to bacterial glycerol channels. *Plant Physiology* **139**, 287–295.

Hachez C., Besserer A., Chevalier A.S. & Chaumont F. (2013) Insights into plant plasma membrane aquaporin trafficking. *Trends in Plant Science* **18**, 344–352.

Hachez C., Heinen R., Draye X. & Chaumont F.o. (2008) The expression pattern of plasma membrane aquaporins in maize leaf highlights their role in hydraulic regulation. *Plant Molecular Biology* **68**, 337–353.

Hachez C., Laloux T., Reinhardt H., Cavez D., Degand H., Grefen C., … Chaumont F. (2014) Arabidopsis SNAREs SYP61 and SYP121 coordinate the trafficking of plasma membrane aquaporin PIP2;7 to modulate the cell membrane water permeability. *Plant Cell* **26**, 3132–3147.

Hachez C., Moshelion M., Zelazny E., Cavez D. & Chaumont F. (2006) Localization and quantification of plasma membrane aquaporin expression in maize primary root: a clue to understanding their role as cellular plumbers. *Plant Molecular Biology* **62**, 305–323.

Hanba Y.T., Shibasaka M., Hayashi Y., Hayakawa T., Kasamo K., Terashima I. & Katsuhara M. (2004) Overexpression of the barley aquaporin HvPIP2;1 increases internal CO_2 conductance and CO_2 assimilation in the leaves of transgenic rice plants. *Plant and Cell Physiology* **45**, 521–529.

Hanson D.T. & Rice S.K. (2014) *Photosynthesis in Bryophytes and Early Land Plants*. Springer, Dordrecht, Netherlands.

Harmer S.L., Hogenesch J.B., Straume M., Chang H.-S., Han B., Zhu T., … Kay S.A. (2000) Orchestrated transcription of key pathways in Arabidopsis by the circadian clock. *Science* **290**, 2110–2113.

Heckwolf M., Pater D., Hanson D.T. & Kaldenhoff R. (2011) The *Arabidopsis thaliana* aquaporin AtPIP1;2 is a physiologically relevant CO_2 transport facilitator. *Plant Journal* **67**, 795–804.

Heinen R.B., Bienert G.P., Cohen D., Chevalier A.S., Uehlein N., Hachez C., … Chaumont F. (2014) Expression and characterization of plasma membrane aquaporins in stomatal complexes of *Zea mays*. *Plant Molecular Biology* **86**, 335–350.

Heinen R.B., Ye Q. & Chaumont F. (2009) Role of aquaporins in leaf physiology. *Journal of Experimental Botany* **60**, 2971–2985.

Heymann J.B. & Engel A. (1999) Aquaporins: phylogeny, structure, and physiology of water channels. *News in Physiological Sciences* **14**, 187–193.

Hooijmaijers C., Rhee J.Y., Kwak K.J., Chung G.C., Horie T., Katsuhara M. & Kang H. (2012) Hydrogen peroxide permeability of plasma membrane aquaporins of *Arabidopsis thaliana*. *Journal of Plant Research* **125**, 147–153.

Horie T., Kaneko T., Sugimoto G., Sasano S., Panda S.K., Shibasaka M. & Katsuhara M. (2011) Mechanisms of water transport mediated by pip aquaporins and their regulation via phosphorylation events under salinity stress in barley roots. *Plant and Cell Physiology* **52**, 663–675.

Hsu J.-L., Wang L.-Y., Wang S.-Y., Lin C.-H., Ho K.-C., Shi F.-K. & Chang F. (2009) Functional phosphoproteomic profiling of phosphorylation sites in membrane fractions of salt-stressed *Arabidopsis thaliana*. *Proteome Science* **7**, 1.

Hu W., Hou X., Huang C., Yan Y., Tie W., Ding Z., … Jin Z. (2015) Genome-wide identification and expression analyses of aquaporin gene family during development and abiotic stress in banana. *International Journal of Molecular Sciences* **16**, 19728–19751.

Hu W., Yuan Q., Wang Y., Cai R., Deng X., Wang J., … He G. (2012) Overexpression of a wheat aquaporin gene, TaAQP8, enhances salt stress tolerance in transgenic tobacco. *Plant and Cell Physiology* **53**, 2127–2141.

Huang C., Zhou S., Hu W., Deng X., Wei S., Yang G. & He G. (2014) The wheat aquaporin gene TaAQP7 confers tolerance to cold stress in transgenic tobacco. *Zeitschrift Fur Naturforschung Section C-a Journal of Biosciences* **69**, 142–148.

Hub J.S. & de Groot B.L. (2006) Does CO2 permeate through aquaporin-1? *Biophysical Journal* **91**, 842–848.

Ishikawa-Sakurai J., Hayashi H. & Murai-Hatano M. (2014) Nitrogen availability affects hydraulic conductivity of rice roots, possibly through changes in aquaporin gene expression. *Plant and Soil* **379**, 289–300.

Ishikawa F., Suga S., Uemura T., Sato M.H. & Maeshima M. (2005) Novel type aquaporin SIPs are mainly localized to the ER membrane and show cell-specific expression in *Arabidopsis thaliana*. *Febs Letters* **579**, 5814–5820.

Itel F., Al-Samir S., Oberg F., Chami M., Kumar M., Supuran C.T., … Endeward V. (2012) CO_2 permeability of cell membranes is regulated by membrane cholesterol and protein gas channels. *Faseb Journal* **26**, 5182–5191.

Jang J.Y., Kim D.G., Kim Y.O., Kim J.S. & Kang H. (2004) An expression analysis of a gene family encoding plasma membrane aquaporins in response to abiotic stresses in *Arabidopsis thaliana*. *Plant Molecular Biology* **54**, 713–725.

Jang J.Y., Lee S.H., Rhee J.Y., Chung G.C., Ahn S.J. & Kang H. (2007) Transgenic Arabidopsis and tobacco plants overexpressing an aquaporin respond differently to various abiotic stresses. *Plant Molecular Biology* **64**, 621–632.

Javot H., Lauvergeat V., Santoni V., Martin-Laurent F., Guclu J., Vinh J., … Maurel C. (2003) Role of a single aquaporin isoform in root water uptake. *Plant Cell* **15**, 509–522.

Javot H. & Maurel C. (2002) The role of aquaporins in root water uptake. *Annals of Botany* **90**, 301–313.

Jiao Y., Wickett N.J., Ayyampalayam S., Chanderbali A.S., Landherr L., Ralph P. E., … dePamphilis C.W. (2011) Ancestral polyploidy in seed plants and angiosperms. *Nature* **473**, 97–100.

Johanson U. & Gustavsson S. (2002) A new subfamily of major intrinsic proteins in plants. *Molecular Biology and Evolution* **19**, 456–461.

Johansson I., Karlsson M., Shukla V.K., Chrispeels M.J., Larsson C. & Kjellbom P. (1998) Water transport activity of the plasma membrane aquaporin PM28A is regulated by phosphorylation. *Plant Cell* **10**, 451–459.

Jozefkowicz C., Rosi P., Sigaut L., Soto G., Isabel P.L., Amodeo G. & Alleva K. (2013) Loop A is critical for the functional interaction of two *Beta vulgaris* PIP aquaporins. *Plos One* **8**e57993.

Jozefkowicz C., Sigaut L., Scochera F., Soto G., Ayub N., Pietrasanta L.I., … Alleva K. (2016) PIP water transport and its pH dependence are regulated by tetramer stoichiometry. *Biophysical Journal* **110**, 1312–1321.

Kai L. & Kaldenhoff R. (2014) A refined model of water and CO_2 membrane diffusion: effects and contribution of sterols and proteins. *Scientific Reports* **4**, 6665.

Kaldenhoff R. (2012) Mechanisms underlying CO_2 diffusion in leaves. *Current Opinion in Plant Biology* **15**, 276–281.

Kaldenhoff R. & Fischer M. (2006) Functional aquaporin diversity in plants. *Biochimica et Biophysica Acta (BBA) – Biomembranes* **1758**, 1134–1141.

Kaldenhoff R., Grote K., Zhu J.-J. & Zimmermann U. (1998) Significance of plasmalemma aquaporins for water transport in *Arabidopsis thaliana*. *The Plant Journal* **14**, 121–128.

Kaldenhoff R., Kai L. & Uehlein N. (2014) Aquaporins and membrane diffusion of CO_2 in living organisms. *Biochimica Et Biophysica Acta-General Subjects* **1840**, 1592–1595.

Kaldenhoff R., Ribas-Carbo M., Flexas J., Lovisolo C., Heckwolf M. & Uehlein N. (2008) Aquaporins and plant water balance. *Plant, Cell and Environment* **31**, 658–666.

Kammerloher W., Fischer U., Piechottka G.P. & Schaffner A.R. (1994) Water channels in the plant plasma-membrane cloned by immunoselection from a mammalian expression system. *Plant Journal* **6**, 187–199.

Katsuhara M., Akiyama Y., Koshio K., Shibasaka M. & Kasamo K. (2002) Functional analysis of water channels in barley roots. *Plant and Cell Physiology* **43**, 885–893.

Katsuhara M., Hanba Y.T., Shiratake K. & Maeshima M. (2008) Expanding roles of plant aquaporins in plasma membranes and cell organelles. *Functional Plant Biology* **35**, 1–14.

Katsuhara M., Koshio K., Shibasaka M., Hayashi Y., Hayakawa T. & Kasamo K. (2003) Over-expression of a barley aquaporin increased the shoot/root ratio and raised salt sensitivity in transgenic rice plants. *Plant and Cell Physiology* **44**, 1378–1383.

Katsuhara M. & Shibasaka M. (2007) Barley root hydraulic conductivity and aquaporins expression in relation to salt tolerance. *Soil Science and Plant Nutrition* **53**, 466–470.

Kawase M., Hanba Y.T. & Katsuhara M. (2013) The photosynthetic response of tobacco plants overexpressing ice plant aquaporin McMIPB to a soil water deficit and high vapor pressure deficit. *Journal of Plant Research* **126**, 517–527.

Kelly G., Sade N., Attia Z., Secchi F., Zwieniecki M., Holbrook N.M., … Granot D. (2014) Relationship between hexokinase and the aquaporin PIP1 in the regulation of photosynthesis and plant growth. *Plos One* **9**, e87888.

Khan K., Agarwal P., Shanware A. & Sane V.A. (2015) Heterologous expression of two jatropha aquaporins imparts drought and salt tolerance and improves seed viability in transgenic *Arabidopsis thaliana*. *Plos One* **10**, e0128866.

Khandelia H., Jensen M.Ø. & Mouritsen O.G. (2009) To gate or not to gate: using molecular dynamics simulations to morph gated plant aquaporins into constitutively open conformations. *The Journal of Physical Chemistry B* **113**, 5239–5244.

Kim T-H., Böhmer M., Hu H.H., Nishimura N. & Schroeder J.I. (2010) Guard cell signal transduction network: advances in understanding abscisic acid, CO2, and Ca2+ signaling. *Annual Review of Plant Biology* **61**, 561–591.

Kline K.G., Barrett-Wilt G.A. & Sussman M.R. (2010) In planta changes in protein phosphorylation induced by the plant hormone abscisic acid. *Proceedings of the National Academy of Sciences* **107**, 15986–15991.

Komsic-Buchmann K., Wöstehoff L. & Becker B. (2014) The contractile vacuole as a key regulator of cellular water flow in *Chlamydomonas reinhardtii*. *Eukaryotic Cell* **13**, 1421–1430.

Kreida S. & Tornroth-Horsefield S. (2015) Structural insights into aquaporin selectivity and regulation. *Current Opinion in Structural Biology* **33**, 126–134.

Krishnan D., Liu L., Wiebe S.A., Casey J.R., Cordat E. & Alexander R.T. (2015) Carbonic anhydrase II binds to and increases the activity of the epithelial sodium–proton exchanger, NHE3. *American Journal of Physiology. Renal Physiology* **309**, F383–392.

Kubásek J., Hájek T. & Glime J.M. (2014) Bryophyte photosynthesis in sunflecks: greater relative induction rate than in tracheophytes. *Journal of Bryology* **36**, 110–117.

Kukulski W., Schenk A.D., Johanson U., Braun T., de Groot B.L., Fotiadis D., … Engel A. (2005) The 5A structure of heterologously expressed plant aquaporin SoPIP2;1. *Journal of Molecular Biology* **350**, 611–616.

Kustu S. & Inwood W. (2006) Biological gas channels for NH_3 and CO_2: evidence that Rh (Rhesus) proteins are CO_2 channels. *Transfusion Clinique et Biologique* **13**, 103–110.

Laur J. & Hacke U.G. (2013) Transpirational demand affects aquaporin expression in poplar roots. *Journal of Experimental Botany* **64**, 2283–2293.

Laur J. & Hacke U.G. (2014) Exploring *Picea glauca* aquaporins in the context of needle water uptake and xylem refilling. *New Phytologist* **203**, 388–400.

Lee S.H., Chung G.C., Jang J.Y., Ahn S.J. & Zwiazek J.J. (2012) Overexpression of PIP2;5 aquaporin alleviates effects of low root temperature on cell hydraulic conductivity and growth in Arabidopsis. *Plant Physiology* **159**, 479–488.

Leliaert F., Smith D.R., Moreau H., Herron M.D., Verbruggen H., Delwiche C.F. & De Clerck O. (2012) Phylogeny and molecular evolution of the green algae. *Critical Reviews in Plant Sciences* **31**, 1–46.

Li G.-W., Zhang M.-H., Cai W.-M., Sun W.-N. & Su W.-A. (2008) Characterization of OsPIP2;7, a water channel protein in rice. *Plant and Cell Physiology* **49**, 1851–1858.

Li J., Yu G., Sun X., Liu Y., Liu J., Zhang X., … Pan H. (2015a) AcPIP2, a plasma membrane intrinsic protein from halophyte *Atriplex canescens*, enhances plant growth rate and abiotic stress tolerance when overexpressed in *Arabidopsis thaliana*. *Plant Cell Reports* **34**, 1401–1415.

Li L., Wang H., Gago J., Cui H., Qian Z., Kodama N., … Dong H. (2015b) Harpin Hpa1 interacts with aquaporin PIP1;4 to promote the substrate transport and photosynthesis in *Arabidopsis*. *Scientific Reports* **5**, 17207.

Li L.G., Li S.F., Tao Y. & Kitagawa Y. (2000) Molecular cloning of a novel water channel from rice: its products expression in Xenopus oocytes and involvement in chilling tolerance. *Plant Science* **154**, 43–51.

Li X., Liu Y., Alvarez B.V., Casey J.R. & Fliegel L. (2006) A novel carbonic anhydrase II binding site regulates NHE1 activity. *Biochemistry* **45**, 2414–2424.

Li X., Wang X., Yang Y., Li R., He Q., Fang X., … Lin J. (2011) Single-molecule analysis of PIP2;1 dynamics and partitioning reveals multiple modes of Arabidopsis plasma membrane aquaporin regulation. *Plant Cell* **23**, 3780–3797.

Lian H.L., Yu X., Ye Q., Ding X.S., Kitagawa Y., Kwak S.S., … Tang Z.C. (2004) The role of aquaporin RWC3 in drought avoidance in rice. *Plant and Cell Physiology* **45**, 481–489.

Lienard D., Durambur G., Kiefer-Meyer M.C., Nogue F., Menu-Bouaouiche L., Charlot F., … Lassalles J.P. (2008) Water transport by aquaporins in the extant plant *Physcomitrella patens*. *Plant Physiology* **146**, 1207–1218.

Liu L.H., Ludewig U., Gassert B., Frommer W.B. & von Wiren N. (2003) Urea transport by nitrogen-regulated tonoplast intrinsic proteins in Arabidopsis. *Plant Physiology* **133**, 1220–1228.

Lopez D., Bronner G., Brunel N., Auguin D., Bourgerie S., Brignolas F., … Venisse J.S. (2012) Insights into Populus XIP aquaporins: evolutionary expansion, protein functionality, and environmental regulation. *Journal of Experimental Botany* **63**, 2217–2230.

Lopez D., Venisse J.-S., Fumanal B., Chaumont F., Guillot E., Daniels M.J., … Gousset-Dupont A. (2013) Aquaporins and leaf hydraulics: poplar sheds new light. *Plant and Cell Physiology* **54**, 1963–1975.

Lopez F., Bousser A., Sissoëff I., Gaspar M., Lachaise B., Hoarau J. & Mahé A. (2003) Diurnal regulation of water transport and aquaporin gene expression in maize roots: contribution of PIP2 proteins. *Plant and Cell Physiology* **44**, 1384–1395.

Loque D., Ludewig U., Yuan L. & von Wiren N. (2005) Tonoplast intrinsic proteins AtTIP2;1 and AtTIP2;3 facilitate NH3 transport into the vacuole. *Plant Physiology* **137**, 671–680.

Ludewig U. & Dynowski M. (2009) Plant aquaporin selectivity: where transport assays, computer simulations and physiology meet. *Cellular and Molecular Life Sciences* **66**, 3161–3175.

Luu D.T. & Maurel C. (2013) Aquaporin trafficking in plant cells: an emerging membrane-protein model. *Traffic* **14**, 629–635.

Ma N., Xue J.Q., Li Y.H., Liu X.J., Dai F.W., Jia W.S., … Gao J.P. (2008) Rh-PIP2;1, a rose aquaporin gene, is involved in ethylene-regulated petal expansion. *Plant Physiology* **148**, 894–907.

Mahdieh M., Mostajeran A., Horie T. & Katsuhara M. (2008) Drought stress alters water relations and expression of PIP-type aquaporin genes in *Nicotiana tabacum* plants. *Plant and Cell Physiology* **49**, 801–813.

Majeran W., Zybailov B., Ytterberg A.J., Dunsmore J., Sun Q. & van Wijk K.J. (2008) Consequences of C-4 differentiation for chloroplast membrane Proteomes in maize mesophyll and bundle sheath cells. *Molecular & Cellular Proteomics* **7**, 1609–1638.

Mao Z. & Sun W. (2015) Arabidopsis seed-specific vacuolar aquaporins are involved in maintaining seed longevity under the control of ABSCISIC ACID INSENSITIVE 3. *Journal of Experimental Botany* **66**, 4781–4794.

Martinoia E., Maeshima M. & Neuhaus H.E. (2007) Vacuolar transporters and their essential role in plant metabolism. *Journal of Experimental Botany* **58**, 83–102.

Martins C.P., Pedrosa A.M., Du D., Goncalves L.P., Yu Q., Gmitter F.G. Jr. & Costa M.G. (2015) Genome-wide characterization and expression analysis of major intrinsic proteins during abiotic and biotic stresses in sweet orange (*Citrus sinensis* L. Osb.). *PLoS One* **10**e0138786.

Martre P., Morillon R., Barrieu F., North G.B., Nobel P.S. & Chrispeels M.J. (2002) Plasma membrane Aquaporins play a significant role during recovery from water deficit. *Plant Physiology* **130**, 2101–2110.

Masalkar P., Wallace I.S., Hwang J.H. & Roberts D.M. (2010) Interaction of cytosolic glutamine synthetase of soybean root nodules with the C-terminal domain of the symbiosome membrane nodulin 26 aquaglyceroporin. *Journal of Biological Chemistry* **285**, 23880–23888.

Maurel C., Boursiac Y., Doan-Trung L., Santoni V., Shahzad Z. & Verdoucq L. (2015) Aquaporins in plants. *Physiological Reviews* **95**, 1321–1358.

Maurel C., Reizer J., Schroeder J.I. & Chrispeels M.J. (1993) The vacuolar membrane-protein gamma-TIP creates water specific channels in *Xenopus*-oocytes. *Embo Journal* **12**, 2241–2247.

Maurel C., Tacnet F., Guclu J., Guern J. & Ripoche P. (1997) Purified vesicles of tobacco cell vacuolar and plasma membranes exhibit dramatically different water permeability and water channel activity. *Proceedings of the National Academy of Sciences of the United States of America* **94**, 7103–7108.

Maurel C., Verdoucq L., Luu D.-T. & Santoni V. (2008) Plant aquaporins: membrane channels with multiple integrated functions. *Annual Review of Plant Biology* **59**, 595–624.

Missner A., Kuegler P., Antonenko Y.N. & Pohl P. (2008a) Passive transport across bilayer lipid membranes: overton continues to rule. *Proceedings of the National Academy of Sciences of the United States of America* **105**, E123–E123.

Missner A., Kugler P., Saparov S.M., Sommer K., Mathai J.C., Zeidel M.L. & Pohl P. (2008b) Carbon dioxide transport through membranes. *Journal of Biological Chemistry* **283**, 25340–25347.

Missner A. & Pohl P. (2009) 110 years of the Meyer–Overton rule: predicting membrane permeability of gases and other small compounds. *Chemphyschem* **10**, 1405–1414.

Mizokami Y., Noguchi K., Kojima M., Sakakibara H. & Terashima I. (2015) Mesophyll conductance decreases in the wild type but not in an ABA-deficient mutant (aba1) of *Nicotiana plumbaginifolia* under drought conditions. *Plant, Cell and Environment* **38**, 388–398.

Monshausen G.B. & Gilroy S. (2009) The exploring root – root growth responses to local environmental conditions. *Current Opinion in Plant Biology* **12**, 766–772.

Monshausen G.B. & Haswell E.S. (2013) A force of nature: molecular mechanisms of mechanoperception in plants. *Journal of Experimental Botany* **64**, 4663–4680.

Mori I.C., Rhee J., Shibasaka M., Sasano S., Kaneko T., Horie T. & Katsuhara M. (2014) CO_2 transport by PIP2 aquaporins of barley. *Plant and Cell Physiology* **55**, 251–257.

Mosa K.A., Kumar K., Chhikara S., Mcdermott J., Liu Z., Musante C., … Dhankher O.P. (2012) Members of rice plasma membrane intrinsic proteins subfamily are involved in arsenite permeability and tolerance in plants. *Transgenic Research* **21**, 1265–1277.

Mosa K.A., Kumar K., Chhikara S., Musante C., White J.C. & Dhankher O.P. (2016) Enhanced boron tolerance in plants mediated by bidirectional transport through plasma membrane intrinsic proteins. *Scientific Reports* **6**, 21640.

Moshelion M., Becker D., Biela A., Uehlein N., Hedrich R., Otto B., … Kaldenhoff R. (2002) Plasma membrane aquaporins in the motor cells of *Samanea saman*: diurnal and circadian regulation. *The Plant Cell* **14**, 727–739.

Moshelion M., Halperin O., Wallach R., Oren R. & Way D.A. (2015) Role of aquaporins in determining transpiration and photosynthesis in water-stressed plants: crop water-use efficiency, growth and yield. *Plant, Cell and Environment* **38**, 1785–1793.

Mühlhausen S. & Kollmar M. (2013) Whole genome duplication events in plant evolution reconstructed and predicted using myosin motor proteins. *BMC Evolutionary Biology* **13**, 202.

Musa-Aziz R., Chen L.M., Pelletier M.F. & Boron W.F. (2009) Relative CO_2/NH_3 selectivities of AQP1, AQP4, AQP5, AmtB, and RhAG. *Proceedings of the National Academy of Sciences of the United States of America* **106**, 5406–5411.

Nakhoul N.L., Davis B.A., Romero M.F. & Boron W.F. (1998) Effect of expressing the water channel aquaporin-1 on the CO_2 permeability of *Xenopus* oocytes. *American Journal of Physiology-Cell Physiology* **43**, C543–C548.

Navarro-Rodenas A., Barzana G., Nicolas E., Carra A., Schubert A. & Morte A. (2013) Expression analysis of aquaporins from desert truffle mycorrhizal symbiosis reveals a fine-tuned regulation under drought. *Molecular Plant-Microbe Interactions* **26**, 1068–1078.

Niemietz C.M. & Tyerman S.D. (1997) Characterization of water channels in wheat root membrane vesicles. *Plant Physiology* **115**, 561–567.

Niemietz C.M. & Tyerman S.D. (2002) New potent inhibitors of aquaporins: silver and gold compounds inhibit aquaporins of plant and human origin. *Febs Letters* **531**, 443–447.

Noronha H., Agasse A., Martins A.P., Berny M.C., Gomes D., Zarrouk O., … Geros H. (2014) The grape aquaporin VvSIP1 transports water across the ER membrane. *Journal of Experimental Botany* **65**, 981–993.

Nyblom M., Frick A., Wang Y., Ekvall M., Hallgren K., Hedfalk K., … Tornroth-Horsefield S. (2009) Structural and functional analysis of SoPIP2;1 mutants adds insight into plant aquaporin gating. *Journal of Molecular Biology* **387**, 653–668.

Oparka K.J. & Roberts A.G. (2001) Plasmodesmata. A not so open-and-shut case. *Plant Physiology* **125**, 123–126.

Otto B., Uehlein N., Sdorra S., Fischer M., Ayaz M., Belastegui-Macadam X., … Kaldenhoff R. (2010) Aquaporin tetramer composition modifies the function of tobacco aquaporins. *Journal of Biological Chemistry* **285**, 31253–31260.

Pandey B., Sharma P., Pandey D.M., Sharma I. & Chatrath R. (2013) Identification of new aquaporin genes and single nucleotide polymorphism in bread wheat. *Evol Bioinform Online* **9**, 437–452.

Pang Y.Q., Li L.J., Ren F., Lu P.L., Wei P.C., Cai J.H., … Wang X.C. (2010) Overexpression of the tonoplast aquaporin AtTIP5;1 conferred tolerance to boron toxicity in Arabidopsis. *Journal of Genetics and Genomics* **37**, 389–U352.

Park J.H. & Saier M.H. Jr. (1996) Phylogenetic characterization of the MIP family of transmembrane channel proteins. *Journal of Membrane Biology* **153**, 171–180.

Park W., Scheffler B.E., Bauer P.J. & Campbell B.T. (2010) Identification of the family of aquaporin genes and their expression in upland cotton (*Gossypium hirsutum* L.). *BMC Plant Biology* **10**, 142.

Peng J. & Huang C.H. (2006) Rh proteins vs Amt proteins: an organismal and phylogenetic perspective on CO_2 and NH_3 gas channels. *Transfusion Clinique et Biologique* **13**, 85–94.

Peng Y., Lin W., Cai W. & Arora R. (2007) Overexpression of a Panax ginseng tonoplast aquaporin alters salt tolerance, drought tolerance and cold acclimation ability in transgenic Arabidopsis plants. *Planta* **226**, 729–740.

Pommerrenig B., Diehn T.A. & Bienert G.P. (2015) Metalloido-porins: essentiality of nodulin 26-like intrinsic proteins in metalloid transport. *Plant Science* **238**, 212–227.

Postaire O., Tournaire-Roux C., Grondin A., Boursiac Y., Morillon R., Schaeffner A.R. & Maurel C. (2010) A PIP1 aquaporin contributes to hydrostatic pressure-induced water transport in both the root and rosette of *Arabidopsis*. *Plant Physiology* **152**, 1418–1430.

Prado K., Boursiac Y., Tournaire-Roux C., Monneuse J.M., Postaire O., Da Ines O., … Maurel C. (2013) Regulation of *Arabidopsis* leaf hydraulics involves light-dependent phosphorylation of aquaporins in veins. *Plant Cell* **25**, 1029–1039.

Prado K. & Maurel C. (2013) Regulation of leaf hydraulics: from molecular to whole plant levels. *Frontiers in Plant Science* **4**, 255.

Prak S., Hem S., Boudet J., Viennois G., Sommerer N., Rossignol M., … Santoni V. (2008) Multiple phosphorylations in the C-terminal tail of plant plasma membrane aquaporins: role in subcellular trafficking of AtPIP2;1 in response to salt stress. *Molecular and Cellular Proteomics* **7**, 1019–1030.

Preston G.M. & Agre P. (1991) Isolation of the cDNA for erythrocyte integral membrane protein of 28 kilodaltons: member of an ancient channel family. *Proceedings of the National Academy of Sciences* **88**, 11110–11114.

Preston G.M., Carroll T.P., Guggino W.B. & Agre P. (1992) Appearance of water channels in *Xenopus* oocytes expressing red-cell CHIP28 protein. *Science* **256**, 385–387.

Pushkin A., Abuladze N., Gross E., Newman D., Tatishchev S., Lee I., … Kurtz I. (2004) Molecular mechanism of kNBC1-carbonic anhydrase II interaction in proximal tubule cells. *Journal of Physiology* **559**, 55–65.

Qian Z.-J., Song J.-J., Chaumont F. & Ye Q. (2015) Differential responses of plasma membrane aquaporins in mediating water transport of cucumber seedlings under osmotic and salt stresses. *Plant, Cell and Environment* **38**, 461–473.

Quigley F., Rosenberg J.M., Shachar-Hill Y. & Bohnert H.J. (2001) From genome to function: the Arabidopsis aquaporins. *Genome Biology* **3**RESEARCH0001.

Ranganathan K., El Kayal W., Cooke J.E.K. & Zwiazek J.J. (2016) Responses of hybrid aspen over-expressing a PIP2;5 aquaporin to low root temperature. *Journal of Plant Physiology* **192**, 98–104.

Raven J.A. & Beardall J. (2016) The ins and outs of CO_2. *Journal of Experimental Botany* **67**, 1–13.

Raven J.A. & Doblin M.A. (2014) Active water transport in unicellular algae: where, why, and how. *Journal of Experimental Botany* **65**, 6279–6292.

Reddy P.S., Rao T.S.R.B., Sharma K.K. & Vadez V. (2015) Genome-wide identification and characterization of the aquaporin gene family in *Sorghum bicolor* (L.). *Plant Gene* **1**, 18–28.

Rensing S.A. (2014) Gene duplication as a driver of plant morphogenetic evolution. *Current Opinion in Plant Biology* **17**, 43–48.

Reuscher S., Akiyama M., Mori C., Aoki K., Shibata D. & Shiratake K. (2013) Genome-wide identification and expression analysis of aquaporins in tomato. *PLoS One* **8**e79052.

Royles J., Ogee J., Wingate L., Hodgson D.A., Convey P. & Griffiths H. (2013) Temporal separation between CO_2 assimilation and growth? Experimental and theoretical evidence from the desiccation-tolerant moss Syntrichia ruralis. *New Phytologist* **197**, 1152–1160.

Ruhfel B.R., Gitzendanner M.A., Soltis P.S., Soltis D.E. & Burleigh J.G. (2014) From algae to angiosperms – inferring the phylogeny of green plants (Viridiplantae) from 360 plastid genomes. *BMC Evolutionary Biology* **14**, 23.

Sabir F., Leandro M.J., Martins A.P., Loureiro-Dias M.C., Moura T.F., Soveral G. & Prista C. (2014) Exploring three pips and three tips of grapevine for transport of water and atypical substrates through heterologous expression in aqy-null yeast. *PLoS ONE* **9**e102087.

Sachdeva R. & Singh B. (2014) Insights into structural mechanisms of gating induced regulation of aquaporins. *Progress in Biophysics and Molecular Biology* **114**, 69–79.

Sade N., Galle A., Flexas J., Lerner S., Peleg G., Yaaran A. & Moshelion M. (2014a) Differential tissue-specific expression of NtAQP1 in *Arabidopsis thaliana* reveals a role for this protein in stomatal and mesophyll conductance of CO2 under standard and salt-stress conditions. *Planta* **239**, 357–366.

Sade N., Gebretsadik M., Seligmann R., Schwartz A., Wallach R. & Moshelion M. (2010) The role of tobacco aquaporin1 in improving water use efficiency, hydraulic conductivity, and yield production under salt stress. *Plant Physiology* **152**, 245–254.

Sade N., Shatil-Cohen A., Attia Z., Maurel C., Boursiac Y., Kelly G., … Moshelion M. (2014b) The role of plasma membrane aquaporins in regulating the bundle sheath-mesophyll continuum and leaf hydraulics. *Plant Physiology* **166**, 1609–1620.

Sade N., Vinocur B.J., Diber A., Shatil A., Ronen G., Nissan H., … (2009) Improving plant stress tolerance and yield production: is the tonoplast aquaporin SlTIP2;2 a key to isohydric to anisohydric conversion? *New Phytologist*, **181**, 651–661.

Sakr S., Alves G., Morillon R., Maurel K., Decourteix M., Guilliot A., … Chrispeels M.J. (2003) Plasma membrane aquaporins are involved in winter embolism recovery in walnut tree. *Plant Physiology* **133**, 630–641.

Sakurai J., Ahamed A., Murai M., Maeshima M. & Uemura M. (2008) Tissue and cell-specific localization of rice aquaporins and their water transport activities. *Plant and Cell Physiology* **49**, 30–39.

Sakurai J., Ishikawa F., Yamaguchi T., Uemura M. & Maeshima M. (2005) Identification of 33 rice aquaporin genes and analysis of their expression and function. *Plant and Cell Physiology* **46**, 1568–1577.

Secchi F., Schubert A. & Lovisolo C. (2016) Changes in air CO_2 concentration differentially alter transcript levels of NtAQP1 and NtPIP2; 1 aquaporin genes in tobacco leaves. *International Journal of Molecular Sciences* **17**, 567.

Secchi F. & Zwieniecki M.A. (2013) The physiological response of *Populus tremula* × *alba* leaves to the down-regulation of PIP1 aquaporin gene expression under no water stress. *Frontiers in Plant Science* **4**, 507.

Secchi F. & Zwieniecki M.A. (2014) Down-regulation of plasma intrinsic protein1 aquaporin in poplar trees is detrimental to recovery from embolism. *Plant Physiology* **164**, 1789–1799.

Shatil-Cohen A., Attia Z. & Moshelion M. (2011) Bundle-sheath cell regulation of xylem-mesophyll water transport via aquaporins under drought stress: a target of xylem-borne ABA? *The Plant Journal* **67**, 72–80.

Shelden M.C., Howitt S.M., Kaiser B.N. & Tyerman S.D. (2009) Identification and functional characterisation of aquaporins in the grapevine, *Vitis vinifera*. *Functional Plant Biology* **36**, 1065–1078.

Shibasaka M., Sasano S., Utsugi S. & Katsuhara M. (2012) Functional characterization of a novel plasma membrane intrinsic protein2 in barley. *Plant Signaling & Behavior* **7**, 1648–1652.

Siefritz F., Tyree M.T., Lovisolo C., Schubert A. & Kaldenhoff R. (2002) PIP1 plasma membrane aquaporins in tobacco: from cellular effects to function in plants. *Plant Cell* **14**, 869–876.

Sjohamn J. & Hedfalk K. (2014) Unraveling aquaporin interaction partners. *Biochimica et Biophysica Acta* **1840**, 1614–1623.

Smart L.B., Moskal W.A., Cameron K.D. & Bennett A.B. (2001) MIP genes are down-regulated under drought stress in *Nicotiana glauca*. *Plant and Cell Physiology* **42**, 686–693.

Sorieul M., Santoni V., Maurel C. & Luu D.T. (2011) Mechanisms and effects of retention of over-expressed aquaporin AtPIP2;1 in the endoplasmic reticulum. *Traffic* **12**, 473–482.

Soto G., Alleva K., Mazzella M.A., Amodeo G. & Muschietti J.P. (2008) AtTIP1;3 and AtTIP5;1, the only highly expressed Arabidopsis pollen-specific aquaporins, transport water and urea. *Febs Letters* **582**, 4077–4082.

Soupene E., Inwood W. & Kustu S. (2004) Lack of the Rhesus protein Rh1 impairs growth of the green alga *Chlamydomonas reinhardtii* at high CO2. *Proceedings of the National Academy of Sciences of the United States of America* **101**, 7787–7792.

Soupene E., King N., Feild E., Liu P., Niyogi K.K., Huang C.-H. & Kustu S. (2002) Rhesus expression in a green alga is regulated by CO_2. *Proceedings of the National Academy of Sciences* **99**, 7769–7773.

Sreedharan S., Shekhawat U.K.S. & Ganapathi T.R. (2013) Transgenic banana plants overexpressing a native plasma membrane aquaporin MusaPIP1;2 display high tolerance levels to different abiotic stresses. *Plant Biotechnology Journal* **11**, 942–952.

Sreedharan S., Shekhawat U.K.S. & Ganapathi T.R. (2015) Constitutive and stress-inducible overexpression of a native aquaporin gene (MusaPIP2;6) in transgenic banana plants signals its pivotal role in salt tolerance. *Plant Molecular Biology* **88**, 41–52.

Steudle E. (2000) Water uptake by plant roots: an integration of views. *Plant and Soil* **226**, 45–56.

Suga S. & Maeshima M. (2004) Water channel activity of radish plasma membrane aquaporins heterologously expressed in yeast and their modification by site-directed mutagenesis. *Plant and Cell Physiology* **45**, 823–830.

Takase T., Ishikawa H., Murakami H., Kikuchi J., Sato-Nara K. & Suzuki H. (2011) The circadian clock modulates water dynamics and aquaporin expression in Arabidopsis roots. *Plant and Cell Physiology* **52**, 373–383.

Tao P., Zhong X., Li B., Wang W., Yue Z., Lei J., … Huang X. (2014) Genome-wide identification and characterization of aquaporin genes (AQPs) in Chinese cabbage (*Brassica rapa* ssp pekinensis). *Molecular Genetics and Genomics* **289**, 1131–1145.

Temmei Y., Uchida S., Hoshino D., Kanzawa N., Kuwahara M., Sasaki S. & Tsuchiya T. (2005) Water channel activities of *Mimosa pudica* plasma membrane intrinsic proteins are regulated by direct interaction and phosphorylation. *FEBS Letters* **579**, 4417–4422.

Terashima I. & Ono K. (2002) Effects of $HgCl_2$ on CO_2 dependence of leaf photosynthesis: evidence indicating involvement of aquaporins in CO_2 diffusion across the plasma membrane. *Plant and Cell Physiology* **43**, 70–78.

Tian S., Wang X., Li P., Wang H., Ji H., Xie J., … Dong H. (2016) Plant aquaporin AtPIP1;4 links apoplastic H_2O_2 induction to disease immunity pathways. *Plant Physiology* **171**, 1635–1650.

Tornroth-Horsefield S., Wang Y., Hedfalk K., Johanson U., Karlsson M., Tajkhorshid E., … Kjellbom P. (2006) Structural mechanism of plant aquaporin gating. *Nature* **439**, 688–694.

Tosens T., Nishida K., Gago J., Coopman R.E., Cabrera H.M., Carriqui M., … Flexas J. (2016) The photosynthetic capacity in 35 ferns and fern allies: mesophyll CO_2 diffusion as a key trait. *New Phytologist* **209**, 1576–1590.

Tournaire-Roux C., Sutka M., Javot H., Gout E., Gerbeau P., Luu D.T., … Maurel C. (2003) Cytosolic pH regulates root water transport during anoxic stress through gating of aquaporins. *Nature* **425**, 393–397.

Tsiavaliaris G., Itel F., Hedfalk K., Al-Samir S., Meier W., Gros G. & Endeward V. (2015) Low CO_2 permeability of cholesterol-containing liposomes detected by stopped-flow fluorescence spectroscopy. *Faseb Journal* **29**, 1780–1793.

Tsuchihira A., Hanba Y.T., Kato N., Doi T., Kawazu T. & Maeshima M. (2010) Effect of overexpression of radish plasma membrane aquaporins on water-use efficiency, photosynthesis and growth of Eucalyptus trees. *Tree Physiology* **30**, 417–430.

Tyerman S.D., Niemietz C.M. & Bramley H. (2002) Plant aquaporins: multifunctional water and solute channels with expanding roles. *Plant, Cell and Environment* **25**, 173–194.

Uehlein N., Lovisolo C., Siefritz F. & Kaldenhoff R. (2003) The tobacco aquaporin NtAQP1 is a membrane CO_2 pore with physiological functions. *Nature* **425**, 734–737.

Uehlein N., Otto B., Eilingsfeld A., Itel F., Meier W. & Kaldenhoff R. (2012a) Gas-tight triblock-copolymer membranes are converted to CO_2 permeable by insertion of plant aquaporins. *Scientific Reports* **2**, 538.

Uehlein N., Otto B., Hanson D.T., Fischer M., McDowell N. & Kaldenhoff R. (2008) Function of *Nicotiana tabacum* aquaporins as chloroplast gas pores challenges the concept of membrane CO_2 permeability. *Plant Cell* **20**, 648–657.

Uehlein N., Sperling H., Heckwolf M. & Kaldenhoff R. (2012b) The Arabidopsis aquaporin PIP1;2 rules cellular CO_2 uptake. *Plant, Cell & Environment* **35**, 1077–1083.

Uemura M., Joseph R.A. & Steponkus P.L. (1995) Cold-acclimation of *Arabidopsis thaliana* – effect on plasma-membrane lipid-composition and freeze-induced lesions. *Plant Physiology* **109**, 15–30.

Vandeleur R.K., Mayo G., Shelden M.C., Gilliham M., Kaiser B.N. & Tyerman S. D. (2009) The role of plasma membrane intrinsic protein aquaporins in water transport through roots: diurnal and drought stress responses reveal different strategies between isohydric and anisohydric cultivars of grapevine. *Plant Physiology* **149**, 445–460.

Venkatesh J., Yu J.W. & Park S.W. (2013) Genome-wide analysis and expression profiling of the *Solanum tuberosum* aquaporins. *Plant Physiology and Biochemistry* **73**, 392–404.

Verdoucq L., Grondin A. & Maurel C. (2008) Structure–function analysis of plant aquaporin AtPIP2;1 gating by divalent cations and protons. *Biochemical Journal* **415**, 409–416.

Verma R.K., Gupta A.B. & Sankararamakrishnan R. (2015a) Major intrinsic protein superfamily: channels with unique structural features and diverse selectivity filters. *Methods in Enzymology* **557**, 485–520.

Verma R.K., Prabh N.D. & Sankararamakrishnan R. (2015b) Intra-helical salt-bridge and helix destabilizing residues within the same helical turn: role of functionally important loop E half-helix in channel regulation of major intrinsic proteins. *Biochimica et Biophysica Acta* **1848**, 1436–1449.

Vilas G., Krishnan D., Loganathan S.K., Malhotra D., Liu L., Beggs M.R., … Alexander R.T. (2015) Increased water flux induced by an aquaporin-1/carbonic anhydrase II interaction. *Molecular Biology of the Cell* **26**, 1106–1118.

von Caemmerer S., Evans J., Cousins A., Badger M. & Furbank R. (2007) C_4 photosynthesis and CO_2 diffusion. In *Charting New Pathways to C_4 Rice* (eds Sheehy J., Mitchell P. & Hardy B.), pp. 95–115. International Rice Research Institute, Los Banos, Philippines.

von Caemmerer S. & Evans J.R. (2015) Temperature responses of mesophyll conductance differ greatly between species. *Plant, Cell and Environment* **38**, 629–637.

von Caemmerer S., Evans J.R., Hudson G.S. & Andrews T.J. (1994) The kinetics of ribulose-1,5-bisphosphate carboxylase/oxygenase *in vivo* inferred from measurements of photosynthesis in leaves of transgenic tobacco. *Planta* **195**, 88–97.

von Caemmerer S. & Farquhar G.D. (1981) Some relationships between the biochemistry of photosynthesis and the gas exchange of leaves. *Planta* **153**, 376–387.

von Caemmerer S. & Furbank R.T. (2016) Strategies for improving C4 photosynthesis. *Current Opinion in Plant Biology* **31**, 125–134.

Wang C., Hu H., Qin X., Zeise B., Xu D., Rappel W.-J., … Schroeder J.I. (2016) Reconstitution of CO_2 regulation of SLAC1 anion channel and function of CO_2-permeable PIP2;1aquaporin as CARBONIC ANHYDRASE4 interactor. *The Plant Cell* **28**, 568–582.

Wang L.-L., Chen A.-P., Zhong N.-Q., Liu N., Wu X.-M., Wang F., … Xia G.-X. (2014) The *Thellungiella salsuginea* tonoplast aquaporin TsTIP1; 2 functions in protection against multiple abiotic stresses. *Plant and Cell Physiology* **55**, 148–161.

Wang W., Vinocur B. & Altman A. (2003) Plant responses to drought, salinity and extreme temperatures: towards genetic engineering for stress tolerance. *Planta* **218**, 1–14.

Wang Y., Cohen J., Boron W.F., Schulten K. & Tajkhorshid E. (2007) Exploring gas permeability of cellular membranes and membrane channels with molecular dynamics. *Journal of Structural Biology* **157**, 534–544.

Wang Y., Stessman D.J. & Spalding M.H. (2015) The CO_2 concentrating mechanism and photosynthetic carbon assimilation in limiting CO_2: how Chlamydomonas works against the gradient. *Plant Journal* **82**, 429–448.

Weig A., Deswarte C. & Chrispeels M.J. (1997) The major intrinsic protein family of arabidopsis has 23 members that form three distinct groups with functional aquaporins in each group. *Plant Physiology* **114**, 1347–1357.

Willmer C.M. & Sexton R. (1979) Stomata and plasmodesmata. *Protoplasma* **100**, 113–124.

Xu Y., Hu W., Liu J., Zhang J., Jia C., Miao H., … Jin Z. (2014) A banana aquaporin gene, MaPIP1;1, is involved in tolerance to drought and salt stresses. *BMC Plant Biology* **14**, 59.

Yaneff A., Sigaut L., Marquez M., Alleva K., Isabel P.L. & Amodeo G. (2014) Heteromerization of PIP aquaporins affects their intrinsic permeability. *Proceedings of the National Academy of Sciences of the United States of America* **111**, 231–236.

Yaneff A., Vitali V. & Amodeo G. (2015) PIP1 aquaporins: intrinsic water channels or PIP2 aquaporin modulators? *Febs Letters* **589**, 3508–3515.

Yoo Y.J., Lee H.K., Han W., Kim D.H., Lee M., Jeon J., … Hwang I. (2016) Interactions between transmembrane helices within monomers of the aquaporin AtPIP2;1 play a crucial role in tetramer formation. *Molecular Plant* .

Yoshida S. & Uemura M. (1986) Lipid composition of plasma membranes and tonoplasts isolated from etiolated seedlings of mung bean (*Vigna radiata* L.). *Plant Physiology* **82**, 807–812.

Yu G., Li J., Sun X., Zhang X., Liu J. & Pan H. (2015) Overexpression of AcNIP5; 1, a novel nodulin-like intrinsic protein from halophyte *Atriplex canescens*, enhances sensitivity to salinity and improves drought tolerance in Arabidopsis. *Plant Molecular Biology Reporter* **33**, 1864–1875.

Yu Q., Hu Y., Li J., Wu Q. & Lin Z. (2005) Sense and antisense expression of plasma membrane aquaporin BnPIP1 from *Brassica napus* in tobacco and its effects on plant drought resistance. *Plant Science* **169**, 647–656.

Zelazny E., Borst J.W., Muylaert M., Batoko H., Hemminga M.A. & Chaumont F. (2007) FRET imaging in living maize cells reveals that plasma membrane aquaporins interact to regulate their subcellular localization. *Proceedings of the National Academy of Sciences of the United States of America* **104**, 12359–12364.

Zelazny E., Miecielica U., Borst J.W., Hemminga M.A. & Chaumont F. (2009) An N-terminal diacidic motif is required for the trafficking of maize aquaporins ZmPIP2;4 and ZmPIP2;5 to the plasma membrane. *Plant Journal* **57**, 346–355.

Zhang D.Y., Ali Z., Wang C.B., Xu L., Yi J.X., Xu Z.L., … Ma H.X. (2013) Genome-wide sequence characterization and expression analysis of major intrinsic proteins in soybean (*Glycine max* L.). *PLoS One* **8**e56312.

Zhang M.H., Lu S.Q., Li G.W., Mao Z.L., Yu X., Sun W.N., … Su W.A. (2010) Identification of a residue in helix 2 of rice plasma membrane intrinsic proteins that influences water permeability. *Journal of Biological Chemistry* **285**, 41982–41992.

Zhang Y., Wang Z., Chai T., Wen Z. & Zhang H. (2008) Indian mustard aquaporin improves drought and heavy-metal resistance in tobacco. *Molecular Biotechnology* **40**, 280–292.

Zhao M., Tan H.T., Scharwies J., Levin K., Evans J.R. & Tyerman S.D. (2016) Association between water and carbon dioxide transport in leaf plasma membranes: assessing the role of aquaporins. *Plant, Cell & Environment* doi:10.1111/pce.12830.

hou L., Wang C., Liu R., Han Q., Vandeleur R.K., Du J., … Shou H. (2014) Constitutive overexpression of soybean plasma membrane intrinsic protein GmPIP1;6 confers salt tolerance. *BMC Plant Biology* **14**, doi:10.1186/1471-2229-14-181.

Zhou S., Hu W., Deng X., Ma Z., Chen L., Huang C., … He G. (2012) Overexpression of the wheat aquaporin gene, TaAQP7, enhances drought tolerance in transgenic tobacco. *PLoS ONE* **7**e52439.

Zhou Y., Setz N., Niemietz C., Qu H., Offler C.E., Tyerman S.D. & Patrick J.W. (2007) Aquaporins and unloading of phloem-imported water in coats of developing bean seeds. *Plant, Cell and Environment* **30**, 1566–1577.

Zhu C., Schraut D., Hartung W. & Schäffner A.R. (2005) Differential responses of maize MIP genes to salt stress and ABA. *Journal of Experimental Botany* **56**, 2971–2981.

Zhuang L., Liu M., Yuan X., Yang Z. & Huang B. (2015) Physiological effects of aquaporin in regulating drought tolerance through overexpressing of *Festuca arundinacea* aquaporin gene FaPIP2; 1. *Journal of the American Society for Horticultural Science* **140**, 404–412.

Zimmermann H.M., Hartmann K., Schreiber L. & Steudle E. (2000) Chemical composition of apoplastic transport barriers in relation to radial hydraulic conductivity of corn roots (*Zea mays* L.). *Planta* **210**, 302–311.

Zou Z., Gong J., An F., Xie G., Wang J., Mo Y. & Yang L. (2015a) Genome-wide identification of rubber tree (*Hevea brasiliensis* Muell. Arg.) aquaporin genes and their response to ethephon stimulation in the laticifer, a rubber-producing tissue. *BMC Genomics* **16**, 1001.

Zou Z., Gong J., Huang Q., Mo Y., Yang L. & Xie G. (2015b) Gene structures, evolution, classification and expression profiles of the aquaporin gene family in castor bean (*Ricinus communis* L.). *Plos One* **10**, doi:10.1371/journal.pone.0141022.

Zou Z., Yang L., Gong J., Mo Y., Wang J., Cao J., … Xie G. (2016) Genome-wide identification of *Jatropha curcas* aquaporin genes and the comparative analysis provides insights into the gene family expansion and evolution in *Hevea brasiliensis*. *Frontiers in Plant Science* **7**, 395.

Zwieniecki M.A., Brodribb T.J. & Holbrook N.M. (2007) Hydraulic design of leaves: insights from rehydration kinetics. *Plant, Cell and Environment* **30**, 910–921.

Received 19 May 2016; received in revised form 1 September 2016; accepted for publication 22 September 2016

SUPPORTING INFORMATION

Additional Supporting Information may be found in the online version of this article at the publisher's web-site:

Figure S1. Interacting residues in different gated states
Table S1. Mutagenesis of residues involved in gating.
Table S2. Mutagenesis of residues involved in other parts of the aquaporin protein.

frontiers in Plant Science

ORIGINAL RESEARCH
published: 01 December 2016
doi: 10.3389/fpls.2016.01815

Roles of Aquaporins in *Setaria viridis* Stem Development and Sugar Storage

Samantha A. McGaughey[1,2], Hannah L. Osborn[3], Lily Chen[1,3], Joseph L. Pegler[1], Stephen D. Tyerman[2], Robert T. Furbank[3], Caitlin S. Byrt[2†] and Christopher P. L. Grof[1†]*

[1] Centre for Plant Science, School of Environmental and Life Sciences, University of Newcastle, Callaghan, NSW, Australia, [2] Australian Research Council Centre of Excellence in Plant Energy Biology, Waite Research Institute and School of Agriculture, Food and Wine, University of Adelaide, Glen Osmond, SA, Australia, [3] Australian Research Council Centre of Excellence for Translational Photosynthesis, College of Medicine, Biology and Environment, Australian National University, Canberra, ACT, Australia

Setaria viridis is a C_4 grass used as a model for bioenergy feedstocks. The elongating internodes in developing *S. viridis* stems grow from an intercalary meristem at the base, and progress acropetally toward fully expanded cells that store sugar. During stem development and maturation, water flow is a driver of cell expansion and sugar delivery. As aquaporin proteins are implicated in regulating water flow, we analyzed elongating and mature internode transcriptomes to identify putative aquaporin encoding genes that had particularly high transcript levels during the distinct stages of internode cell expansion and maturation. We observed that *SvPIP2;1* was highly expressed in internode regions undergoing cell expansion, and *SvNIP2;2* was highly expressed in mature sugar accumulating regions. Gene co-expression analysis revealed *SvNIP2;2* expression was highly correlated with the expression of five putative sugar transporters expressed in the *S. viridis* internode. To explore the function of the proteins encoded by *SvPIP2;1* and *SvNIP2;2*, we expressed them in *Xenopus laevis* oocytes and tested their permeability to water. SvPIP2;1 and SvNIP2;2 functioned as water channels in *X. laevis* oocytes and their permeability was gated by pH. Our results indicate that SvPIP2;1 may function as a water channel in developing stems undergoing cell expansion and SvNIP2;2 is a candidate for retrieving water and possibly a yet to be determined solute from mature internodes. Future research will investigate whether changing the function of these proteins influences stem growth and sugar yield in *S. viridis*.

Keywords: aquaporin, stem, water transport, sugar accumulation, grasses

OPEN ACCESS

Edited by:
Rupesh Kailasrao Deshmukh, Laval University, Canada

Reviewed by:
Manoj Prasad, National Institute of Plant Genome Research, India
Kapil Kumar Tiwari, Sardarkrushinagar Dantiwada Agricultural University, India

***Correspondence:**
Caitlin S. Byrt
caitlin.byrt@adelaide.edu.au

† These authors have contributed equally to this work.

Specialty section:
This article was submitted to Plant Physiology, a section of the journal Frontiers in Plant Science

Received: *15 August 2016*
Accepted: *17 November 2016*
Published: *01 December 2016*

Citation:
McGaughey SA, Osborn HL, Chen L, Pegler JL, Tyerman SD, Furbank RT, Byrt CS and Grof CPL (2016) Roles of Aquaporins in Setaria viridis Stem Development and Sugar Storage. Front. Plant Sci. 7:1815. doi: 10.3389/fpls.2016.01815

INTRODUCTION

The panicoid grasses sugarcane (*Saccharum officinarum*), sorghum (*Sorghum bicolor*), switchgrass (*Panicum virgatum*), and miscanthus (*Miscanthus X giganteum*) provide the majority of soluble sugars and lignocellulosic biomass used for food and biofuel production worldwide (Somerville et al., 2010; Waclawovsky et al., 2010). A closely related grass with a smaller genome, *Setaria viridis*, is used as a model for these crops in photosynthesis research and for the study of biomass generation and sugar accumulation (Li and Brutnell, 2011; Bennetzen et al., 2012; Brutnell et al., 2015; Martin et al., 2016). The mechanisms that regulate cell expansion and photoassimilate delivery in

the stems of these grasses are of interest because they influence the yields of soluble sugars and cell wall biomass produced (Byrt et al., 2011).

Grass stems have repeating units consisting of an internode positioned between two nodes that grow from intercalary meristems at the base; sugar, primarily sucrose, accumulates and is stored in mature cells at the top of the internode (Grof et al., 2013). Along this developmental gradient there is also a transition from synthesis and deposition of primary cell walls through to establishment of thicker secondary cell walls. Sucrose that is not used for growth and maintenance is primarily accumulated intracellularly in the vacuoles of storage parenchyma cells that surround the vasculature (Glasziou and Gayler, 1972; Hoffmann-Thoma et al., 1996; Rae et al., 2005) or in the apoplasm (Tarpley et al., 2007). The mature stems of grasses such as sugarcane can accumulate up to 1M sucrose, with up to 428 mM sucrose stored in the apoplasm (Hawker, 1985; Welbaum and Meinzer, 1990). In addition to a high capacity for soluble sugar storage, carbohydrates are also stored in cell walls of stem parenchyma cells (Botha and Black, 2000; Ermawar et al., 2015; Byrt et al., 2016a).

Historically, increases in sugar yields in the stems of panicoid grasses have been achieved by increasing sugar concentration in stem cells without increasing plant size (McCormick et al., 2009). Sugarcane and sorghum stem sugar content has been increased by years of selecting varieties with the highest culm sucrose content, but these gains have begun to plateau (Grof and Campbell, 2001; Pfeiffer et al., 2010). It may be that we are approaching a physiological ceiling that limits the potential maximum sucrose concentration in the stems of these grasses. Increasing the size of grass stems as a sink may be an effective strategy to increase stem biomass and the potential for greater soluble sugar yield as a relationship exists between stem size and capacity to import and accumulate photoassimilates (sink strength) as soluble sugars or cell wall carbohydrates. Hence, improved stem sugar yields have also been achieved in some sorghum hybrids by expanding stem volume through increased plant height and stem diameter (Pfeiffer et al., 2010; Slewinski, 2012).

In elongating stems, water and dissolved photoassimilates are imported from the phloem into the stem by bulk-flow, or translocation, to drive cell expansion or otherwise be used for growth, development and storage (Schmalstig and Cosgrove, 1990; Wood et al., 1994). In non-expanding storage sinks, water delivering sucrose is likely to be effluxed to the apoplasm and then recycled into the xylem transportation stream to be exported to other tissues (Lang and Thorpe, 1989; Lang, 1990). In addition to vacuolar accumulation of sugars delivered for storage, sugars may also accumulate in the apoplasm with apoplasmic barriers preventing leakage back into the vasculature (Moore, 1995; Patrick, 1997).

The flow of water from the phloem into growth and storage sinks involves the diffusion of water across plant cell membranes facilitated by aquaporins (Kaldenhoff and Fischer, 2006; Zhang et al., 2007). Aquaporins are a highly conserved family of transmembrane channel proteins that enable plants to rapidly and reversibly alter their membrane water permeability or permeability to other solutes depending on the isoform. In maize (*Zea mays*) and rice (*Oryza sativa*) genomes 30–70 aquaporin homologs have been identified, respectively (Chaumont et al., 2001; Sakurai et al., 2005). These large numbers of isoforms can be divided into five sub-families by sequence homology; plasma membrane intrinsic proteins (PIPs), tonoplast intrinsic proteins (TIPs), nodulin-like intrinsic proteins (NIPs), and small basic intrinsic proteins (SIPs; Johanson and Gustavsson, 2002). In dicotyledonous plants but not monocotyledonous plants there is also a group referred to as X intrinsic proteins (XIPs; Danielson and Johanson, 2008).

As aquaporins have important roles in controlling water potential, they are prospective targets for manipulating stem biomass and sugar yields (Maurel, 1997). The crucial role of aquaporins in water delivery to expanding tissues and water recycling in mature tissues is indicated by their high expression in these regions (Barrieu et al., 1998; Chaumont et al., 1998; Wei et al., 2007). Here, we explore the transcriptional regulation of aquaporins in meristematic, expanding, transitional and mature *S. viridis* internodal tissues to identify candidate water channels involved in cell expansion and water recycling after sugar delivery in mature internode tissues.

MATERIALS AND METHODS

Phylogenetic Tree

Setaria viridis aquaporins were identified from *S. italica* (Azad et al., 2016), *Arabidopsis* (Johanson et al., 2001), rice (Sakurai et al., 2005), barley (Hove et al., 2015) and maize (Chaumont et al., 2001) aquaporins, and predicted *S. viridis* aquaporins from transcriptomic data (Martin et al., 2016) (Supplementary Table S1) using the online HMMER tool phmmer (Finn et al., 2015[1]). Protein sequences used to generate the phylogenetic tree were obtained for *S. viridis* and *Z. mays* from Phytozome 11.0.5 (*S. viridis* v1.1, DOE-JGI[2]; last accessed July 19, 2016) (Supplementary Table S2). The phylogenetic tree was generated using the neighbor-joining method in the Geneious Tree Builder program (Geneious 9.0.2).

Elongating Internode Transcriptome Analysis and Aquaporin Candidate Selection

Expression data on identified *S. viridis* aquaporins was obtained from a transcriptome generated from *S. viridis* internode tissue (Martin et al., 2016). Protein sequences of selected putative aquaporin candidates expressed in the elongating *S. viridis* transcriptome were analyzed by HMMscan (Finn et al., 2015[1]).

Plant Growth Conditions

Seeds of *S. viridis* (Accession-10; A10) were grown in 2 L pots, two plants per pot, in a soil mixture that contained one part

[1]http://www.ebi.ac.uk/Tools/hmmer/

[2]http://phytozome.jgi.doe.gov/

coarse river sand, one part perlite, and one part coir peat. The temperatures in the glasshouse, located at the University of Newcastle (Callaghan, NSW, Australia) were 28°C during the day (16 h) and 20°C during the night (8 h). The photoperiod was artificially extended from 5 to 8 am and from 3 to 9 pm by illumination with 400 W metal halide lamps suspended ∼40 cm above the plant canopy. Water levels in pots were maintained with an automatic irrigation system that delivered water to each pot for 2 min once a day. Osmocote® exact slow release fertilizer (Scotts Australia Pty Ltd, Sydney, NSW, Australia) was applied at 20 g per pot, 2 weeks post-germination. Additional fertilization was applied using Wuxal® liquid foliar nutrient and Wuxal® calcium foliar nutrient (AgNova Technologies, Box Hill North, VIC, Australia) alternately each week.

Harvesting Plant Tissues, RNA Extraction, and cDNA Library Synthesis

Harvesting of plant material from a developing internode followed Martin et al. (2016). Total RNA was isolated from plant material ground with mortar and pestle cooled with liquid nitrogen, using Trizol® Reagent (Thermo Fisher Scientific, Scoresby, VIC, Australia) as per manufacturer's instruction. Genomic DNA was removed using an Ambion TURBO DNase Kit (Thermo Fisher Scientific) following the manufacturer's instructions. cDNA was synthesized from 230 ng of isolated RNA from the cell expansion, transitional, and maturing developmental zones as described in Martin et al. (2016) using the Superscript III cDNA synthesis kit (Thermo Fisher Scientific) with an oligo d(T) primer and an extension temperature of 50°C as per the manufacturer's instructions.

Reverse-Transcriptase Quantitative PCR (RT-qPCR)

Reverse-transcriptase-qPCR was performed using a Rotor-Gene Q (QIAGEN, Venlo, Netherlands) and GoTaq® Green Master Mix 2x (Promega, Madison, WI, USA). A two-step cycling program was used following the manufacturer's instructions. The green channel was used for data acquisition. Gene expression of the candidate genes was measured as relative to the housekeeper *S. viridis PP2A* (*SvPP2A*; accession no.: Sevir.2G128000). The *PP2A* gene was selected as a housekeeper gene because it is established as a robust reference gene in many plant species (Czechowski et al., 2005; Klie and Debener, 2011; Bennetzen et al., 2012) and it was consistently expressed across the developmental internode gradient in the transcriptome and cDNA libraries (Martin et al., 2016; Supplementary Figure S1). The forward (F) and reverse (R) primers used for RT-qPCR for were: SvPIP2;1-F (5′-CTCTACATCGTGGCGCAGT-3′) and SvPIP2;1-R (5′–ACGAAGGTGCCGATGATCT-3′), and SvNIP2;2-F (5′–AGTTCACGGGAGCGATGT- 3′) and SvNIP2;2-R (5′–CTAACCCGGCCAACTCAC-3′). SvPIP2;1 and SvNIP2;2 primer sets amplified 161 and 195 base pair fragments from the CDS, respectively. SvPP2A primer set sequences were SvPP2A-F (5′–GGCAACAAGAAGCTCACTCC-3′) and SvPP2A-R (5′-TTGCACATCAATGGAATCGT-3′) and amplified a 164 base pair fragment from the 3′UTR.

Gene Co-expression Network Analysis

Raw FPKM values of putative aquaporins and sugar transporters were extracted from the *S. viridis* elongating internode transcriptome (Martin et al., 2016). Putative *S. viridis* sugar transporters from the Sucrose Transporter (SUT), Sugar Will Eventually be Exported Transporter (SWEET), and Tonoplast Monosaccharide Transporter (TMT) families were identified by homology to rice SUT, SWEET, and TMT genes (Supplementary Table S3; Supplementary Figures S2–S4). FPKM values were normalized by Log_2 transformation and Pearson's correlation coefficients calculated by Metscape (Karnovsky et al., 2012). A gene network was generated for Pearson's correlation coefficients between 0.8 and 1.0 and visualized with the Metscape app in Cytoscape v3.4.0. Significance of Pearson's correlation coefficients were calculated using SPSS (IBM Corp. Released 2013. IBM SPSS Statistics for Windows, Version 22.0. Armonk, NY, USA) (Supplementary Table S4). The 1.5Kb 5′ promoter region, directly upstream of the transcriptional start site, of the two aquaporin candidates and the highly correlated putative sugar transporter genes were screened for the presence of *cis*-acting regulatory elements registered through the PlantCARE online database (Lescot et al., 2002[3]) and *cis*-acting elements of *Arabidopsis* and rice SUT genes reported by Ibraheem et al. (2010).

Photometric Swelling Assay

Extracted consensus coding sequences for *SvPIP2;1* and *SvNIP2;2*, from *S. viridis* transcriptome data (Martin et al., 2016), were synthesized commercially by GenScript (Piscataway, NJ, USA). *SvPIP2;1* and *SvNIP2;2* cDNA fragments were inserted into a gateway enabled pGEMHE vector. pGEMHE constructs were linearized using NheI (New England Biolabs, Ipswich, MA, USA) and purified using the MinElute PCR Purification Kit (QIAGEN). Complimentary RNA (cRNA) for *SvPIP2;1* and *SvNIP2;2* was transcribed using the Ambion mMessage mMachine Kit (Life Technologies, Carlsbad, CA, USA).

Xenopus laevis oocytes were injected with 46 ng of *SvPIP2;1* or *SvNIP2;2* cRNA in 46 μL of water, or 46 μL of water alone as a control. Injected oocytes were incubated for 72 h in Ca-Ringer's solution. Prior to undertaking permeability assays oocytes were transferred into ND96 solution pH 7.4 (96 mM NaCl, 2 mM KCl, 1.8 mM $CaCl_2$, 1 mM $MgCl_2$, 500 $\mu g.mL^{-1}$ Streptomycin, 500 $\mu g.mL^{-1}$ Tetracycline; 204 osmol/L) and allowed to acclimate for 30 min. Oocytes were then individually transferred into a 1:5 dilution of ND96 solution (42 osmol/L), pH 7.4, and swelling was measured for 1 min for *SvPIP2;1* injected oocytes and 2 min for *SvNIP2;2* injected oocytes. Oocytes were viewed under a dissecting microscope (Nikon SMZ800 light microscope, Japan) at 2× magnification. The changes in volume were captured with a Vicam color camera (Pacific Communications, Australia) at 2× magnification and recorded with IC Capture 2.0 software (The Imagine Source, US) as AVI format video files. Images were acquired every 2.5 s for 2 min measurements and every 2 s for 1 min measurements. The osmotic permeability (P_f) was calculated for water injected

[3]http://bioinformatics.psb.ugent.be/webtools/plantcare/html/

and cRNA injected oocytes from the initial rate of change in relative volume $(dV_{rel}/dt)_I$ determined from the cross sectional area images captured assuming the oocytes were spherical:

$$P_f = \frac{V_i \times (dV_{rel}/dt)_i}{A_i \times V_w \times \Delta C_0},$$

Where V_i and A_i are the initial volume and area of the oocyte, respectively, V_w is the partial molar volume of water and ΔC_o is the change in external osmolality. The osmolality of each solution was determined using a Fiske® 210 Micro-Sample freezing point osmometer (Fiske, Norwood, MA, USA). pH inhibition of oocyte osmotic permeability was determined as above where oocytes where bathed in 1:5 diluted ND96 solution with the addition of 50 mM Na-Acetate, pH 5.6. Topological prediction models of SvPIP2;1 and SvNIP2;2 were generated in TMHMM[4] (Krogh et al., 2001) and TMRPres-2D (Spyropoulos et al., 2004) to assess potential mechanisms of pH gating.

RESULTS

Identification of Putative *Setaria viridis* Aquaporins

Previously published *S. viridis* elongating internode transcriptome data (Martin et al., 2016), and protein sequences of aquaporins identified in *Arabidopsis*, *S. italica*, barley, maize and rice were used to identify genes predicted to encode aquaporins that were highly expressed in stages of cell expansion and sugar accumulation. The nomenclature assigned to the putative aquaporins followed their relative homology to previously named maize aquaporins determined by phylogenetic analysis of protein sequences (Chaumont et al., 2001; **Figure 1**). *S. viridis* proteins separated as expected into the major aquaporin subfamilies referred to as PIPs, TIPs, NIPs, and SIPs. Within *S. viridis* 41 full length aquaporins were identified: 12 PIPs, 14 TIPs, 12 NIPs, and three SIPs. One predicted aquaporin identified in the genome, transcript Sevir.6G061300.1, has very high similarity to SvNIP5;3 (Sevir.6G06000.1) but may be a pseudogene as it has two large deletions in the transcript relative to SvNIP5;3. Sevir.6G061300.1 only encodes for two out of the typical six transmembrane domains characteristic of aquaporins, and no transcripts have been detected in any of the *S. viridis* RNA-seq libraries available through the Joint Genome Institute (JGI) Plant Gene Atlas Project (Grigoriev et al., 2011). Another truncated NIP-like transcript, Sevir.5G141800.1, was identified. It is predicted to encode a protein 112 amino acids in length with only two transmembrane domains. As it is unlikely to generate an individually functioning aquaporin it has not been named. However, unlike Sevir.6G061300.1, Sevir.5G141800.1 was included in the phylogenetic tree as it was shown to be highly expressed in several tissue types in *S. viridis* RNA-seq libraries available through the JGI Plant Gene Atlas Project (Grigoriev et al., 2011) and may be of interest to future studies of *Setaria* aquaporin-like genes.

[4]http://www.cbs.dtu.dk/services/TMHMM/

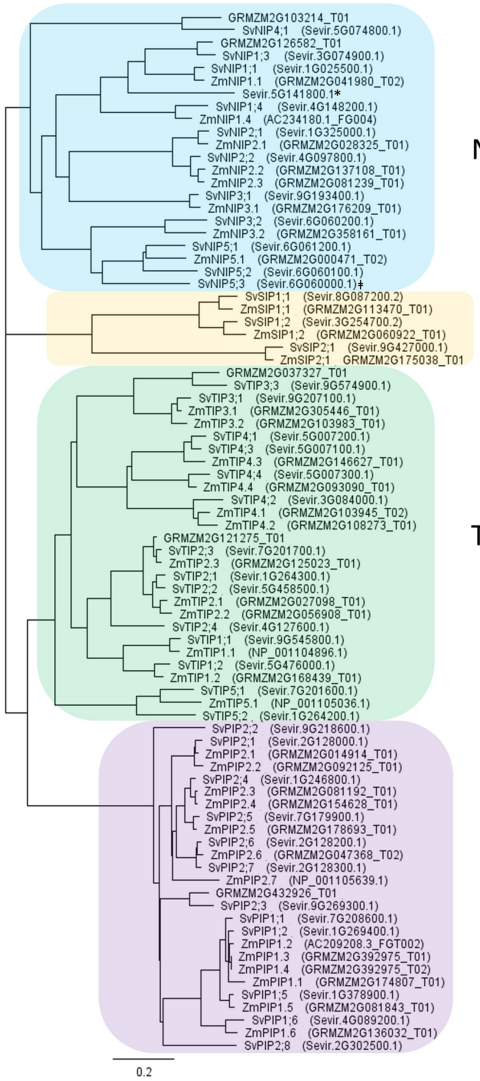

FIGURE 1 | Phylogenetic tree based on protein sequences of aquaporins from *Setaria viridis* and *Zea mays*. *S. viridis* aquaporins were identified in the genome via HMMER search using aquaporins sequences from *Arabidopsis*, barley, maize, and rice. Maize aquaporins were included in the phylogenetic tree for ease of interpretation. The addition of aquaporin sequences from other grasses did not change the groupings. Tree was generated by neighbor-joining method using the Geneious Tree Builder program, Geneious 9.0.2. The scale bar indicates the evolutionary distance, expressed as changes per amino acid residue. Aquaporins can be grouped into four subfamilies: PIPs (plasma membrane intrinsic proteins), TIPs (tonoplast intrinsic proteins), NIPs (nodulin-like intrinsic proteins), and SIPs (small basic intrinsic proteins). *Sevir.5G141800.1 protein sequence is truncated, 112 amino acids in length. ‡SvNIP5;3 (Sevir.6G06000.1) may have a related pseudogene Sevir.6G061300.1.

Analysis of *Setaria viridis* Aquaporin Transcripts in Stem Regions

We compared the relative transcript levels of putative *S. viridis* aquaporin encoding genes in the different developmental regions of an elongating internode (**Figure 2**). We observed that *SvPIP1;2*

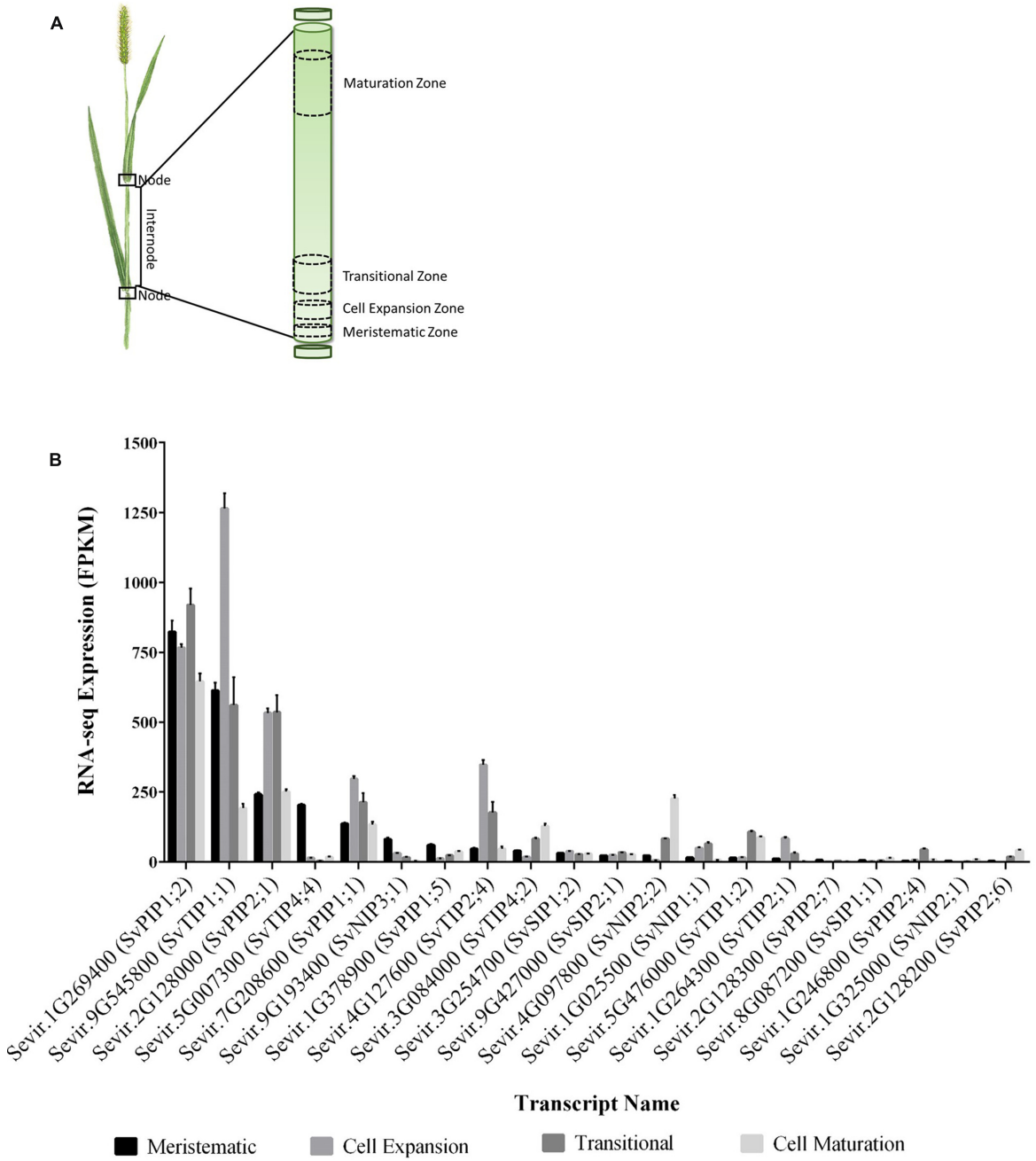

FIGURE 2 | Expression of putative aquaporins across the developmental zones of an elongating *S. viridis* internode. (A) Schematic of the developmental regions in an elongating internode of *S. viridis* as reported by Martin et al. (2016): meristematic zone, residing at the base of the internode, where cell division occurs; the cell expansion zone where cells undergo turgor driven expansion; transitional zone where cells begin to differentiate and synthesize secondary cell walls; and the maturation zone whereby expansion, differentiation and secondary cell wall synthesis cease and sugar is accumulated. **(B)** The expression profiles of putative *S. viridis* aquaporins, as identified by phylogeny to *Z. mays* aquaporins, were mined in the *S. viridis* elongating internode transcriptome (Martin et al., 2016). RNA-seq data is presented as mean FPKM ± SEM for four biological replicates from each developmental zone.

transcripts were abundant in all regions; and *SvTIP1;1* transcripts were also abundant, particularly in cell expansion regions. *SvPIP2;1*, *SvPIP1;1*, *SvTIP2;2*, and *SvTIP2;1* transcripts were detected in all regions with the highest transcript levels in cell expansion and transitional regions. Transcripts for *SvTIP4;4*, *SvNIP3;1*, and *SvPIP1;5* were highest in the meristem relative to other regions; whereas *SvTIP4;2*, *SvNIP2;2*, and *SvTIP1;2* transcripts were at their highest in transitional or mature regions. Low transcript levels were observed for *SvSIP1;2*, *SvNIP1;1*, and *SvPIP2;4* in all regions, with maximum transcripts for

SvNIP1;1 and *SvPIP2;4* detected in the transitional region, and very low transcript levels were detected for *SvPIP2;6*, *SvSIP1;1*, and *SvNIP2;1*.

Overall the highest aquaporin transcript levels detected across the internode developmental zones were those of *SvPIP1;2* (**Figure 2**). Previous research has indicated that the related ZmPIP1;2 interacts with PIP2 subgroup proteins targeting PIP2s to plasma membrane, and a number of PIP1 aquaporins are not associated with osmotic water permeability when expressed alone in oocytes (Fetter et al., 2004; Luu and Maurel, 2005; Zelazny et al., 2007). Our interest lay in identifying water permeable aquaporins that might be preferentially involved in delivering water to the growing stem cells and in sucrose accumulation in mature stem regions. As candidates *SvPIP2;1* and *SvNIP2;2* met these criteria we focussed on these two genes. *SvPIP2;1* had the high transcript levels in the region of cell expansion and transcript levels of *SvNIP2;2* were highest in mature stem regions (**Figure 2B**). The protein sequences of *SvPIP2;1* and *SvNIP2;2* were analyzed by the HMMER tool HMMscan which identified these candidates as belonging to the aquaporin (Major Intrinsic Protein) protein family.

To confirm our RNA-seq expression profile observations, we measured the transcript levels of *SvPIP2;1* and *SvNIP2;2* in the *S. viridis* internode regions by RT-qPCR. Stem samples were harvested from *S. viridis* plants grown under glasshouse conditions with the light period artificially supplemented by use of metal halide lamps to replicate as closely as possible the conditions used by Martin et al. (2016) for the RNA-seq analysis. We assessed the relative fold change of gene expression normalized to the cell expansion zone and similar trends were observed for the RT-qPCR expression data compared to the RNA-seq transcriptome data (**Figure 3**). *SvPIP2;1* transcript levels were high in the cell expansion region and decreased toward the maturation region and *SvNIP2;2* transcript levels were highest in mature stem tissues.

We are interested in the coordination of water and sugar transport related processes in developing grass stems. As a tool to investigate this, we further analyzed the stem transcriptome data to test whether any aquaporin and sugar transport related genes were co-expressed. Putative *S. viridis* sugar transporters were identified from the internode transcriptome (Martin et al., 2016) by homology to the rice sugar transporter families: SUTs, SWEETs, and TMTs (Supplementary Figures S2–S4). A co-expression gene network of the aquaporins and sugar transporters expressed in the *S. viridis* stem was generated in Cytoscape v3.4.0 using Pearson's correlation coefficients calculated by MetScape (Karnovsky et al., 2012) (**Figure 4**). This analysis revealed that for a number of aquaporins and sugar transport related genes there was a high correlation in expression: *SvPIP2;1* expression correlated with the expression of *SvPIP2;3*, *SvTIP2;1,* and *SvNIP1;1* (0.8–0.9); and the correlation coefficients for co-expression of *SvPIP2;1* with *SvPIP2;5*, *SvTIP4;1*, *SvTIP1;2*, and *SWEET1a* were in the range of 0.8–0.9. Most notable was the high correlation (0.95–1.0) of expression of *SvNIP2;2* with sugar transport related genes *SvSUT5*, *SvSUT1*, *SvSWEET4a* and with *SvTIP4;2* and *SvPIP2;6*. The correlation between expression of *SvNIP2;2* and *SvSWEET13b* and *SvSWEET16* was also high (0.9–0.95). The *cis*-acting regulatory elements of the promoter regions of the aquaporin candidates *SvNIP2;2* and *SvPIP2;1*, and the putative sugar transporter genes *SvSUT1*, *SvSUT5*, and *SvSWEET4a* were analyzed (Supplementary Figure S5). There was no obvious relationship between the correlation of expression of *SvNIP2;2* and *SvSUT1, SvSUT5* and *SvSWEET4a* and their *cis*-acting regulatory elements.

Characterisation of *Setaria viridis* PIP2;1 and NIP2;2 in *Xenopus laevis* Oocytes

To explore whether the proteins encoded by *SvPIP2;1* and *SvNIP2;2* function as water channels they were expressed in the heterologous *X. laevis* oocytes system. Water with or without 46 ng of *SvPIP2;1* and *SvNIP2;2* cRNA was injected into oocytes and the swelling of these oocytes in response to bathing in a hypo-osmotic solution (pH 7.4) was measured (**Figure 5A**). The osmotic permeability (P_f) of cRNA injected oocytes was calculated and compared to the osmotic permeability of water injected oocytes. Water injected oocytes had a P_f of $0.60 \pm 0.08 \times 10^{-2}$ mm s^{-1}. Relative to water injected control oocytes *SvPIP2;1* and *SvNIP2;2* cRNA injected oocytes had significantly higher P_f of $14.13 \pm 1.66 \times 10^{-2}$ mm s^{-1} and $3.22 \pm 0.28 \times 10^{-2}$ mm s^{-1}, respectively ($p < 0.05$).

The effect of lowering oocyte cytosolic pH was determined by bathing oocytes in an external hypo-osmotic solution at pH 5.6 with the addition of Na-Acetate (**Figure 5B**). Reduced osmotic permeability of the cRNA injected oocyte membrane was observed in response to the low pH treatment. A reduction in P_f was observed for *SvPIP2;1* and *SvNIP2;2* cRNA injected oocytes bathed in an external hypo-osmotic solution at pH 5.6 relative to the pH 7.4 solution indicating that SvPIP2;1 and SvNIP2;2 have pH gating mechanisms (**Figure 5B**). Water injected oocytes in the pH 5.6 Na-Acetate solution had P_f of $0.84 \pm 0.13 \times 10^{-2}$ mm s^{-1}. *SvNIP2;2* and *SvPIP2;1* cRNA injected oocytes in the pH 5.6 solution had significantly lower P_f of $2.46 \pm 0.32 \times 10^{-2}$ mm s^{-1} and $0.97 \pm 0.13 \times 10^{-2}$ mm s^{-1}, respectively, compared to those in pH 7.4 solution ($p < 0.05$). SvPIP2;1 and SvNIP2;2 associated osmotic permeability and pH gating observations indicate that these proteins can function as water channels. The mechanism of pH gating for other plant aquaporins is the protonation of a Histidine residue in the Loop D structure; topological modeling of SvPIP2;1 and SvNIP2;2 predicted that the Loop D of SvPIP2;1 contains a Histidine residue while SvNIP2;2 Loop D does not contain a His residue (Supplementary Figure S6).

DISCUSSION

Roles of Aquaporins in Grass Stem Development

On the basis of amino acid sequence comparison with known aquaporins in *Arabidopsis*, rice and maize, the genomes of sugarcane, sorghum and *S. italica* include 42, 41, and 42 predicted aquaporin encoding genes, respectively (da Silva et al., 2013; Reddy et al., 2015; Azad et al., 2016). In *S. viridis* 41 aquaporin encoding genes were identified that group into four clades

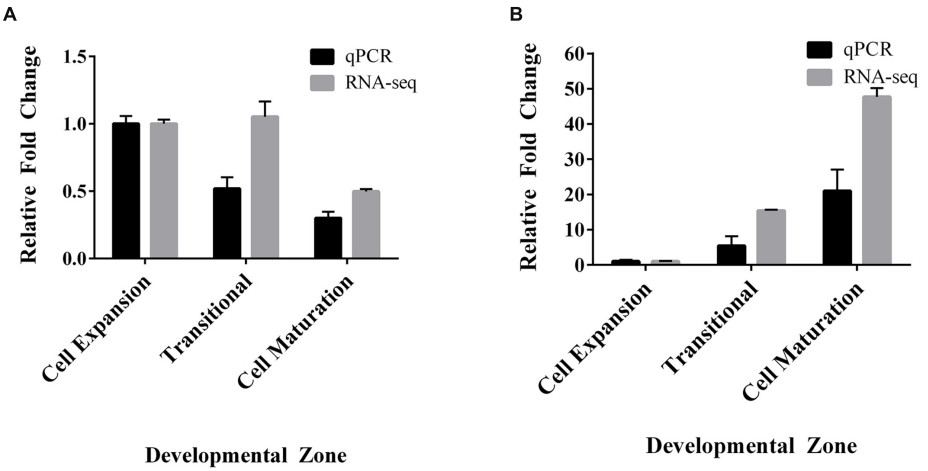

FIGURE 3 | Comparison of relative fold changes between RNA-seq and RT-qPCR of *SvPIP2;1* and *SvNIP2;2* in an elongating internode of S. viridis. (A) *SvPIP2;1*. **(B)** *SvNIP2;2*. Data is mean relative fold change in expression ± SEM. Data for RNA-seq and RT-qPCR was normalized relative to the cell expansion zone expression level.

corresponding to NIPs, TIPs, SIPs, and PIPs (**Figure 1**). We note that Azad et al. (2016) named the *Setaria* aquaporins in an order consecutive with where they are found in the genome. For ease of comparing related aquaporins in C_4 grasses of interest, we named the *Setaria* aquaporins based on their homology to previously named maize aquaporins (**Figure 1**) (Chaumont et al., 2001), of course high homology and the same name does not infer the same function. In the *S. viridis* elongating internode transcriptome, we detected transcripts for 19 putative aquaporin encoding genes, including 5 NIPs, 6 TIPs, 2 SIPs, and 6 PIPs (**Figures 2** and **3**; Martin et al., 2016). In mature *S. viridis* internode tissues, the transcript levels of TIPs and NIPs was generally low with the exception of *SvNIP2;2, SvTIP4;2,* and *SvTIP1;2.* In a sorghum stem transcriptome report investigating SWEET gene involvement in sucrose accumulation, we note that transcripts for all 41 sorghum aquaporins were detected in pith and rind tissues in 60-day-old plants (Reddy et al., 2015; Mizuno et al., 2016). Of those 41 aquaporins the expression of 16, primarily NIPs and TIPs, was relatively low. However, *PIP1;2, PIP2;1,* and *NIP2;2* homologs were all highly expressed in pith and rind of sorghum plants after heading, which is consistent with our findings for the *S. viridis* homologs of these genes (**Figure 2**; Mizuno et al., 2016). Comparisons with other gene expression studies for C_4 grass stem tissues were not possible as in most studies the internode tissue has not been separated into different developmental zones or the study has not reported aquaporin expression (Carson and Botha, 2000, 2002; Casu et al., 2007).

Relationships between Sink Strength, Sink Size, Water Flow, and the Function of Aquaporins

The molecular and physiological mechanisms that determine stem cell number and cell size in turn determine the capacity of the stem as a sink (Ho, 1988; Herbers and Sonnewald, 1998). Examples have been reported in the literature where stem volume and sucrose concentration has been increased, in sugarcane and sorghum, by increasing cell size (Slewinski, 2012; Patrick et al., 2013). Larger cell size may improve sink strength by increasing membrane surface area available to sucrose transport (increasing import capacity), increasing single cell capacity to accumulate greater concentrations of sucrose in parenchyma cell vacuoles due to increased individual cell volume (increasing storage capacity), and increasing lignocellulosic biomass.

Cell expansion and growth are highly sensitive to water potential. This is because expansion requires a continuous influx of water into the cell to maintain turgor pressure (Hsiao and Acevedo, 1974; Cosgrove, 1986, 2005). The diffusion of water across a plant cell membrane is facilitated by aquaporins (Kaldenhoff and Fischer, 2006). Aquaporins function throughout all developmental stages, but several PIP aquaporins have been found to be particularly highly expressed in regions of cell expansion (Chaumont et al., 1998; Maurel et al., 2008; Besse et al., 2011). Here, we report that in the *S. viridis* internode, *SvPIP2;1* was highly expressed in regions undergoing cell expansion (**Figure 2**). Positive correlations have been reported for the relationship between PIP mRNA and protein expression profiles of PIP isoforms in the expanding regions of embryos, roots, hypocotyls, leaves, and reproductive organs indicating that gene expression is a key mechanisms to regulate PIP function (Maurel et al., 2002; Hachez et al., 2008; Liu et al., 2008). Therefore, high expression of *SvPIP2;1* in the expanding zone of *S. viridis* internodes indicates that this gene may be involved in the process of water influx in this tissue to maintain turgor pressure for growth.

The roles of a number of PIP proteins in hydraulic conductivity in plant roots and leaves have been reported but PIP function in stems is largely unexplored. The regulation of the hydraulic properties of expanding root tissues by PIP expression was analyzed by Péret et al. (2012) and they reported

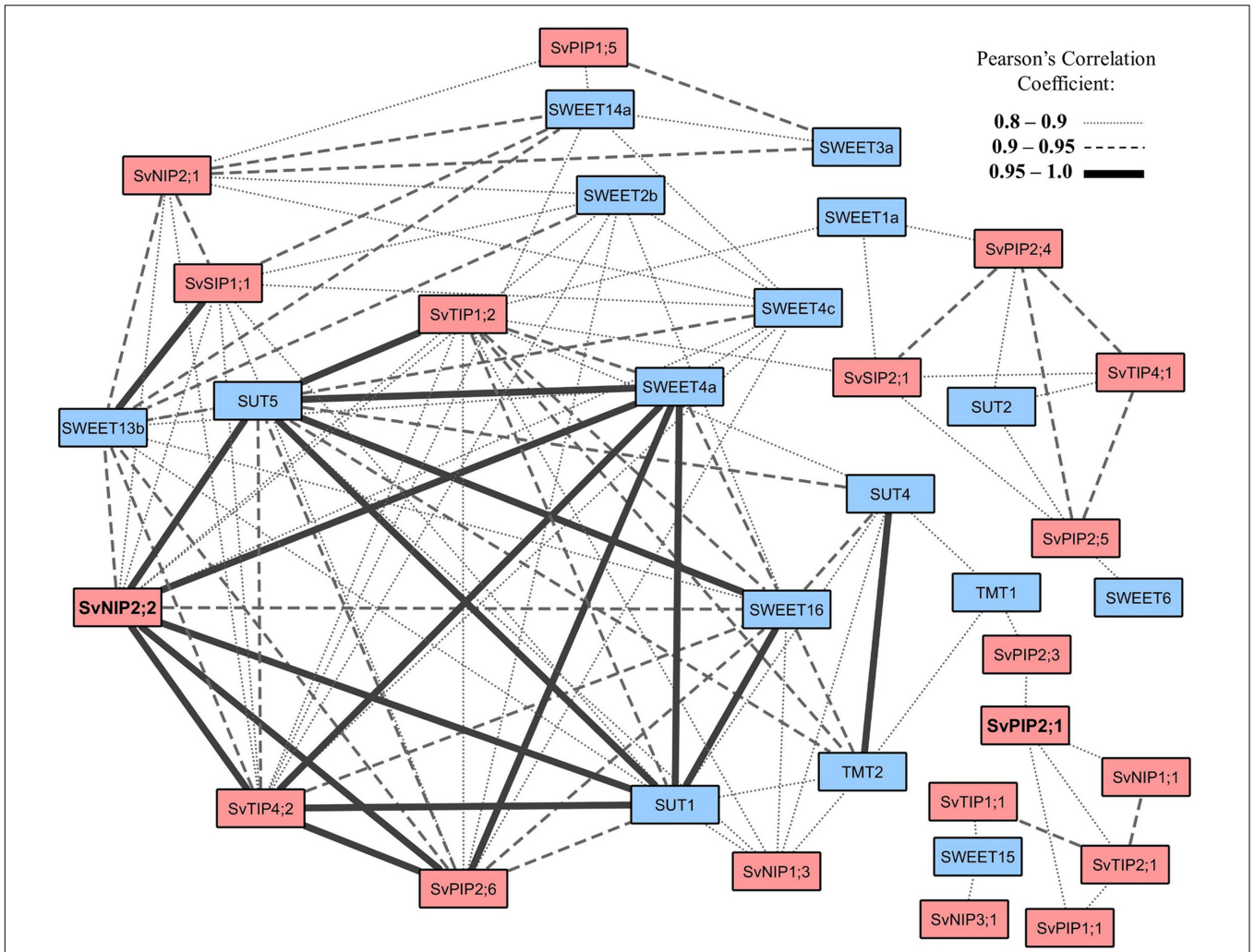

FIGURE 4 | Co-expression network of putative *S. viridis* aquaporin and sugar transporter genes identified in an elongating internode. The co-expressed gene network was generated from the stem specific aquaporins (**Figure 2**) and sugar transporters identified in the *S. viridis* elongating internode transcriptome reported by Martin et al. (2016). Raw FPKM values were Log_2 transformed and Pearson's correlation coefficients (0.8–1.0) were calculated in the MetScape app in Cytoscape v3.4.0. Sugar transporters in the *S. viridis* elongating internode were identified by homology to rice sugar transporter genes (Supplementary Figures S2–S4). Sugar transport related genes are color filled with blue and aquaporin genes with orange. *SvNIP2;2* and *SvPIP2;1* are in bold font.

that auxin mediated reduction of *Arabidopsis thaliana* (At) PIP gene expression resulted in delayed lateral root emergence. Previously *AtPIP2;2* anti-sense mutants were reported to have lower (25–30%) hydraulic conductivity of root cortex cells than control plants (Javot et al., 2003). PIP2 family aquaporins, involved in cellular water transport in roots have also been linked to water movement in leaves, seeds, and reproductive organs (Schuurmans et al., 2003; Bots et al., 2005). The roles of PIP proteins in maintenance of hydraulic conductivity and cell expansion in stems are likely to be equally as important as the roles reported for PIPs in the expanding tissues of roots and leaves. One study in rice reported OsPIP1;1 and OsPIP2;1 as being highly expressed in the zone of cell expansion in rapidly growing internodes (Malz and Sauter, 1999). Expression analysis of sugarcane genes associated with sucrose content identified that some unnamed PIP isoforms were highly expressed in immature internodes, and in high sugar yield cultivars (Papini-Terzi et al., 2009). Proteins from the PIP2 subfamily in particular in maize, spinach and *Arabidopsis* have been shown to be highly permeable to water (Johansson et al., 1998; Chaumont et al., 2000; Kaldenhoff and Fischer, 2006). Here, we demonstrate, by expression of SvPIP2;1 in *Xenopus* oocytes and analysis of water permeability, that this protein functions as a water channel (**Figure 5A**).

Aquaporin Function and Sugar Accumulation in Mature Grass Stems

The accumulation of sucrose to high concentrations in panicoid stems rapidly increases with the cessation of cell expansion, which is also associated with the deposition of secondary cell walls (Hoffmann-Thoma et al., 1996). In the mature regions of the stem internodes, imported sucrose is no longer required for

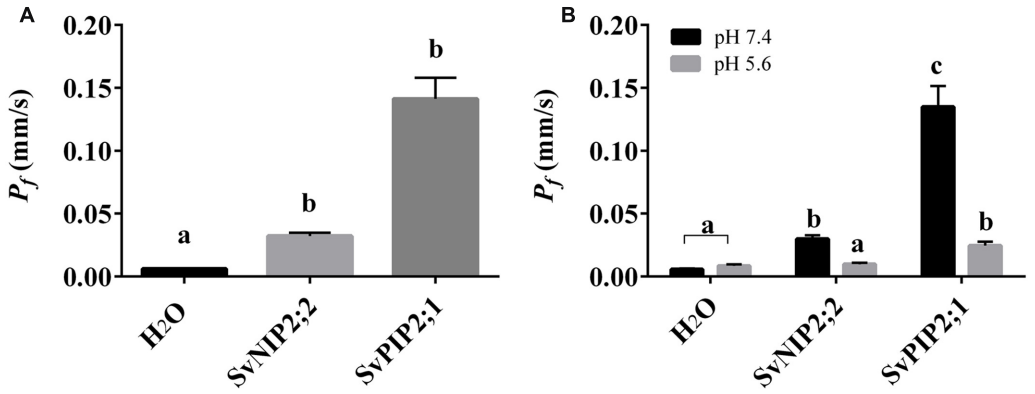

FIGURE 5 | Osmotic permeability (P_f) of *Xenopus laevis* oocytes injected with *SvNIP2;2* and *SvPIP2;1* cRNA. (A) Osmotic permeability (P_f) of water (H_2O) injected and *SvNIP2;2* and *SvPIP2;1* cRNA (46 ng) injected oocytes. Oocytes were transferred into a hypo-osmotic solution, pH 7.4, and P_f was calculated by video monitoring of the rate of oocyte swelling. **(B)** Effect of lowering oocyte cytosolic pH on osmotic permeability (P_f) of H_2O and *SvNIP2;2* and *SvPIP2;1* cRNA injected oocytes by bathing in hypo-osmotic solution supplemented with 50 mM Na-acetate, pH 5.6, $n = 12$–14; a = non-significant; b = $p < 0.05$; c = $p < 0.005$.

growth, development, or as a necessary precursor to structural elements and it is stored in the vacuoles of ground parenchyma cells or the apoplasm (Rae et al., 2009). Phloem unloading and the delivery of sucrose to these storage cells may occur via an apoplasmic pathway as in sorghum or a symplasmic pathway as in sugarcane (Welbaum and Meinzer, 1990; Walsh et al., 2005). The degree of suberisation and/or lignification of cell walls surrounding the phloem may influence stem sucrose storage traits by restricting apoplasmic pathways of sucrose transport. In potato tubers and *Arabidopsis* ovules a switch between apoplasmic and symplasmic pathways of delivering sucrose to storage sites has been reported (Viola et al., 2001; Werner et al., 2011). Similarly, a switch from symplasmic to apoplasmic transport pathways has been proposed for sorghum as internodes approach maturity (Tarpley et al., 2007; Milne et al., 2015). Both apoplasmic and symplasmic mechanisms of phloem unloading require the maintenance of low sugar concentration in the cytoplasm of parenchymal storage cells. Control of hydrostatic pressure is facilitated by the sequestration of sucrose into the vacuole by tonoplast localized SUTs or into the apoplasm by plasma membrane localized SUTs (Slewinski, 2011). Members of the SUT and TMT families have been shown to function on the tonoplast to facilitate sucrose accumulation in the vacuole (Reinders et al., 2008; Wingenter et al., 2010; Bihmidine et al., 2016). In mature stem tissue plasma membrane localized SWEETs, SUTs, and possibly some NIPs may have a role in transporting sugar into the apoplasm (Milne et al., 2013; Chen, 2014).

The cell maturation zone is characterized by cells that have ceased expansion and differentiation and have realized their sugar accumulation capacity (Rohwer and Botha, 2001; McCormick et al., 2009). In mature sink tissues, the movement of water and dissolved photoassimilates from the phloem to storage parenchyma cells may be driven by differences in solute concentration and hydrostatic pressure (Turgeon, 2010; De Schepper et al., 2013). However, the movement of water and sucrose by diffusion or bulk-flow requires the continued maintenance of low cytosolic sucrose concentrations by accumulation of sucrose into the vacuole or efflux into the apoplasm for storage (Grof et al., 2013). Throughout internode development, the internal cell pressure of storage parenchyma cells in sugarcane remains relatively constant despite increasing solute concentrations toward maturation (Moore and Cosgrove, 1991). As mature cells tend to have heavily lignified cell walls that limit the ability of the protoplast to expand in response to water flux the equilibration of storage parenchyma cell turgor is likely to be achieved by the partitioning of sucrose into the vacuole and apoplasm, and efflux of water into the apoplasm (Moore and Cosgrove, 1991; Vogel, 2008; Keegstra, 2010; Moore and Botha, 2013). Phloem water effluxed into the apoplasm may then be recycled back to the vascular bundles (Welbaum et al., 1992).

Members of the NIPs are candidates for water and neutral solute permeation, and some NIPs could have a role in water and solute efflux to the apoplasm in mature stem cells (Takano et al., 2006; Kamiya et al., 2009; Li et al., 2009; Hanaoka et al., 2014). The NIP subfamily is divided into the subgroups NIP I, NIP II, and NIP III based on the composition of the ar/R selectivity filter (Liu and Zhu, 2010). NIP III subgroup homologs have reported permeability to water, urea, boric acid, and silicic acid (Bienert et al., 2008; Ma et al., 2008; Ma and Yamaji, 2008; Li et al., 2009). In grasses NIP2;2 homologs, from the NIP III subgroup, have been shown to localize to the plasma membrane (Ma et al., 2006).

In the *S. viridis* internode, *SvNIP2;2* had relatively high transcript levels in mature stem tissue where sugar accumulates, and it can function as a water channel, although with a relatively low water permeability compared to SvPIP2;1 (**Figures 2** and **5A**). Our analysis of gene co-expression in stem tissues revealed high correlation between the expression of *SvNIP2;2* and five putative *S. viridis* sugar transporter genes (**Figure 4**). Co-expression can indicate that genes are controlled by the same transcriptional regulatory program, may be functionally related, or be members of the same pathway or protein complex (Eisen et al., 1998;

Yonekura-Sakakibara and Saito, 2013). The strong correlation between expression of *SvNIP2;2* and key putative sugar transport related genes such as *SvSUT5*, *SvSUT1*, *SvSWEET4a*, *SvSWEET13b*, and *SvSWEET16* indicates that they may be involved in a related biological process such as stem sugar accumulation. It is likely that one or more of the SWEETs have roles in transporting sugars out of the stem parenchyma cells into the apoplasm. SvNIP2;2 may be permeable to neutral solutes as well as water and the role of this protein in the mature stem could be in effluxing a solute to adjust osmotic pressure allowing for greater sugar storage capacity. The rice and soybean (*Glycine max* L.) NIP2;2 proteins are permeable to silicic acid and silicon, respectively (Ma et al., 2006; Zhao et al., 2010; Deshmukh et al., 2013). The deposition of silicic acid into the apoplasm, where it associates with the cell wall matrix as a polymer of hydrated amorphous silica (Epstein, 1994; Ma et al., 2004; Coskun et al., 2016), strengthens the culm to reduce lodging events, and increases plant resistance to pathogens and abiotic stress factors (Mitani, 2005).

SvNIP2;2 water permeability was gated by pH (**Figure 5B**). Gating of water channel activity has been reported for PIPs, including SvPIP2;1 (**Figure 5B**), and for the TIP2;1 isoform found in grapevine (Törnroth-Horsefield et al., 2006; Leitao et al., 2012; Frick et al., 2013). The mechanism of pH gating for these AQPs is the protonation of a Histidine residue located on the cytoplasmic Loop D where site-directed mutagenesis studies of the Loop D His residue results in a loss of pH dependent water permeability (Tournaire-Roux et al., 2002; Leitao et al., 2012; Frick et al., 2013). However, although SvNIP2;2 water permeability was pH dependent the predicted Loop D structure does not contain a His residue (Supplementary Figure S5), hence for SvNIP2;2 the mechanism for pH gating is not clear.

CONCLUSION

Our observations of high transcript levels of *SvPIP2;1* in expanding *S. viridis* stem regions and high transcript levels of *SvNIP2;2* in mature stems inspired us to test the function of the proteins encoded by these genes. We found that SvPIP2;1 and SvNIP2;2 can function as pH gated water channels. We hypothesize that in stem tissues SvPIP2;1 is involved in cell growth and that SvNIP2;2 may facilitate water movement and potentially the flow of other solutes into the apoplasm to sustain solute transportation by bulk-flow, and possibly 'recycle' water used for solute delivery back to the xylem. It is expected that SvPIP2;1 could have additional roles, as other PIP water channels have been shown to also be permeable to CO_2, hydrogen peroxide, urea, sodium and arsenic (Siefritz et al., 2001; Uehlein et al., 2003; Mosa et al., 2012; Bienert and Chaumont, 2014; Byrt et al., 2016b). SvNIP2;2 could have roles such as transporting neutral solutes to the apoplasm, as previous studies report silicic acid, urea, and boric acid permeability for other NIPS (Bienert et al., 2008; Ma et al., 2008; Ma and Yamaji, 2008; Li et al., 2009; Deshmukh et al., 2013). Transporting solutes other than sucrose into the apoplasm in mature stem tissues may be an important part of the processes that supports high sucrose accumulation capacity in grass stem parenchyma cells. The next steps in establishing the respective functions of SvPIP2;1 and SvNIP2;2 in stem growth and sugar accumulation in *S. viridis* will require testing of the permeability of these proteins to a range of other solutes and modification of their function *in planta*.

AUTHOR CONTRIBUTIONS

CG conceived and designed the work. SM, HO, LC, and JP acquired the data. SM, ST, CB, and CG analyzed and interpreted the data. SM and CB drafted and revised the work. All authors commented on the manuscript. SM, ST, RF, CB, and CG revised the work critically for intellectual content.

FUNDING

This research was supported by The Australian Research Council (ARC) Centre of Excellence in Plant Energy Biology (CE140100008) and CB (ARC DE150100837).

ACKNOWLEDGMENT

We thank Wendy Sullivan for preparation of oocytes. We thank Kate Hutcheon for advice on qPCR and Antony Martin for comments on early planning documents and cloning plans.

SUPPLEMENTARY MATERIAL

The Supplementary Material for this article can be found online at: http://journal.frontiersin.org/article/10.3389/fpls.2016.01815/full#supplementary-material

REFERENCES

Azad, A. K., Ahmed, J., Alum, A., Hasan, M., Ishikawa, T., Sawa, Y., et al. (2016). Genome-wide characterization of major intrinsic proteins in four grass plants and their non-aqua transport selectivity profiles with comparative perspective. *PLoS ONE* 11:e0157735. doi: 10.1371/journal.pone.0157735

Barrieu, F., Chaumont, F., and Chrispeels, M. J. (1998). High expression of the tonoplast aquaporin ZmTIP1 in epidermal and conducting tissues of maize. *Plant Physiol.* 117, 1153–1163. doi: 10.1104/pp.117.4.1153

Bennetzen, J. L., Schmutz, J., Wang, H., Percifield, R., Hawkins, J., Pontaroli, A. C., et al. (2012). Reference genome sequence of the model plant *Setaria*. *Nat. Biotechnol.* 30, 555–564. doi: 10.1038/nbt.2196

Besse, M., Knipfer, T., Miller, A. J., Verdeil, J.-L., Jahn, T. P., and Fricke, W. (2011). Developmental pattern of aquaporin expression in barley (*Hordeum vulgare* L.) leaves. *J. Exp. Bot.* 62, 4127–4142. doi: 10.1093/jxb/err175

Bienert, G. P., and Chaumont, F. (2014). Aquaporin-facilitated transmembrane diffusion of hydrogen peroxide. *Biochim. Biophys. Acta.* 1840, 1596–1604. doi: 10.1016/j.bbagen.2013.09.017

Bienert, G. P., Thorsen, M., Schüssler, M. D., Nilsson, H. R., Wagner, A., Tamás, M. J., et al. (2008). A subgroup of plant aquaporins facilitate the bi-directional

diffusion of As(OH)3 and Sb(OH)3 across membranes. *BMC Biol.* 6:26. doi: 10.1186/1741-7007-6-26

Bihmidine, S., Julius, B. T., Dweikat, I., and Braun, D. M. (2016). Tonoplast sugar transporters (SbTSTs) putatively control sucrose accumulation in sweet sorghum stems. *Plant Signal. Behav.* 11:e1117721. doi: 10.1080/15592324.2015.1117721

Botha, F. C., and Black, K. G. (2000). Sucrose phosphate synthase and sucrose synthase activity during maturation of internodal tissue in sugarcane. *Aust. J. Plant Physiol.* 27, 81–85.

Bots, M., Feron, R., Uehlein, N., Weterings, K., Kaldenhoff, R., and Mariani, T. (2005). PIP1 and PIP2 aquaporins are differentially expressed during tobacco anther and stigma development. *J. Exp. Bot.* 56, 113–121.

Brutnell, T. P., Bennetzen, J. L., and Vogel, J. P. (2015). Brachypodium distachyon and *Setaria viridis*: Model genetic systems for the grasses. *Annu. Rev. Plant Biol.* 66, 465–485. doi: 10.1146/annurev-arplant-042811-105528

Byrt, C. S., Betts, N. S., Tan, H.-T., Lim, W. L., Ermawar, R. A., Nguyen, H. Y., et al. (2016a). Prospecting for energy-rich renewable raw materials: sorghum stem case study. *PLoS ONE* 11:e0156638. doi: 10.1371/journal.pone.0156638

Byrt, C. S., Grof, C. P. L., and Furbank, R. T. (2011). C4 plants as biofuel feedstocks: optimising biomass production and feedstock quality from a lignocellulosic perspective. *J. Integr. Plant Biol.* 53, 120–135. doi: 10.1111/j.1744-7909.2010.01023.x

Byrt, C. S., Zhao, M., Kourghi, M., Bose, J., Henderson, S. W., Qiu, J., et al. (2016b). Non-selective cation channel activity of aquaporin AtPIP2;1 regulated by Ca^{2+} and pH. *Plant Cell Environ.* doi: 10.1111/pce.12832 [Epub ahead of print].

Carson, D., and Botha, F. (2002). Genes expressed in sugarcane maturing internodal tissue. *Plant Cell Rep.* 20, 1075–1081. doi: 10.1007/s00299-002-0444-1

Carson, D. L., and Botha, F. C. (2000). Preliminary analysis of expressed sequence tags for sugarcane. *Crop Sci.* 40:1769. doi: 10.2135/cropsci2000.4061769x

Casu, R. E., Jarmey, J. M., Bonnett, G. D., and Manners, J. M. (2007). Identification of transcripts associated with cell wall metabolism and development in the stem of sugarcane by Affymetrix GeneChip sugarcane genome array expression profiling. *Funct. Integr. Genomics* 7, 153–167. doi: 10.1007/s10142-006-0038-z

Chaumont, F., Barrieu, F., Herman, E. M., and Chrispeels, M. J. (1998). Characterization of a maize tonoplast aquaporin expressed in zones of cell division and elongation. *Plant Physiol.* 117, 1143–1152. doi: 10.1104/pp.117.4.1143

Chaumont, F., Barrieu, F., Jung, R., and Chrispeels, M. J. (2000). Plasma membrane intrinsic proteins from Maize cluster in two sequence subgroups with differential aquaporin activity. *Plant Physiol.* 122, 1025–1034. doi: 10.1104/pp.122.4.1025

Chaumont, F., Barrieu, F., Wojcik, E., Chrispeels, M. J., and Jung, R. (2001). Aquaporins constitute a large and highly divergent protein family in Maize. *Plant Physiol.* 125, 1206–1215. doi: 10.1104/pp.125.3.1206

Chen, L.-Q. (2014). SWEET sugar transporters for phloem transport and pathogen nutrition. *New Phytol.* 201, 1150–1155. doi: 10.1111/nph.12445

Cosgrove, D. (1986). Biophysical control of plant growth. *Ann. Rev. Plant Physiol.* 37, 377–405. doi: 10.1146/annurev.pp.37.060186.002113

Cosgrove, D. J. (2005). Growth of the plant cell wall. *Nat. Rev. Mol. Cell Biol.* 6, 850–861. doi: 10.1038/nrm1746

Coskun, D., Britto, D. T., Huynh, W. Q., and Kronzucker, H. J. (2016). The role of silicon in higher plants under salinity and drought stress. *Front. Plant Sci.* 7:1072. doi: 10.3389/fpls.2016.01072

Czechowski, T., Stitt, M., Altmann, T., Udvardi, M. K., and Scheible, W.-R. (2005). Genome-wide identification and testing of superior reference genes for transcript normalization in *Arabidopsis*. *Plant Physiol.* 139, 5–17. doi: 10.1104/pp.105.063743

da Silva, M. D., Silva, R. L. D. O., Costa Ferreira Neto, J. R., Guimarães, A. C. R., Veiga, D. T., Chabregas, S. M., et al. (2013). Expression analysis of Sugarcane aquaporin genes under water deficit. *J. Nucleic Acids* 2013, 1–14. doi: 10.1155/2013/763945

Danielson, J. Å, and Johanson, U. (2008). Unexpected complexity of the Aquaporin gene family in the moss Physcomitrella patens. *BMC Plant Biol.* 8:45. doi: 10.1186/1471-2229-8-45

De Schepper, V., De Swaef, T., Bauweraerts, I., and Steppe, K. (2013). Phloem transport: a review of mechanisms and controls. *J. Exp. Bot.* 64, 4839–4850. doi: 10.1093/jxb/ert302

Deshmukh, R. K., Vivancos, J., Guerin, V., Sonah, H., Labbe, C., Belzile, F., et al. (2013). Identification and functional characterization of silicon transporters in soybean using comparative genomics of major intrinsic proteins in *Arabidopsis* and rice. *Plant Mol. Biol.* 83, 303–315. doi: 10.1007/s11103-013-0087-3

Eisen, M. B., Spellman, P. T., Brown, P. O., and Botstein, D. (1998). Cluster analysis and display of genome-wide expression patterns. *Genetics* 95, 14863–14868.

Epstein, E. (1994). The anomaly of silicon in plant biology. *Proc. Natl. Acad. Sci. U.S.A.* 91, 11–17. doi: 10.1073/pnas.91.1.11

Ermawar, R. A., Collins, H. M., Byrt, C. S., Henderson, M., O'Donovan, L. A., Shirley, N. J., et al. (2015). Genetics and physiology of cell wall polysaccharides in the model C4 grass, *Setaria viridis* spp. *BMC Plant Biol.* 15:236. doi: 10.1186/s12870-015-0624-0

Fetter, K., Van Wilder, V., Moshelion, M., and Chaumont, F. (2004). Interactions between plasma membrane aquaporins modulate their water channel activity. *Plant Cell* 16, 215–228. doi: 10.1105/tpc.017194

Finn, R. D., Clements, J., Arndt, W., Miller, B. L., Wheeler, T. J., Schreiber, F., et al. (2015). HMMER web server: 2015 update. *Nucleic Acids Res.* 43, 30–38. doi: 10.1093/nar/gkv397

Frick, A., Järvå, M., and Törnroth-Horsefield, S. (2013). Structural basis for pH gating of plant aquaporins. *FEBS Lett.* 587, 989–993. doi: 10.1016/j.febslet.2013.02.038

Glasziou, K. T., and Gayler, K. R. (1972). Storage of sugars in stalks of sugar cane. *Bot. Rev.* 36, 471–488. doi: 10.1007/BF02859248

Grigoriev, I. V., Nordberg, H., Shabalov, I., Aerts, A., Cantor, M., Goodstein, D., et al. (2011). The genome portal of the department of energy joint genome institute. *Nucleic Acids Res.* 42, D26–D31.

Grof, C. P. L., Byrt, C. S., and Patrick, J. W. (2013). "Phloem transport of resources," in *Sugarcane: Physiology, Biochemistry, and Functional Biology*, eds P. Moore and F. Botha (Chichester: John Wiley & Sons Ltd), 267–305.

Grof, C. P. L., and Campbell, J. A. (2001). Sugarcane sucrose metabolism: scope for molecular manipulation. *Aust. J. Plant Physiol.* 28, 1–12.

Hachez, C., Heinen, R. B., Draye, X., and Chaumont, F. (2008). The expression pattern of plasma membrane aquaporins in maize leaf highlights their role in hydraulic regulation. *Plant Mol. Biol.* 68, 337–353. doi: 10.1007/s11103-008-9373-x

Hanaoka, H., Uraguchi, S., Takano, J., Tanaka, M., and Fujiwara, T. (2014). OsNIP3;1, a rice boric acid channel, regulates boron distribution and is essential for growth under boron-deficient conditions. *Plant J.* 78, 890–902. doi: 10.1111/tpj.12511

Hawker, J. S. (1985). "Sucrose," in *Biochemistry of Storage Carbohydrates in Green Plants*, eds P. Dey and R. Dixon (New York, NY: Academic Press), 1–51.

Herbers, K., and Sonnewald, U. (1998). Molecular determinants of sink strength. *Curr. Opin. Plant Biol.* 1, 207–216. doi: 10.1016/S1369-5266(98)80106-4

Ho, L. C. (1988). Metabolism and compartmentation of imported sugars in sink organs in relation to sink strength. *Ann. Rev. Plant Physiol.* 39, 355–378. doi: 10.1146/annurev.pp.39.060188.002035

Hoffmann-Thoma, G., Hinkel, K., Nicolay, P., and Willenbrink, J. (1996). Sucrose accumulation in sweet sorghum stem internodes in relation to growth. *Physiologia* 97, 277–284. doi: 10.1034/j.1399-3054.1996.970210.x

Hove, R. M., Ziemann, M., and Bhave, M. (2015). Identification and expression analysis of the barley (*Hordeum vulgare* L.) aquaporin gene family. *PLoS ONE* 10:e0128025. doi: 10.1371/journal.pone.0128025

Hsiao, T. C., and Acevedo, E. (1974). Plant responses to water deficits, water-use efficiency, and drought resistance. *Agric. Meteorol.* 14, 59–84. doi: 10.1016/0002-1571(74)90011-9

Ibraheem, O., Botha, C. E. J., and Bradley, G. (2010). In silico analysis of cis-acting regulatory elements in 5' regulatory regions of sucrose transporter gene families in rice (*Oryza sativa* Japonica) and *Arabidopsis thaliana*. *Comput. Biol. Chem.* 34, 268–283. doi: 10.1016/j.compbiolchem.2010.09.003

Javot, H., Lauvergeat, V., Santoni, V., Martin-Laurent, F., Güçlü, J., Vinh, J., et al. (2003). Role of a single aquaporin isoform in root water uptake. *Plant Cell* 15, 509–522. doi: 10.1105/tpc.008888

Johanson, U., and Gustavsson, S. (2002). A new subfamily of major intrinsic proteins in plants. *Mol. Biol. Evol* 19, 456–461. doi: 10.1093/oxfordjournals.molbev.a004101

Johanson, U., Karlsson, M., Johansson, I., Gustavsson, S., Sjö, S., Fraysse, L., et al. (2001). The complete set of genes encoding Major Intrinsic Proteins in *Arabidopsis* provides a framework for a new nomenclature for Major Intrinsic Proteins in plants. *Plant Physiol.* 126, 1358–1369. doi: 10.1104/pp.126.4.1358

Johansson, I., Karlsson, M., Shukla, V. K., Chrispeels, M. J., Larsson, C., and Kjellbom, P. (1998). Water transport activity of the plasma membrane aquaporin PM28A is regulated by phosphorylation. *Plant Cell* 10, 451–459. doi: 10.1105/tpc.10.3.451

Kaldenhoff, R., and Fischer, M. (2006). Functional aquaporin diversity in plants. *Biochim. Biophys. Acta-Biomembr.* 1758, 1134–1141. doi: 10.1016/j.bbamem.2006.03.012

Kamiya, T., Tanaka, M., Mitani, N., Ma, J. F., Maeshima, M., and Fujiwara, T. (2009). NIP1; 1, an aquaporin homolog, determines the arsenite sensitivity of *Arabidopsis thaliana*. *J. Biol. Chem.* 284, 2114–2120. doi: 10.1074/jbc.M806881200

Karnovsky, A., Weymouth, T., Hull, T., Tarcea, V. G., Scardoni, G., Laudanna, C., et al. (2012). Metscape 2 bioinformatics tool for the analysis and visualization of metabolomics and gene expression data. *Bioinforma. Orig. Pap.* 28, 373–380.

Keegstra, K. (2010). Plant cell walls. *Plant Physiol.* 154, 483–486. doi: 10.1104/pp.110.161240

Klie, M., and Debener, T. (2011). Identification of superior reference genes for data normalisation of expression studies via quantitative PCR in hybrid roses (Rosa hybrida). *BMC Res. Notes* 41:518.

Krogh, A., Larsson, B., von Heijne, G., and Sonnhammer, E. L. (2001). Predicting transmembrane protein topology with a hidden markov model: application to complete genomes. *J. Mol. Biol.* 305, 567–580. doi: 10.1006/jmbi.2000.4315

Lang, A. (1990). Xylem, phloem and transpiration flows in developing Apple fruits. *J. Exp. Bot.* 41, 645–651. doi: 10.1093/jxb/41.6.645

Lang, A., and Thorpe, M. R. (1989). Xylem, phloem and transpiration flows in a grape: application of a technique for measuring the volume of attached fruits to high resolution using archimedes'. *Principle. J. Exp. Bot.* 40, 1069–1078. doi: 10.1093/jxb/40.10.1069

Leitao, L., Prista, C., Moura, T. F., Loureiro-Dias, M. C., and Soveral, G. (2012). Grapevine aquaporins: gating of a tonoplast intrinsic protein (TIP2;1) by cytosolic pH. *PLoS ONE* 7:e33219. doi: 10.1371/journal.pone.0033219

Lescot, M., Déhais, P., Thijs, G., Marchal, K., Moreau, Y., Van De Peer, Y., et al. (2002). PlantCARE, a database of plant cis-acting regulatory elements and a portal to tools for in silico analysis of promoter sequences. *Nucleic Acids Res.* 30, 325–327. doi: 10.1093/nar/30.1.325

Li, P., and Brutnell, T. P. (2011). Setaria viridis and *Setaria italica*, model genetic systems for the Panicoid grasses. *J. Exp. Bot.* 62, 3031–3037. doi: 10.1093/jxb/err096

Li, R. Y., Ago, Y., Liu, W. J., Mitani, N., Feldmann, J., McGrath, S. P., et al. (2009). The rice aquaporin Lsi1 mediates uptake of methylated arsenic species. *Plant Physiol.* 150, 2071–2080. doi: 10.1104/pp.109.140350

Liu, D., Tu, L., Wang, L., Li, Y., Zhu, L., and Zhang, X. (2008). Characterization and expression of plasma and tonoplast membrane aquaporins in elongating cotton fibers. *Plant Cell Rep.* 27, 1385–1394. doi: 10.1007/s00299-008-0545-6

Liu, Q. P., and Zhu, Z. J. (2010). Functional divergence of the NIP III subgroup proteins involved altered selective constraints and positive selection. *BMC Plant Biol.* 10:256. doi: 10.1186/1471-2229-10-256

Luu, D. T., and Maurel, C. (2005). Aquaporins in a challenging environment: molecular gears for adjusting plant water status. *Plant Cell Environ.* 28, 85–96. doi: 10.1111/j.1365-3040.2004.01295.x

Ma, J. F., Mitani, N., Nagao, S., Konishi, S., Tamai, K., Iwashita, T., et al. (2004). Characterization of the silicon uptake system and molecular mapping of the silicon transporter gene in rice. *Plant Physiol.* 136, 3284–3289. doi: 10.1104/pp.104.047365

Ma, J. F., Tamai, K., Yamaji, N., Mitani, N., Konishi, S., Katsuhara, M., et al. (2006). A silicon transporter in rice. *Nature* 440, 688–691. doi: 10.1038/nature04590

Ma, J. F., and Yamaji, N. (2008). Functions and transport of silicon in plants. *Cell. Mol. Life Sci.* 65, 3049–3057. doi: 10.1007/s00018-008-7580-x

Ma, J. F., Yamaji, N., Mitani, N., Xu, X.-Y., Su, Y.-H., Mcgrath, S. P., et al. (2008). Transporters of arsenite in rice and their role in arsenic accumulation in rice grain. *Proc. Natl. Acad. Sci. U.S.A.* 105, 9931–9935. doi: 10.1073/pnas.0802361105

Malz, S., and Sauter, M. (1999). Expression of two PIP genes in rapidly growing internodes of rice is not primarily controlled by meristem activity or cell expansion. *Plant Mol. Biol.* 40, 985–995. doi: 10.1023/A:1006265528015

Martin, A. P., Palmer, W. M., Brown, C., Abel, C., Lunn, J. E., Furbank, R. T., et al. (2016). A developing *Setaria viridis* internode: an experimental system for the study of biomass generation in a C4 model species. *Biotechnol. Biofuels* 9, 1–12. doi: 10.1186/s13068-016-0457-6

Maurel, C. (1997). Aquaporins and water permeability of plant membranes. *Annu. Rev. Plant Physiol. Plant Mol. Biol.* 48, 399–429. doi: 10.1146/annurev.arplant.48.1.399

Maurel, C., Javot, H., Lauvergeat, V., Gerbeau, P., Tournaire, C., Santoni, V., et al. (2002). Molecular physiology of aquaporins in plants. *Int. Rev. Cytol.* 215, 105–148. doi: 10.1016/S0074-7696(02)15007-8

Maurel, C., Verdoucq, L., Luu, D.-T. T., and Santoni, V. (2008). Plant aquaporins: membrane channels with multiple integrated functions. *Annu. Rev. Plant Biol.* 59, 595–624. doi: 10.1146/annurev.arplant.59.032607.092734

McCormick, A. J., Watt, D. A., and Cramer, M. D. (2009). Supply and demand: sink regulation of sugar accumulation in sugarcane. *J. Exp. Bot.* 60, 357–364. doi: 10.1093/jxb/ern310

Milne, R. J., Byrt, C. S., Patrick, J. W., and Grof, C. P. L. (2013). Are sucrose transporter expression profiles linked with patterns of biomass partitioning in Sorghum phenotypes? *Front. Plant Sci.* 4:223. doi: 10.3389/fpls.2013.00223

Milne, R. J., Offler, C. E., Patrick, J. W., and Grof, C. P. L. (2015). Cellular pathways of source leaf phloem loading and phloem unloading in developing stems of Sorghum bicolor in relation to stem sucrose storage. *Funct. Plant Biol.* 42, 957–970. doi: 10.1071/FP15133

Mitani, N. (2005). Uptake system of silicon in different plant species. *J. Exp. Bot.* 56, 1255–1261. doi: 10.1093/jxb/eri121

Mizuno, H., Kasuga, S., and Kawahigashi, H. (2016). The sorghum SWEET gene family: stem sucrose accumulation as revealed through transcriptome profiling. *Biotechnol. Biofuels* 9, 1–12. doi: 10.1186/s13068-016-0546-6

Moore, P. H. (1995). Temporal and spatial regulation of sucrose accumulation in the sugarcane stem. *Aust. J. Plant Physiol* 22, 661–679. doi: 10.1071/PP9950661

Moore, P. H., and Botha, F. C. (2013). *Sugarcane: Physiology, Biochemistry and Functional Biology*. Hoboken, NJ: John Wiley & Sons.

Moore, P. H., and Cosgrove, D. J. (1991). Developmental changes in cell and tissue water relations parameters in storage parenchyma of sugarcane. *Plant Physiol.* 96, 794–801. doi: 10.1104/pp.96.3.794

Mosa, K. A., Kumar, K., Chhikara, S., Mcdermott, J., Liu, Z. J., Musante, C., et al. (2012). Members of rice plasma membrane intrinsic proteins subfamily are involved in arsenite permeability and tolerance in plants. *Transgenic Res.* 21, 1265–1277. doi: 10.1007/s11248-012-9600-8

Papini-Terzi, F. F. S., Rocha, F. R. F., Vencio, R. R. Z., Felix, J. J. M., Branco, D. S., Waclawovsky, A. J. A., et al. (2009). Sugarcane genes associated with sucrose content. *BMC Genomics* 10:120. doi: 10.1186/1471-2164-10-120

Patrick, J. W. (1997). Phloem unloading: Sieve element unloading and post-sieve element transport. *Annu. Rev. Plant Physiol. Plant Mol. Biol.* 48, 191–222. doi: 10.1146/annurev.arplant.48.1.191

Patrick, J. W., Botha, F. C., and Birch, R. G. (2013). Metabolic engineering of sugars and simple sugar derivatives in plants. *Plant Biotechnol. J.* 11, 142–156. doi: 10.1111/pbi.12002

Péret, B., Li, G., Zhao, J., Band, L. R., Voß, U., Postaire, O., et al. (2012). Auxin regulates aquaporin function to facilitate lateral root emergence. *Nat. Cell Biol.* 14, 991–998. doi: 10.1038/ncb2573

Pfeiffer, T. W., Bitzer, M. J., Toy, J. J., and Pedersen, J. F. (2010). Heterosis in sweet sorghum and selection of a new sweet sorghum hybrid for use in syrup production in appalachia. *Crop Sci.* 50, 1788–1794. doi: 10.2135/cropsci2009.09.0475

Rae, A. L., Grof, C. P. L., and Casu, R. E. (2005). Sucrose accumulation in the sugarcane stem: pathways and control points for transport and compartmentation. *Field Crop. Res.* 92, 159–168. doi: 10.1016/j.fcr.2005.01.027

Rae, A. L., Jackson, M. A., Nguyen, C. H., and Bonnett, G. D. (2009). Functional specialization of vacuoles in sugarcane leaf and stem. *Trop. Plant Biol.* 2, 13–22. doi: 10.1007/s12042-008-9019-9

Reddy, P. S., Rao, T. S. R. B., Sharma, K. K., and Vadez, V. (2015). Genome-wide identification and characterization of the aquaporin gene family in *Sorghum bicolor* (L.). *Plant Gene* 1, 18–28. doi: 10.1016/j.plgene.2014.12.002

Reinders, A., Sivitz, A. B., Starker, C. G., Gantt, J. S., and Ward, J. M. (2008). Functional analysis of LjSUT4, a vacuolar sucrose transporter from *Lotus japonicus*. *Plant Mol. Biol.* 68, 289–299. doi: 10.1007/s11103-008-9370-0

Rohwer, J. M., and Botha, F. C. (2001). Analysis of sucrose accumulation in the sugar cane culm on the basis of in vitro kinetic data. *Biochem. J.* 358, 437–445. doi: 10.1042/bj3580437

Sakurai, J., Ishikawa, F., Yamaguchi, T., Uemura, M., and Maeshima, M. (2005). Identification of 33 rice aquaporin genes and analysis of their expression and function. *Plant Cell Physiol.* 46, 1568–1577. doi: 10.1093/pcp/pci172

Schmalstig, J. G., and Cosgrove, D. J. (1990). Coupling of solute transport and cell expansion in pea stems. *Plant Physiol.* 94, 1625–1633. doi: 10.1104/pp.94.4.1625

Schuurmans, J. A. M., van Dongen, J. T., Rutjens, B. P. W., Boonman, A., Pieterse, C. M. J., and Borstlap, A. C. (2003). Members of the aquaporin family in the developing pea seed coat include representatives of the PIP, TP and NIP subfamilies. *Plant Mol. Biol.* 53, 655–667. doi: 10.1023/B:PLAN.0000019070.60954.77

Siefritz, F., Biela, A., Eckert, M., Otto, B., Uehlein, N., and Kaldenhoff, R. (2001). The tobacco plasma membrane aquaporin NtAQP1. *J. Exp. Bot.* 52, 1953–1957. doi: 10.1093/jexbot/52.363.1953

Slewinski, T. L. (2011). Diverse functional roles of monosaccharide transporters and their homologs in vascular plants: a physiological perspective. *Mol. Plant* 4, 641–662. doi: 10.1093/mp/ssr051

Slewinski, T. L. (2012). Non-structural carbohydrate partitioning in grass stems: a target to increase yield stability, stress tolerance, and biofuel production. *J. Exp. Bot.* 63, 4647–4670. doi: 10.1093/jxb/ers124

Somerville, C., Youngs, H., Taylor, C., Davis, S. C., and Long, S. P. (2010). Feedstocks for lignocellulosic biofuels. *Science*. 329, 790–792. doi: 10.1126/science.1189268

Spyropoulos, I. C., Liakopoulos, T. D., Bagos, P. G., and Hamodrakas, S. J. (2004). TMRPres2D: High quality visual representation of transmembrane protein models. *Bioinformatics* 20, 3258–3260. doi: 10.1093/bioinformatics/bth358

Takano, J., Wada, M., Ludewig, U., Schaaf, G., Von Wirén, N., and Fujiwara, T. (2006). The *Arabidopsis* major intrinsic protein NIP5; 1 is essential for efficient boron uptake and plant development under boron limitation. *Plant Cell* 18, 1498–1509. doi: 10.1105/tpc.106.041640

Tarpley, L., Vietor, D. M., Tarpley, L., Vietor, D., Miller, F., Guimarães, C., et al. (2007). Compartmentation of sucrose during radial transfer in mature sorghum culm. *BMC Plant Biol.* 7:33. doi: 10.1186/1471-2229-7-33

Törnroth-Horsefield, S., Wang, Y., Hedfalk, K., Johanson, U., Karlsson, M., Tajkhorshid, E., et al. (2006). Structural mechanism of plant aquaporin gating. *Nature* 439, 688–694. doi: 10.1038/nature04316

Tournaire-Roux, C., Sutka, M., Javot, H. H., Gout, E. E., Gerbeau, P., Luu, D.-T. T., et al. (2002). Cytosolic pH regulates root water transport during anoxic stress through gating of aquaporins. *Nature* 425, 187–194.

Turgeon, R. (2010). The puzzle of phloem pressure. *Plant Physiol.* 154, 578–581. doi: 10.1104/pp.110.161679

Uehlein, N., Lovisolo, C., Siefritz, F., and Kaldenhoff, R. (2003). The tobacco aquaporin NtAQP1 is a membrane CO_2 pore with physiological functions. *Nature* 425, 734–737. doi: 10.1038/nature02027

Viola, R., Roberts, A. G., Haupt, S., Gazzani, S., Hancock, R. D., Marmiroli, N., et al. (2001). Tuberization in potato involves a switch from apoplastic to symplastic phloem unloading. *Plant Cell* 13, 385–398. doi: 10.1105/tpc.13.2.385

Vogel, J. (2008). Unique aspects of the grass cell wall. *Curr. Opin. Plant Biol.* 11, 301–307. doi: 10.1016/j.pbi.2008.03.002

Waclawovsky, A. J., Sato, P. M., Lembke, C. G., Moore, P. H., and Souza, G. M. (2010). Sugarcane for bioenergy production: an assessment of yield and regulation of sucrose content. *Plant Biotechnol. J.* 8, 263–276. doi: 10.1111/j.1467-7652.2009.00491.x

Walsh, K. B., Sky, R. C., and Brown, S. M. (2005). The anatomy of the pathway of sucrose unloading within the sugarcane stalk. *Funct. Plant Biol.* 32, 367–374. doi: 10.1071/FP04102

Wei, W. X., Alexandersson, E., Golldack, D., Miller, A. J., Kjellborn, P. O., and Fricke, W. (2007). HvPIP1;6, a barley (*Hordeum vulgare* L.) plasma membrane water channel particularly expressed in growing compared with non-growing leaf tissues. *Plant Cell Physiol.* 48, 1132–1147. doi: 10.1093/pcp/pcm083

Welbaum, G. E., and Meinzer, F. C. (1990). Compartmentation of solutes and water in developing sugarcane stalk tissue. *Plant Physiol.* 93, 1147–1153. doi: 10.1104/pp.93.3.1147

Welbaum, G. E., Meinzer, F. C., Grayson, R. L., and Thornham, K. T. (1992). Evidence for the consequences of a barrier to solute diffusion between the apoplast and vascular bundles in sugarcane stalk tissue. *Funct. Plant Biol.* 19, 611–623.

Werner, D., Gerlitz, N., and Stadler, R. (2011). A dual switch in phloem unloading during ovule development in *Arabidopsis*. *Protoplasma* 248, 225–235. doi: 10.1007/s00709-010-0223-8

Wingenter, K., Schulz, A., Wormit, A., Wic, S., Trentmann, O., Hoermiller, I. I., et al. (2010). Increased activity of the vacuolar monosaccharide transporter TMT1 alters cellular sugar partitioning, sugar signaling, and seed yield in *Arabidopsis*. *Plant Physiol.* 154, 665–677. doi: 10.1104/pp.110.162040

Wood, R., Patrick, J. W., and Offler, C. E. (1994). The cellular pathway of short-distance transfer of photosynthates and potassium in the elongating stem of *Phaseolus vulgaris* L. Stem anatomy, solute transport and pool sizes. *Ann. Bot.* 73, 151–160. doi: 10.1006/anbo.1994.1018

Yonekura-Sakakibara, K., and Saito, K. (2013). Transcriptome coexpression analysis using ATTED-II for integrated transcriptomic/metabolomic analysis. *Methods Mol. Biol.* 1011, 317–326. doi: 10.1007/978-1-62703-414-2_25

Zelazny, E., Borst, J. W., Muylaert, M., Batoko, H., Hemminga, M. A., and Chaumont, F. (2007). FRET imaging in living maize cells reveals that plasma membrane aquaporins interact to regulate their subcellular localization. *Proc. Natl. Acad. Sci. U.S.A.* 104, 12359–12364. doi: 10.1073/pnas.0701180104

Zhang, W.-H., Zhou, Y., Dibley, K. E., Tyerman, S. D., Furbank, R. T., Patrick, J. W., et al. (2007). Nutrient loading of developing seeds. *Funct. Plant Biol.* 34, 314–331. doi: 10.1071/FP06271

Zhao, X. Q., Mitani, N., Yamaji, N., Shen, R. F., and Ma, J. F. (2010). Involvement of silicon influx transporter OsNIP2;1 in selenite uptake in rice. *Plant Physiol.* 153, 1871–1877. doi: 10.1104/pp.110.157867

Conflict of Interest Statement: The authors declare that the research was conducted in the absence of any commercial or financial relationships that could be construed as a potential conflict of interest.

Journal of Experimental Botany, Vol. 68, No. 2 pp. 299–310, 2017
doi:10.1093/jxb/erw357 Advance Access publication 4 October 2016
This paper is available online free of all access charges (see http://jxb.oxfordjournals.org/open_access.html for further details)

RESEARCH PAPER

Effects of reduced carbonic anhydrase activity on CO_2 assimilation rates in *Setaria viridis*: a transgenic analysis

Hannah L. Osborn[1], Hugo Alonso-Cantabrana[1,*], Robert E. Sharwood[1], Sarah Covshoff[2], John R. Evans[1], Robert T. Furbank[1] and Susanne von Caemmerer[1]

[1] Australian Research Council Centre of Excellence for Translational Photosynthesis, Division of Plant Sciences, Research School of Biology, The Australian National University, Acton, ACT 2601, Australia
[2] Department of Plant Sciences, University of Cambridge, Cambridge CB2 3EA, UK

* Correspondence: Hugo.Alonso@anu.edu.au

Received 19 July 2016; Accepted 5 September 2016

Editor: Christine Raines, University of Essex

Abstract

In C_4 species, the major β-carbonic anhydrase (β-CA) localized in the mesophyll cytosol catalyses the hydration of CO_2 to HCO_3^-, which phospho*enol*pyruvate carboxylase uses in the first step of C_4 photosynthesis. To address the role of CA in C_4 photosynthesis, we generated transgenic *Setaria viridis* depleted in β-CA. Independent lines were identified with as little as 13% of wild-type CA. No photosynthetic defect was observed in the transformed lines at ambient CO_2 partial pressure (pCO_2). At low pCO_2, a strong correlation between CO_2 assimilation rates and CA hydration rates was observed. $C^{18}O^{16}O$ isotope discrimination was used to estimate the mesophyll conductance to CO_2 diffusion from the intercellular air space to the mesophyll cytosol (g_m) in control plants, which allowed us to calculate CA activities in the mesophyll cytosol (C_m). This revealed a strong relationship between the initial slope of the response of the CO_2 assimilation rate to cytosolic pCO_2 (AC_m) and cytosolic CA activity. However, the relationship between the initial slope of the response of CO_2 assimilation to intercellular pCO_2 (AC_i) and cytosolic CA activity was curvilinear. This indicated that in *S. viridis*, mesophyll conductance may be a contributing limiting factor alongside CA activity to CO_2 assimilation rates at low pCO_2.

Key words: Carbonic anhydrase, $C^{18}O^{16}O$ isotope discrimination, C_4 photosynthesis, mesophyll conductance, *Setaria viridis*, transformation

Introduction

C_4 plants have evolved a CO_2-concentrating mechanism (CCM) that enables the elevation of CO_2 around the active sites of Rubisco by a combination of anatomical and biochemical specialization (Hatch, 1987). C_4 photosynthesis has independently evolved >60 times, providing one of the most widespread and effective solutions for remedying the catalytic inefficiency of Rubisco (Sage *et al.*, 2012; Christin and Osborne, 2013). The key carboxylases in C_4 plants are localized to different cellular compartments. Phospho*enol*pyruvate carboxylase (PEPC) is localized to the cytosol of mesophyll cells and Rubisco to the chloroplasts of bundle sheath cells. For the CCM to operate effectively, PEPC activity must exceed Rubisco activity to balance leakage of CO_2 out of the bundle sheath compartment. This maintains a high bundle sheath CO_2 level but prevents wasteful overcycling of the mesophyll CO_2 'pump' (von Caemmerer and Furbank, 2003). As PEPC utilizes HCO_3^- and not CO_2, the first committed enzyme of the C_4 pathway is carbonic anhydrase (CA) which

catalyses the reversible conversion of CO_2 and HCO_3^- in the cytosol of mesophyll cells. C_4 acids produced by PEPC then diffuse into the bundle sheath cells where they are decarboxylated, supplying CO_2 for Rubisco.

Within higher plants, there are multiple forms of the α-CA, β-CA, and γ-CA families which share little sequence homology (Moroney *et al.*, 2001). β-CAs are the most prevalent CA family in land plants. CA is an abundant enzyme in C_3 plants, representing up to 2% of the soluble leaf protein (Okabe *et al.*, 1984). In C_3 plants, the role of CA is unclear (Badger and Price, 1994) as it does not appear to limit photosynthesis but does influence stomatal conductance, guard cell movement, and amino acid biosynthesis (Hu *et al.*, 2010; DiMario *et al.*, 2016; Engineer *et al.*, 2016).

It has long been contended that the uncatalysed rate of CO_2 conversion to HCO_3^- is insufficient to support C_4 photosynthetic flux (Hatch and Burnell, 1990; Badger and Price, 1994). This hypothesis was supported by experiments in the C_4 dicot *Flaveria bidentis*, where antisense plants with <10% of wild-type CA activity required high CO_2 for growth and showed reduced CO_2 assimilation rates (von Caemmerer *et al.*, 2004; Cousins *et al.*, 2006). However, in the C_4 monocot *Zea mays* mutant plants with reduced CA activity (3% of wild type), no limitation to CO_2 assimilation rates at ambient CO_2 was observed (Studer *et al.*, 2014). CA activity has been shown to vary widely between species (Cousins *et al.*, 2008), and it is unclear whether CA activities are limiting at high CO_2 assimilation rates, as has previously been suggested (Hatch and Burnell, 1990; Gillon and Yakir, 2000).

We examined the role of CA in the model C_4 monocot species *Setaria viridis* (green foxtail millet). *Setaria viridis* is closely related to agronomically important C_4 crops including *Z. mays* (maize), *Sorghum bicolor* (sorghum), and *Saccharum officinarum* (sugarcane) (Brutnell *et al.*, 2010). It is an ideal model species due to its rapid generation time, small stature, high seed production, diploid status, and small genome that is sequenced and publicly available (Doust *et al.*, 2009; Brutnell *et al.*, 2010; Li and Brutnell, 2011). Here we used a stable transformation approach to examine the role of CA in *S. viridis* and could show that *S. viridis* is a useful model species that lends itself to molecular manipulation of the C_4 photosynthetic pathway. Two constructs both targeting the major leaf β-CA (Si003882m.g) were used to generate three independent transformed lines with reduced CA activity. A strong correlation between the CO_2 assimilation rate at low pCO_2 and CA activity was observed. Our combined measurements of mesophyll conductance and CA activity suggest that increasing mesophyll conductance may be an important way to increase the CO_2 assimilation rate at low intercellular pCO_2, as may occur under drought.

Materials and methods

Plant growth conditions

T_1 seeds were incubated in 5% liquid smoke (Wrights) for 24 h to promote germination, and germinated in garden soil mix fertilized with Osmocote (Scotts, Australia) in small containers before being transferred to individual 2 litre pots. Plants were grown in controlled environmental chambers, irradiance 500 µmol photons m^{-2} s^{-1}, 16 h photoperiod, 28 °C day, 24 °C night, 2% CO_2. Pots were watered daily.

Construct generation

Two different constructs were used to generate three lines of reduced CA activity. First, an RNAi was targeted to the primary leaf β-CA Si003882m which generated lines 2.1 and 5.3. A region of Si003882m.g was amplified by PCR using gene-specific primers (Supplementary Table S1 at *JXB* online) and reverse-transcribed RNA from *S. viridis* leaves ligated into pENTR/D-TOPO (ThermoFisher), and verified by sequencing. The fragment was inserted via a double Gateway system LR reaction (Invitrogen) into the hairpin RNAi binary vector pSTARGATE (Greenup *et al.*, 2010) to form a stem–loop region under the control of the ubiquitin promoter/intron (UBI) and octopine synthase (OCS) terminator to form the RNAi vector pSG/*CAa*.

Secondly, an overexpression approach, which resulted in gene silencing, generated the third transformed line, 1.1. The coding sequence of the maize β-CA gene (GRMZM2G348512), *ZmCA2* (Studer *et al.*, 2014), was amplified by reverse transcription–PCR (RT–PCR) from total RNA extracted from B73 maize. Total RNA was isolated using hot acid phenol and chloroform, and then treated with RQ1 RNase-free DNase (Promega). The reverse transcription and PCRs were performed as per the manufacturer's protocols with Superscript II (ThermoFisher) and Phusion High-Fidelity DNA polymerase (NEB), respectively (for primers, see Supplementary Table S1). The sequence encoding an AcV5 epitope tag (Lawrence *et al.*, 2003) was added to the C-terminal end of *ZmCA2*. The resulting *ZmCA2* amplicon was cloned into pENTR/D-TOPO and verified by sequencing. LR Gateway cloning (ThermoFisher) was used to insert the *ZmCA2* coding sequence into the overexpression vector, pSC110. pSC110 was created by Gibson Assembly (Gibson *et al.*, 2009) from two modified pMDC164 vectors (Curtis and Grossniklaus, 2003), kindly provided to us by Udo Gowik (Heinrich-Heine University, Dusseldorf, Germany). *ZmCA2* expression from pSC110 was driven by the B73 *ZmPEPC* promoter. pSC110 and pSC110/*ZmCA2* were verified by sequencing.

Both constructs were transformed into *Agrobacterium tumefaciens* strain AGL1 for stable plant transformation.

Callus induction and plant transformation

Stable transformation of *S. viridis* (accession A10.1) was carried out as described by Brutnell *et al.* (2010). Seed coats were mechanically removed from mature *S. viridis* seeds to improve germination. Seeds were sterilized before plating on callus induction medium [CIM; 4.3 g l^{-1} Murashige and Skoog (MS) salts, pH 5.8, 10 ml l^{-1} 100× MS vitamins stock, 40 g l^{-1} maltose, 35 mg l^{-1} $ZnSO_4 \cdot 7H_2O$, 0.6 mg l^{-1} $CuSO_4 \cdot 5H_2O$, 4 g l^{-1} Gelzan, 0.5 mg l^{-1} kinetin, 2 mg l^{-1} 2,4-D]. After 4 weeks in the dark at 24 °C, any seedling structures or gelatinous calli were removed and remaining calli transferred to fresh CIM. After a further 2 weeks, calli were divided and replated onto fresh CIM. One week later, transformations were performed.

AGL1 containing the construct of interest were grown in the presence of 50 µg l^{-1} kanamycin and 50 µg l^{-1} rifampicin at 28 °C to OD_{600}=0.5 and then resuspended in CIM without Gelzan and hormones. Acetosyringone (200 mM) and synperonic [0.01% (w/v)] were added to the *Agrobacterium* solution before incubating the calli in the medium for 5 min at room temperature. The calli were blotted dry on sterile filter paper and incubated at 22 °C for 3 d in the dark. The calli were then transferred to selective CIM (CIM containing 40 mg l^{-1} hygromycin, 150 mg l^{-1} timentin) and incubated in the dark at 24 °C for 16 d. Calli were then transferred to selective plant regeneration medium (PRM) containing 4.3 g l^{-1} MS salts, pH 5.8, 10 ml l^{-1} 100× MS vitamins, 20 g l^{-1} sucrose, 7 g l^{-1} Phytoblend, 2 mg l^{-1} kinetin, 150 mg l^{-1} timentin, 15 mg l^{-1} hygromycin. Calli were maintained at 24 °C under a 16 h light:8 h dark photoperiod and a light

intensity of 60 µmol photons m^{-2} s^{-1}. Developing shoots were transferred to selective rooting medium (RM) containing 2.15 g l^{-1} MS salts, pH 5.7, 10 ml l^{-1} 100× MS vitamins, 30 g l^{-1} sucrose, 7 g l^{-1} Phytoblend, 150 mg l^{-1} timentin, 20 mg l^{-1} hygromycin. Shoots that survived and developed roots were genotyped using primers against the hygromycin phosphotransferase gene (Supplementary Table S1) by PCR, and positive transformants were transplanted to soil.

Selection of plants for analysis

The progeny of three independent T_0 transformation events were analysed for CA hydration rates (Supplementary Fig. S1). One T_1 plant with low CA hydration rates was selected from each transformation event (labelled 5.3, 2.1, and 1.1) and its progeny (T_2) used for all future analysis. Two sets of experiments were performed on the T_2 plants. First, gas exchange and biochemical analysis on lines 5.3, 2.1, and 1.1 (Table 1) and, secondly, gas exchange and oxygen discrimination on lines 5.3 and 1.1 (Table 2). Each T_2 plant was genotyped prior to experiments using primers against the hygromycin phosphotransferase gene (Supplementary Table S1). The progeny of a plant which went through the *S. viridis* transformation process and tested negative for the hygromycin phosphotransferase gene were used as null controls.

Insertion number estimation

DNA was isolated from a fully expanded leaf using a CTAB (cetyltrimethylammonium bromide) extraction buffer [2% CTAB (v/v), 20 mM Tris–HCl pH 8, 1.4 M NaCl, 20 mM EDTA, 1% polyvinylpyrrolidone (PVP)-40 (w/v), 0.2% (v/v) β-mercaptoethanol] followed by extraction with phenol/chloroform/isoamylalcohol (25:24:1) and ethanol clean-up. DNA quality and quantity was determined using a NanoDrop spectrophotometer (Thermo Scientific).

IDNA genetics (UK) performed quantitative real-time PCR (qPCR) analysis to estimate the numbers of transgene copies in the CA transformed lines following the procedure described in Bartlett *et al.* (2008) with some modifications. The hygromycin phosphotransferase gene (with a FAM reporter) and the internal positive control (IPC, with a VIC reporter) were amplified together in a multiplex reaction (15 min denaturation, then 40 cycles of 15 s at 95 °C and 60 s at 60 °C) in an ABI1900 real-time PCR machine. Fluorescence from the FAM and VIC fluorochromes was measured during each 60 °C step and the Ct values obtained. The difference between the Ct values for the hygromycin phosphotransferase gene and the IPC (the Delta Ct) was used to allocate the assayed samples into groups with the same gene copy number.

RNA extraction and reverse transcription–quantitative PCR (RT–qPCR)

Leaf discs (0.78 cm^2) frozen and stored at −80 °C were lysed using the Qiagen TissueLyser II. RNA was extracted using the Trizol extraction method and in the presence of RNase inhibitor (Ambion). DNA was removed using the TURBO DNA free kit (Ambion), and RNA quantity and quality were determined using a NanoDrop (Thermo Scientific).

RNA (200 ng) was reverse transcribed into cDNA using Qiagen's RT^2 HT First Strand cDNA synthesis kit. RT–qPCR and melt curve analysis were performed on a Viia7 Real-time PCR system using the Power SYBR green PCR Master Mix (Thermo Fisher) according

Table 1. *Physiological and biochemical characteristics of CA transformants under ambient CO_2 conditions*

Net CO_2 assimilation rate (A), stomatal conductance (g_s), mesophyll pCO_2 (C_m), the rate constant of CA hydration (k_{CA}), and enzyme activities were measured from the uppermost, fully expanded leaf of 5-week-old plants grown at 2% CO_2. Gas exchange measurements were made at 25 °C leaf temperature, flow rate at 500 µmol m^{-2} s^{-1}, and irradiance of 1500 µmol photons m^{-2} s^{-1}. Three T_2 plants from three different transformation events were measured.

	A	g_s	C_m	k_{CA}	Rubisco	PEPC	NADP-ME
	µmol m^{-2} s^{-1}	mol m^{-2} s^{-1}	µbar	mol m^{-2} s^{-1} bar^{-1}	µmol m^{-2} s^{-1}	µmol m^{-2} s^{-1}	µmol m^{-2} s^{-1}
Null	22.5 ± 0.6 a	0.19 ± 0.01 a	132.4 ± 3.3 a	6.1 ± 0.8 a	18.7 ± 1.5 a	229.6 ± 19.3 a	59.8 ± 4.3 a
5.3	21.7 ± 2.6 a	0.2 ± 0.02 a	118.9 ± 13.1 a	3.3 ± 0.2 b	18.8 ± 1.8 a	249.3 ± 24.6 a	54.5 ± 5.8 a
2.1	18.5 ± 1.9 a	0.16 ± 0.01 a	152.9 ± 15.2 a	2.0 ± 0.2 b,c	20.9 ± 2.9 a	181.5 ± 25.4 a	47.3 ± 2.6 a
1.1	19.1 ± 1.2 a	0.19 ± 0.02 a	153.9 ± 4.4 a	0.8 ± 0.1 c	19.7 ± 1.8 a	180.3 ± 18.4 a	43.6 ± 3.9 a

Significant differences are based on one-way ANOVA and Tukey post-hoc analysis (SPSS statistics version 22; P=0.05).

Table 2. *Physiological characteristics of CA transformants at ambient CO_2 measured using LI-6400XT coupled to a tunable diode laser*

Net CO_2 assimilation rate (A), stomatal conductance (g_s), mesophyll pCO_2 (C_m), the ratio of intercellular to ambient pCO_2 (C_i/C_a), the rate constant of CA hydration (k_{CA}), online $\Delta^{18}O$ discrimination, and the length of mesophyll cells exposed to intercellular airspace (S_m) were measured on the uppermost, fully expanded leaf of 5-week-old plants grown at 2% CO_2. Gas exchange measurements were made at 2% O_2, 25 °C leaf temperature, flow rate at 500 µmol m^{-2} s^{-1}, and irradiance of 1500 µmol photons m^{-2} s^{-1}. Three T_2 plants from two different transformation events were measured.

	A	g_s	C_m	C_i/C_a	k_{CA}	$\Delta^{18}O$	S_m
	µmol m^{-2} s^{-1}	mol m^{-2} s^{-1}	µbar	µbar	mol m^{-2} s^{-1} bar^{-1}	‰	m^2 m^{-2}
Null	30.0 ± 1.4 a	0.30 ± 0.03 a	144.6 ± 5.9 a	0.39 ± 0.03 a	8.4 ± 0.7 a	18.0 ± 1.4 a	10.2 ± 0.4 a
5.3	29.2 ± 0.9 a	0.29 ± 0.02 a	157.9 ± 10.5 a	0.34 ± 0.01 a	2.5 ± 0.3 b	13.6 ± 0.7 a,b	–
1.1	24.5 ± 1.6 a	0.26 ± 0.03 a	178.1 ± 13.5 a	0.43 ± 0.02 a	0.8 ± 0.2 b	10.9 ± 0.6 b	10.2 ± 0.9 a

Significant differences are based on one-way ANOVA and Tukey post-hoc analysis (SPSS statistics version 22; P=0.05).

to the manufacturer's instructions. Primers (Supplementary Table S1) were designed using Primer3 in Geneious R7.1.6, ensuring products spanned an intron. Primer amplification efficiencies were determined by the Ct slope method; efficiencies for all primer pairs were comparable (~95%) and no amplification was detected in the no template control. Relative fold change was calculated by the ΔΔCt method, using the average of three nulls as reference, as described by Livak and Schmittgen (2001). The geometric mean of the Ct values for three reference genes was used for normalization (Vandesompele *et al.*, 2002). Statistics were performed with SigmaPlot (version 11.0).

Determination of enzyme activities

For CA activity, leaf discs (0.78 cm^2) were collected from the uppermost fully expanded leaf of 5-week-old *S. viridis* plants and frozen in liquid nitrogen. Soluble protein was extracted by grinding one frozen leaf disc in ice-cold glass homogenizers (Tenbroek) in 500 µl of extraction buffer [50 mM HEPES, pH 7.8, 1% (w/v) PVP, 1 mM EDTA, 10 mM dithiothreitol, 0.1% (v/v) Triton X-100, 2% (v/v) protease inhibitor cocktail (Sigma)]. Crude extracts were centrifuged at 4 °C for 1 min at 13 000 *g* and the supernatant collected for the soluble CA assay. Activity was measured on a membrane inlet mass spectrometer to measure the rates of ^{18}O exchange from labelled $^{13}C^{18}O_2$ to $H_2{}^{16}O$ at 25 °C (Badger and Price, 1989; von Caemmerer *et al.*, 2004). The hydration rates were calculated as described by Jenkins *et al.* (1989).

For Rubisco, PEPC, and NADP-malic enzyme (ME) activities, soluble protein was extracted from fresh leaf discs collected from leaves used for gas exchange analysis. Spectrophotometric assays were then performed as described previously (Pengelly *et al.*, 2010, 2012; Sharwood *et al.*, 2016).

Gas exchange measurements

Net photosynthesis (A) was measured over a range of intercellular pCO_2 (C_i) on the uppermost, fully expanded leaf of 5-week-old *S. viridis* plants using a portable gas exchange system LI-COR 6400XT (LI-COR Biosciences). Measurements were made after leaves had equilibrated at 380 µbar, flow rate 500 µmol s^{-1}, leaf temperature 25 °C, and irradiance 1500 µmol photons m^{-2} s^{-1}. CO_2 response curves were measured in a stepwise increase (3 min intervals) in CO_2 partial pressure 380, 0, 23.75, 47.5, 71.25, 95, 142.5, 190, 285, 380, 570, 760, and 950 µbar whilst maintaining leaf temperature and irradiance conditions.

Measurements of $C^{18}O^{16}O$ discrimination ($\Delta^{18}O$)

Simultaneous measurements of exchange of CO_2, H_2O, $C^{18}O^{16}O$, and $H_2{}^{18}O$ were made by coupling two LI-6400XT gas exchange systems to a tunable diode laser (TDL: TGA200A, Campbell Scientific Inc., Logan, UT, USA) to measure $C^{18}O^{16}O$ and a Cavity Ring-Down Spectrometer (L2130-i, Picarro Inc., Sunnyvale, CA, USA) to measure the oxygen isotope composition of water vapour. The system is essentially that described by Tazoe *et al.* (2011) except that the TGA100 was replaced by a TGA200A and the additional laser for water vapour measurements has been added together with a 16 port distribution manifold. To generate gas flows to the gas exchange systems, N_2 and O_2 were mixed by mass flow controllers (Omega Engineering Inc., Stamford, CT, USA) to generate CO_2-free air with 2% O_2. The humidity of incoming air was adjusted by varying the temperature of water circulating around a Nafion tube (Permapure, MH-110-12P-4) but was kept constant in this set of experiments to supply water vapour of a constant ^{18}O composition. To supply flow to the TDL and the L2130-i from the sample and reference gas streams, two T junctions were inserted into the match valve tubing and in the reference line of the LI-6400XT, respectively. This allowed leaves of two plants to be measured in sequence, with each LI-6400XT sampled by the TDL at 4 min intervals for 20 s at the sample and reference line. The Picarro Cavity Ring Down spectrometer sampled for 3 min, so that leaves were sampled at 6 min intervals.

Supplementary Fig. 5 shows the CO_2 dependence of the standard error of $\delta^{18}O$ of CO_2 in the reference gas of repeated measurements on the TGA200A. The ^{18}O isotopic composition of the CO_2 calibration gas was 22.17 ± 0.04‰ for Vienna mean oceanic water (VSMOW) and was checked against standards on an Isoprime mass spectrometer. We monitored the ^{18}O composition of water vapour of the reference air streams daily, and the values were −6.07 ± 0.08‰ and −6.34 ± 0.08‰ (VSMOW) for LI-6400XT L1 and L2 references, respectively. We attribute the small difference between the reference lines to differences in the Nafion tubing. At the end of the experiment, the calibration of the Picarro L2130-i was confirmed by collecting water vapour samples from the gas stream of the LI-6400XT reference lines going to the Picarro as described by Cousins *et al.* (2006) and assaying these water samples against standards on a Picarro 1102i, which was set up to measure the ^{18}O isotopic composition of water samples.

Gas exchange was measured on the uppermost fully expanded leaf of 5-week-old *S. viridis* plants at 25 °C, and leaves were equilibrated at ambient CO_2 (380 µbar), irradiance 1500 µmol photons m^{-2} s^{-1}, and 2% O_2. The flow rate was 200 µmol s^{-1}. CO_2 concentration was adjusted from 380 to 760, 570, 380, and 190 µbar at 1 h intervals. Immediately following gas exchange measurements, leaf discs were collected and stored at −80 °C until measurements of CA activity were made.

Calculations of $C^{18}O^{16}O$ ($\Delta^{18}O$) discrimination and mesophyll conductance (g_m)

Discrimination against ^{18}O in CO_2 during photosynthesis, $\Delta^{18}O$, was calculated from the isotopic composition of the CO_2 entering δ_{in} and exiting δ_{out} the leaf chamber and the CO_2 concentration entering C_{in} and exiting C_{out} (all measured with the TDL) (Evans *et al.*, 1986; Barbour *et al.*, 2016;):

$$\Delta^{18}O = \frac{\xi(\delta_{out} - \delta_{in})}{1 + \delta_{out} - \xi(\delta_{out} - \delta_{in})} \quad (1)$$

where $\xi = C_{in}/C_{in} - C_{out}$. Sample streams were passed through a Nafion drying tube before entering the TDL, and CO_2 values presented are all at zero water vapour concentration.

Following the derivation by Barbour *et al.* (2016) and Farquhar and Cernusak (2012) photosynthetic $\Delta^{18}O$ discrimination was used to calculate pCO_2 in the mesophyll cytosol, C_m, with the assumption that C_m is equal to the pCO_2 at the site of CO_2–H_2O exchange and assuming that cytosolic CO_2 is in full isotopic equilibrium with local cytosolic water. This allowed g_m to be calculated from

$$g_m = A / (C_i - C_m) \quad (2)$$

$$C_m = C_i \left(\frac{\delta_i - a_w - \delta_A (1 + a_w)}{\delta_c - a_w - \delta_A (1 + a_w)} \right) \quad (3)$$

Equation 3 is the same as equation 21 of Barbour *et al.* (2016), and is a rearrangement of equation 18 of Farquhar and Cernusak (2012) using their notation. The oxygen isotope ratios are expressed relative to the standard, (VSMOW) $\left(\delta_x = \frac{\left(^{18}O / {}^{16}O\right)_x}{\left(^{18}O / {}^{16}O\right)_{std}} - 1\right)$. Intercellular pCO_2 is denoted by C_i, and a_w is the discrimination against $C^{16}O^{18}O$ during liquid phase diffusion and dissolution (0.8‰).

The isotopic composition of CO_2 being assimilated, δ_A, is given by

$$\delta_A = \frac{\delta_a - \Delta^{18}O}{1 + \Delta^{18}O}, \quad (4)$$

where δ_a is the isotopic composition of ambient air (in our case $\delta_a=\delta_{out}$).

The oxygen isotope composition of CO_2 in the intercellular airspaces, δ_i, including ternary corrections proposed by Farquhar and Cernusak (2012), is given by

$$\delta_i = \frac{\delta_{io} + t\left[\delta_A\left(\frac{C_a}{C_i}+1\right) - \delta_a\frac{C_a}{C_i}\right]}{1+t} \quad (5)$$

where C_a is the pCO_2 in the ambient air. The ternary correction factor, t, is given by

$$t = \frac{\left(1+\frac{a_{18bs}}{1000}\right)E}{2g_{ac}} \quad (6)$$

where g_{ac} is the total conductance to CO_2, E the transpiration rate, and a_{18bs} is the weighted discrimination of $C^{16}O^{18}O$ diffusion across the boundary layer and stomata in series given by:

$$a_{18bs} = \frac{(C_a - C_s)a_{18b} - (C_s - C_i)a_{18s}}{(C_a - C_i)} \quad (7)$$

where C_s is the pCO_2 at the leaf surface and a_{18s} and a_{18b} are the discriminations against $C^{16}O^{18}O$ through stomata and the boundary layer (8‰ and 5.8‰, respectively).

The isotopic composition of intercellular CO_2 ignoring ternary corrections is given by

$$\delta_{io} = \delta_A\left(1-\frac{C_a}{C_i}\right)(1+a_{18bs}) - \frac{C_a}{C_i}(\delta_a - a_{18bs}) + a_{18bs} \quad (8)$$

To calculate C_m, we assume that the isotopic composition of CO_2 in the cytosol, δ_c, is the isotopic composition of CO_2 equilibrated with cytosolic water, δ_{cw}, and

$$\delta_{cw} = \delta_w + \varepsilon_w \quad (9)$$

where δ_w is the stable oxygen isotope composition of water in the cytosol at the site of evaporation and ε_w is the isotopic equilibrium between CO_2 and water (dependent on temperature T_K in K (Barbour *et al.*, 2016, and references therein).

$$\varepsilon_w(‰) = \frac{17604}{T_K} - 17.93 \quad (10)$$

Calculation of the isotopic composition of water at the site of evaporation from the isotopic composition of transpired water

The isotopic composition of water at the site of evaporation, δ_w, can be estimated from the Craig and Gordon model of evaporative enrichment (Craig and Gordon, 1965; Farquhar and Lloyd, 1993)

$$\delta_w = \delta_t + \varepsilon^* + \varepsilon_k + \frac{e_a}{e_i}(\delta_{wa} - \varepsilon_k - \delta_t) \quad (11)$$

where ε^* is the equilibrium fractionation during evaporation, ε_k is the kinetic fractionation during vapour diffusion in air, δ_t is the oxygen isotopic composition of transpired water, e_a/e_i is the ratio of ambient to intercellular vapour pressure, and δ_a is the isotopic composition of ambient air. ε^* is dependent on temperature:

$$\varepsilon^* = 2.644 - 3.206\left(\frac{10^3}{T_K}\right) + 1.534\left(\frac{10^6}{T_K^2}\right) \quad (12)$$

ε_k is dependent on stomatal and boundary layer conductances and associated fractionation factors (Barbour *et al.*, 2016, and references therein):

$$\varepsilon_k = \frac{28g_s^{-1} + 19g_b^{-1}}{g_s^{-1} + g_b^{-1}} \quad (13)$$

The isotopic composition of transpired water δ_t can be calculated from mass balance knowing the isotopic composition of the water entering δ_{win} and exiting δ_{wout} the leaf chamber (measured with the Picarro) and the water vapour concentration entering w_{in} and exiting w_{out} (measured with the LI-6400XT):

$$\delta_t = \left(\delta_{wout}(1-w_{in}) - \delta_{win}\frac{w_{in}}{w_{out}}(1-w_{out})\right)\frac{w_{out}}{w_{out}-w_{in}} \quad (14)$$

Calculation of the proportion of mesophyll cytosolic CO_2 in equilibration with leaf water, θ

If C_m is known, it is possible to calculate the isotopic composition of cytosolic CO_2 from measurements of $\Delta^{18}O$ using equation 18 from Farquhar and Cernusak (2012):

$$\delta_c = \delta_A\left(1-\frac{C_i}{C_m}\right)(1+a_w) + \frac{C_i}{C_m}(\delta_i - a_w) + a_w. \quad (15)$$

This can then be compared with δ_{cw} (Equation 9), the isotopic composition of CO_2 in equilibrium with water at the site of evaporation. We calculated mesophyll conductance, g_m, in the *S. viridis* null plants assuming that $\delta_c=\delta_{cw}$ and then used this g_m to estimate C_m in the *S. viridis* transgenics to calculate the proportion of cytosolic CO_2 in equilibration with leaf water, θ using equations developed by Cernusak *et al.* (2004)

$$\theta = \frac{\delta_c - \delta_a + a_{18}\left(1+\frac{C_c}{C_a}\right)}{\delta_{cw} - \delta_a + a_{18}\left(1+\frac{C_c}{C_a}\right)} \quad (16)$$

where a_{18} is the weighted discrimination of $C^{16}O^{18}O$ diffusion across the boundary layer, stomata, and the liquid phase in series given by:

$$a_{18} = \frac{a_b(C_a - C_s) + a_s(C_s - C_i) + a_w(C_i - C_m)}{(C_a - C_m)}. \quad (17)$$

Leaf anatomical measurements and estimation of g_m from anatomical measurements

Fully expanded leaves from 5-week-old T_2 plants, null and line 1.1, were collected and cut into ~0.5 × 2 mm pieces. Leaf slices were fixed in 2.5% (v/v) glutaraldehyde, 2% (v/v) paraformaldehyde, 0.1 M phosphate buffer, and 0.01% (v/v) Tween-20 under vacuum for 20 min, then replaced with buffer containing no Tween-20 and fixed overnight at 4 °C. Leaf pieces were washed in phosphate buffer and post-fixed in 1% (w/v) osmium tetroxide for 2 h. Fixed leaf pieces were then dehydrated in an ethanol series (10, 30, 50, 70, 80, 95, 100%) followed by infiltration with LR white. Leaf sections were finally placed in moulds filled with resin and baked at 60 °C for 24 h. Sections of 0.5 µm thickness were cut using glass knives on a Reichert ultramicrotome, stained with toluidine blue, and heat fixed to glass slides. Slides were viewed using a Zeiss Axioskop light microscope at ×400 magnification. Three images were taken from each slide for analysis, each containing a leaf cross-section in the same orientation and showing at least two vascular bundles. Fiji quantification

software (Schindelin *et al.*, 2012) was used to select regions of interest. Mesophyll surface area exposed to intercellular airspace to leaf area ratio (S_m) was calculated using Equation 18 where CCF is the curvature correction factor of 1.43 (Evans *et al.*, 1994).

$$S_m = \frac{\text{Length of mesophyll cells exposed to intercellular airspace}}{\text{Interveinal distance}} \times \text{CCF} \quad (18)$$

The values of S_m together with measurements of cell wall thickness and cytosol thickness were used to derive an estimate of g_m from anatomical parameters. The cell wall thickness (0.113 ± 0.005 µm) was kindly estimated from transmission electron micrographs of *S. viridis* grown under similar conditions by Florence Danila (Danila *et al.*, 2016). Calculations followed equations 1–5 of von Caemmerer and Evans (2015) using the membrane permeability of Gutknecht for a lipid bilayer of 3.5×10^{-3} m s^{-1} since only the plasma membrane needs to be transversed for diffusion of CO_2 from he intercellular airspace to mesophyll cytosol (Gutknecht *et al.*, 1977) and a cytosol thickness of 0.3 µm (von Caemmerer and Evans, 2015). These calculations give a g_m of 0.68 mol m^{-2} s^{-1} bar^{-1}.

Statistical analysis

One-way ANOVAs with post-hoc Tukey test analyses were performed for all measurements of gas exchange and enzyme activities with P=0.05 using the IBM SPSS Statistics 22 package.

Results

Generation of transgenic S. viridis *with reduced β-CA*

In *S. viridis* we identified four β-CA genes: Si002140m.g (with one other isoform Si002148m), Si002669m.g, Si030616m.g (with two other isoforms Si030928m and Si030803m), and Si003882m.g. There is very low sequence identity between these β-CA genes, ~37% (Supplementary Fig. S2). Si003882m.g has been shown to be the major leaf β-CA (Christin *et al.*, 2013; John *et al.*, 2014).

Three independent transformation events resistant to hygromycin and with reduced CA activity were generated using two different approaches. First, one line (1.1) was generated through gene suppression upon transformation with the overexpression construct pSC110/*ZmCA2*. The coding sequences of *ZmCA2* and Si003882m.g show 87% identity (Supplementary Fig. S3). Most probably, expression of *ZmCA2* therefore caused suppression of the primary *S. viridis* β-CA gene, resulting in reduced CA activity in line 1.1. The second approach was to target Si003882m.g using the RNAi construct pSG/*CAa* which generated stably transformed lines from two different events (2.1 and 5.3). Plants were grown at high pCO_2 for all experiments.

To determine the specificity of the RNAi construct and check which β-CA was suppressed in line 1.1, RT–qPCR was performed against the β-CAs in *S. viridis*. Expression of the primary leaf β-CA Si003882m.g was significantly down-regulated, between 83% and 96%, in lines from all three transformation events (Fig. 1A). Transcript levels of Si030616m.g and Si002140m.g were unchanged relative to expression in the null plants (Fig. 1B, C) while Si002669m.g transcript was undetectable in all samples (data not shown). Therefore, expression of only the target β-CA gene was affected in the three transformed lines.

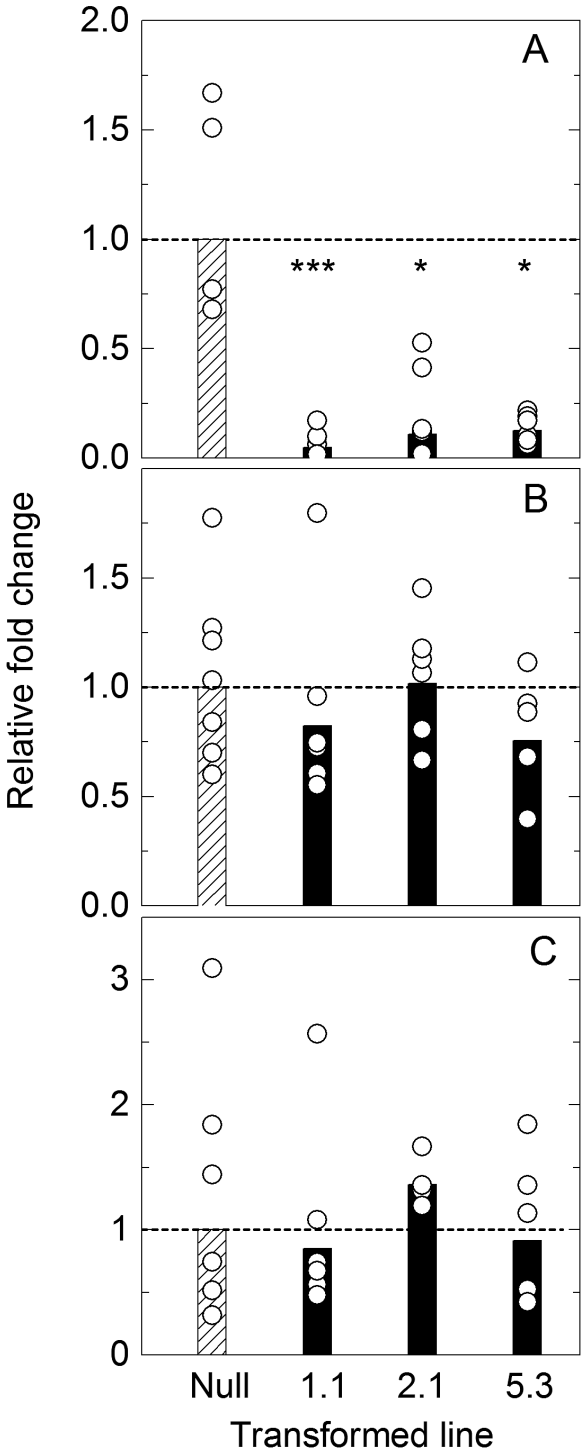

Fig. 1. Expression level of β-CA transcripts. (A) Si003882m.g, (B) Si002140m.g, and (C) Si030616m.g in null control and CA transformed lines 1.1, 2.1, and 5.3 as measured by RT–qPCR and analysed by ΔΔCt. Fold change relative to the null transformant is shown; bars represent mean fold change, and circles show the data range of T_2 plants (n=5–7 plants) from each transformation event measured in triplicate. The dotted line indicates average null fold change. Expression level of the major leaf β-CA transcript Si003882m.g (A) is significantly lower compared with the null control in all three transformed lines, calculated using one-way ANOVA.

qPCR was used to estimate the number of insertions in the transgenic plants, based on the number of copies of the hygromycin phosphotransferase gene. Three T_2 plants of the

three lines were analysed and there were two, four, and more than four transgene insertions detected for plants of line 5.3, 2.1, and 1.1, respectively. The high copy number in the over-expressing line of 1.1 is the likely cause of the suppression of transcript accumulation.

CA and photosynthetic enzyme activity and leaf anatomy

T_1 progeny of the three independent transformation events showed a range of CA hydration rates as measured on the soluble leaf fraction on a membrane inlet mass spectrometer. Compared with the null control, lines 1.1, 2.1, and 5.3 had on average (n=7 T_2 plants) an 87, 70, and 50% reduction of CA activity, respectively (Fig. 2). The CA hydration rate in the null plants was 934 ± 92 µmol m^{-2} s^{-1} as calculated at a mesophyll pCO_2 (C_m) of 140 µbar (Equation 2).

The activities of the photosynthetic enzymes Rubisco, PEPC, and NADP-ME were unchanged in lines 5.3, 2.1, and 1.1 compared with the nulls (Table 1) and showed no correlation with CA hydration rates (one-way ANOVA and Tukey post-hoc analysis (SPSS statistics version 22; P=0.05).

No significant differences were observed for the surface area of mesophyll cells exposed to intercellular airspace per unit leaf area (S_m) in embedded leaf sections of nulls (10.22 ± 0.35 m^2 m^{-2}) and plants from line 1.1 (10.18 ± 0.95 m^2 m^{-2}). These anatomical measurements were used to estimate an anatomical g_m of 0.68 mol m^{-2} s^{-1} bar^{-1} (see the Materials and methods).

CA activity and CO_2 assimilation rates

The response of CO_2 assimilation rate (A) to increasing intercellular pCO_2 (C_i) was investigated to examine the effect of reduced CA activity on CO_2 assimilation rates (Fig. 3). There were no statistical differences in the maximum rate of CO_2 assimilation under ambient or high CO_2 conditions between null control and progeny of transformant lines. At low pCO_2, CO_2 assimilation rates were reduced to varying degrees in the progeny of the transformed lines compared with the null control. Individuals of line 1.1 with the lowest CA hydration rate had the lowest initial slopes of the AC_i curves.

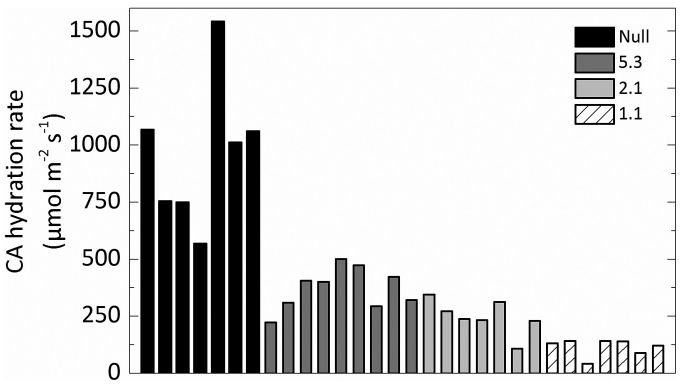

Fig. 2. Range of CA hydration rates at mesophyll pCO_2 (C_m) measured using a membrane inlet mass spectrometer in the null control and T_2 plants from lines 5.3, 2.1, and 1.1.

The initial slopes of the AC_i and AC_m curve were plotted against the CA hydration rate constant (k_{CA}; Fig. 4). Mesophyll cytosolic pCO_2, C_m, was calculated from Equation 2, using the average null g_m (0.9 mol m^{-2} s^{-1} bar^{-1}) since there was no difference in S_m. A strong correlation between the initial slope from the AC_m curve and k_{CA} was observed, with the initial slope increasing as CA hydration rates increase (R^2=0.845; Fig. 4). There was a curvilinear response between the initial slope of the AC_i curves indicating other limitations. No difference in stomatal conductance (g_s) was observed across a range of intercellular pCO_2 between null controls and any of the transformed lines during the rapid measurements of CO_2 responses (Fig. 5).

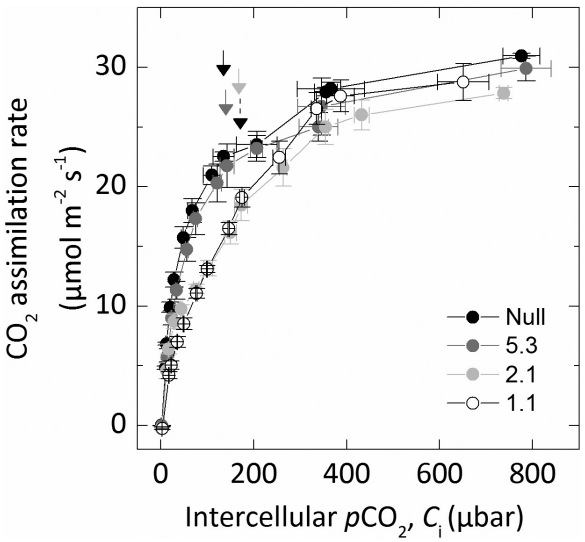

Fig. 3. CO_2 assimilation rate of transformed lines over a range of intercellular pCO_2 (C_i). Average of three T_2 plants from each line. Plants were grown at 2% CO_2, and the uppermost, fully expanded leaves of 5-week-old plants were measured using a LI-6400XT at 25 °C leaf temperature at an irradiance of 1500 µmol photons m^{-2} s^{-1}. Arrows mark ambient pCO_2 for each line; note that the dotted arrow is line 1.1.

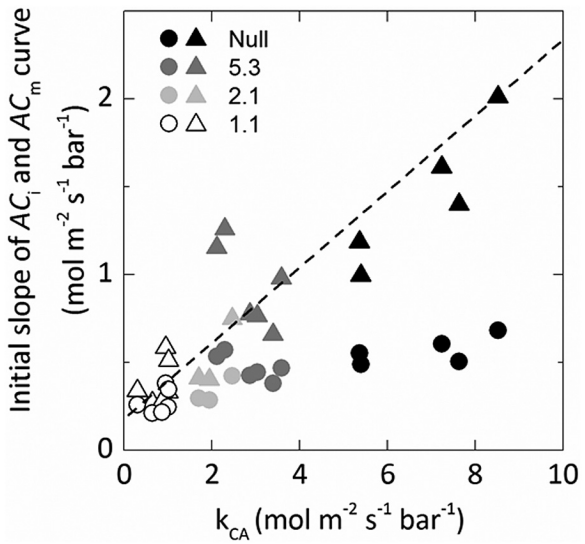

Fig. 4. Relationship between the initial slope of the AC_m (triangles) or AC_i (circles) curves and the rate constant of CA hydration rates (k_{CA}), AC_m R^2=0.846. Each point represents a measurement made on an individual leaf of a T_2 plant.

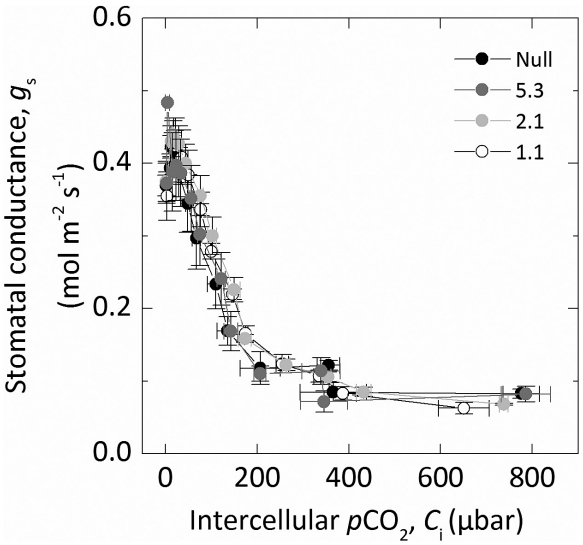

Fig. 5. Stomatal conductance (g_s) over a range of intercellular pCO_2 (C_i). Measurements were made concurrently with those in Fig. 4.

Oxygen isotope discrimination measurements

Oxygen ($\Delta^{18}O$) isotope discrimination and CO_2 assimilation rates were measured in response to changes in pCO_2 using a LI-6400XT coupled to a TDL trace gas analyser to measure $C^{18}O^{16}O$ and a Cavity Ring-Down Spectrometer to measure the oxygen isotope composition of water vapour. Transformed plants with reduced CA hydration rates had lower $\Delta^{18}O$ compared with the nulls, but only line 1.1 was significantly lower (Table 2).

In the null controls, measurements of $\Delta^{18}O$ were used to estimate conductance of CO_2 from the intercellular airspace to the sites of CO_2 and H_2O exchange in the cytosol (g_m) with the assumption that CO_2 was in full isotopic equilibrium with leaf water in the cytosol (Equation 2; Fig. 6). Although g_m appeared to increase with decreasing C_i, there were no significant differences between g_m estimated at the different C_i, and the average value was 0.94 ± 0.06 mol m^{-2} s^{-1} bar^{-1} (Fig. 6B). C_i–C_m indicates the drawdown of CO_2 from the intercellular airspace to the site of fixation, and for the null controls there is an increasing gradient of pCO_2 as C_i increases (Fig. 6C).

$\Delta^{18}O$ at ambient pCO_2 showed statistically significant differences between line 1.1 (with the lowest CA activity) and null plants (Table 2). When plotted against C_m/C_a, $\Delta^{18}O$ measurements closely correspond to theoretical curves representing θ (Equation 16) under different scenarios either where cytosolic CO_2 is at full isotopic equilibrium with the cytosolic water (null lines) or where there is only partial equilibrium (such as line 1.1; Fig. 7). Calculated values for line 5.3 which showed a 50% reduction in CA activity relative to the null controls fell in between these two theoretical lines. This is illustrated again with theta (θ) of lines 1.1 and 5.3 over a range of C_m (Fig. 8). When CO_2 is at full isotopic equilibrium with the cytosolic water, θ would be 1, whereas in lines 1.1 and 5.3 (with reduced CA hydration rates relative to the null control) θ is <1. There was no CO_2 dependence of θ over the range of pCO_2 measured.

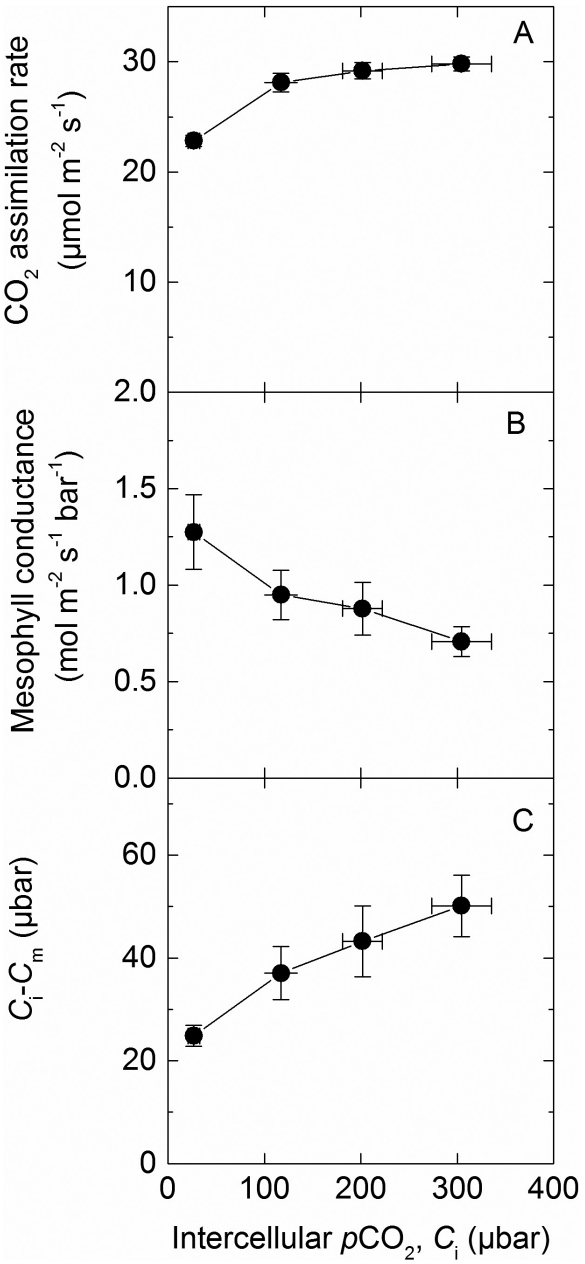

Fig. 6. (A) CO_2 assimilation rate, (B) mesophyll conductance (g_m; Equation 2), and (C) C_i–C_m over a range of intercellular pCO_2 in null controls measured using a LI-6400XT coupled to a tunable diode laser. Plants were grown at 2% CO_2 and the uppermost, fully expanded leaves of 5-week-old plants were measured at 25 °C leaf temperature, flow rate 200 µmol m^{-2} s^{-1}, 2% O_2 at an irradiance of 1500 µmol photons m^{-2} s^{-1}.

Discussion

Setaria viridis *as a model species to study photosynthetic physiology in a C_4 monocot*

Flaveria bidentis, a readily transformable model C_4 dicot, has been successfully used to study the regulation of C_4 photosynthesis using antisense and RNAi technology (Furbank *et al.*, 1997; Matsuoka *et al.*, 2001; von Caemmerer *et al.*, 2004; Pengelly *et al.*, 2012). This work has been crucial in quantifying the rate-limiting steps in the C_4 pathway by 'titrating' out levels of target enzymes by gene suppression and observing

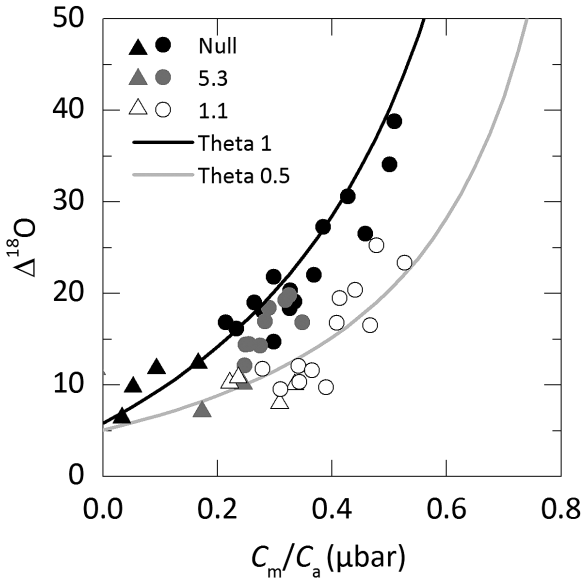

Fig. 7. Oxygen isotope discrimination ($\Delta^{18}O$) as a function of the ratio of mesophyll pCO_2 to ambient pCO_2 (C_m/C_a) in null and lines 5.3 and 1.1. Each point represents a measurement made on an individual leaf of a T_2 plant. Triangular symbols represent measurements made at low pCO_2. Theoretical curves represent the scenario where cytosolic CO_2 is at full isotopic equilibrium with cytosolic water (θ=1, black) or under partial equilibrium (θ=0.5, grey) of ^{18}O in the leaf. The equations for the curves are given by $\Delta^{18}O = a_{18} + \frac{C_m}{C_a - C_m}(\delta_c - \delta_a)$ and a_{18}=5.85‰ and δ_c–δ_a=33‰ at full equilibration or a_{18}=5.1‰ and δ_c–δ_a=15‰ (Farquhar and Lloyd, 1993).

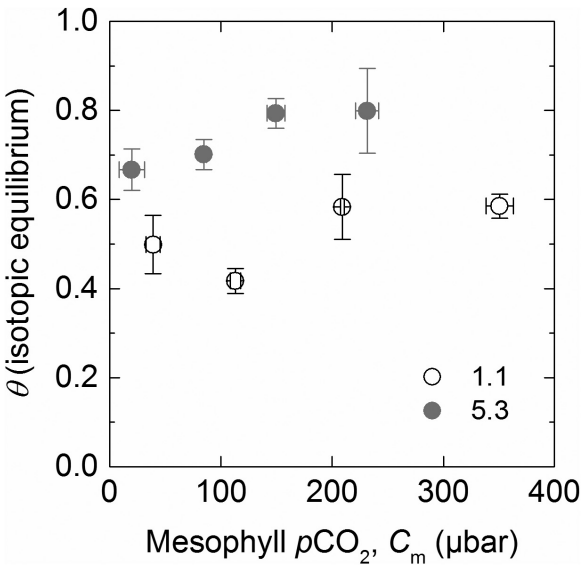

Fig. 8. Average isotopic equilibrium (theta, θ) over a range of mesophyll pCO_2 in two reduced CA lines 5.3 (grey) and 1.1 (white). Measured values of θ were determined from $\Delta^{18}O$ using Equation 16. Each point represents the average measurement of three T_2 plants.

the effects on physiological characteristics of the resultant transgenics (Furbank *et al.*, 1997). There are, however, important differences between C_4 dicots and the C_4 monocots which make up the majority of agriculturally important C_4 species. *Setaria viridis* has emerged as a new model grass to study C_4 photosynthesis in crops and related bioenergy species. *Setaria viridis* is an appropriate biochemical model species for *Z. mays* and *S. bicolor* as all three use NADP-ME as the primary decarboxylation enzyme. We generated transgenic *S. viridis* plants with reduced CA activity to compare the effect with previous results obtained with *F. bidentis* and *Z. mays* (von Caemmerer *et al.*, 2004; Studer *et al.*, 2014) and to explore the effect that a reduction in CA activity has on the initial slope of the AC_i and AC_m curves. In these lines, only the major leaf isoform of β-CA was reduced (Fig. 1). The transgenic plants had a range of different CA activities (Fig. 2), but showed no changes in PEPC and Rubisco activity (Table 1) or anatomical parameters (Table 2), making these plants ideal for exploring the role of CA activity in *S. viridis*.

Initial slope of AC$_i$ curves in C$_4$ plants

Models of C_4 photosynthesis suggest that the initial slope of the AC_i curve is determined by three possible limitations: (i) the mesophyll conductance to CO_2 diffusion from the intercellular airspace to the mesophyll cytosol (g_m); (ii) the rate of CO_2 hydration by CA; and (iii) the rate of PEP carboxylation (von Caemmerer, 2000). However, it is not readily known which is the major limitation in C_4 species. Studies with PEPC mutants from the C_4 dicot *Amaranthus edulis* indicate that PEPC activity may not be the major limitation as a 60% reduction in PEPC leads to only a 20% reduction in the CO_2 assimilation rate at ambient pCO_2 accompanied by a small reduction in initial slope for the AC_i curves (Dever *et al.*, 1992; Dever, 1997; Cousins *et al.*, 2007). This study with *S. viridis* confirms that substantial reductions in CA activity are possible before a reduction in steady-state CO_2 assimilation rate and initial slope of the AC_i curve are observed. This is in accordance with previous observations in *F. bidentis* and *Z. mays* (von Caemmerer *et al.*, 2004; Studer *et al.*, 2014).

The Michaelis–Menten constant for CO_2 for CA is >2 mM (~5% CO_2) which makes it appropriate to quantify CA activity by its first-order rate constant (Jenkins *et al.*, 1989; Hatch and Burnell, 1990) and simplifies species comparisons. In *S. viridis*, the lowest rate constant recorded was 0.8 mol m^{-2} s^{-1} bar^{-1} compared with values of 0.1 for the *ca1ca2* double mutant in *Z. mays* and 0.47 for transgenic *F. bidentis* (von Caemmerer *et al.*, 2004; Studer *et al.*, 2014). With this low rate constant, *F. bidentis* had very low CO_2 assimilation rates and the CO_2 response curves did not saturate at high CO_2. In contrast, for both *S. viridis* transgenics and *Z. mays* mutants, CO_2 assimilation rates were only slightly less than in the controls, suggesting that *S. viridis* is more similar to *Z. mays* in its CA requirements. This suggests that these two monocot species can make better use of leaf CA activity or that *in vivo* CA activity is greater than that estimated *in vitro*.

Mesophyll conductance and the initial slope of AC$_m$ curves

Next, we used recently established techniques that utilize ^{18}O discrimination measurements to quantify g_m in our null controls (Fig. 6B; Barbour *et al.*, 2016). This estimates the

diffusion of CO_2 from the intercellular airspace through the cell wall, plasma membrane, and cytosol to the sites of CA activity. At ambient pCO_2, the g_m observed for the null plants were similar to those reported by Barbour *et al.* (2016). A key assumption for the calculation of g_m is that CA activity is not limiting and that CO_2 is in isotopic equilibrium with HCO_3^-; consequently g_m was not measured in the transgenic lines with reduced CA activity. In C_3 species, g_m (in this instance from the intercellular airspace to the chloroplast stroma) has been shown to be proportional to the chloroplast surface area appressing the intercellular airspace per unit leaf area (Evans *et al.*, 1994). Evans and von Caemmerer (1996) hypothesized that in C_4 species g_m may correlate with the mesophyll surface area exposed to intercellular airspace per unit leaf area (S_m). Since S_m was similar between the nulls and line 1.1 plants, we assumed that g_m may also be similar between the plants. In C_3 species, g_m has been shown to, in some instances, increase with decreasing pCO_2 (Flexas *et al.*, 2007; Tazoe *et al.*, 2011; Alonso-Cantabrana and von Caemmerer, 2016). These changes to g_m which may be important in regulating and maintaining photosynthesis were also observed here in the *S. viridis* null plants, with g_m increasing slightly at low pCO_2. However, because the differences in g_m at different pCO_2 were not significant, we used the average g_m estimated for the null plants to calculate mesophyll cytosolic pCO_2 (C_m) in the transgenics.

As shown in Fig. 4, a strong almost linear relationship was found between AC_m and k_{CA}, whereas a saturating relationship was observed with AC_i. This indicates that the CO_2 assimilation rate is limited by cytosolic CA activity, with the relationship becoming clearer after accounting for g_m. It is tempting to speculate that the differences between the two monocot species and *F. bidentis* relate to differences in limitations imposed by g_m which affects cytosolic pCO_2 and hence *in vivo* CA activity, but this is not borne out by comparative measurements of g_m made by Barbour *et al.* (2016). CA activity increases with increasing pH, so variation in cytosolic pH can also contribute to variations in *in vivo* CA activity; however, these effects are not large (Jenkins *et al.*, 1989). The interaction of β-CA and a CO_2-permeable aquaporin in *Arabidopsis thaliana* has indicated that CA can be localized near the plasma membrane rather than dispersed throughout the mesophyll cytosol (Wang *et al.*, 2016). This may also impact on CA activity and result in another difference between the C_4 species. Other possibilities pertain to differences in anatomical characteristics of leaves. Both CA and PEPC are cytosolic enzymes, and differences in S_m may affect the efficiency with which CA is used. Our results suggest that increasing g_m may be an important way to increase the CO_2 assimilation rate at low intercellular pCO_2, a scenario that may, for example, occur under drought.

Oxygen isotope discrimination and the CO_2 dependence of isotopic equilibrium

As had previously been observed, $\Delta^{18}O$ decreased with reductions in CA activity as CA facilitates the exchange of O_2 between cytosolic water and CO_2 (Fig. 7; Williams *et al.*, 1996; Cousins *et al.*, 2006). Previous reports, which have estimated the proportion of cytosolic CO_2 in equilibrium with leaf water (θ) in C_4 species, have generally assumed a relatively large g_m value and this then led to lower estimates of θ (Cousins *et al.*, 2006, 2008). Here we assumed that in the *S. viridis* null plants there is sufficient CA for isotopic equilibrium to be reached, as discussed by Barbour *et al.* (2016). For comparison, we also estimated g_m from anatomical estimates of S_m, and cell wall and cytosolic thickness following calculations outlined by von Caemmerer and Evans (2015). This gives a g_m value of 0.68 mol m^{-2} s^{-1} bar^{-1} which is less than the value of 0.9 mol m^{-2} s^{-1} bar^{-1} calculated from $\Delta^{18}O$ measurements and highlights the anatomical constraints for CO_2 diffusion dictated by the photosynthetic pathway in leaves of C_4 plants (von Caemmerer *et al.*, 2007).

Reduction in CA activity led to significant reductions in θ but it is interesting to note that θ did not vary significantly with pCO_2. This is explained by the fact that CA activity increases linearly with pCO_2 so that although there is more CO_2 that needs to equilibrate with leaf water, there is also proportionally more CA activity. The fact that neither transgenic line showed a CO_2 dependence suggests that the decrease in the ratio of CA hydrations to PEP carboxylations is not affecting the isotopic equilibration of CO_2 with leaf water. These results have important implications for the interpretation of the ^{18}O signature of atmospheric CO_2 (Yakir and Sternberg, 2000; Gillon and Yakir, 2001; Wingate *et al.*, 2009).

Reduction of CA in S. viridis *does not alter the stomatal reponse to CO_2*

The CO_2 regulation of stomatal conductance remains an open question (Engineer *et al.*, 2016). It has been previously shown that in the *ca1*/*ca4* double mutant of *A. thaliana*, the degree of stomatal closure in response to increasing pCO_2 was reduced (Hu *et al.*, 2010; Wang *et al.*, 2016). It is clear that CA is part of a complex signal transduction network. However, nothing is currently known about the role of CA in stomatal CO_2 responses in C_4 species. In our study, where only one β-CA isoform was reduced, we found no change in the response of stomatal conductance to CO_2. The *S. viridis* β-CA reduced here (Si003882m.g) has low sequence identity (<50%) to all of the Arabidopsis β-CAs, but we would predict that multiple reductions in β-CA isoforms would be required to observe a similar stomatal phenotype in *S. viridis*.

Conclusion

Under current atmospheric conditions, CA activity was not rate limiting for C_4 photosynthesis in *S. viridis.* At lower C_i, which may, for example, occur under conditions of drought, our results suggest that g_m may pose a greater limitation than CA activity. However, it is important to investigate the role of CA on C_4 photosynthesis under a range of environmental conditions such as high temperatures which have recently been suggested to deactivate CA activity in *S. viridis* (Boyd *et al.*, 2015). Here we have shown that *S. viridis* is a useful

model monocot C_4 species that lends itself to molecular manipulation of the C_4 photosynthetic pathway.

Supplementary Data

Supplementary data are available at *JXB* online.

Table S1. Primers used in this study

Figure S1. CA hydration rates at mesophyll pCO_2 in the T_1 plants.

Figure S2. Very low sequence identity (~37%) between the four main *S. viridis* β-CAs.

Figure S3. High sequence identity (87%) of Si003882m.g to the *ZmCA2* (GRMZM2G348512).

Figure S4. CO_2 assimilation rate of the TDL experiment.

Figure S5. Standard error of $\delta^{18}O$ in the reference gas of repeated measurements with the TGA200A.

Acknowledgements

We thank Jasper Pengelly for assisting with construct generation, Xueqin Wang for assisting with *S. viridis* transformations, Soumi Bala for help with biochemical assays, gas exchange, and TDL measurements, and Murray Badger for making the MIMS available for measurements of CA activity. We thank Hilary Stuart-Williams for calibrating standard gases and water samples, and Joyce van Eck and Tom Brutnell for helpful discussions regarding *S. viridis* transformations. We thank Joanne Lee and the Centre for Advanced Microscopy at ANU for technical assistance with microscopy. This research was supported by the Bill and Melinda Gates Foundation's funding for the C_4 Rice consortium and by the Australian Research Council Centre of Excellence for Translational Photosynthesis (CE140100015). RES is funded by ARC DECRA (DE130101760).

References

Alonso-Cantabrana H, von Caemmerer S. 2016. Carbon isotope discrimination as a diagnostic tool for C_4 photosynthesis in C_3–C_4 intermediate species. Journal of Experimental Botany **67,** 3109–3121.

Badger MR, Price GD. 1989. Carbonic anhydrase activity associated with the cyanobacterium Synechococcus PCC7942. Plant Physiology **89,** 51–60.

Badger MR, Price GD. 1994. The role of carbonic anhydrase in photosynthesis. Annual Review of Plant Biology **45,** 369–392.

Barbour MM, Evans JR, Simonin KA, von Caemmerer S. 2016. Online CO_2 and H_2O oxygen isotope fractionation allows estimation of mesophyll conductance in C_4 plants, and reveals that mesophyll conductance decreases as leaves age in both C_4 and C_3 plants. New Phytologist **210,** 875–889

Bartlett JG, Alves SC, Smedley M, Snape JW, Harwood WA. 2008. High-throughput Agrobacterium-mediated barley transformation. Plant Methods **4,** 1–12.

Boyd RA, Gandin A, Cousins AB. 2015. Temperature response of C_4 photosynthesis: biochemical analysis of Rubisco, phosphoenolpyruvate carboxylase and carbonic anhydrase in *Setaria viridis*. Plant Physiology **160,** 1850–1861.

Brutnell TP, Wang L, Swartwood K, Goldschmidt A, Jackson D, Zhu X-G, Kellogg E, Van Eck J. 2010. *Setaria viridis*: a model for C_4 photosynthesis. The Plant Cell **22,** 2537–2544.

Cernusak LA, Farquhar GD, Wong SC, Stuart-Williams H. 2004. Measurement and interpretation of the oxygen isotope composition of carbon dioxide respired by leaves in the dark. Plant Physiology **136,** 3350–3363.

Christin P-A, Boxall SF, Gregory R, Edwards EJ, Hartwell J, Osborne CP. 2013. Parallel recruitment of multiple genes into C_4 photosynthesis. Genome Biology and Evolution **5,** 2174–2187.

Christin PA, Osborne CP. 2013. The recurrent assembly of C_4 photosynthesis, an evolutionary tale. Photosynthesis Research **117,** 163–175.

Cousins AB, Badger MR, von Caemmerer S. 2006. A transgenic approach to understanding the influence of carbonic anhydrase on $C^{18}OO$ discrimination during C_4 photosynthesis. Plant Physiology **142,** 662–672.

Cousins AB, Badger MR, von Caemmerer S. 2008. C_4 photosynthetic isotope exchange in NAD-ME-and NADP-ME-type grasses. Journal of Experimental Botany **59,** 1695–1703.

Cousins AB, Baroli I, Badger MR, Ivakov A, Lea P, Leegood RC, von Caemmerer S. 2007. The role of phosph*enol*pyruvate carboxylase during C_4 photosynthetic isotope exchange and stomatal conductance. Plant Physiology **145,** 1–12.

Craig H, Gordon LI. 1965. Deuterium and oxygen 18 variations in the ocean and the marine atmosphere. In: Tongiorgi E, ed. Proceedings of a Conference on stable isotopes in oceanographic studies and paleotemperatures. Pisa, Italy: Consiglio Nazionale delle Ricerche, Laboratorio di Geologia Nucleare, 9–130.

Curtis MD, Grossniklaus U. 2003. A Gateway cloning vector set for high-throughput functional analysis of genes *in planta*. Plant Physiology **133,** 462–469.

Danila F, Quick WP, White RG, Furbank RT, von Caemmerer S. 2016. The metabolite pathway between bundle sheath and mesophyll: quantification of plasmodesmata in leaves of C_3 and C_4 monocots. The Plant Cell **28,** 1461–1471.

Dever LV. 1997. Control of photosynthesis in *Amaranthus edulis* mutants with reduced amounts of PEP carboxylase. Australian Journal of Plant Physiology **24,** 469–476.

Dever LV, Lea PJ, Blackwell RD, Leegood RC. 1992. The isolation of mutants of C_4 photosynthesis. In: Murata N, ed. Research in Photosynthesis, **Vol. 111**. Kluwer Academic Publishers, 891–894.

DiMario RJ, Quebedeaux JC, Longstreth D, Dassanayake M, Hartman MM, Moroney JV. 2016. The cytoplasmic carbonic anhydrases βCA2 and βCA4 are required for optimal plant growth at low CO_2. Plant Physiology **171,** 280–293.

Doust AN, Kellogg EA, Devos KM, Bennetzen JL. 2009. Foxtail millet: a sequence-driven grass model system. Plant Physiology **149,** 137–141.

Engineer CB, Hashimoto-Sugimoto M, Negi J, Israelsson-Nordstrom M, Azoulay-Shemer T, Rappel WJ, Iba K, Schroeder JI. 2016. CO_2 sensing and CO_2 regulation of stomatal conductance: advances and open questions. Trends in Plant Science **21,** 16–30.

Evans J, Sharkey T, Berry J, Farquhar G. 1986. Carbon isotope discrimination measured concurrently with gas exchange to investigate CO_2 diffusion in leaves of higher plants. Functional Plant Biology **13,** 281–292.

Evans JR, Caemmerer S, Setchell BA, Hudson GS. 1994. The relationship between CO_2 transfer conductance and leaf anatomy in transgenic tobacco with a reduced content of Rubisco. Functional Plant Biology **21,** 475–495.

Evans JR, von Caemmerer S. 1996. Carbon dioxide diffusion inside leaves. Plant Physiology **110,** 339–346.

Farquhar GD, Cernusak LA. 2012. Ternary effects on the gas exchange of isotopologues of carbon dioxide. Plant, Cell and Environment **35,** 1221–1231.

Farquhar G, Lloyd J. 1993. Carbon and oxygen isotope effects in the exchange of carbon dioxide between terrestrial plants and the atmosphere. In: Elheringer JR, Hall AE, Farquhar G, eds. Stable isotopes and plant carbon–water relations. New York: Academic Press, 47–70.

Flexas J, Diaz-Espejo A, GalmES J, Kaldenhoff R, Medrano H, Ribas-Carbo M. 2007. Rapid variations of mesophyll conductance in response to changes in CO2 concentration around leaves. Plant, Cell and Environment **30,** 1284–1298.

Furbank RT, Chitty JA, Jenkins CLD, Taylor WC, Trevanion SJ, von Caemmerer S, Ashton AR. 1997. Genetic manipulation of key photosynthetic enzymes in the C_4 plant *Flaveria bidentis*. Australian Journal of Plant Physiology **24,** 477–485.

Gibson DG, Young L, Chuang RY, Venter JC, Hutchison CA 3rd, Smith HO. 2009. Enzymatic assembly of DNA molecules up to several hundred kilobases. Nature Methods **6,** 343–345.

Gillon J, Yakir D. 2001. Influence of carbonic anhydrase activity in terrestrial vegetation on the ^{18}O content of atmospheric CO_2. Science **291,** 2584–2587.

Gillon JS, Yakir D. 2000. Naturally low carbonic anhydrase activity in C_4 and C_3 plants limits discrimination against $C^{18}OO$ during photosynthesis. Plant, Cell and Environment **23,** 903–915.

Greenup AG, Sasani S, Oliver SN, Talbot MJ, Dennis ES, Hemming MN, Trevaskis B. 2010. ODDSOC2 is a MADS box floral repressor that is down-regulated by vernalization in temperate cereals. Plant Physiology **153,** 1062–1073.

Gutknecht J, Bisson MA, Tosteson FC. 1977. Diffusion of carbon dioxide through lipid bilayer membranes. Effects of carbonic anhydrase, bicarbonate, and unstirred layers. Journal of General Physiology **69,** 779–794.

Hatch MD. 1987. C_4 photosynthesis: a unique blend of modified biochemistry, anatomy and ultrastructure. Biochimica et Biophysica Acta **895,** 81–106.

Hatch MD, Burnell JN. 1990. Carbonic anhydrase activity in leaves and its role in the first step of C_4 photosynthesis. Plant Physiology **93,** 825–828.

Hu H, Boisson-Dernier A, Israelsson-Nordstrom M, Bohmer M, Xue S, Ries A, Godoski J, Kuhn JM, Schroeder JI. 2010. Carbonic anhydrases are upstream regulators of CO_2-controlled stomatal movements in guard cells. Nature Cell Biology **12,** 87–93.

Jenkins CLD, Furbank RT, Hatch MD. 1989. Mechanism of C_4 photosynthesis: a model describing the inorganic carbon pool in bundle sheath cells. Plant Physiology **91,** 1372–1381.

John CR, Smith-Unna RD, Woodfield H, Covshoff S, Hibberd JM. 2014. Evolutionary convergence of cell-specific gene expression in independent lineages of C_4 grasses. Plant Physiology **165,** 62–75.

Lawrence SD, Novak NG, Slack JM. 2003. Epitope tagging: a monoclonal antibody specific for recombinant fusion proteins in plants. Biotechniques **35,** 488–492.

Li P, Brutnell TP. 2011. *Setaria viridis* and *Setaria italica*, model genetic systems for the Panicoid grasses. Journal of Experimental Botany **62,** 3031–3037.

Livak KJ, Schmittgen TD. 2001. Analysis of relative gene expression data using real-time quantitative PCR and the 2(-Delta Delta C(T)) Method. Methods **25,** 402–408.

Matsuoka M, Furbank RT, Fukayama H, Miyao M. 2001. Molecular engineering of C_4 photosynthesis. Annual Review of Plant Physiology and Plant Molecular Biology **52,** 297–314.

Moroney JV, Bartlett SG, Samuelsson G. 2001. Carbonic anhydrases in plants and algae. Plant, Cell and Environment **24,** 141–153.

Okabe K, Yang S-Y, Tsuzuki M, Miyachi S. 1984. Carbonic anhydrase: its content in spinach leaves and its taxonomic diversity studied with anti-spinach leaf carbonic anhydrase antibody. Plant Science Letters **33,** 145–153.

Pengelly JJL, Sirault XRR, Tazoe Y, Evans JR, Furbank RT, von Caemmerer S. 2010. Growth of the C_4 dicot *Flaveria bidentis*: photosynthetic acclimation to low light through shifts in leaf anatomy and biochemistry. Journal of Experimental Botany **61,** 4109–4122.

Pengelly JJL, Tan J, Furbank RT, von Caemmerer S. 2012. Antisense reduction of NADP-malic enzyme in *Flaveria bidentis* reduces flow of CO_2 through the C_4 cycle. Plant Physiology **160,** 1070–1080.

Sage RF, Sage TL, Kocacinar F. 2012. Photorespiration and the evolution of C4 photosynthesis. Annual Review of Plant Biology **63,** 19–47.

Schindelin J, Arganda-Carreras I, Frise E, *et al*. 2012. Fiji: an open-source platform for biological-image analysis. Nature Methods **9,** 676–682.

Sharwood RE, Sonawane BV, Ghannoum O, Whitney SM. 2016. Improved analysis of C_4 and C_3 photosynthesis via refined in vitro assays of their carbon fixation biochemistry. Journal of Experimental Botany **67,** 3137–3148.

Studer AJ, Gandin A, Kolbe AR, Wang L, Cousins AB, Brutnell TP. 2014. A limited role for carbonic anhydrase in C_4 photosynthesis as revealed by a ca1ca2 double mutant in maize. Plant Physiology **165,** 608–617.

Tazoe Y, von Caemmerer S, Estavillo GM, Evans JR. 2011. Using tunable diode laser spectroscopy to measure carbon isotope discrimination and mesophyll conductance to CO_2 diffusion dynamically at different CO_2 concentrations. Plant, Cell and Environment **34,** 580–591.

Vandesompele J, De Preter K, Pattyn F, Poppe B, Van Roy N, De Paepe A, Speleman F. 2002. Accurate normalization of real-time quantitative RT–PCR data by geometric averaging of multiple internal control genes. Genome Biology **3**, Research0034.

von Caemmerer S. 2000. Biochemical models of leaf photosynthesis. Collingwood, Australia: CSIRO Publishing.

von Caemmerer S, Evans JR. 2015. Temperature responses of mesophyll conductance differ greatly between species. Plant, Cell and Environment **38,** 629–637.

von Caemmerer S, Evans JR, Cousins AB, Badger MR, Furbank RT. 2007. C_4 photosynthesis and CO_2 diffusion. In: Sheehy JE, Mitchell PL, Hardy B, eds. Charting new pathways to C_4 rice. Philippines: IRRI, 95–115.

von Caemmerer S, Furbank RT. 2003. The C_4 pathway: an efficient CO_2 pump. Photosynthesis Research **77,** 191–207.

von Caemmerer S, Quinn V, Hancock N, Price G, Furbank R, Ludwig M. 2004. Carbonic anhydrase and C_4 photosynthesis: a transgenic analysis. Plant, Cell and Environment **27,** 697–703.

Wang C, Hu H, Qin X, Zeise B, Xu D, Rappel W-J, Boron WF, Schroeder JI. 2016. Reconstitution of CO_2 regulation of SLAC1 anion channel and function of CO_2-permeable PIP2;1 aquaporin as CARBONIC ANHYDRASE4 interactor. The Plant Cell **28,** 568–582.

Williams TG, Flanagan LB, Coleman JR. 1996. Photosynthetic gas exchange and discrimination against $^{13}CO_2$ and $C^{18}O^{16}O$ in tobacco plants modified by an antisense construct to have low chloroplastic carbonic anhydrase. Plant Physioogy **112,** 319–326.

Wingate L, Ogee J, Cuntz M, *et al*. 2009. The impact of soil microorganisms on the global budget of delta ^{18}O in atmospheric CO_2. Proceedings of the National Academy of Sciences, USA **106,** 22411–22415.

Yakir D, Sternberg LDL. 2000. The use of stable isotopes to study ecosystem gas exchange. Oecologia **123,** 297–311.